Geometric morphometric exploration of the skull phenotypic matrix of Columbimorphae (Pteroclidiformes, Mesitornithiformes and Columbiformes):

Allometry, heterochrony, ecological factors, modularity, biomechanics, diet, and domestication



César Augusto Espinoza Campuzano

St Hugh's College

University of Oxford

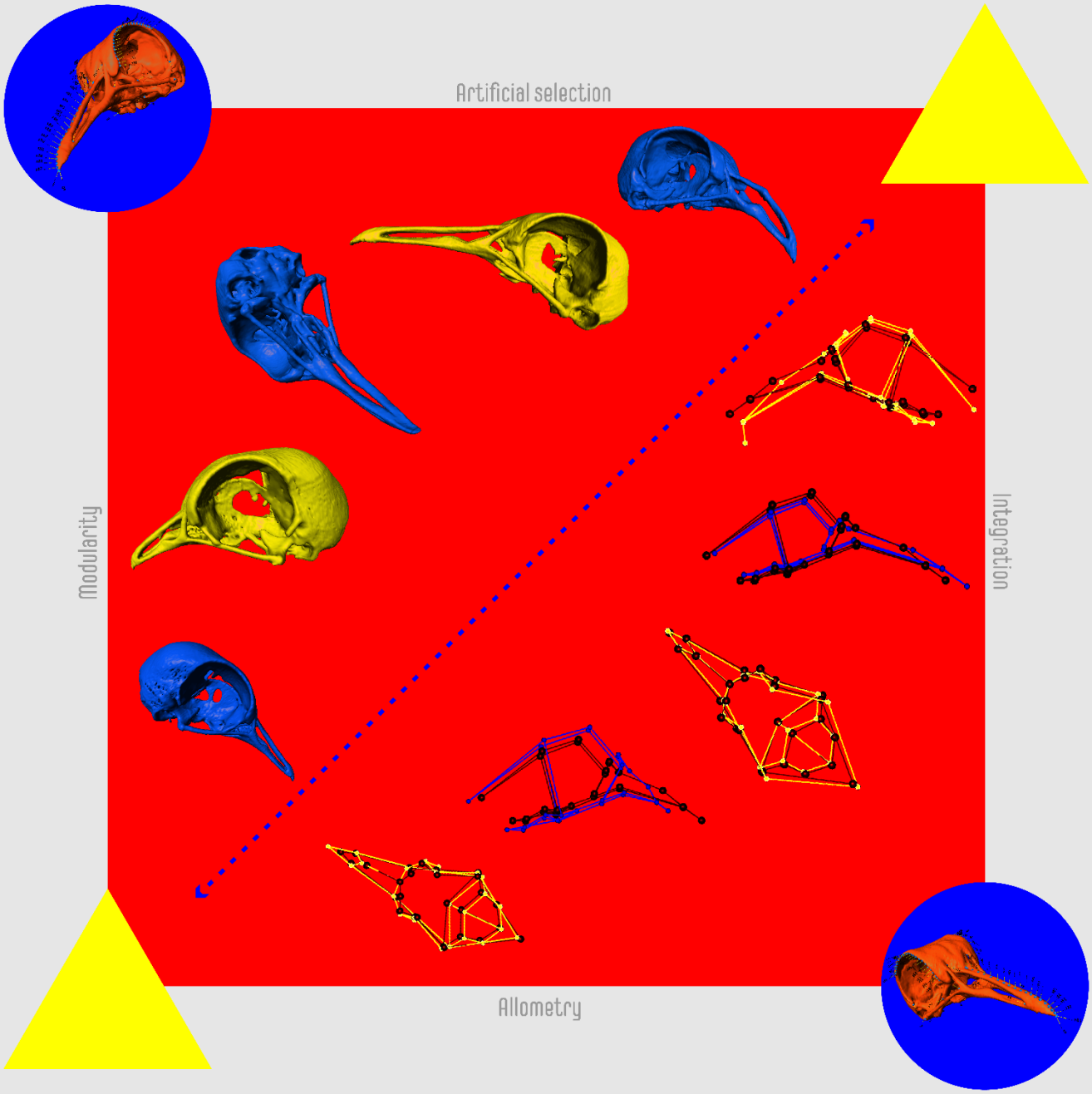
A thesis submitted for the degree of

Doctor of Philosophy

Michaelmas 2018

Geometric Morphometrics

The **Fancy** Pigeon Deconstructed



The common pigeon (**Columba livia**) is the second oldest domesticated animal after dogs. Domestication allowed this species to expand their natural habitat range from rock cliffs to a wide variety of human environments. It is believed that pigeons were originally domesticated for food. The homing habit of pigeons was discovered at least 5000 years ago, by the Egyptians and Babylonians. Though pigeons are now rarely used for food, a variety of distinct breeds have been selected for utility (messenger pigeons, racing pigeons, thief pigeons) and for aesthetic reasons (**'fancy pigeons'**).

Fancy pigeons have obtained a wide range of morphologies (shown). They were bred and described by Charles Darwin in the 19th century and were fundamental to the construction of the theory of evolution by natural selection, helping Darwin to see the principles of artificial selection at first hand. Now, new research based on X-ray computer tomography and mathematical shape characterization is **deconstructing** the fancy pigeon to uncover its secrets

By Cesar A. Espinoza-Campuzano

-To my mother Claudia, who always knew what needed to be done and whose wisdom and love I miss.

In sadness and tough times, always remember “Arriba y adelante, usted es la trompa de la maquina”

-To my daughter Lilith, who makes me proud and constantly reminded me of my deadline with her allometric growth.

-To my wife Viridiana, for sharing this experience with me

-To my family, who I left ten long years ago but are always with me

“The hardest thing of all is to find a black cat in a dark room,

especially if there is no cat.”

-misatributed to many people

Acknowledgements

Academic

Foremost, I want to thank my supervisors Matt Friedman and Roger Benson for the supervision, advise, and directions given to me during my D. Phil. They have unequivocally shaped this research and allowed me to, hopefully, become a better scientist. Furthermore, this work would not have been possible without the support provided by them, not only academically but for material and µCT-scanning funds.

I would also like to thank and recognize all the curators that were involved in my research: Judith White (Natural History Museum, Tring) who was responsible for allowing me to µCT scan most of the skulls in the sample, including the time consuming and delicate matter of scanning the fancy pigeons collected by Darwin. Janet Hinshaw (University of Michigan Museum of Zoology) for the freedom she granted me when browsing through the collections. I would also like to acknowledge the Mathew Lowe (collection manager) and Mike Brooke (curator of birds) in the University Museum of Zoology Cambridge. I would also like to thank Mark Carnall (curator) and Paul Smith (director) at the Oxford University Museum of Natural History, who allowed me to obtain a structured light surface scan of the Oxford dodo.

I would like to acknowledge people that made possible to µCT my sample. Again, Mathew Lowe and Mike Brooke from the University Museum of Zoology Cambridge CT scanning Cambridge. Farah Ahmed (Natural History Museum, London). Finally, I would like to thank Luis Alberto Medina (Instituto Nacional de Cancerología; INCAN) for allowing me to spend a week CT-Scanning the Mexican fancy pigeon sample, granting me access to one of the

few micro CT scanners in Mexico at the time, free of charge. The Mexican fancy pigeon sample were processed in the Faculty of Sciences (UNAM, Mexico), I would like to acknowledge Alejandro Gordillo Martínez for providing the dermestid colony and installations necessary for the skeletonization of the sample. I would also like to thank Perla Alejandra Román Torres for taking the job of giving the final touch to the skeletons.

Throughout my D. Phil. I have also been helped by other curators like Robert Faucett (University of Washington Burke Museum) who allowed me to browse for an entire month through their bird wing collection, allowing me to gather a sample of 1,000 genera. This sample remains to be analysed because of the long time it took investigate all the captivating aspects of the pigeon morphology. Hein Van Grouw also helped me to check the wing collection of the Natural History Museum, Tring. I would especially like to thank Robert Prys (Natural History Museum, Tring) who casually mentioned the Darwin fancy pigeon material to me. This material became the foundation for my thesis.

I was also able to gain access to cloud points of different dodo specimens, which ultimately were not included in the sample in favour of the surface scan of the Oxford dodo. However, I would like to thank the curators and researcher who shared their dodo data with me: Charlotte Brassey (Manchester Metropolitan University), Judith white (Natural History Museum, Tring), Delphine Brabant and Christine Lefèvre (Muséum national d'Histoire naturelle, Paris).

I also surveyed and transcribed the wing measurement database made by Colonel Meinertzhagen, which was not included in the thesis. However, the access to this material would have been impossible without Alison Harding (Natural History Museum, Tring). I

would also like to tank Robert Prys (Natural History Museum, Tring) because of the insights in the mind of Colonel Meinertzhagen.

I want to thank people whit whom I have had enlightening scientific talks throughout my D. Phil., I would like to thank Felipe de la Parra; Andrzej Wolniewicz, Gemma Benevento, Neil Brocklehurst; Jose Guerrero Castro; Serjoscha Evers; Donald Davesne; Mimi Beckett; and David Ford. I would especially like to thank Gemma Benevento and Serjoscha Evers for their input over my work.

Personal

I want to thank my wife Viridiana for her continuous support and love (and for continuous proofread of my work) during these years and for understanding the long trips and late nights demanded by my D. Phil.

I want to thank my family for supporting me, in every imaginable way, during this process.

I would also like to thank my friends in Oxford: Felipe de la Parra; Andrzej Wolniewicz, Gemma Benevento; Serjoscha Evers; Jose Guerrero Castro; Donald Davesne; Perla Alejandra Román Torres; Neil Brocklehurst; Mimi Beckett; David Ford; and many others.

Finally, I would like to thank my fellow Mexican students for electing me as their absolute leader, in charge of the Oxford Mexican Society.

Funding

I would like to acknowledge the Consejo Nacional de Ciencia y Tecnología (CONACyT, soon to become CONAHCyT) because of the funding and stipend provided.

My repeated travels to the United States, to attend international conferences and visit museum collections, would have been impossible without the support of St. Hugh's College. My college granted me the Barbinder Watson Fund and the MCR Travel Grant.

I would also like to acknowledge the Consejo Zacatecano de Ciencia, Tecnología e Innovación (COZCTI, formerly COZCyT) which granted me yearly travel funds throughout my D. Phil. and MSc.

Declaration

The contents of this thesis are all my own work, except where otherwise stated. The views and opinions expressed herein are mine and not necessarily those of any other person or body unless so attributed.



César Augusto Espinoza Campuzano

Michaelmas 2018

Abstract

Geometric morphometric exploration of the skull phenotypic matrix of Columbimorphae (Pteroclidiformes, Mesitornithiformes and Columbiformes): Allometry, heterochrony, ecological factors, modularity, biomechanics, diet and, domestication

Cesar Augusto Espinoza Campuzano
St-Hugh's College, University of Oxford
A thesis submitted for the degree of Doctor of Philosophy
Michaelmas 2018

This thesis deals with the interplay between developmental constraints and ecomorphological factors in the skull shape evolution in Columbimorphae. Columbimorphae is a group of birds that includes the Mesitornithiformes (mesites), Pteroclidiformes (sandgrouses), and Columbiformes (pigeons and doves). Columbiformes have a wide geographical distribution, exhibit a wide range of body sizes, and have high ecological and morphological diversity. It includes iconic species like the dodo (*Raphus cucullatus*), the Rodrigues solitaire (*Pezophaps solitaria*), and the passenger pigeon (*Ectopistes migratorius*).

This diversity shown in Columbiformes, along with their well resolved phylogenetic relationships makes this clade a good study system to perform macro-evolutionary research. This thesis is focussed on a pluralistic view of phenotypical evolution. For this reason, I tested ecological factors (distribution, body size, centroid size, feeding strategy and biomechanical performance) and developmental factors (allometry, heterochrony, modularity, integration) to examine the skull evolution.

My research sheds light into various evolutionary phenomena, showing that the dodo and the Rodrigues solitaire follow allometry and heterochrony; that modularity and integration are not sufficient to explain the columbiform skull shape; that ecomorphological factors have shaped the pigeon skull; that differences in biomechanical performance are

associated with different feeding strategies; that domestication does not only increases the amount of morphological disparity using existent axes of variation but successfully explores and incorporates new axis of variation; and that different phenotypic matrices are not usually comparable and generalizable because matrices of wild Columbiformes, domestic (*Columba livia*) and feral individuals (*C. livia*) are unequal and do not share the same axes of variation.

My overall results suggest that both ecomorphology and development influenced the evolution of the pigeon skull. My research also warns against the generalization of species patterns of constraints (modularity and integration) across taxonomic scales.

Extended Abstract

Adaptationism is the view of evolution in which traits (morphological, physiological biomechanical) are products from past selection towards a function. The correct implementation of the adaptationist program is done in a comparative framework after taking evolutionary constraints into account. Some of the evolutionary constraints are related to the "cohesion" of the genotype, which implies that there is an amount of integration and modularity in the organisms. This cohesion is better exemplified by the covariation and the correlation observed in the additive genetic and phenotypic matrices. When a selection pressure is applied in a selection regime (*e.g.*, artificial selection towards larger brain size), the covariation and correlation of the traits in the matrix will change the response to selection and may even produce the inverse effect to the selection pressure.

For these reasons, it is paramount to account for developmental constraints in evolutionary research. However, the prominent role of the search for developmental constraints in recent macroevolutionary research might obscure the fact that ecomorphology is also important for phenotypic evolution. For this reason, I take a pluralistic view of evolution throughout this thesis, in which multiple drivers of evolution can be accepted. I tested the influence of developmental (allometry, heterochrony, integration and modularity) and ecomorphological factors (distribution, size, biomechanics, diet, and foraging behaviour) in the phenotypic evolution of the skull of Columbimorphae.

Columbimorphae is a clade of birds that includes the Mesitornithiformes (mesites), Pteroclidiformes (sandgrouses), and Columbiformes (pigeons and doves); the latter of which is the most diverse, containing more than 300 species. This group of birds is globally distributed, inhabiting most oceanic islands and almost all continents, except Antarctica. This group includes iconic species like the passenger pigeon (*Ectopistes migratorius*) and

the seasonally poisonous pink pigeon (*Nesoenas mayeri*). This clade also includes extinct giant flightless species like dodo (*Raphus cucullatus*) and the Rodrigues solitaire (*Pezophaps solitaria*). Columbimorphae shows different diets (frugivorous, granivorous or both) and foraging behaviours (arboreal, terrestrial or both). The extant Columbimorphae range in body mass from 32 grams in the diamond dove (*Geopelia cuneata)* to 2 kg in the Victoria crowned pigeon (*Goura cristata*). Furthermore, the extinct flightless pigeons (Raphini): the dodo (Raphus cucullatus) and the Rodrigues solitaire (*Pezophaps solitaria*) could have weighed an order of magnitude more, at 21 and 28 kilograms respectively. Throughout this thesis I use the skulls of Columbimorphae, in a geometric morphometric framework, to assess a series of ecomorphological and developmental factors that might explain the evolution of the phenotype in this clade.

In Chapter One, I set the background for the ecomorphology versus developmental debate and my stance on it. I also give a general account of Columbimorphae and a general outline for the thesis.

In Chapter Two, I dealt with developmental factors (allometry and heterochrony). I analysed the allometric patterns in the three bird orders in Columbimorphae. I analysed both the allometry of skull centroid size versus body mass and the allometry of skull shape in comparison to size. I propose a new method to identify heterochronic species. This test uses the prediction of size based on shape in an allometric framework. This approach allowed me to explain the shape of some pigeons with peculiar skull morphology. Paedomorphosis was found in the skull shape of Pteroclidiformes, while peramorphosis accounted for the skull shape of Mesitornithiformes. I further discuss how a large proportion of the shape changes observed in the dodo and the Rodrigues solitaire can be accounted for by allometry and heterochrony. Based on skull shape, the pigeon furthest

away from the mean columbiform skull shape is the Samoan tooth-billed pigeon (*Didunculus strigirostris*). This species has a skull shape that is impervious to allometric or heterochronic explanations. I noted that some pigeons with skull shapes not predicted by allometry or heterochrony like *Didunculus*, or the genera *Treron* and *Ptilinopus*, are frugivorous species.

In Chapter Three, I dealt with both ecomorphological (biomechanics, diet, foraging behaviour, size, and distribution) and developmental factors (integration and modularity). I proposed a new feeding behaviour classification for pigeons, based on the hierarchical clustering of both feeding and foraging characters. This feeding classification takes into account the complexity of the feeding behaviour and separates the pigeons into eight feeding clusters. Next, I propose the use of a new visualization of the phylogeny in a feeding behaviour space, this "phylofeedingspace" is reminiscent of the commonly used "phylomorphospace" approach used in geometric morphometrics. Using this phylofeedingspace and ancestral character reconstruction I recognized that the ancestral feeding strategy for pigeons is granivorous terrestrial feeding and that pigeons have invaded other parts of the feeding space at least three times. I evaluate the biomechanical landscape of empirical and theoretical pigeon shapes to assess the "principle of frustration" in a "fitness landscape" framework. The biomechanical landscape allowed me to find performance differences between feeding modes. Frugivorous pigeons present a higher bending resistance and muscle area while granivorous pigeons present straighter thinner rostra with low bending resistance. I test the hypothesis of modularity and integration of the columbiform skull, finding that it is a globally disintegrated structure, with weak modularity and moderate integration. However, biomechanics and ecomorphology have a greater influence on the rostra than on the braincase.

Using information from the principal coordinated analysis of diet and biomechanical characters, I identify that feeding variables can account for skull shape and biomechanics

In Chapter Four, I dealt with developmental factors (matrix correlation, response to selection and evolution across lines of least evolutionary resistance). I evaluated the phenotypic matrix of domesticated pigeons by comparing the variation and covariation of domestic *Columba livia*, feral individuals of the same species and wild Columbiformes (analysed in previous chapters). I identify that artificial selection is not restricted to act along the same axes of variation as natural selection, thus challenging a popular view about phenotypic variation which argues in favour of the uniformity of axes of variation across all avian skulls. Despite finding that artificial selection and natural selection may work in different dimensions, I found that the amount of phenotypic change produced by artificial selection is higher when selection is aligned with the axis of higher morphological variation in wild Columbiformes. However, my results suggest that domestication has successfully explored other axes of variation and produced new ones, possibly by the incorporation of novel mutations during the domestication process.

The overall results warn against the generalization of modularity and integration of one species across taxonomic scales. While I argue in favour of a pluralistic view of phenotypic evolution, I also discuss how factors like geometrical scaling expectations are not accounted for in some of the current methods used to identify modularity and integration. Not accounting for a baseline of similarity expectation might bias the results of modularity and integration analyses because some patterns of similarity observed across species or taxonomic scales might be a result of geometrical scaling rather than constraints in the developmental pathways of organisms.

Contents

ACKNOWLEDGEMENTS ..... **I**

DECLARATION ..... **V**

ABSTRACT ..... **VII**

EXTENDED ABSTRACT ..... **IX**

CONTENTS ..... **XIII**

LIST OF FIGURES ..... **XXI**

LIST OF TABLES ..... **XXV**

CHAPTER ONE. INTRODUCTION **1**

DEVELOPMENT VERSUS NATURAL SELECTION IN PHENOTYPIC EVOLUTION, A LONGSTANDING DEBATE 1

COLUMBIMORPHAE 8

Diversity *9*

Systematics *11*

Raphidae *13*

Age of diversification *14*

Distribution and conservation *15*

Feeding behaviour *17*

Drinking behaviour *20*

Crop milk *21*

Domestication *22*

THESIS OUTLINE AND OBJECTIVES 30

Chapter Two: Allometry and heterochrony in the skull of Columbimorphae *30*

Chapter Three: Ecological factors and their relationship with skull shape in Columbiformes *30*

Chapter Four. Artificial and natural selection work on different axes of variation *31*

CHAPTER TWO: ALLOMETRY AND HETEROCHRONY IN THE SKULL OF COLUMBIMORPHAE (MESITORNITHIFORMES, PTEROCLIDIFORMES AND COLUMBIFORMES): THE DODO WASN'T THE STRANGEST PIGEON **33**

ABSTRACT 33

INTRODUCTION 36

Allometry in shape *42*

METHODS 47

Institutional abbreviations. *47*

Materials examined *47*

Computed tomography and surface scanning *48*

Geometric morphometrics *48*

Body size and phylogenetic information *52*

Statistical hypothesis tests *54*

Multidimensional shape visualization *63*

RESULTS 65

Allometry of head size against body mass *65*

Allometric shape changes of shape against size *68*

Heterochrony in skull shape versus size *76*

DISCUSSION 83

Allometry of head size against body size *83*

Allometry of skull shape against size *84*

Heterochrony in columbiform evolution *85*

Distribution likely influences the skull shape in Columbiformes *87*

Influence of allometry and heterochrony on the outlier skull shape *88*

Allometry and heterochrony are not enough to explain the "strange" skull of the Raphini *93*

Morphological disparity of Raphidae *94*

Ecomorphology and the skull shape in Columbiformes *95*

CONCLUSIONS 99

Allometry of head size against body size *99*

Allometry of skull shape against size *99*

Heterochrony in columbiform evolution *100*

Skull shape, allometry and heterochrony of outlier species *100*

Diet and skull shape *101*

The "strange" skull of Raphini and the high morphological diversity of Raphinae *102*

Mass prediction and its significance for the "fat" dodo (Appendix One) *102*

SUPPLEMENTARY MATERIAL (S2) 103

Supplementary figures *103*

Supplementary Tables *105*

CHAPTER THREE. ECOLOGICAL FACTORS AND THEIR RELATIONSHIP WITH SKULL SHAPE IN COLUMBIFORMES. 119

ABSTRACT 119

INTRODUCTION 121

Why is morphology expected to covary with other factors? *121*

Columbiformes *122*

Biomechanical performance *127*

Integration and modularity *129*

METHODS 131

Sample *131*

Phylogeny *131*

Size *132*

Distribution *133*

Feeding behaviour (diet plus foraging) *133*

Biomechanical performance *135*

Biomechanical variables *136*

Ecological and biomechanical factors correlation with skull shape *144*

Modularity and integration *148*

Variables that explain skull shape (distance-based regression) *151*

RESULTS 155

Cluster analyses of feeding (diet and foraging) *155*

Principal coordinates analysis of feeding behaviour *161*

Phylogeny and feeding behaviour ("Phylofeedingspace") *161*

Biomechanics *162*

Modularity and integration *164*

Two-block partial least squares *165*

Three-way comparison between feeding, shape, and biomechanical blocks (z-scores) *179*

Factors explaining shape (regression setting) *181*

DISCUSSION 187

Diet classification of Pigeons *187*

Feeding evolution (phylofeedingspace) *187*

Biomechanical landscape *188*

Modularity and integration *189*

Correlation between shape and biomechanics *191*

Correlation of biomechanics on shape and diet *191*

Factors that explain skull and module shape *192*

Factors that explain biomechanics *192*

Effect of feeding behaviour and biomechanics on skull shape, evidence for a columbiform adaptive radiation *194*

CONCLUSIONS 199

Main text *199*

Appendix Two. Columbiform feeding (diet and foraging) classification *202*

Appendix Three. Biomechanical landscape *202*

SUPPLEMENTARY MATERIAL (S3) 204

Detailed results for the two-block PLS of skull and modules vs feeding and biomechanics *204*

Factors explaining module shape (ordinary regression setting) *215*

Supplementary figures *217*

Supplementary tables *231*

CHAPTER FOUR. ARTIFICIAL AND NATURAL SELECTION WORK ON DIFFERENT AXES OF VARIATION: EXAMINING THE PHENOTYPIC MATRICES OF WILD COLUMBIFORMES AND DOMESTIC AND FERAL *COLUMBA LIVIA* **241**

ABSTRACT 241

INTRODUCTION 243

METHODS 255

Landmarks *256*

Geometric morphometrics *257*

Naïve comparison of principal axis of variation (descriptive tests) *258*

Statistical tests for matrix similarities *263*

RESULTS 281

Morphospace *281*

Identified shape changes *284*

Overlap of n-dimensional hypervolumes *287*

Geometric angles, scale and difference between vectors *289*

Krzanowski principal component comparison (Krzanowski, 1979) *290*

Test for correlation of matrices (Krzanowski, 1993) *298*

Random skewers *299*

Lines of least evolutionary resistance *300*

DISCUSSION 307

A cautionary view about the expectations of similarity between patterns of variation in a geometric morphometrics framework. *313*

SUPPLEMENTARY MATERIAL (S4) 317

Supplementary tables *320*

CHAPTER FIVE. CONCLUSIONS **329**

ALLOMETRY AND HETEROCHRONY IN THE SKULL OF COLUMBIMORPHAE 329

Ecological factors and their relationship with skull shape in Columbiformes 331
Artificial and natural selection work on different axes of variation 332
Summary 333

REFERENCES 335

APPENDIX ONE. COMMON ALLOMETRIC COMPONENT AND BODY MASS RESULTS 351

Common allometric component results 351
Detailed mass results 354
Detailed discussion: shape-based mass prediction and its significance for the "fat" dodo hypothesis 356

APPENDIX TWO: NEW CLASSIFICATION AND EVOLUTION OF FEEDING BEHAVIOUR IN COLUMBIFORMES 359

Results for the phylogeny and feeding behaviour ("phylofeedingspace") 360
Discussion of diet classification and feeding evolution in Columbiforms 362
Diet classification of Pigeons 362
Feeding evolution (phylofeedingspace) 364

APPENDIX THREE. BIOMECHANICAL LANDSCAPE AND ITS RELATIONSHIP WITH DIET OF COLUMBIFORMES AND RAPHINI (DODO AND RODRIGUES SOLITAIRE) 371

Detailed biomechanical landscape results 371
Input force (muscle centroid size) 372
Mechanical advantage 376
Effort distance and output force 377
Output distance and mouth opening 377
Velocity of bite 378
Eye size 378
Dorsoventral height (thickness) at mid length of the rostra 380
Moment of area 380
The lever length (Dlever) 383
Moment of mass 383

DETAILED DISCUSSION OF COLUMBIFORM BIOMECHANICAL LANDSCAPE..... 384

APPENDIX FOUR. SCRIPTS.....387

A) Script used in Chapter Two 387

B) Script used in Chapter Three 391

C) Script used in Chapter Four 395

List of Figures

Figure 1.1. Relationship between ecomorphology and developmental factors in evolutionary hypothesis. 4

Figure 1.2. Skull morphology of Raphini and Goura cristata. 11

Figure 1.3. Phylogenetic relationships between the Genera in Columbiformes 13

Figure 1.4. Maps of distribution of the three orders in Columbimorphae. 16

Figure 2.1. Plots of the regression models of head versus body size. 65

Figure 2.2. Changes in pigeon skull shape due to size changes 72

Figure 2.3. Comparison of three species along the allometric axis 72

Figure 2.4. Shape outliers. Sum of shape residuals plotted against the centroid size. 73

Figure 2.5. Shape outliers (real and predicted shape) 75

Figure 2.6. Shape of heterochronic Pteroclidiformes. 76

Figure 2.7. Linear model fit for the empirical and predicted sizes 77

Figure S2.1. The 27 landmarks used in this study displayed in *Columba livia* 103

Figure S2.2. Differences in the ordination obtained for Young et al. (2017) when the original landmark system is used versus the reduced landmark system used in this chapter 104

Figure 3.1. First, three principal coordinates (PCO) axes plotted against the binary feeding characters 160

Figure 3.4. Feeding PLS scores (YScores) in PLS dimension one (A) and two (B) 169

Figure 3.5. Standardized biomechanical characters versus PLS scores 172

Figure 3.2. PLS dimension one 174

Figure 3.3. PLS dimension two 176

Figure 3.6. Z-scores of all two-block PLS analyses. 180

Figure S3.1. Complete linkage clustering of the feeding behaviour 218

Figure S3.2. Tanglegram showing the differences in clustering 219
Figure S3.3. Principal coordinates axes (3-6) plotted against the binary feeding characters 222
Figure S3.4. Biomechanical model of pigeon skull as a simple machine. 222
Figure S3.5. PLS dimension one 223
Figure S3.6. Predicted shapes for the maximum and minimum values of XScores in the PLS dimension one.....224
Figure S3.7. PLS Shape (XScores) versus other data blocks (YScores), PLS dimension two 225
Figure S3.8. Predicted shapes for the maximum and minimum values of XScores in the PLS dimension two. 226
Figure S3.9. Feeding PLS scores (YScores) in PLS dimension one 227
Figure S3.10. Feeding PLS scores (YScores) in PLS dimension two 228
Figure S3.11. Standardized biomechanical characters versus PLS dimension one scores 229
Figure S3.12. Standardized biomechanical characters versus PLS dimension two 230
Figure 4.1. Random skewer method for comparison of phenotypic or additive genetic covariance matrices 273
Figure 4.2. Principal component analysis of the complete sample 283
Figure 4.3. Shape changes associated with the first two principal components 285
Figure 4.4. Permutation results for the principal component comparison (Krzanowski, 1979) 292
Figure 4.5. Bisector between the first four subspace dimensions 293
Figure 4.6. Lines of least evolutionary resistance (LLER). 303

Figure 4.7. Lines of least evolutionary resistance (LLER) using PC axes two, three, and four as $\mathbf{p}_{max}$. 306

Figure S4.1. Shape changes associated with PC3 and PC4 of the three samples. 317

Figure S4.2. Difference between closest vectors. 318

Figure S4.3. Correlation between random vectors and random or isometric vectors.....320

Figure A1.1. Right plots show the comparison between Common Allometric Components (CAC) and the Residual Shape Component (RSC) 352

Figure A2.1. Phylogenetic feeding space (phylofeedingspace) 360

Figure A2.2. Phylogeny of Columbiformes with the feeding clusters mapped 367

Figure A3.1. Biomechanical landscape in PC1 and PC2. 374

Figure A3.2. Biomechanical landscape in PC1 and PC2 (continued). 376

Figure A3.3. Biomechanical landscape in PC3 and PC4. 380

Figure A3.4. Biomechanical landscape in PC3 and PC4 (continued). 383

List of Tables

Table 1.1. Ten most diverse bird orders 9

Table 2.1. Allometry of skull centroid size against body mass 67

Table 2.2. Allometry of skull shape against size 69

Table 2.3. Predicted size and improvement in shape prediction obtained by using heterochronic size in the allometric model. 78

Table 2.4. Phylogenetic generalized least squares models 81

Table S2.1. Dodo and Rodrigues solitaire mass estimates 105

Table S2.2. Specimens in the sample, missing landmarks, and missing landmarks after reflection 106

Table S2.3. Landmark description and equivalence to Young *et al.* (2017) 111

Table S2.4. Missing landmark characterization 112

Table S2.5. Centroid size and body mass range in Columbiformes and Pteroclidiformes 115

Table S2.6. Empirical, predicted, and reported species mass 115

Table 3.1. Feeding clustering of Columbiformes using average and complete linkage algorithms 156

Table 3.2. Integration, modularity and global integration in the skull of the comparative sample of Columbiformes 164

Table 3.3. Two-block partial least squares correlation and significance results 166

Table 3.4. PLS vectors (from the phylogenetic two-block PLS analysis) of the right block data (biomechanical performance or feeding PCO) 167

Table 3.5. PLS vectors of the phylogenetic two-block PLS analysis of diet versus biomechanical blocks 178
Table 3.6. Results for the ordinary least squares (ols) and phylogenetic generalized least squares models of skull shape versus candidate explanatory variables 182
Table 3.7. Results for the ordinary least squares (ols) and phylogenetic generalized least squares models of biomechanical performance versus a series of candidate explanatory variables 184
Table S3.1. Ecological indicators, other than feeding behaviour, collected for the sample 231
Table S3.2. Landmarks system and assigned modules 234
Table S3.3. Biomechanical performance calculated on the Procrustes aligned coordinates 235
Table S3.4. Proportion of the covariation between blocks explained by the first four PLS dimensions 238
Table S3.5. Results for the ordinary least squares (ols) and phylogenetic generalized least squares models of rostrum shape versus candidate explanatory variables 239
Table S3.6. Results for the ordinary least squares (ols) and phylogenetic generalized least squares models of braincase shape versus candidate explanatory variables 240
Table 4.2. Variation explained by each PCA. PCA and phylogenetic PCA results 281
Table 4.1. Overlap of variance explained by the multidimensional centroids of different subsets of pigeons.....288
Table 4.3. Principal component comparison Krzanowski (1979) 292
Table 4.4. Subspace comparison of all samples.....297

Table 4.5. Correlation matrices test Krzanowski (1993).....298

Table 4.6. Random skewers correlation (Cheverud and Marroig, 2007) 300

Table 4.7. Lines of least evolutionary resistance (Marroig and Cheverud, 2005).....301

Table S4.1. Domestic pigeon specimens and missing landmarks.....320

Table S4.2. Angles and closest eigenvector between the first 10 eigenvectors of each sample.....325

Table S4.3. Scale of vectors 327

Chapter One. Introduction

Development versus natural selection in phenotypic evolution, a longstanding debate

The relative importance of ecology and development in influencing patterns of phenotypic evolution has been a topic of heated debate for a long time. Adaptationism is the view that traits of an organism (morphology, physiology, and behaviour) are the result of past natural selection (Mayr, 1983). For this reason, the adaptationist program is an eminently ecomorphological approach. In an influential and harsh critique to the adaptationist program, Gould and Lewontin (1979) portrayed the extreme adaptationist research as assuming *a priori* that all aspects of organisms are adaptively optimal solutions to ecological problems. They stressed the important role of developmental constraints and argued in favour of a pluralistic view of evolution, similar to that held by Darwin (1859), in which evolutionary history was determined not only by natural selection, but also by other factors (Gould and Lewontin, 1979). The factors originally proposed by Darwin (1853) included: chance during selection (*i.e.*, genetic drift and founder effect; Motoo Kimura, 1968; Futuyma and Kirkpatrick, 2018) in which, for example, random individuals survive a catastrophic event (i.e., flooding, wildfire) or colonise a new distribution area; heritance of acquired characters, proposed by Lamarckian theories; intrinsic directive forces like orthogenesis in which evolution follows a non-random direction; and saltational speciation like the hopeful monsters in which sudden morphological change can originate new species.

By the time Gould and Lewontin (1979) publication, most of the alternatives to natural selection initially proposed by Darwin (1853) had been discredited (e.g., heritance of acquired characters, intrinsic directive forces, and saltational speciation), and the drivers to evolution were reduced to only two options: natural selection or chance (Mayr, 1983). However, evidence for some factors other than natural selection and chance during selection has emerged and these other evolutionary factors are recognized nowadays. Examples include epigenetics (allowing inheritance of acquired characters; Asano *et al.*, 2013) and the major role of hybridization in plant evolution (in some ways resembling saltational evolution; Goulet, Roda and Hopkins, 2017). The existence of the aforementioned alternative drivers to evolution suggests that the "synthetic" view of evolution, which resulted from the refutation of alternative drivers to evolution (Mayr, 1993), is not adequate.

Some of the historical critiques to the adaptationist program stressed the important role of developmental constraints resulting from the cohesion of the genotype, integration, and modularity (Gould and Lewontin, 1979; Mayr, 1983). The result of this is that natural selection does not operate separately on individual traits. Instead, the fitness of a genotype is determined by all the traits (and their performance) it can produce in a given environment (Dobzhansky, 1956).

Numerous constraints act on genotypes (Mayr, 1983). These constraints act before natural selection, thus, they limit the phenotypic variation that is available for selection in the first place. One of these constraints is the cohesion of the genotype (Mayr, 1983). "Cohesion" arises because development is controlled by complex regulatory systems which are tightly

interconnected (Mayr, 1983). The “cohesion” of the phenotype is exemplified by the concepts of integration and modularity. These concepts refer to the amount of covariation between traits in an structure that is hypothesized to present different sub-sections or modules (Klingenberg, 2014; Adams, 2016). Integration refers to a system in which most variation occurs between modules. Individuals are more or less modular at all levels, to different degrees (Van Valen, 2009). Integration is generally thought to be more substantial in regions that form a “functional matrix”: a coherent anatomical domain balancing diverse functional criteria that persists over a growth trajectory (Bookstein, 2015). Modularity refers to the opposite case when most variation occurs within different modules. Modularity permits flexibility among functionally coordinated units (limiting the effects of mutations to sets of related traits) while inhibiting deleterious disruption of this coordination within modules (Hallgrímsson *et al.*, 2009; Van Valen, 2009). Modularity and integration can be investigated by examining the additive genetic or phenotypic matrix of organisms (Klingenberg, 2008; Goswami and Polly, 2010; Penna *et al.*, 2017).

Because of the apparent lack of alternatives to natural selection at the time, Mayr (1983) proposed that evolutionary research, implementing the adaptationist program, should attempt to explain biological phenomena as the product of natural selection. Alternative hypotheses could only be accepted when all attempts of explaining a trait by natural selection had failed. However, two considerations need to be taken into account when implementing the “adaptationist program” (Mayr, 1983): (1) evolutionary constraints and (2) a robust comparative framework which enables the statistical identification of common ecomorphological responses to ecological or environmental variables. If these factors are

accounted for, then it is possible to avoid falling into the reductionist extreme adaptationism (Gould and Lewontin, 1979; Mayr, 1983).

Nowadays, the adaptationist program is still subject to similar critiques as before, a large proportion of which are based on the proposal of alternative factors to natural selection (Wilkins and Godfrey-Smith, 2009). Some of these factors may place inherent limitations on the degree to which an organism can adapt. Two such factors are the role of historical constraints, and the importance of mechanistic factors (underlying genetic or developmental mechanisms; Wilkins and Godfrey-Smith, 2009).

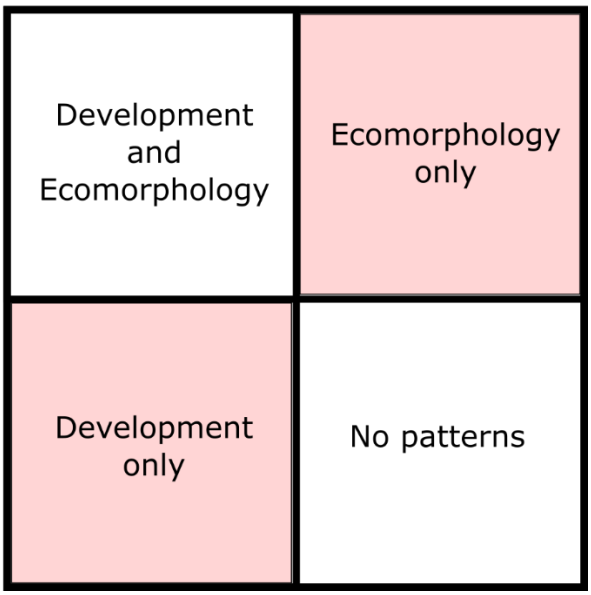


Figure 1.1. Relationship between ecomorphology and developmental factors in evolutionary hypothesis. Pink areas represent the extremes of a false dichotomy. White top-left sector shows the pluralistic view of evolution defended by Darwin (1859) and Mayr (1983).

Today, developmental constraints are regarded as being very important. Because of this, the search for patterns of modularity and integration has taken a prominent role in evolutionary research (Dobzhansky, 1956; Gould and Lewontin, 1979; Mayr, 1983;

Klingenberg, 2008; Wilkins and Godfrey-Smith, 2009). Here, I argue that in some examples, the predominance of developmental explanations for observed patterns, resemble the old extreme adaptationist view of evolution. This is exemplified by the trend in recent macroevolutionary literature to establish development as the most important factor driving evolution in interpretation of observed pattern of morphological evolution (Bright *et al.*, 2016; Cooney *et al.*, 2017; Felice and Goswami, 2017; Young *et al.*, 2017). Furthermore, this research tends to minimize the importance of the interplay between developmental and ecomorphological factors and treat these two factors as a strict dichotomy (red squares, Figure 1.1).

Extreme views that might be detrimental to evolutionary research can emerge if the interplay between factors is disregarded, and these factors are considered as a dichotomy (Figure 1.1). Recent macroevolutionary research usually acknowledge the possibility of ecomorphological explanations and does not hold a totalitarian developmental view. However, it does embody a particular approach which generally tends to favour developmental explanations. Focussing in one evolutionary explanation and neglecting other evolutionary factors might be detrimental in the long run. No exclusive, end-member view of an evolutionary phenomena is likely to adequately address evolutionary questions (Mayr, 1983). Here, I argue for a pluralistic view of evolution as Darwin (1859), Mayr (1983) or Gould and Lewontin (1979) did in previous contexts.

Furthermore, I highlight that the distinction between the developmental and ecomorphological components of phenotypic evolution might be less straightforward than usually portrayed. Research on developmental constraints is based on the analysis of the

aforementioned additive genetic variance matrix or the phenotypic matrices (Lande, 1979; Marroig and Cheverud, 2005; Hansen and Houle, 2008; Klingenberg, 2008). However, constraints such as integration and modularity can themselves be modified by selection (Van Valen, 2009). This modification by natural selection makes it difficult to distinguish between ecomorphological and developmental factors and complicating the interpretation of observed patterns of modularity and integration (Figure 1.1). Furthermore, there is evidence that our ability to identify constraints like modularity and integration depends not only on the tendency of a developmental system to produce covariation ("covariabilty") but on the variation present in the examined sample (Hallgrímsson *et al.*, 2009). If variation is absent from the sample or if major morphological changes occur because one mutation this can dramatically change the detected integration and modularity (Hallgrímsson *et al.*, 2009).

Finally, I will use allometry to illustrate another unaccounted factor that might impact on the significance of identified constraints. Negative allometry is usually identified in a regression with a slope less than one. However, when allometry of head size against body size is analysed, it is necessary interpret the slopes considering the expected geometrical scaling (Gould, 1966). Geometric scaling is the result of a purely geometrical phenomenon: linear measurements increase at a lower rate than areas or volumes. Thus, the isometric expectation given by geometric scaling is a slope of 0.33 which provides a baseline to interpret the identified allometry. Considering the geometric scaling allows the correct interpretation of slopes. A slope of head size against body size equal to 0.45 would no longer be considered as negative allometry instead it would correctly be interpreted as positive allometry.

Currently, there is no baseline for the expected integration of a structure. This baseline could be influenced, for example, by geometric scaling alone. If no baseline is considered, then the identified constraints and shared patterns could be incorrectly interpreted (for example resulting purely from allometry). Approaches looking into integration and modularity usually test their results against the null hypothesis of random association by permuting either taxa or landmarks between modules (Cheverud and Marroig, 2007; Hansen and Houle, 2008; Goswami and Polly, 2010; Aguirre *et al.*, 2014; Adams, 2016). But other factors like sample variation are usually overlooked (Hallgrímsson *et al.*, 2009). The patterns of integration and modularity are, without any doubt, real mathematical phenomena and show that the detected patterns are different from random association. However, these patterns might not reflect biological or developmental evolutionary constraints, but the expected similarity produced by geometric scaling or other factors.

In this research I used a pluralistic view of evolution to assess the evolution of the skull shape in Columbiformes, taking both developmental (allometry, heterochrony, modularity, and integration) and ecomorphological (diet, foraging, biomechanics) factors into account to explain the evolution of skull shape in this group.

Columbimorphae

Throughout this thesis I analysed a relatively understudied (in a macroevolutionary setting) group of birds, Columbimorphae (Jetz et al., 2012; Jarvis et al., 2014; Prum et al., 2015; Soares et al., 2016), which includes the Mesitornithiformes (mesites), Pteroclidiformes (sandgrouses), and Columbiformes (pigeons and doves). Variation in skull shape among columbimorphs has mainly been studied at a descriptive/anecdotical level, which summarizes the known information of the group (Goodwin, 1983; Gibbs, Barnes and Cox, 2010; Hoyo et al., 2017). However, evolutionary hypotheses about this group have rarely been tested.

There are two notable exceptions of research focused on the macroevolution of Columbimorphae. (1) Lapiedra *et al.* (2013) found that changes in foraging behaviour have influenced the rates of evolution in Columbiformes. They also identified terrestrial foraging to be the ancestral foraging behaviour in pigeons. Furthermore, they identified an evolutionary constraint that prevents regression from arboreal foraging towards terrestrial or generalist strategies. (2) Pereira *et al.* (2007) studied the phylogeny and divergence time of Columbiformes. However, besides their time calibrated phylogeny they performed an stochastic reconstruction of ancestral distribution areas. They found a Gondwanaland origin for columbiforms and multiple dispersals between Australasian and Afro-Eurasian regions.

This relative lack of macroevolutionary research in Columbimorphae is somewhat paradoxical when the existence of comprehensive macroevolutionary research dealing with all birds (Jetz et al., 2012; Rolland et al., 2014; Caswell et al., 2017; Cooney et al., 2017)

is considered. These big macroevolutionary studies, by their own nature, explore extremely large samples and cannot discuss every detail of the obtained results. The lack of macroevolutionary research focused directly on Columbimorphae might produce the illusion of this clade lacking any noteworthy evolutionary process. However, in this chapter I aim to first explain why Columbimorphae are a clade with a complex evolutionary and ecological history, and second to show why the analysis of Columbimorphae might help to shed light into the development versus adaptation debate.

Table 1.1. Ten most diverse bird orders according to IOC World Bird List, 8.1 (Gill and Donsker, 2018)

	Order	Spp. number
1	Passeriformes	6456
2	Caprimulgiformes	604
3	Piciformes	445
4	Psittaciformes	398
5	Charadriiformes	383
6	**Columbimorphae**	343
7	Galliformes	300
8	Accipitriformes	266
9	Strigiformes	243
10	Gruiformes	189

Diversity

Birds (class Aves) are the most diverse class of extant tetrapod vertebrates with around 10,000 species (Jetz *et al.*, 2012; Prum *et al.*, 2015; Clements *et al.*, 2017). Roughly two thirds of these species are in the order Passeriformes. Columbimorphae is the sixth most speciose clade when compared with other bird orders (Table 1.1), and includes three bird orders: Mesitornithiformes (mesites), Pteroclidiformes (sandgrouses) and Columbiformes (pigeons and doves; Jetz *et al.*, 2012; Jarvis *et al.*, 2014; Prum *et al.*, 2015). The diversity of

two of these orders is relatively low: Mesitornithiformes includes two genera (three species), while Pteroclidiformes is composed by two genera (16 species). Columbiformes have a much higher biodiversity, formed of 49 genera and around 350 species (Hoyo *et al.*, 2017). Within columbiforms, one of the most diverse clades is the genus *Columba*, which contains 51 species (Hoyo *et al.*, 2017).

Two of the most iconic taxa in Columbiformes are the dodo (*Raphus cucullatus*) and the Rodrigues solitaire (*Pezophaps solitaria*; Figure 1.2). These two taxa and the correlation of their skull shape with development and ecomorphology are analysed throughout Chapters Two and Thee. These extinct species were highly distinct from other columbiform species, due to their large body sizes (Livezey, 1993; Angst, Buffetaut and Abourachid, 2011; Louchart and Mourer-Chauviré, 2011; Brassey et al., 2016; van Heteren et al., 2017), flightlessness, and morphology (Owen, 1866; Livezey, 1993; Claessens, Meijer and Hume, 2015). For example, these species exhibit crania with proportionally smaller braincases; 'vulture-like' beaks; broad frontals; and flat parietals (Figure 1.2; Owen, 1866; Claessens, Meijer and Hume, 2015).

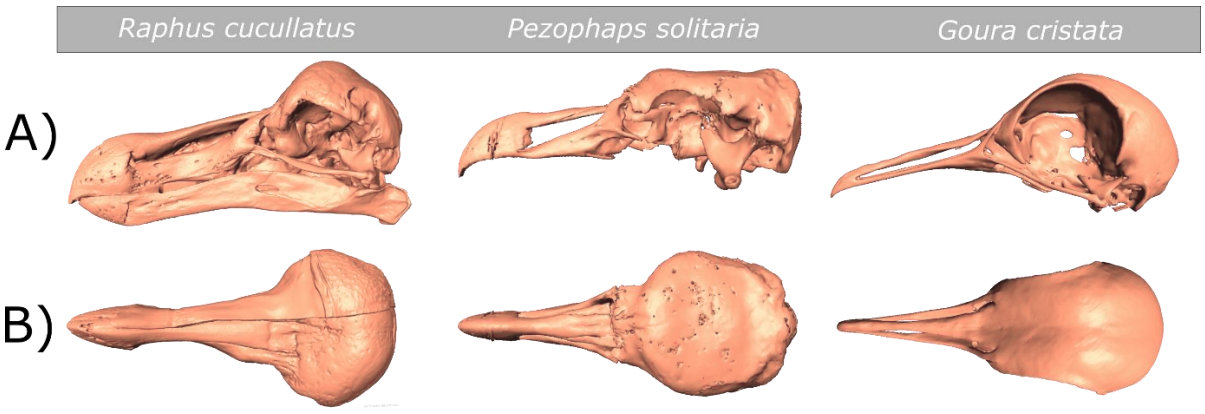


Figure 1.2. Skull morphology of Raphini and Goura cristata. A) left lateral view; B) dorsal view

Systematics

Whenever possible, a phylogenetic comparative framework was used throughout the thesis. Columbiformes has a well resolved phylogeny which makes possible to analyse the factors that influenced shape in the evolution of Columbimorphae in a phylogenetic framework. All recent genomic phylogenies recover the clade Columbimorphae (see avobe; Jetz *et al.*, 2012; Jarvis *et al.*, 2014; Prum *et al.*, 2015) in the Neoaves. Neoaves are all crown birds excluding Galloanserae (ducks, chicken and kin) and Paleognathae (ratites). Columbimorphae is the sister clade to Otidimorphae: Cuculiformes (cuckoos), Musophagiformes (turacos), and Otidiformes (bustards; Prum *et al.*, 2015). The phylogenetic relationships between the three orders in Columbimorphae are well constrained. Mesitornithiformes and Pteroclidiformes are closely related, and together they form the sister clade to Columbiformes (Jarvis *et al.*, 2014; Prum *et al.*, 2015).

Columbiformes is composed of a single family (Columbidae). Conversely, historically two other families were placed along Columbidae inside Columbiformes. (1) Raphidae (*Raphus* and *Pezophaps*; Janoo, 2005). However, molecular phylogenetic analyses have demonstrated that Raphidae, in spite of its morphological distinctiveness, is nested within Columbidae (Shapiro *et al.*, 2002; Janoo, 2005; Pereira *et al.*, 2007). (2) Pteroclididae (sandgrouses) was historically also placed within Columbiformes, because of morphological and behavioural characters (drinking mode; Zweers, 1982).

The phylogenetic relationships within Columbiformes are well constrained. The phylogenetic analysis of half of the pigeon species diversity (Lapiedra *et al.*, 2013) and the

global phylogeny of birds (Jetz *et al.*, 2012) have found similar phylogenetic relationships in pigeons (Figure 1.3). Three main clades of pigeons are usually proposed (Figure 1.3). These three clades can be summarized as follows (Pereira *et al.*, 2007): Neotropical ground doves (clade 1); New World pigeons and allies (clade 3); and Afro-Eurasian and Australasian taxa (clade 2).

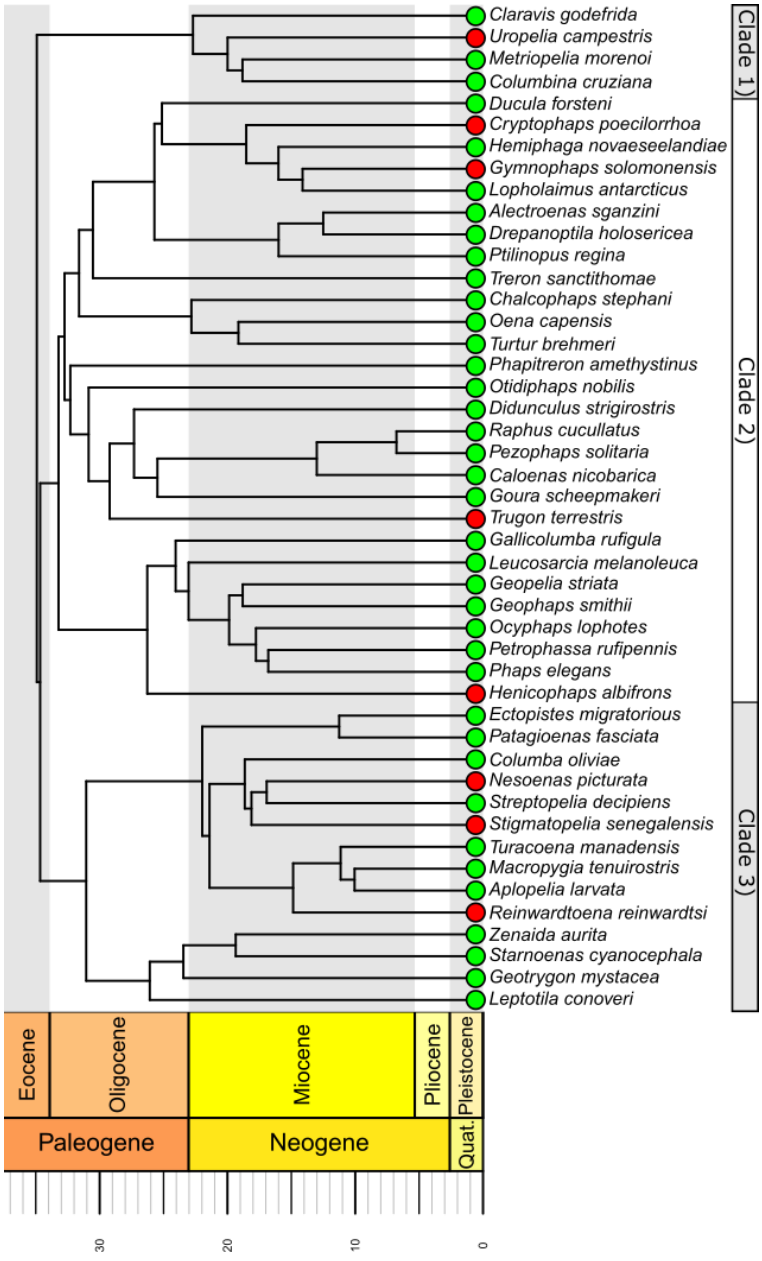


Figure 1.3. Phylogenetic relationships between the Genera in Columbiformes (Jetz et al., 2012). The tree was randomly selected from the posterior sample of trees with the Hacket et al., (2008) backbone (BirdTree.org, Jetz et al., 2012). This phylogeny closely corresponds to the one reported by Lapiedra et al. (2018). Green circles show the genera included in my sample. Pezophaps and Raphus were added as sister taxa to Caloenas nicobarica (Shapiro et al., 2002; Janoo, 2005; Pereira et al., 2007). Ectopistes migratorius (passenger pigeon) was added as the sister taxa to the Patagioenas clade (Johnson et al., 2010).

Similar clades were found when analysing mitochondrial and nuclear data (Pereira *et al.*, 2007). The main difference between the three-clade hypotheses is which clade is recovered as basal, clade 1 (Jetz *et al.*, 2012; Lapiedra *et al.*, 2013) or clade 3 (Pereira *et al.*, 2007). However, Soares *et al.* (2016) obtained two main clades within Columbiformes when they analysed complete mitochondrial DNA. These two clades were: an Indo-Pacific clade which includes the genera in clade 2, and a Holarctic clade + New world clade (clade 3). However, they did not include any member of clade 1 in their analysis, so they did not falsify the three-clade hypothesis. The general agreement of the phylogenetic information available allowed for the pigeons to be used to test macroevolutionary questions in a phylogenetic framework.

Raphidae

Raphidae was originally a family that contained the morphologically-distinct giant flightless genera *Raphus* and *Pezophaps* (Janoo, 2005). This family was placed outside of Columbidae but within Columbiformes. However molecular evidence shows that *Pezophaps* and *Raphus* are included in the Indo-Pacific clade of Columbidae (Soares *et al.*, 2016). Throughout this thesis, the name Raphini is used to define the clade composed of *Raphus* and *Pezophaps*. In Chapter Two, I take in account the phylogenetic position of Raphini to assess the morphological disparity of this clade.

The place of Raphini within Columbidae is well constrained. The sister taxa to Raphini is the Nicobar pigeon (*Caloenas nicobarica*; Shapiro *et al.*, 2002; Janoo, 2005; Pereira *et al.*, 2007). All molecular analyses place the Raphini inside a clade which includes the genera *Goura*, *Didunculus* and *Caloenas* (Shapiro *et al.*, 2002; Pereira *et al.*, 2007; Soares *et al.*, 2016). *Otidiphaps* and *Trugon* have also been recovered as part of this clade by some analyses (Pereira *et al.*, 2007; Lapiedra *et al.*, 2013). For convenience, this more inclusive clade of pigeons will be referred to as Raphidae here.

Age of diversification

The origin of Columbiformes has been a topic of debate, and estimates have varied widely from Lower-Upper Cretaceous (Pereira *et al.*, 2007) to Eocene-Palaeocene (Soares *et al.*, 2016). However, the age of the crown columbiform diversification is more constrained: Earlier Eocene to Middle Miocene (Pereira *et al.*, 2007) to late Oligocene to Miocene (Soares *et al.*, 2016).

The age of divergence of Raphini has also been topic of debate. This is because the age of divergence is key to interpret the geographical distribution of these taxa with Indo-Pacific affinities. The divergence of *Raphus* and *Pezophaps* from *Caloenas* has been estimated at 43 mya (Shapiro *et al.*, 2002), 33mya (Pereira *et al.*, 2007), and 18 Mya (Soares *et al.*, 2016). While the divergence between *Raphus* and *Pezophaps* has been estimated at 25 mya (Shapiro *et al.*, 2002), 23mya (Pereira *et al.*, 2007), and 13.1mya (9.5–17.3mya; Soares *et al.* (2016). The divergence time is important because both of these taxa were flightless species, but their ancestor was most likely flighted, facilitating the colonization of the Rodrigues and Mauritius islands. However, Mauritius emerged 6.8 to 7.8mya and Rodrigues

emerged 1.5mya (Shapiro *et al.*, 2002). Older divergence estimates would point to stepping-stone dispersal (Shapiro *et al.*, 2002). Whatever the diversification time might have been, the Raphini achieved extreme morphological disparity when compared with other Columbiformes since colonizing their respective islands.

Distribution and conservation

Geographic distribution of the analysed species is another variable which could explain the columbiform skull shape (observed in Chapter Two and assessed in Chapter Three). Island distributions have been related to both peculiar morphological changes associated with insular taxa as well as prolific adaptive radiations resulting from the colonization of isolated habitats (Millien, 2006; Harmon *et al.*, 2010; Presgraves and Glor, 2010). Island distribution can accelerate evolutionary rates through ecological release or other factors (Van Valen, 1965; Millien, 2006; Parent and Crespi, 2009; Presgraves and Glor, 2010; Tokita *et al.*, 2016).

The three mesitornithiform species are distributed in Madagascar (Figure 1.4C; Hoyo *et al.*, 2017). The 16 pteroclidiform species are distributed in the Old World: in arid areas of Europe, Africa and Asia (Figure 1.4B; Hoyo *et al.*, 2017). Unlike these two orders, columbiforms are distributed across every continent but Antarctica, and are also absent from the driest parts of the Sahara and high Arctic (Figure 1.4A). Pigeons and doves have colonized oceanic islands (*e.g.*, Polynesia and the Chatham Islands in the Pacific Ocean; Mauritius, the Seychelles and Réunion in the Indian Ocean; the Azores in the Atlantic Ocean) (Goodwin, 1983; Gibbs, Barnes and Cox, 2010; Hoyo *et al.*, 2017).

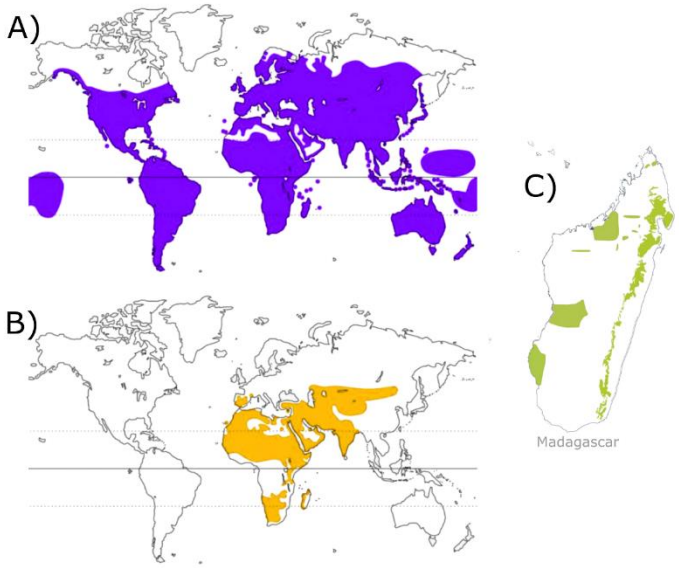


Figure 1.4. Maps of distribution of the three orders in Columbimorphae. A) Columbiformes; B) Pteroclidiformes; C) Mesitornithiformes. The maps were modified from the maps available at HBW.com (Hoyo et al., 2017) and show the distributional areas for all species per bird order.

They range from endemic species with restricted areas of distribution like the Samoan tooth-billed pigeon (*Didunculus strigirostris;* ca. 2900 km^2) and the Taiwan green-pigeon (*Treron formosae*; 101,000 km_2), to species with wide geographic distributions like the rock dove, *C. livia*, which has expanded its geographic range following human cities and towns (61,000,000 km^2) and the common woodpigeon (*Columba palumbus*; 31,800,000 km^2), which inhabits most of Europe, the northern of Africa and parts of Turkey.

Unsurprisingly, most of the extinct (16/17), critically endangered (10/12) or endangered (19/20) columbiform species are island inhabitants (Rauzon, 2007; Hoyo *et al.*, 2017; BirdLife International, 2018). Island taxa like *Pezophaps* and *Raphus* probably went extinct because of the introduction of exotic species (Livezey, 1993; Janoo, 2005; Hume, 2012). Another iconic extinct pigeon species, with continental distribution, was the passenger pigeon (*Ectopistes migratorius*). *Ectopistes* was once the most abundant bird in the world

with an estimated population of three to five billion birds in North America (Goodwin, 1983; del Hoyo, Elliott and Christie, 2004; Gibbs, Barnes and Cox, 2010; Hung *et al.*, 2014). This bird species likely went extinct because of a number of anthropic factors (exploitation and deforestation; Blockstein and Tordoff, 1985) combined with natural low fluctuations in the population size (Hung *et al.*, 2014).

The island and archipelago distributions of many Columbiformes might have allowed them to exploit new niches and might have allowed them to undergo similar adaptive radiations to other bird groups like Galapagos finches (Geospizinae: Darwin, 1859; Foster, Podos, and Hendry, 2008), Hawaiian honeycreepers (Drepanidinae: Tokita, Yano, James, and Abzhanov, 2016) and Madagascan vangas (Vangidae: Jønsson et al., 2012). For this reason, Columbiformes is a good candidate to show phenotypic change because of ecomorphological factors (Mayr, 1983).

Feeding behaviour

Adaptation to different a feeding behaviour (diet and foraging) is a classical ecomorphological variable used in an adaptationist framework (Mayr, 1983). Columbiformes are a good candidate to find an ecomorphological signal because they present different diets and foraging behaviours (see below). In Chapter Three I analyse the influence of feeding and integration on the skull shape of Columbiformes.

Diet and foraging habits are the two components of the pigeon feeding behaviour by which the pigeons have traditionally been classified. Pigeon diet can be broadly divided in three types: frugivorous, granivorous and a mixture of both (Gibbs, Barnes and Cox, 2010; Hoyo *et al.*, 2017). Most pigeons take food items whole, irrespective of item size. For this reason,

granivorous pigeons usually store grit in their gizzard to assist in digestion (Hoyo *et al.*, 2017). Pigeons whose diets consist of larger items exhibit gizzards with structures (horny plates, hard ridges, nodules, raised processes) that assist in breaking nuts (*Caloenas*) or in de-fleshing fruits. After the fruit has been de-fleshed, the fruit stone passes intact through the digestive tract (Hoyo *et al.*, 2017). The size of the fruit that pigeons can eat is associated with the gape size of the bird (Diamond, 1973). The exceptions to these general rules of diet in pigeons are the genus *Treron*, which can cut fruit into smaller morsels using their beak, and *Didunculus*, which can open the tough capsules containing the seeds of the wild mahogany tree (*Dyosoxylum* spp.).

Many species supplement their diet by including invertebrates (insects and snails; Gibbs, Barnes and Cox, 2010; Hoyo *et al.*, 2017). *Ectopistes* was reported to seize and eat earthworms (Hoyo *et al.*, 2017). Pigeons of the genera *Gallicolumba* and *Geotrygon* seem to take more invertebrates than most pigeons (Hoyo *et al.*, 2017). The most extreme example of live prey consumption in pigeons is the atoll fruit dove (*Ptilinopus coralensis*) which includes insects and lizards in their diet (Hoyo *et al.*, 2017). Diet can have collateral effects, for example the Mascarene pink pigeon (*Nesoenas mayeri*) becomes seasonally poisonous, putatively because of the consumption of fandamane (*Aphloia theiformis*) and fangame (*Stillingia lineata*; Hume, 2011).

The foraging behaviour can be divided into three types: arboreal, terrestrial or both (Goodwin, 1983; Gibbs, Barnes and Cox, 2010; Hoyo *et al.*, 2017). Some arboreal foragers remove fruits from stems by seizing the fruit or nut with the bill and making a twisting movement with the head (Hoyo *et al.*, 2017). Some arboreal foragers can also hang upside-

down from the branches in order to gain access to fruit. Other arboreal foragers like *Alectroenas pulcherrimus* are incapable of standing on the ground because of their tightly clenched feet (Hume, 2011). Terrestrial feeders take the seeds from the ground or search for seeds and invertebrates by sweeping leaves and soil using their bill (Gibbs, Barnes and Cox, 2010; Hoyo *et al.*, 2017). The foraging strategy of the Galapagos dove (*Zenaida galapagoensis*) is unique among pigeons because it uses its curved beak to dig into the soil in search for seeds (Gibbs, Barnes and Cox, 2010; Hoyo *et al.*, 2017). While species in the genus *Gallicolumba* can use their feet to hold a grass stem while eating its seeds. This diversity of diets and foraging strategies also shows Columbiformes might be a group where ecomorphological influence on shape can be detected. Furthermore, the aforementioned correlation between pigeon size and fruit size (Diamond, 1973) might emphasize the role of size as the line of least evolutionary resistance (Schluter, 1996; Marroig and Cheverud, 2010) in Columbiformes.

The skull shape of the Raphini (Figure 1.2), especially the dodo, has been hypothesized to be related to the sporadic inclusion of animals in the diet (Owen, 1866; Livezey, 1993). However, the Raphini diet probably would have consisted primarily of fallen fruits, seeds, and bulbs which were accessible to these obligate ground-dwelling birds (Owen, 1866; Goodwin, 1983; Livezey, 1993; Angst, Buffetaut and Abourachid, 2011). Apart from diet, heterochrony (see below) has been used to explain the morphology of these taxa, pointing at the possible overdeveloped peramorphic skull size in comparison to the paedomorphic scapular girdle (Owen, 1866; Livezey, 1993). The “strange” skull shape of Raphini makes these species ideal candidates to test evolutionary hypotheses of allometry and heterochrony.

Drinking behaviour

The aforementioned feeding mode of most pigeons (swallowing food items, either fruits or seeds, as a whole) could constraint the skull shape of these species. Furthermore, the drinking behaviour of pigeons (suction feeding) and the use of crop milk to feed their young (see below) could place additional constraints to the columbiform skull. Multiple functional constraints could indicate that the columbiform skull fits the definition of a functional matrix (anatomical domain balancing diverse functional criteria; Bookstein, 2015). Integration is expected to be found in functional matrices (Bookstein, 2015). The integration (and modularity) of the columbiform skull is assessed in Chapter Three.

Drinking in birds can be classified as tip up and tip down drinking (Zweers, 1982, 1992). Tip up drinking (Zweers, 1992) or scooping (Goodwin, 1983) is the type of drinking shown by most birds, in which the bills are immersed in water and the head is moved in a scooping movement, allowing water to reach the oesophagus by gravity. This drinking method depends on capillarity forces in some birds and has been comparatively classified as ladling (Kim and Bush, 2012). Ladling is the drinking method used by animals in which the geometry of their cheeks does not allow sucking water (*e.g.*, Felidae, *Canis*; Kim and Bush, 2012). Remarkably, the drinking behaviour in pigeons is different than in most birds. Kim and Brush (2012) classified pigeons as inertial suction drinkers along with turtles, snakes, and mammals like sheep, humans, and donkey. However, pigeons are not the only birds that show suction drinking (Zweers, 1982), one of the other birds that can suction drink are the pteroclidiforms. Historically, this was the primary reason to place this family within Columbiformes (Zweers, 1982).

The homology of drinking behaviour in Pteroclidiformes and Columbiformes has been contested using several lines of evidence (Zweers, 1982): (1) not all pigeons and not all sandgrouse show this behaviour; (2) the drinking mechanism seems to be only superficially similar between families; (3) suction drinking is also shown by some Australian estrildid finches (*Poephila* spp.), mousebirds (Coliiformes), and the gardener warbler (*Sylvia borin*). (4) similar drinking to that of pteroclidiforms is shown by the fork-tailed drongo (*Dicrurus adsimilis*) and in some hanging parrots (*Loriculus* spp.). The biomechanical requirements of drinking behaviour in Columbiformes might place constraints to the extent of morphological change in these species. For example, the only pigeon that is not capable of suction drinking is *Didunculus*, which shows a remarkable bulky bill and has a different feeding behaviour than other pigeons. These evolutionary constraints might be detectable in the statistical analyses of this group.

Crop milk

Crop milk is a secretion of the lining of the crop, produced by male and female pigeons to feed the young (Gibbs, Barnes and Cox, 2010; Gillespie *et al.*, 2012; Hoyo *et al.*, 2017). The crop milk in pigeons and mammal milk show some remarkable similarities: the hormone prolactin regulate the production of crop milk in both mammals and pigeons, both secretions are highly nutritious and both secretions contain immunoglobulin-A antibodies, promoting the immune system development (Gillespie *et al.*, 2012). However, crop milk is not only produced by pigeons, but also by male and female flamingos (Phoenicopteridae) and male penguins (Spheniscidae; Gillespie *et al.*, 2012). Crop milk is required for normal pigeon development, without it the young do not normally survive (Gillespie *et al.*, 2012).

Some domestic pigeon breeds (short-faced tumbler) are incapable of feeding their young because of their extremely short bills (Young *et al.*, 2017), requiring other pigeons to act as "wet nurses". This could suggest that an evolutionary constraint to bill length might be detectable in Columbiformes. Overall this clade of birds is an often overlooked ecologically and morphologically diverse clade that will benefit from focussed macroevolutionary research.

Domestication

In Chapter Three, I analyse the morphologic variation in domestic fancy pigeons and compare it with the variation of feral pigeons and a comparative sample of wild Columbiformes. Here, I provide context about the time and mode of pigeon domestication and the role of hybridisation on the morphological variation of domestic pigeons. Previous research of pigeon domestication is provided along with the reasons for analysing heterochronic patterns instead of processes in throughout this research.

Common pigeons (*Columba livia*) were domesticated around 5,000 (6,000 to 4,000) years ago (Johnston and Janinga, 1995; Sol, 2008; Larson and Fuller, 2014). Pigeons are the first bird that entered a domestic relationship with people from Western Eurasia (Larson and Fuller, 2014). Several distinct breeds of domestic pigeons are still kept for utility (messenger pigeons, racing pigeons, thief pigeons) and for aesthetic reasons ('fancy pigeons') (Darwin, 1868; Martínez-Gómez *et al.*, 2009). Fancy pigeons in particular have obtained a wide range of morphologies, presenting more variation than seen within any other bird species (Price, 2002; Stringham *et al.*, 2012). Fancy pigeons were fundamental to the construction of the theory of evolution by natural selection, helping Darwin to see the principles of artificial

selection first hand (Darwin, 1859, 1868; Martínez-Gómez *et al.*, 2009; Young *et al.*, 2017). Fancy pigeons exhibit patterns of variation similar to dog breeds: modularity and integration between the rostrum and braincase (Young *et al.*, 2017). The variation in fancy pigeons has also been hypothesised to recapitulate the natural variation across the entire Columbiformes order (Martínez-Gómez *et al.*, 2009). For these reasons, the comparison of the variation in domestication and from natural selection can shed light on common developmental constraints.

The role of hybridization in the variability of domestic Columba livia.

Hybridization and introgression (transfer of genetic information from one species to another as a result of hybridization and repeated backcrossing) can increase the variation of domestic species (Larson and Fuller, 2014). These phenomena do not seem to play a major role (see below) in the morphological variation of domestic the fancy pigeons (*C. livia*). If hybridization played a major role in fancy pigeon variation the results of the comparison of axis of variation between domestic C. livia and wild Columbiformes (Chapter Three) could be affected.

While arguing in favour of all domestic pigeon breeds coming from *C. livia*, Darwin (1868 pp. 193-194) recounted the instances of interspecific pigeon crosses (*C. oenas* x *C. livia*, *C. oenas* x *C. gymnophthalmos* (*Patagioenas corensis*), *Turtur vulgaris* x *T. risorii*, *T. vulgaris* x *Ectopistes migratorius*, *Goura coronate* x *G. Victoria*) and their viability and fecundity. All interspecies crosses in his account produced eggs that did not hatch or infertile hybrids. This hybrid inviability provided evidence for all domestic pigeon breeds and their morphological variation originating from a single species (*C. livia)*. However, modern data

(Lijtmaer, Mahler and Tubaro, 2003) shows that some interspecies hybrids are fertile (although the percentage of unhatched eggs is high). Furthermore, the checkered pattern of some pigeons originated introgression from a *C. livia* x *C. guinea* hybrid (Vickrey *et al.*, 2018). Despite the fertility of some hybrids, the inviability of these columbiform hybrids increases along with species divergence time. Pigeons follow Haldane's rule: sterility and inviability appearing first in the heterogametic sex (Lijtmaer, Mahler and Tubaro, 2003). Mean divergence time for total inviability in columbiforms is 6.5 million years (or 13% of sequence divergence of cytochrome *b*).

As pointed out by the hybridization experiments (Lijtmaer, Mahler and Tubaro, 2003), hybrids are unlikely to overcome pre and postzygotic barriers (except in *C. oenas*) and provide new variation to fancy domestic pigeons. Furthermore, the genera that have been recorded to hybridize with *C. livia* are other members of *Columba* or the closely related genus *Streptopelia*, which do not exhibit exaggerated morphologies characteristic of fancy pigeon breeds (Darwin, 1868; Martínez-Gómez *et al.*, 2009). Therefore, Darwin's (1868) assessment of fancy pigeon variation originating from the variation in *C. livia* is likely to be true. In the case of the present thesis, hybridization is unlikely to have significantly increased the natural variation int the pigeon skull because of the close morphologies of closely related species. This putatively small contribution of variation from interspecific hybridization contrasts with the widespread introgressive capture in dogs (Caniedae), cats (Felidae; Hailer and Leonard 2008; Davis et al. 2015; Li et al. 2016; Gopalakrishnan et al. 2018), chickens (Phasianidae), pigs (Suidae), African cattle (Bovidae), and horses (Equidae; Larson and Fuller 2014).

Previous pigeon domestication research

Some morphological characters of fancy pigeons (head crest, plumage colour, feathered feet, feather growth polarity, and limb identity) have been characterised from the genetics standpoint (Shapiro *et al.*, 2013; Domyan and Shapiro, 2016). This genetic characterisation has also allowed analysing the evolution and dispersion of these traits in domestic pigeon breeds (Shapiro *et al.*, 2013; Domyan and Shapiro, 2016). Furthermore, the convergence in these morphological traits (Stringham *et al.*, 2012) and the geographic origin of domestic pigeon breeds (Stringham *et al.*, 2012; Shapiro *et al.*, 2013) has also been a topic of study. The parallels between morphological characters (orbital rings, nose ceres, bill length, small or large body mass, feathered tarsi, head crests, number of rectrices, and tail length) present in some wild columbiforms and some domestic pigeons has been used to argue for a convergence on mutations causing these traits (Martínez-Gómez *et al.*, 2009).

Feral pigeons (all street pigeons) are descendants of domesticated pigeons (*C. livia*) that escaped captivity (Johnston, 1992). Size and a series of univariate skeletal traits have been compared between feral and homing pigeons (semidomesticated pigeons living in dovecots; Johnston, 1990). Homing pigeons presented a significantly larger size (principal component one) than feral *C. livia* or wild individuals of the same species. Skeletal traits have also been used to assess how natural selection has "reconstructed" the wild phenotype of *C. livia* in feral pigeons (descendants of domestic pigeons; Johnston, 1992; Sol, 2008). In fact, this "reconstruction" of the wild phenotype has occurred at least two times: once in North America and once the old world (Johnston, 1992). Darwin (1859, 1868) was inspired by pigeons (and other domestic animals) when he formulated the analogy between natural and artificial selection. In modern times, domestic pigeons have been used

as a model to explain the speciation, and the acquisition of novel characters through time, by sexual selection (Price, 2002).

After extensive research, I found only one study of pigeon domestication in a geometric morphometric framework. This study is an influential paper written by Young *et al.*, 2017. In it, the patterns of variation were compared between a sample of adult individuals of 20 birds of different orders versus a sample of 15 feral pigeons and 58 domestic pigeons (belonging to 36 breeds). They found that the patterns of variation and covariation in domesticated pigeons are predictive of avian cranial evolution. They argued that selection on variation (in a conserved developmental system: bird skull) could explain the evolution of skull shapes across all birds and even in a broad diversity of vertebrate species. The 58 domestic pigeons analysed by Young *et al.* (2017) are re-analysed, along with new specimens of domestic pigeons (modern and other collected by Darwin) in Chapter Three.

Despite the lack of further geometric morphometric research on the pigeon domestication, a broader context for this phenomenon can be obtained by considering the morphological variation of other domestic birds. Chickens (*Gallus gallus*) exhibit similar patterns to those found in pigeons (Young *et al.*, 2017): high morphological variation (higher than their wild counterparts) and changes in the magnitude of trait variation (but not in the covariance patterns; Stange *et al.*, 2018). Chickens present highly integrated skulls with low evidence of modularity. Unlike chickens, pigeons and mammals show modularity and integration in their skull (Young *et al.*, 2017; Stange *et al.*, 2018). Other difference is that allometry explains less variance in chickens (R^2= 6.6%; Stange *et al.*, 2018) than in pigeons (20.2%; Young *et al.*, 2017).

Embryology and the domestication of pigeons

Domestic pigeons show characteristics (fertility, genetic characterisation, easiness for husbandry, large morphological variation) that makes them an outstanding model to be used in embryology (Helms and Brugmann, 2007). Paradoxically, pigeons are not common in modern comparative embryological studies (Helms and Brugmann, 2007). Embryos of ducks, chickens, and pigeons have been compared (Liu, Rooker and Helms, 2010) to show the existence of a minimal divergence stage in embryologic development (i.e., hourglass model; see below). Embryology (used along geometric morphometrics) has also found that the onset of facial morphological differentiation between pigeon breeds starts at mid-gestation while the morphology is indistinguishable at earlier stages (Helms and Brugmann, 2007; Liu, Rooker and Helms, 2010).

The domestication process can be interpreted on the light of embryology and development of other birds. Young *et al.* (2014) studied the development of mammals, snakes, lizards, turtles, crocodilians, and birds (*Gallus gallus*: chicken, *Coturnix coturnix*: quail, and *Anas platyrhynchos*: Peking duck) and found evidence for the hourglass model. This model states that during the embryonic development, the distinct faces of amniotes become more similar to each other at one developmental stage after which they diverge. Evidence for the hourglass model in pigeons had been previously found (Liu, Rooker and Helms, 2010) and Young *et al.* (2014) argued that the hourglass model is a result of developmental constraints. Deviations from the convergent developmental stage increase the likelihood of clefting (uncoordinated fusion of prominences). However, Smith *et al.* (2015) studied the embryonic development on three bird species birds (*G. gallus*, *Coturnix japonica*: Japanese quail, and *A. platyrhynchos*) and found no convincing evidence of the convergent stage

predicted by the hourglass model (although a marked divergence in morphology of two species after the prominence fusion stage was found). Smith *et al.* (2015) found evidence for evolutionary relevant differences arising in early development which support the evidence found in pigeons (Helms and Brugmann, 2007; Liu, Rooker and Helms, 2010).

My research can only take the embryological evidence into account when interpreting results. All analyses in this thesis are performed on a sample of adults (such as the one of Young *et al.*, 2017) in which only the static or evolutionary effects of development (patterns or downstream results of processes) can be studied. The capacity of my research to shed light into developmental processes (upstream developmental mechanisms) is thus very limited. Nevertheless, it is possible that similar developmental processes which affect the neural crest derivates play an important role in pigeons as well as chickens (Stange *et al.*, 2018) and mammals (Sánchez-Villagra, Geiger and Schneider, 2016). Conversely, domestic pigeons might display only some of the expected symptoms (maybe increased docility, increased skilfulness in using human cues, and shortening of the rostrum) of the domestication syndrome (usually associated with neural crest development changes; Sánchez-Villagra, Geiger and Schneider, 2016).

Heterochrony in pigeon domestication

Heterochrony refers to differences timing of in development changes. It can be studied in an evolutionary context, (comparing adult of individuals from different species), in individuals of the same species (polymorphism or phenotypic plasticity) or even in a single individual (serially homologous structures develop at different stages in one ontogeny; Richardson *et al.*, 2009). Heterochrony can be divided into two relative terms (as the

aforementioned developmental changes): upstream ‘‘process’’ (changes in developmental mechanisms that generate such patterns) and downstream “patterns” (phenotypic expressions of timing change). This distinction between process and pattern highlight the complexity of heterochrony. There are “nonheterochronic process heterochronies” in which heterochronic processes do not produce any measurable heterochronic patterns in later development. For example, some salamander species differ in the sequence of development of limb primordia but end up developing very similar adult limb skeletons (Richardson *et al*., 2009).

In this thesis, I analyse a sample of skulls of adult birds; thus, I am unable to study the developmental processes that lead to heterochrony. However, I will explore the evolutionary effects (patterns) that heterochronic changes had in pigeon evolution. Furthermore, heterochrony does not seem to be a major factor in domestication (Drake, 2011; Sánchez-Villagra, Geiger and Schneider, 2016; Evin *et al.*, 2017) and there is conflicting evidence between some paedomorphic morphological characters and some peramorphic characters like sexual maturation (Sánchez-Villagra, Geiger and Schneider, 2016). Because of this, I will focus my heterochronic assessment on the evolutionary patterns in Columbimorphae (Chapter Two) rather than on its role in domestication (Chapter Four).

Thesis outline and objectives

I aim to test the factors influencing the skull shapes in Columbimorphae. Because of the pluralist approach followed here, I evaluate both developmental and ecomorphological factors affecting shape throughout three research chapters:

Chapter Two: Allometry and heterochrony in the skull of Columbimorphae

In this chapter, I explore one of the most basic evolutionary trends. Allometry is the change in proportional size or shape of a structure, related to changes in overall size.

- I test allometric trends in skull size and shape in Columbimorphae.
- I assess the changes in the morphological clock (heterochrony) that might explain the shape variation in Columbimorphae.

Chapter Three: Ecological factors and their relationship with skull shape in Columbiformes

In this section I assess the influence of a series of ecological factors in the columbiform skull shape and biomechanics.

- To obtain the relevant feeding (diet and foraging) variables I propose a new algorithmic characterization of the feeding characters of Columbiformes
- I assess the biomechanical performance landscape of Columbiformes to obtain the relevant biomechanical characters. The correlation of biomechanical characters and skull shape is evaluated.
- In this chapter I also assess the developmental constraints (modularity and integration) of the columbiform skull and the influence of feeding and biomechanics on different modules.

Chapter Four. Artificial and natural selection work on different axes of variation

In the last research chapter, I assess how the axes of variation of one species (*C. livia*) can predict the axes of variation across taxonomic scales. To do so, I compare the variation in nature to that of a large sample of domesticated pigeons.

- I evaluate how similar are the phenotypic matrices of pigeons under domestication (*C. livia*), and under natural selection (feral *C. livia* and a comparative columbiform sample). I test this within a strong multivariate framework.

- I modify and use the lines of least resistance approach to test, in a phylogenetic framework, if axes of variation (other than the maximum axis of variation) have been explored during domestication.

Chapter Two: Allometry and heterochrony in the skull of Columbimorphae (Mesitornithiformes, Pteroclidiformes and Columbiformes): The dodo wasn't the strangest pigeon

Abstract

Evolutionary allometry is the change in shape associated with the change in size across species. Heterochrony is the change of the allometric patterns in descendant species compared to the ancestral patterns of allometry. Columbimorphae is a clade of non-passerine birds which includes three orders: Mesitornitiformes (3 spp.), Pteroclidiformes (16 spp.), and Columbiformes (351 spp.). Within Columbiformes, the clade Raphini includes iconic and morphologically-disparate species: the dodo (*Raphus cucullatus*) and the Rodrigues solitaire (*Pezophaps solitaria*). Adaptationist and heterochronic hypotheses have been proposed to explain or describe the shape of these disparate species. However, if these species follow the common allometric patterns of Columbimorphae, this could preclude additional evolutionary explanations. Here I show allometry accounts for only 11% of the skull shape variation in Columbimorphae. However, allometry and heterochrony can account for a large proportion of the skull shape in Raphini. A new test for heterochrony was implemented: this test is based on the size prediction using the shape of a structure in an allometric setting. Heterochrony is a significant variable that provides independent information when considered after allometry. Heterochrony can describe the skull shape of 18 analysed spp. including Pteroclidiformes (paedomorphosis) and Mesitornithiformes (peramorphosis). I found that the skull of *Didunculus strigirostris* diverges most from the

overall columbimorph sample. The skull shape of *Didunculus* is not easily attributable to allometry or heterochrony, highlighting that ecological factors might explain the peculiar shape of this species.

Introduction

The bird clade Columbimorphae includes three orders: Mesithornitiformes (mesites), Pteroclidiformes (sandgrouses) and Columbiformes (pigeons and doves; Jarvis *et al.*, 2014; Prum *et al.*, 2015). Columbiformes (pigeons and doves) is the most diverse, including over 310 species and having a nearly global distribution (Sol, 2008). Pigeons and doves occupy an important place in the history of evolutionary biology, beginning with Darwin's (1859) pioneering studies of variation in domesticated *Columba livia* (fancy pigeons). Despite repeated study of *Columba livia* (Darwin, 1868; Johnston, 1992; Larson and Fuller, 2014; Domyan and Shapiro, 2016; Young *et al.*, 2017), relatively little attention has been paid to natural variation within Columbiformes (Martínez-Gómez *et al.*, 2017). Phenotypic disparity and patterns of evolution among wild columbiform species are important for interpreting the variation within domesticated pigeons, and *vice versa*. Analysing only domestic pigeons neglects information about the effects of natural selection and patterns of phenotypic variation in nature. Beyond providing broader context for *C. livia*, Columbiformes is an interesting group in its own right, presenting a wide range of distributions, sizes and foraging habits.

Columbiform species are distributed across every continent but Antarctica, and are also absent from the driest parts of the Sahara and high Arctic. Pigeons and doves have colonized oceanic islands (*e.g.*, Polynesia and the Chatham Islands in the Pacific Ocean; Mauritius, the Seychelles and Réunion in the Indian Ocean; the Azores in the Atlantic Ocean) (Goodwin, 1983; Gibbs, Barnes and Cox, 2010; Hoyo *et al.*, 2017). They range from endemic species with restricted areas of distribution like the extinct Rodrigues solitaire (*Pezophaps solitaria*; ca. 108 km^2), the dodo (*Raphus cucullatus*; ca. 2000 km^2) and the

Samoan tooth-billed pigeon (*Didunculus strigirostris;* ca. 2900 km^2), to species with wide geographic distributions like the rock dove, *C. livia*, which has expanded its geographic range following human cities and towns (61,000,000 km^2) and the common woodpigeon (*Columba palumbus*; 31,800,000 km^2), which inhabits most of Europe, the north of Africa and parts of Asia Minor. The extinct passenger pigeon (*Ectopistes migratorius*) was once the most abundant bird in the world with an estimated population of three to five billion birds in North America (Goodwin, 1983; del Hoyo, Elliott and Christie, 2004; Gibbs, Barnes and Cox, 2010; Hung *et al.*, 2014). Columbiformes range in size from the diamond dove (*Geopelia cuneata*) at around 32 grams to the Victoria crowned pigeon (*Goura cristata*) at 2000 grams. Flightless, extinct species like the dodo and the Rodrigues solitaire have been estimated to have weighed one order of magnitude more, at 21 and 28 kilograms respectively (Goodwin, 1983; Livezey, 1993). Columbiformes show synapomorphies like the ability to drink by suction, unlike other birds (Goodwin, 1983). Another synapomorphy of this group, convergent with Phoenicopteridae (flamingos) and some Spheniscidae (penguins), is the production of crop-milk, a secretion of the crop (expanded, muscular part of the oesophagus; (Baumel, 1993; Stringham *et al.*, 2012) lining that is used to feed the young (Goodwin, 1983; Hoyo *et al.*, 2017). Columbiformes show diverse diets. Broadly speaking they can be granivorous or frugivorous and they also have different foraging habits (from ground to arboreal foraging) (Goodwin, 1983; Hoyo *et al.*, 2017). This leads to questions about how this diversity arose, and how the phenotypes of the pigeons have changed in response to different selective pressures of contrasting environments.

Two emblematic columbiform species are the dodo and its sister taxa the Rodrigues solitaire. These extinct flightless birds of the islands of Mauritius and Rodrigues form the

clade hereafter referred as “Raphini” (Raphinae *sensu* Janoo, 2005). The Raphini are placed within a broader group that also includes the crowned pigeons (*Goura spp.)*, the Nicobar pigeon (*Caloenas sp.*), and the Samoan tooth-billed pigeon (*Didunculus sp.*) (Shapiro *et al.*, 2002). This more inclusive clade is hereafter referred to as “Raphinae”. Raphini are highly distinct from other columbiform species, both in body size (Table S2.1) (Livezey, 1993; Angst, Buffetaut and Abourachid, 2011; Louchart and Mourer-Chauviré, 2011; Brassey *et al.*, 2016; van Heteren *et al.*, 2017) and morphology (Owen, 1866; Livezey, 1993; Claessens, Meijer and Hume, 2015). Differences between the cranial structure of Raphini and those of other pigeons include: (1) a proportionally smaller braincase; (2) a ‘vulture-like’ beak, being anteroposteriorly long, and dorsoventrally deep compared to other pigeons (Owen, 1866); (3) frontals that are broad and convex in comparison to the narrow concave frontals found in other pigeons, resembling the state found in *Didunculus* (Owen, 1866; Claessens, Meijer and Hume, 2015); and (4) parietals that are flat instead of convex, as in other pigeons (Owen, 1866; Livezey, 1993; Claessens, Meijer and Hume, 2015). The skull shape of the Raphini, especially the dodo, has been hypothesized to be related to the inclusion of animals in the diet (Owen, 1866; Livezey, 1993). However, animals would have only been a sporadic component of the diet of Raphini, supplementing fallen fruits, seeds, and bulbs used as a food resources by these obligate ground dwelling birds (Owen, 1866; Goodwin, 1983; Livezey, 1993; Angst, Buffetaut and Abourachid, 2011). Apart from diet, heterochrony (see below) has been used to explain the morphology of these taxa, pointing at the possible overdeveloped peramorphic skull size in comparison to the paedomorphic scapular girdle (Owen, 1866; Livezey, 1993).

Heterochrony can be defined in two contexts: evolutionary and developmental. In an evolutionary context, heterochrony is the change in rates and timing of developmental process. In a developmental context, the definition includes the shifts and relative timing of developmental events during ontogeny. Heterochrony is a consequence of the interplay between size, shape and age (Gould, 1977; Klingenberg, 1998; Mitteroecker, Gunza and Bookstein, 2005). Heterochrony modifies the ontogenetic or developmental trajectories that an organism follows in a multidimensional morphological space during its growth and maturation. This modification of the developmental or ontogenetic process can, over evolutionary time, influence and direct morphological variation among related taxa. The evolutionary definition was used here because this makes it possible to infer heterochrony from the comparison of organisms in the same ontogenetic stage (e.g. adults). Furthermore, this variety of heterochrony can be manifest in two ways: (1) paedomorphosis is the retention of early characters in a later ontogenetic stage, which produces reduced or juvenile characters in adults; (2) peramorphosis is the development of a trait that goes beyond the development of that same trait in the ancestor at the same developmental stage, producing exaggerated traits. Paedomorphosis and peramorphosis are relative terms which can be applied to ancestor-descendant relationships, contemporaneous taxa, conspecifics following different life-history strategies or, sexual dimorphism. However, these definitions are only valid when comparing specific traits (Klingenberg, 1998), but even when valid are descriptive rather than explanatory (Mitteroecker, Gunza and Bookstein, 2005). Heterochrony can be inferred from growth curves (shape versus age) or allometric plots (shape versus size). In this context, it is useful to separate the development from the growth to identify the possible dissociation between size and shape.

The shapes of organismal structures commonly vary with increasing organismal size. This is the concept of allometry (Fitch, 2000; Drake and Klingenberg, 2008; Slater and Van Valkenburgh, 2009; Klingenberg, 2016). The large body size of Raphini, which exceeds those of the largest extant columbiform species by six to ten times, suggests that the differences in skull morphology between this group and other columbiform species could reflect allometric changes. Furthermore, if the peculiar skull shape of these pigeons can be explained in terms of a size/shape correlation, then this would preclude the need for adaptationist or heterochronic explanations for their differences in skull morphology compared to other columbiforms. Allometric explanations have been used previously to explain the emergence of "bizarre" structures like the antlers of the Irish elk (*Megaloceros giganteus;* Gould, 1973, 1974) and the horn-like appendages of brontotheres (Brontotheriidae; Hersh, 1934; however see McKinney and Schoch, 1985).

In its classical sense, the analysis of allometry compares the growth of one structure with body size change either during ontogeny, among individuals in a species, or among species in a higher taxon (Klingenberg, 2016). Allometric analyses allow one to identify a slope that best describes the changes in size of the structure and the body. Because both measurements are log-transformed, the calculated slopes can be interpreted in a biological framework as follows: (1) The null hypothesis of allometry is isometry, which corresponds to a slope of 1.0. Such a relationship for empirical data indicates that the structure grows in fixed proportion to the body. (2) Negative allometry reflects when the structure grows proportionally slower than the rest of the body, so that it is relatively smaller in larger individuals. This is indicated by slopes smaller than 1.0. (3) Positive allometry reflects a structure growing proportionally faster than the body, so it is relatively larger in larger

individuals. This corresponds to slopes higher than 1.0. Allometry has traditionally been examined in two distinct frameworks (Klingenberg, 2016): (1) the Gould–Mosimann approach treats allometry as the covariation of shape with size, and (2) the Huxley–Jolicoeur approach pursues the identification of best fitting lines (allometric trajectories) between two traits (*e.g.*, length of the claw versus body length in crabs). The Huxley–Jolicoeur approach permits the identification of classical allometric tendencies (isometry and positive or negative allometry) (Gould, 1966, 1971; Mitteroecker, Gunza and Bookstein, 2005; Klingenberg, 2016).

These approaches often use single-value measurements of a variety of traits in the estimation of allometry (*e.g.*, skull length versus body mass; Therrien and Henderson (2007), rotational inertia versus body mass, and Henderson and Snively (2004). Allometric estimation has also been performed over multiple measurements of the same structure (skull dimensions versus body mass: Fitch, 2000), or by using multiple measurements in one estimation (Auerbach and Ruff, 2004). Allometric trends tend to be quantified indirectly in attempts to estimate body mass using the size of one structure (*e.g.*, skull length: Fitch, 2000; Auerbach and Ruff, 2004; Henderson and Snively, 2004; Therrien and Henderson, 2007). This is because the basic equation for a general least squares model is:

$$y = mx + b + \mathrm{E} \qquad (2.\ 1)$$

Where *y* is the independent variable that is being estimated and *b* is the intercept or constant. The slope *m* is multiplied by the independent variable *x* to obtain the prediction for a particular *x* value. Finally, Ɛ is the normally distributed error or residual. When

allometry is indirectly quantified, the value of the slope *m* describes the steepness and direction of change between *y* (mass) and *x* (structure). The inverse value of *m* (1/*m*) would describe the relationship of allometric change between *y* (structure) and *x* (mass). However, in most cases this would only be a mediocre estimate of the slope obtained by performing the regression with the variables inverted in the first place (Grafen and Hails, 2002). This is because most regression approaches use Mode I regression (which minimizes the *y* residuals) so the slopes would differ depending on which variable is selected as *y* (McKinney and Schoch, 1985; Grafen and Hails, 2002). Model II regression, which minimizes both x and y residuals, assumes that the error in the relation between x and y is restricted to measurement error. This assumption makes it inadvisable for regression in biological settings (Grafen and Hails, 2002).

Allometry in shape

Shape can also exhibit an allometric signal. However, because of the multivariate nature of shape, the study of allometric trends in shape is more complex than the classical allometric studies performed in an univariate setting (Klingenberg, 2016). Geometric morphometrics allows one to study shape in an allometric context by studying the shape based on Cartesian coordinates called landmarks (Adams, Rohlf and Slice, 2004; McGhee, 2012; MacLeod, 2013a). This approach allows allometric shape changes to be precisely described beyond the classical approaches that considered only linear measurements. While geometric morphometrics can record information about lengths between landmarks (if the scale is added to the specimen), the advantage of this method is that it also records the spatial relationships between all landmarks in the specimen. For example, instead of recording five

linear measurements between ten two-dimensional landmarks, geometric morphometrics allows one to work directly with the ten landmarks for which the precise location is known, allowing calculation of the distance between any of them (representing 45 linear measurements in total).

The first step of geometric morphometrics is to remove the effects of position, size and rotation (Gower, 1975; Rohlf and Slice, 1990). To accomplish this, a generalized Procrustes alignment is applied to the landmark coordinates. This moves the centroid of all specimen constellations to the origin (position), scales them to a unit centroid size (size), and rotates (rotation) them until the sum of squares of the distances between corresponding landmarks is minimized (Gower, 1975; Rohlf and Slice, 1990; Adams and Otárola-Castillo, 2013). These shapes now reside on the surface of the Kendall shape space and can be described mathematically by projecting them to a plane (Gower, 1975; Kendall, 1984; Rohlf and Slice, 1990; Adams and Otárola-Castillo, 2013). To describe these shapes, the Procrustes superimposed coordinates are analysed via Principal Component Analysis (PCA) which characterises the factors (Principal Components: PC) that summarize the shape variation on a given sample. The first PC summarizes most of the variation and subsequent PCs are orthogonal to it, summarizing variation of the sample that is mathematically uncorrelated with previous PCs. However, these axes might be correlated biologically because of the shared evolutionary history of species (Mitteroecker *et al.*, 2004; Goswami and Polly, 2010; Adams and Collyer, 2018).

One caveat of these approaches is the high dimensionality of the data (when the variables measured exceed the number of data points, precluding the use of parametric methods).

For example, there might be twenty different species in a sample from which fifty three-dimensional landmarks are collected from each species. This would mean that subsequent analysis would need to use information from the original 20 species but distributed in 150 different PCs after the PCA. However, the first few PCs would be expected to summarize most of the sample variation. This setting produces an epistemological conundrum: either most statistical procedures cannot be used because of the high dimensionality of the data, or these statistical procedures can be applied to only a few PC (representing an arbitrary proportion of the variation: *e.g.*, 90%), thus breaking the accurate representation of the original data (Adams and Collyer, 2018). Other approaches like principal coordinates analysis (PCo) have been shown to be equivalent to PCA when using the square Euclidian distance matrix (Gower, 1966; MacLeod, 2006; Adams, 2014). PCo could reduce the number of axes in the present example to 20 (*n* = species number); however, in other settings with more species than variables, the similarity matrices would be larger than covariance matrices. PCo is an interesting and versatile tool useful in other settings which deal with different kind of variables in one sample (MacLeod, 2006).

Here I use geometric morphometrics and recently developed multidimensional statistics (Adams and Collyer, 2018) to examine the phenotypic variation in cranium shape across Columbiformes. My sample of 65 species represents 20% of the species diversity and 77% of the generic diversity in that clade (Clements *et al.*, 2017) and includes three iconic extinct species: the passenger pigeon (*Ectopistes*) and the flightless Rodrigues solitaire and dodo. Using these data, I seek to address a series of evolutionary questions about Columbiformes: (1) is there an allometric trend in the head size of pigeons relative to body mass?; (2) does size affect the shape of the columbiform skull?; (3) does heterochrony describe observed

shape changes in the sample and does it account for the unexplained variation after allometry?; and (4) to what extent do the unusual skull morphologies like the dodo and the Rodrigues solitaire deviate from the expectations of allometry and heterochrony?

Methods

Institutional abbreviations.

FMNH, Field Museum of Natural History, Chicago, United States of America; **NHMUK**, Natural History Museum, United Kingdom; **NMS**, National Museum of Scotland, Edinburgh, United Kingdom; **OUMNH** Oxford University Museum of Natural History, University of Oxford, Oxford, United Kingdom; **UMMZ**, University of Michigan Museum of Zoology, University of Michigan, Ann Arbor, Michigan, United States of America; **UMZC**, University Museum of Zoology Cambridge, University of Cambridge, Cambridge, United Kingdom.

Materials examined.

To examine the morphological diversity in the skull of Columbimorphae, 95 skulls from museum collections (Table S2.2) were sampled. Data were collected largely through computed tomography (see below). This sample included wild individuals of *Columba livia* (n = 20), other species of the genus *Columba* (n = 16), and other distinct genera in Columbiformes (n = 37). Three Pteroclidiformes were also included (*Syrraptes paradoxus*, *Pterocles senegallus* and *P. quadricinctus*), along with one mesite (*Monias benschi*).

To avoid biasing the sample with species for which many specimens were sampled, the mean shape of *C. livia* (n = 20) and other species with n > 1 (*Alectroenas madagascariensis*, *Caloenas nicobarica*, *Columba arquatrix*, *Columba palumbus*, *Hemiphaga novaeseelandiae*, *Patagioenas picazuro*, *Patagioenas squamosa*, and *Turtur tympanistria*) was calculated using the `mshape` function of Geomorph (Adams and Otárola-Castillo, 2013) and used in all further analysis.

Computed tomography and surface scanning

Micro-computed tomography (µCT) of the museum specimens was done using Nikon Metrology HMX ST 225 scanners at three different institutions: NHMUK, UMMZ, UMZC. The CT scan data were imported and segmented in Materialise Mimics 18.0 (Materialise NV, Belgium) and exported as .stl and .ply files. The .stl files were simplified using the "Quadratic Mesh decimation" method in MeshLab 2016 (Cignoni *et al.*, 2008). These models were imported to the IDAV Landmark Editor (v.3.5; http://graphics.idav.ucdavis.edu/research/EvoMorph) to place 3D landmarks. To surface scan the Oxford dodo (OUMNH ZC11605), a handheld structured light scanner Artec Spider (resolution: 0.1 mm, accuracy: 0.05 mm) was used.

Geometric morphometrics

Geometric morphometric analyses were performed in R (R Core Team, 2015) using the package Geomorph (Adams and Otárola-Castillo, 2013). A generalized Procrustes analysis was performed to remove the effects of position, size and rotation (Gower, 1975; Rohlf and Slice, 1990). The Procrustes superimposed coordinates were the basis for all allometric analyses of shape.

Landmarks

My landmark scheme (Figure S2.1, Table S2.3) is modified from that of Young *et al.* (2017), who generated a landmark arrangement in their study of domesticated pigeon crania. Five of the thirty-two landmarks used by (Young *et al.*, 2017) were difficult to locate unambiguously, and therefore these landmarks were discarded (landmarks 6, 7, 21, 22, and 29 from Young *et al.*; 2017). The discarded landmarks were either located at the cranial

sutures of the frontal with the nasal and parietal bones or were midpoint landmarks dependent on these sutures. Sutures are difficult to locate in some specimens because the pigeon skull bones are not heavily ossified. Squamosal-quadrate contact landmarks were also discarded because the exact position of this landmark was difficult to replicate in my specimens given its vague anatomical definition: "squamosal and quadrate junction" (Young *et al.*, 2017). The removal of these landmarks sacrifices information about the extent of the frontal, and general information of the skull midline between the cranial hinge and the tip of the occipital crest. Information about the proximal position of the quadrate is also diminished. However, I decided to make a comparison of Young et al. (2017) by using both the complete landmarks and my reduced landmark system. The ordination obtained using both approaches points to the apparent stability of results using both systems (Figure S2.2). Figure S2.2 shows that visible differences in the ordination start to show in PC4 which only accounts for 2.3% of the sample variation. Species in the previous three PC axes distribute similarly in both ordinations and account for most of the sample variation (around 87% of the sample variation). I am confident, therefore, that the landmark system used here summarizes most of the information in the sample.

The landmark system used in this study consists of 27 three-dimensional coordinates (Figure S2.1, Table S2.1), of which seven are midline landmarks, and 20 are paired right/left landmarks. The landmarks were not averaged across the midline to preserve important information that could be used in further analyses (*e.g.*, fluctuating asymmetry; Goswami and Polly, 2010). Landmarks can be classified into three types (Bookstein, 1991; MacLeod, 2013a): Type I landmarks are placed in one point that is biologically and geometrically unambiguous: *e.g.*, the intersection of three bone sutures. Type II landmarks are points

that represent a geometric unambiguous location but lack the biological support: *e.g.*, the maximum curvature point or tip of a bone suture or the midpoint between landmarks A and B. Type III landmarks depend of the position of other landmarks or the orientation of the specimen, these landmarks are also called semilandmarks: *e.g.*, the point furthest away from landmark A, or a series of equidistant landmarks representing a curve (Bookstein, 1996, 1997; MacLeod, 2013a). In total, 24 of the landmarks used in this study are type I landmarks, while the other three are type II landmarks (Landmarks 25-27). These type II landmarks (MacLeod, 2013a) were calculated by placing a series of semilandmarks describing a curve and then calculating the midpoint of this curve using the R (R Core Team, 2015) package Geomorph (Adams and Otárola-Castillo, 2013).

Missing landmarks (Tables S2.2 and S2.4) were present in 22 of the 95 specimens in the sample. In total 45 landmarks were missing in the sample, 1.75% of all the sample landmarks. One specimen (*Raphus*) was missing eight landmarks. Two models were missing five landmarks (*Pezophaps* and *Otidiphaps nobilis*), one model was missing four landmarks (*Columba livia*), three specimens were missing two landmarks (*C. livia*, *Patagioenas picazuro*, and *Columbina talpacoti*). Seventeen more specimens were missing one landmark each. These landmarks were missing either because of the conservation or history of the museum specimens: *e.g.*, (1) one or two of the quadrate bones were displaced or missing from the skulls; (2) the zygomatic arches were broken, possibly because the skull interaction with the rest of the bones in the box; (3) the tip of the premaxilla was damaged, possibly during the rhamphotheca removal during the skeletonization process, and (4) holes were made to mount old specimens (Table S2.4). Where possible, missing landmarks were reconstructed by reflecting them from the

opposite side of the skull using a modified version of the `reflect.coords` internet function that uses a Householder transformation (Griffin, 2017); this code was used because reflection is not available in Geomorph (Adams and Otárola-Castillo, 2013) and was easier to apply to all the database than the `reflectMissingShapes` function of the StereoMorph package (Olsen and Westneat, 2015) . After reflection, the number of missing landmarks in the sample decreased to 17 (0.66% of all landmarks), the *Raphus* landmark set was complete, and two specimens (Pezophaps and *Otidiphaps nobilis* had four missing landmarks each, *Columba livia* (NMS; not registered specimen) was missing two landmarks, and seven other specimens were missing only one landmark each (Table S2.4).

For all subsequent analyses, missing landmarks were estimated using the `estimate.missing` function from the package Geomorph (Adams and Otárola-Castillo, 2013), estimation was done using the "TPS method". Thin plate spine (TPS) method is based on the same logic as sliding semilandmarks on a curve or surface (Bookstein, 1997). First, the specimens are aligned, and the thin plate spline is interpolated based on the existing landmarks and in reference to the Procrustes average shape (Gunz *et al.*, 2009). The final position of the missing landmarks is identified when the "bending energy" of the spline is minimized. The "bending energy" parameter is the result of an integral equation that can be visualized as the energy required to bend an infinitely thin metal plate in order to obtain the target shape by deforming the mean shape (Bookstein, 1996, 1997; Gunz *et al.*, 2009; MacLeod, 2013b). This method avoids the possible overfitting of the data caused by regression-based estimation (Gunz *et al.*, 2009).

Body size and phylogenetic information

Two proxies for size were used: mean body mass of the species and the centroid size of the specific skull included in the analyses. The mean body mass of most species was obtained from the *Handbook of Avian Body Masses* (Dunning and John, 2008). Values for the dodo and the Rodrigues solitaire were obtained from the mean of both sexes using the lowest mass estimates of Livezey (1993) (Table S2.1). These masses were estimated via linear regression of the femoral length of 187 Columbiformes. The increased mass estimates obtained by Livezey (1993) that accounted for flightlessness and fat condition were not used because most recent estimates support mass values closer to the lower mass estimate from Livezey (1993) (Angst, Buffetaut and Abourachid, 2011; Louchart and Mourer-Chauviré, 2011; Brassey *et al.*, 2016; van Heteren *et al.*, 2017) (Table S2.1). I decided to use estimates from Livezey (1993) because more recent literature has focussed on the dodo and has not also estimated the body mass of the Rodrigues solitaire in a comparable framework (Table S2.1). The use of skull centroid size eliminates problems like the possible mismatch between the mean species body masses and the actual body masses of the sampled specimens. Furthermore, head size is not typically isometric with respect to body mass (Fitch, 2000; Therrien and Henderson, 2007), so body mass may not be the most appropriate size measure for analysis of allometric trends in skull shape.

I tested whether skull centroid size or species mean body mass was the best predictor variable for skull shape allometry by comparing the R^2 values obtained from distance-based methods between different models and proxies. Akaike Information Criterion (AIC) values were not calculated because they can be heavily biased by multidimensional data (Bedrick

and Tsai, 1994) and even approaches that take in account this multidimensionality (AICc) are biased towards complex and incorrect models when the regression is calculated in distance matrices (Franckowiak *et al.*, 2017). Skull centroid size was the better predictor of skull shape and therefore was used for most of the subsequent analyses of allometry. Despite not being able to use AIC to discern which model fit the data better, I simply acknowledge that phylogenetic regression methods ask different questions than regular methods and interpreted both results accordingly (see below; Pagel, 1999; Garamszegi, 2014).

A sample of 5,000 phylogenetic trees of the species in the sample was obtained from the global phylogeny of birds (https://birdtree.org/; Jetz *et al.*, 2012) based on the Hackett *et al.*, (2008) backbone. Three monotypic genera in the sample were missing from the phylogenetic trees (*Raphus*, *Pezophaps* and *Ectopistes*), these three species were added to the trees using the `bind.tree` function of phytools (Revell, 2012). The species were added at the midpoint of the branch uniting their sister taxon with its next-closest relative in each phylogeny. The sister taxon used for *Pezophaps* was *Caloenas nicobarica* (Soares *et al.*, 2016), *Pezophaps* was then used as the immediate sister taxon of *Raphus*, *Ectopistes* was placed as sister to the genus *Patagioenas* (Johnson *et al.*, 2010). To avoid the possible influence of using consensus trees instead of source trees, I obtained a random sample of 200 phylogenetic trees out of the 5,000 trees sample. All phylogeny-dependent analysis (phylogenetic generalized least squares and distance based phylogenetic generalized least squares) were performed across this sample of 200 trees to account for phylogenetic uncertainty.

Statistical hypothesis tests

Allometry of head shape

To examine trends in evolutionary allometry, I analysed three subsets of the sample: (1) Columbimorphae, (2) Columbiformes, and (3) Columbiformes-nP (Columbiformes excluding *Pezophaps* and *Raphus*). The third subset was intended to examine the influence of these exceptional, large-bodied taxa on inferences of allometry. Since my sample consists only of adults, I examined the static allometry of head centroid size versus body mass. I used two approaches to identify classic allometric trends in skull size in a Huxley–Jolicoeur framework (Fitch, 2000; Klingenberg, 2016). First, I performed an ordinary least squares (ols) linear regression using the $\log_{10}$ centroid size, and the $\log_{10}$ of mean species body mass. Second, to account for the non-independence of the species, I performed a phylogenetic generalized least squares regression (pgls; Grafen, 1989; Garamszegi, Møller and Erritzøe, 2002) on the two size proxies across the 200 phylogenies (Table 2.1). Both approaches: the 'ordinary' ols and pgls ask different questions. The ols fits the best line that explains most of the variance in the data (diminishing residuals). This method asks what the relation between two variables is given a set of observations (species). The pgls model asks if the detected changes of one variable are related to the changes in the explanatory variable across the phylogenetic history of the group (Benson *et al.*, 2017).

Because closely related species often resemble each other (phylogenetic signal), this results in an expectation of differences in phenotypic covariance among those pairs of species. If evolution in every lineage was independent and each character came from a bivariate normal distribution, then the assumptions of ordinary least squares regression could be

used (Felsenstein, 1985). This would be true only if the measured characters responded immediately to external factors, thus they would behave independently of the shared evolutionary history of the group (Felsenstein, 1985). However, when shared history influences the measured characters, the real correlation between variables can be obscured and even the significance of the models would be affected because of the loss of degrees of freedom (Felsenstein, 1985). In terms of the regression equation, the problem of not taking in account the phylogeny is that the error (Ɛ) of equation 2.1 is correlated among related species and is not normally distributed (Garland, Jr., and Ives, 2000).

The second approach (pgls) first calculates the expected phylogenetic variance-covariance matrix which would theoretically contain the expectation of similar traits being held by closely related species. By calculating this matrix, it is possible to account for differences in the duration of shared ancestry among pairs of species in the phylogeny. Ordinary and phylogenetic least squares slope estimates can differ significantly even with large sample sizes, large ranges of the independent variable (*e.g.*, body mass), and high correlation values (Garland, Jr., and Ives, 2000). Obtaining the "correct" slope and intercept is important because the phylogenetic bias could obscure relationships like isometry (Motani and Schmitz, 2011). Taking phylogenetic signal into account allows for the identification of species that are actually different from the phylogenetic expectation while minimizing the effect of single clades that have deviated from the regular values.

Phylogenetic signal was estimated using Pagel's λ, in its broader sense λ is a scaling parameter of the phylogeny that indicates whether the shared evolutionary histories as specified by the phylogeny produce the patterns of similarity observed in the data (Pagel,

1999). When λ equals 1.0, no scaling is done and the pgls model asks whether the changes inferred along phylogenetic lineages are correlated with each other, this would indicate characters behaving as expected by the shared evolutionary history of the group, while values of $\lambda > 1.0$ suggest traits being more similar among species than expected from their phylogeny; values of $\lambda < 1.0$ suggest the reverse. When $\lambda = 0.0$ the traits behave independently of the shared evolutionary history of the group (Felsenstein, 1985), thus complying with the assumptions of ols and rendering similar results (Garland, Jr., and Ives, 2000; Garamszegi, 2014). This can be geometrically interpreted as observing a star phylogeny in which the branch length between all species is the same and there is no variation in similarity among different pairs of taxa, irrespective of their phylogenetic relationships (Felsenstein, 1985). The pgls model accounts for the strength of the "phylogenetic signal" using the parameter λ. The λ value is used to multiply the off-diagonal elements of the variance-covariance matrix during regression (Garamszegi, 2014). In this context, a λ value of 0 indicates absence of phylogenetic signal in the relationship between two traits, while a λ value of 1 suggests a strong phylogenetic signal in accordance with the Brownian motion model of character evolution (Motani and Schmitz, 2011; Garamszegi, 2014; Benson *et al.*, 2017). However, this λ in pgls applies to residual correlation errors Ɛ, and can differ from the λ calculated for each trait separately (Garamszegi, 2014). Finally, in the visualization of the phylogenetic least squares (Figure 2.1), I calculated the average confidence intervals of 200 pgls models to establish a threshold for interpreting this plot. However, these confidence intervals are not statistically meaningful in a pgls context. The confidence intervals are not useful in predicting any new species because phylogenetic

information also needs to be taken in account when calculating these intervals (Garland, Jr., and Ives, 2000).

Allometry and shape

Usual methods applied in a phylogenetic framework are not appropriate when handling multidimensional data like shape (Adams and Collyer, 2018). For example, some methods based on multivariate likelihood become susceptible to model misspecification in high-dimensional data. Methods that operate on single PCs individually are also not appropriate (Ingram and Mahler, 2013), because these do not account for the non-independence between dimensions and are prone to model misspecification. Other methods using pairwise composite likelihood are sensitive to covariation, orientation and high-dimensionality of the data (Adams and Collyer, 2018). Nevertheless, recent developments of multivariate statistics applied to shape (multivariate phylogenetic comparative toolkit; Adams and Collyer, 2017) allow for the testing of biological hypotheses of shape data without the necessity of reducing the information (e.g., by selecting only the first PCs of shape), by making algebraic generalizations of regular phylogenetic comparative analysis. These generalizations come from statistical equivalency between methods based on covariance matrices (R) and those based on distance matrices (Q) in Euclidian space (see below; Adams, 2014).

Phylogenetic regression is a parametric method based on a variance-covariance matrix, and is therefore an R-mode method (Krzanowski, 2000; Denton and Adams, 2015). R-mode techniques present several problems. First, they become quickly unable to recognize patterns in the data when the number of response variables increases, because the number

of parameters that must be estimated to fit the model also increases (Rao's paradox; Denton and Adams, 2015). Second, when the number of dimensions is higher than the sample size (i.e. number of specimens analysed), it becomes impossible to manipulate (invert) the covariance matrix. This is especially troublesome in a geometric morphometric context that can present an extremely large number of dimensions with respect to the sample.

Distance based techniques (Q-mode) utilize the matrix of pairwise distances among observations (Krzanowski, 2000; Adams, 2014; Adams and Collyer, 2018). These methods are widely applicable in a geometric morphometric framework because of the equivalence between the Q and R matrices in an Euclidean setting (Adams, 2014; Denton and Adams, 2015). The use of Q mode techniques, instead of R mode, are adequate for high dimensional datasets, insensitive to orientation and covariation of the data, and display an appropriate Type I error without sacrificing information by reducing the dataset dimensionality (Adams, 2014; Adams and Collyer, 2018). Permutation tests are used to determine significance to avoid spurious correlations provoked by the multidimensionality of the data. These methods allow hypothesis testing using the complete shape data but present one caveat: because it depends on the calculation of a distance matrix, generating a coordinate system from them, the information of the variation associated with the original coordinate system is not transferred to the new one (Klingenberg, 2014).

Multivariate skull shape data have been studied in a phylogenetic context by distance-based multivariate statistics in relation to their body size (Adams, 2014). I applied this method to pigeons to determine the allometric component of the skull shape in a Gould–

Mosimann framework (Klingenberg, 2016). I applied two approaches of multivariate regression to each of the data subsets. First, I performed a distance-based multivariate regression between the shape coordinates and the log of the size proxies data using the Geomorph (Adams and Otárola-Castillo, 2013) function `procD.lm` (D.ols), this approach does not account for phylogenetic relationships among taxa. Second, I performed another multivariate regression between the shape data and size proxies in a phylogenetic comparative framework (Adams, 2014) using the function `procD.pgls` (D.pgls). The $\log_{10}$ of mass and cranial centroid size were used to estimate head shape to body and head size allometry.

Allometry can also be studied by obtaining the Common Allometric Component (CAC) of the sample. The name of CAC is given because in a multi-species sample this component describes the common variation in all species due to size change, and not the allometric variation within a particular species (Mitteroecker *et al.*, 2004). This common allometry has also been referred to as "evolutionary allometry" in a phylogenetic context (Adams, 2014). CAC (Mitteroecker *et al.*, 2004) allows the size-shape space to be constructed and analysed. To accomplish this, first a size column ($\log_{10}$-centroid size) was added to the Procrustes-superposed shape data. This alters the plane projection of Kendall's shape space (Kendall, 1984) by adding a new dimension representing size (Klingenberg, 2016). Third, a PCA is performed on this shape-size matrix. The first PC (CAC) resulting from this PCA is expected to retrieve most of the allometric variation in the sample because the orientation of this new PC space will be dictated by the dimension with most variance (which is expected to be the size dimension) (Mitteroecker *et al.*, 2004). The CAC is usually visualized against the residual shape components (RSC), which are the PC of the residuals of an allometric

regression, either D.pgls or D.ols. The CAC approach shed light into the heterochrony of *Monias*. However, this analysis was formulated in a developmental context and aims to visualize the allometric trajectories of different species in size-shape space in order to identify allometry. The results of this approach are therefore presented in Appendix One.

To identify shape outliers from the allometric model, I obtained the predicted shape for each species based on its skull centroid size, using the mean D.pgls coefficients based on the sample of 200 phylogenies (multi-D.pgls) of the Columbiform-nP sample (Columbiformes excluding Raphini). Next, the shape-residuals were obtained by subtracting the specimen Procrustes aligned coordinates for each species from their predicted shapes. Afterwards, the sums of the absolute values of these residuals were obtained (hereafter referred as sum of shape residuals; SSR) to obtain a univariate measure of the deviation of the actual shape of each pigeon skull from the allometric model expectation. Finally, I used the mean value of SSR ± two standard errors of the Columbiform-nP sample to establish a threshold value for the expected dissimilarity and to identify the shape outliers. The sum of shape residuals was plotted against the $\log_{10}$ of the centroid size to visualize the outliers.

Heterochrony and shape

Heterochrony was originally defined in a univariate framework (Gould, 1977; Klingenberg, 1998; Mitteroecker, Gunza and Bookstein, 2005). The original definitions of heterochrony are difficult to apply in a multivariate framework such as geometric morphometrics (Klingenberg, 1998; Mitteroecker, Gunza and Bookstein, 2005). For example, heterochrony can be global, local or mosaic (Gould, 1977; Mitteroecker, Gunza and Bookstein, 2005).

Mosaic interactions arise from local hormonal/signalling interactions and tissue dependant responses. However, mosaic allometry is difficult to find in the multivariate context (Mitteroecker, Gunza and Bookstein, 2005).

It is possible to identify some of the allometric trends like peramorphosis and paedomorphosis in a multivariate framework if some base precautions are taken (Mitteroecker, Gunza and Bookstein, 2005). PCA should not be used to identify heterochrony. PC1 is usually regarded as the PC summarizing size, however other factors influence PC1. Furthermore, PC1 can summarize changes in overall size but further PCs can summarize the changes of size of one structure. Also it is impossible to interpret heterochrony in each PC separately because these PCs are mathematically uncorrelated but not biologically uncorrelated (Mitteroecker *et al.*, 2004; Goswami and Polly, 2010; Adams and Collyer, 2018). The use of modules has been proposed as a way to analyse mosaic heterochrony (Mitteroecker, Gunza and Bookstein, 2005). However, the descriptive power of statistical tests diminishes with module size, subdividing the landmark data can diminish the sample variation, and modules are rarely completely independent, so modules are not fit to test heterochronic patterns (Mitteroecker, Gunza and Bookstein, 2005).

To gather the shape variation from the landmark data and take into account most variation in the sample, allometric regression is used (Mitteroecker, Gunza and Bookstein, 2005; Adams, 2014). Heterochrony implies the overlap of allometric or ontogenetic trajectories among taxa. If there is no overlap, then the heterochronic hypothesis can be discarded. In an allometric framework, equal slopes can be used to suggest heterochrony.

Some species in the sample may be heterochronic in relation to Columbiformes. I noted that Pteroclidiformes seem to present a paedomorphic skull, whereas the dodo and the Rodrigues solitaire have been proposed to present a peramorphic skull (Owen, 1866; Livezey, 1993). To test this, I performed a size prediction by comparing the predicted shape to a sequence of predicted shapes along the allometric trajectory and chose the shape that minimized the SSR. In other words, I used my allometric model to predict the size of each skull based on its shape. First, I generated two sequences of 30,000 values. For body mass, these values corresponded to a sequence between 1g and 30kg (larger than the largest estimate for *Raphus* or *Pezophaps* from Livezey (1993), taking into account flightlessness and fat condition). These centroid size values extend between the 0.5*minimum centroid size and 1.5*maximum centroid size. I then predicted the expected shape for each value along these sequences using the mean coefficients of the multi-D.pgls analysis of the Columbiformes-nP sample. To predict the size, I selected the shape value that minimized the SSR from the Procrustes-superposed coordinates (Table 2.3, Figure 2.7). Finally, I fit an ols model to the predicted and empirical sizes and calculated the 95% confidence intervals to identify how interest groups behave in the mass prediction (Figure 2.7).

I used the residuals in a purely allometric model (using the mean coefficients from the distance-based pgls model across 200 phylogenies) to quantify the maximum improvement in shape prediction that could be obtained by heterochronic changes. To do so, I calculated fitted values of each species in the dataset using their empirical size. Using these fitted values and the original coordinates, obtained the sum of squared residuals ($SSR_{allometric}$, as in standard regression procedure). Then, I calculated the fitted values for each species using their predicted (heterochronic size) and got a new sum of squared residuals

($SSR_{heterochronic}$) between the fitted heterochronic values and the empirical shape. Finally, as the metric of improvement I obtained the percentage of sum squared residuals percentage of improvement (SSR %, Table 2.3) using the equation:

$$SSR\% = \frac{SSR_{allometric}}{SSR_{hetrochronic}} * 100$$

(2. 2)

My first part of the heterochronic test proposed here: the heterochronic size prediction is mostly descriptive and is based on the question: what heterochronic size (associated to a shape in an allometric model) improves the shape prediction the most? However, the second part of the test (calculating the percentage of improvement: SSR%) allows to identify the species for which the heterochronic size describes the unexplained variation after allometry. However, the SSR% is also a descriptive measurement rather than a statistical hypothesis test.

Finally, to test the explanatory power of heterochronic size I performed a distance-based phylogenetic least squares using the heterochronic centroid size as the independent variable to predict skull shape. I also evaluated if predicted centroid size and empirical centroid size provide redundant information by using both variables in the same model (Table 2.4).

Multidimensional shape visualization

The common allometric component was plotted against the residual shape component in a phylogenetic framework (Appendix One, Mitteroecker *et al.*, 2004; Adams and Otárola-

Castillo, 2013). I identified that allometric shape changes in both, D.ols and D.pgls analyses. D.ols presented similar patterns to the multi-phylogeny D.pgls analysis. However, because these results do not take in account the phylogenetic relationships or the uncertainty of the phylogeny, I decided to use the mean D.pgls coefficients to represent the shape changes related to skull size (Figure 2.2). I obtained a sequence of five values between the minimum and maximum centroid size values in the sample for Columbimorphae (*Columbina tlapacoti*: 4.5cm to *Raphus*: 30.5cm). To predict these shapes I used the mean regression coefficients from the multi-D.pgls analysis of each of the different samples using a custom R function. As a set of coefficients was obtained for each of the three samples (Columbimorphae, Columbiformes and Columbiformes-nP) and five centroid values to predict, 15 shapes were predicted.

I also used this technique to further explore the allometric shape changes in columbiforms within the extant columbiform body size range. Using the mean coefficients of the Columbiformes-nP multi-D.pgls fit, I predicted the shapes of three species (*Columbina passerina*, *Columba rupestris* and *Goura cristata*) along the centroid size range (4.5cm, 7.6cm, and 12.7 cm respectively) and compared them with their actual landmark constellations (Figure 2.3). To visualize the identified outliers (Figure 2.4), I used the mean coefficients of the Columbiformes-nP D.pgls fits to predict the shapes of these outlier species and compared their predicted landmark constellations against their empirical landmark constellations (Figure 2.5). Finally, I visualized the differences between pteroclidiform and columbiform skull landmark constellations (Figure 2.6).

Results

Allometry of head size against body mass

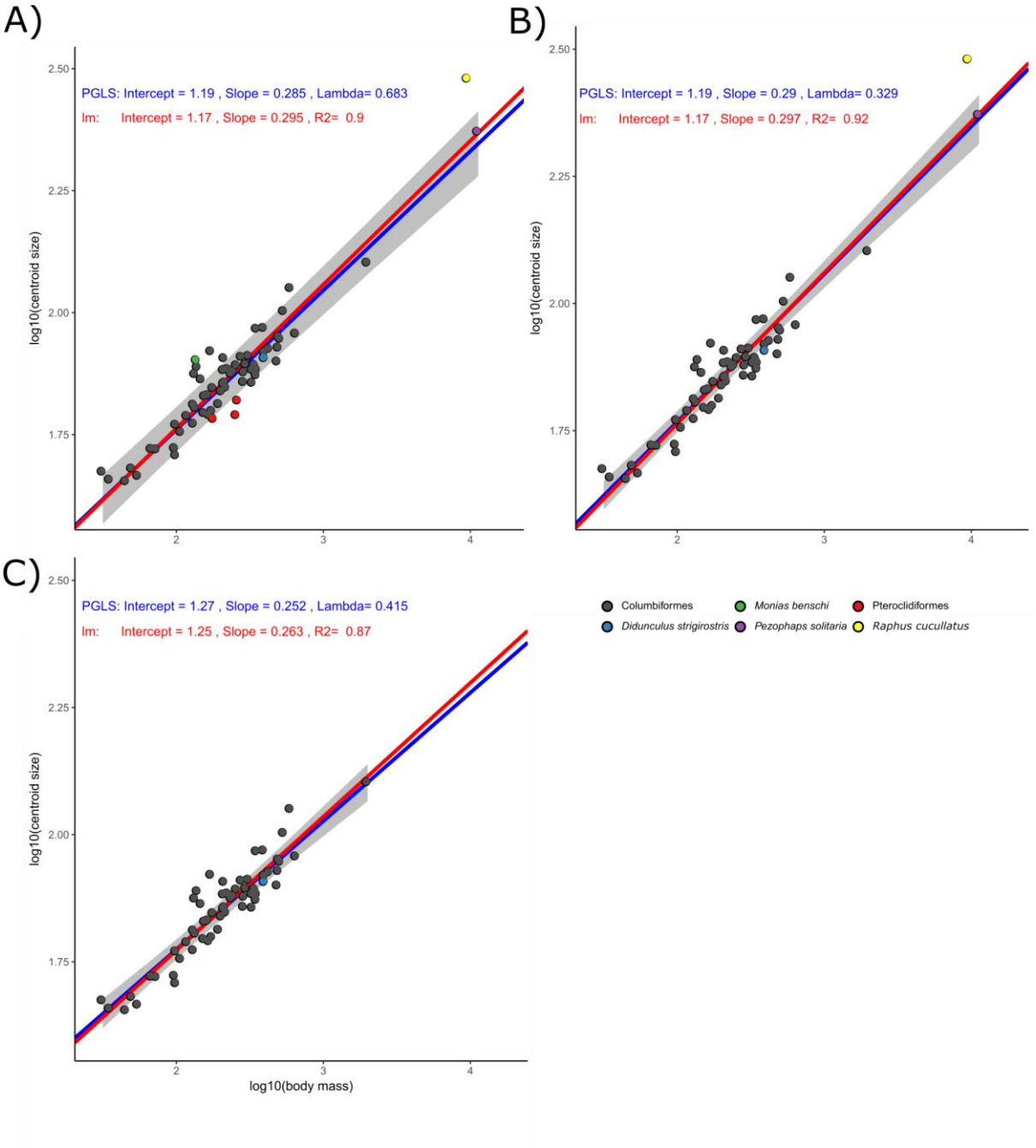


Figure 2.1. Plots of the regression models of head versus body size. for A) Columbimorphae, B) Columbiformes, and C) Columbiformes without the raphini. linear regression line (lm) in red and phylogenetic generalized least squares line (blue). Shaded area shows the average 95% confidence interval for the 200 phylogenetic generalized least squares models.

The mean slopes are lower in the pgls models throughout all samples (Table 2.1). The slope of models was similar for the Columbimorphae (pgls slope (mean)= 0.29, (sd)= 0.00; ols slope= 0.30) and Columbiformes (pgls slope (mean)= 0.29, (sd)= 0.00; ols slope= 0.30) samples, while the slope of the Columbiform-nP sample was lower (pgls slope (mean)= 0.25, (sd)= 0.00; ols slope= 0.26). The mean pgls slope of centroid size against body mass (Figure 2.1, Table 2.1) presents consistent and negatively allometric values (0.25 to 0.39; isometry would be indicated by 0.333) in all three subsets of the data and in both analyses (ols and pgls). The slope values are lower when *Pezophaps* and *Raphus* are excluded from the analyses, taking on values from 0.25 (mean pgls) to 0.26 (ols), once again indicating negative allometry against the isometric expectation.

The predictions of allometry based on the sample of Columbimorphae (Figure 2.1A) show that *Raphus* and the mesithornithiform *Monias* exhibits larger skulls than expected for pigeons of their body masses, and both species fall outside the 95% confidence interval (CI) of the pgls model. The Pteroclidiformes exhibit smaller skulls than expected, and two of them fall outside the 95% confidence interval of the model (*Pterocles quadricinctus* and *Syrrhaptes paradoxus*). *Pezophaps* falls within the skull size predicted for a pigeon of its body mass. *Pezophaps* and *Raphus* show similar positions with respect to the allometric line when only the Columbiformes sample is analysed (Figure 2.1B). When *Pezophaps* and *Raphus* are omitted from the analysis, the R^2 of the ols linear model decreases by 5% (Figure 2.1C).

Table 2.1. Allometry of skull centroid size against body mass

	Columbimorphae	Columbiformes	Columbiformes-nP
Phylogenetic generalized least squares (pgls)			
AIC (median)	-234.31	-227.66	-239.02
AIC (min)	-236.09	-229.05	-240.89
AIC (max)	-232.31	-226.43	-237.25
λ (median)	0.68	0.33	0.42
λ (min)	0.60	0.16	0.29
λ (max)	0.74	0.44	0.55
Intercept (mean)	1.19	1.19	1.27
Intercept (sd)	0.00	0.00	0.00
Slope (mean)	0.29	0.29	0.25
Slope (sd)	0.00	0.00	0.00
Ordinary least squares (ols)			
AIC	-228.83	-226.31	-236.12
Intercept	1.17	1.17	1.25
Slope	0.30	0.30	0.26
R^2	0.90	0.92	0.87

The use of different phylogenies does not seem to influence the results of the analysis of skull centroid size versus body mass (Table 2.1). The analysis of 200 different phylogenetic trees do not cause the values obtained by the pgls analysis (AIC or slope) to overlap among different samples or present a high variation (sd= 0.00). Intermediate levels of phylogenetic signal are present in all pgls analyses (Columbimorphae: λ(median)= 0.68, (range)= 0.60-0.74; Columbiformes: λ(median)= 0.33, (range)=0.16-0.44; Columbiformes-nP: λ(median)= 0.419, range=0.29-0.55). The ranges of λ values (considering phylogenetic uncertainty) overlap for Columbiformes (λ(range)=0.16-0.44) and Columbiformes-nP (λ(range)=0.29-0.55) but not for Columbimorphae (λ(range)=0.6-0.74). The AIC showed that pgls models

fitted the data better than ols models (Columbimorphae: AIC(range)= -236.09 to -232.31; Columbiformes: AIC(range)= -229.05 to -226.43; Columbiformes-nP: AIC(range)=-240.89 to -237.25; Table 2.1). The R^2 values of the ols models indicate that body mass explains between 87 and 92% of variation in head size among samples. Median Pagel's lambda (λ) for pgls analysis across 200 phylogenies is higher in the sample for Columbimorphae (λ(median)= 0.68) than that for Columbiformes (λ(median)= 0.33) or Columbiformes-nP (λ(median)= 0.42).

Allometric shape changes of shape against size

All results of D.ols for skull shape versus body mass or skull centroid size (Table 2.2) were significant (*P*< 0.001). When the D.pgls analysis was performed across 200 phylogenies, a large percentage of the analyses were significant (*P*< 0.05) for centroid size: 92% for Columbimorphae, 91.5% for Columbiformes, and 82.5% for Columbiformes-nP; similar percentages of significant pgls models were obtained for the body mass models (93%, 93%, and 73% respectively). The Columbiformes-nP sample obtained less significant models for both centroid size and body mass. Average *P* values were higher for the pgls models, however, and only the Columbiform-nP sample was non-significant (centroid size model: *P*(average)= 0.079; body mass model: *P*(average)= 0.079). The multi-D.pgls model of skull shape versus body mass (Columbimorphae: *P*(average)= 0.017, (sd)= 0.091; Columbiformes: *P*(average)= 0.017, (sd)= 0.092; Columbiformes-nP: *P*(average)= 0.079, (sd)= 0.162) showed higher significance than the model of skull shape versus skull centroid size (Columbimorphae: *P*(average)= 0.04, (sd)= 0.137, Columbiformes: *P*= 0.039(average),

sd= 0.137) except for the Columbiformes-nP sample, which remained non-significant (*P*(average)= 0.079, (sd)= 0.197).

Table 2.2. Allometry of skull shape against size

Multiple phylogenetic generalized least squares (centroid size)						
	Columbimorphae		Columbiformes		Columbiformes-nP	
	Mean	(sd)	Mean	(sd)	Mean	(sd)
SS	0.006	0.004	0.005	0.004	0.003	0.004
MS	0.006	0.004	0.005	0.004	0.003	0.004
Rsq	0.157	0.044	0.159	0.045	0.114	0.071
F	12.447	4.642	11.788	4.481	8.239	7.777
Z	3.977	1.509	3.929	1.474	2.696	1.309
Pr(>F)	0.04	0.137	0.039	0.137	0.079	0.197
Significance (%)	92		91.5		82.5	
Multiple phylogenetic generalized least squares (body mass)						
SS	0.004	0.004	0.004	0.004	0.002	0.004
MS	0.004	0.004	0.004	0.004	0.002	0.004
Rsq	0.094	0.036	0.099	0.036	0.063	0.053
F	6.942	3.817	6.847	3.63	4.277	5.653
Z	3.63	0.986	3.664	0.951	2.043	0.891
Pr(>F)	0.017	0.091	0.017	0.092	0.079	0.162
Significance (%)	93		93		73.5	
Ordinary least squares (centroid size)						
	Columbimorphae		Columbiformes		Columbiformes-nP	
SS	0.173		0.164		0.064	
MS	0.173		0.164		0.064	
Rsq	0.25		0.289		0.152	
F	21.698		24.785		10.59	
Z	5.008		5.342		4.679	
Pr(>F)	0.001		0.001		0.001	
Ordinary least squares (body mass)						
SS	0.131		0.138		0.05	
MS	0.131		0.138		0.05	
Rsq	0.189		0.242		0.119	

F	15.17	19.508	7.942
Z	4.647	5.105	4.248
Pr(>F)	0.001	0.001	0.001

Skull centroid size appears to consistently be a better predictor of the head shape than body size, explaining around 5% more of the variation of skull shape in all models (Table 2.2). When the Columbimorphae and Columbiformes subsets are compared (both centroid size and body mass models), R^2 is consistently higher in the D.ols models (R^2 = 0.189 to 0.289) than in D.pgls models considering phylogenetic uncertainty (R^2(mean)= 0.094, (sd)= 0.36; to R^2(mean)= 0.159, (sd)=0.045). When *Pezophaps* and *Raphus* are not included in the analysis, R^2 values are lower in the D.ols (R^2 = 0.119 body mass, R^2 = 0.152 centroid size) and drops in the D.pgls (body mass: R^2(mean)= 0.063, (sd)= 0.053; centroid size: R^2(mean)= 0.114, (sd)= 0.071).

The visualized allometric shape changes (Figures 2.2 and 2.3) can be summarized as follows: large skulls are dorsoventrally compressed, resulting in a comparatively dorsally flattened skull roof (frontal and parietal) in the midsagittal plane. In these skulls, the frontal is expanded laterally, and the orbit and braincase are proportionally smaller than the rostrum. Conversely, the visualization also shows that the braincases of small skulls are dorsally expanded in the midsagittal plane, the frontal is mediolaterally narrow between the orbits, the orbit is proportionally large, and the rostrum is proportionally smaller than the braincase. Other allometric shape changes which can only be observed when *Pezophaps* and *Raphus* are included in the sample are: (1) large skulls have dorsoventrally deeper beaks; (2) large skulls also have anteriorly expanded rostra have a decreased beak

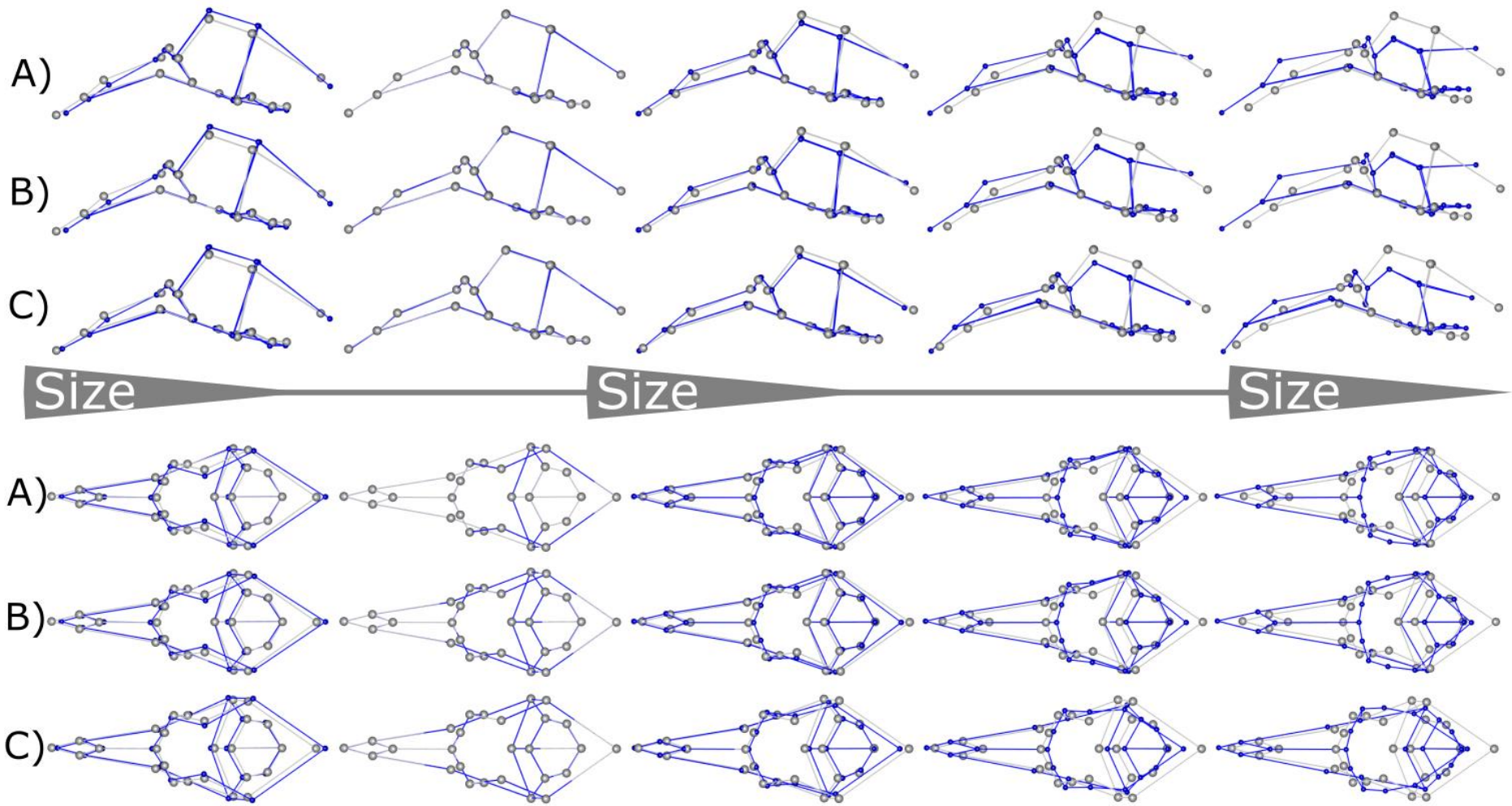

A)
B)
C)
Size
Size
Size
A)
B)
C)

Figure 2.2. Changes in pigeon skull shape due to size changes. Predicted shapes of 5 pigeons along the centroid size range (*Columbina tlapacoti*: 4.5cm to *Raphus*: 30.5cm), using the D.pgls coefficients of different samples for the prediction: A) Columbimorphae, B) Columbiformes, and C) Columbiformes-nP. Grey constellations indicate the mean shape of Columbimorphae. Blue constellations are the predicted shapes. Despite the changes in the sample, all allometric models similar and congruent size related shape changes. The most notable difference occurs in the rostrum height when *Pezophaps* and *Raphus* are omitted from the analysis.

curvature in the midsagittal plane; (3) large skulls also have a decreased basicranial flexion in the midsagittal plane with larger angles than the mean columbiform shape (this becomes evident when compared with small skulls in which the basicranial flexion is at a lower angle than the mean columbiform shape); and (4) large skulls exhibit laterally expanded posterior orbital rims at the frontal and postorbital contacts, while the analysis of smaller pigeons detects the opposite trend. Figure 2.3 shows a good fit of the columbiform species with conservative size and the shapes predicted by the mean coefficients of the D.pgls model of the Columbiformes-nP sample.

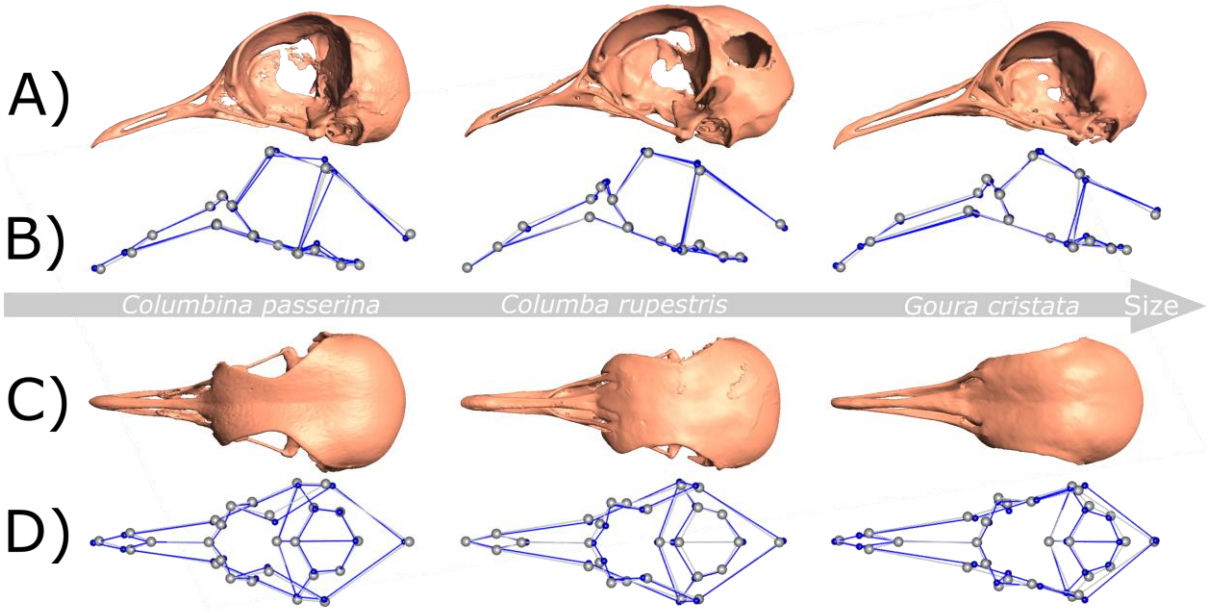


Figure 2.3. Comparison of three species along the allometric axis. The shapes were predicted by the D.pgls model of Columbiformes without *Pezophaps* and *Raphus*. A) Left lateral view of the three-

dimensional models of the shape; B) left lateral view of expected landmark constellations (Grey) versus empirical constellations (Blue); C) dorsal view of the three dimensional models of the shape; D) dorsal view of expected landmark constellations (Grey) versus empirical constellations (Blue).

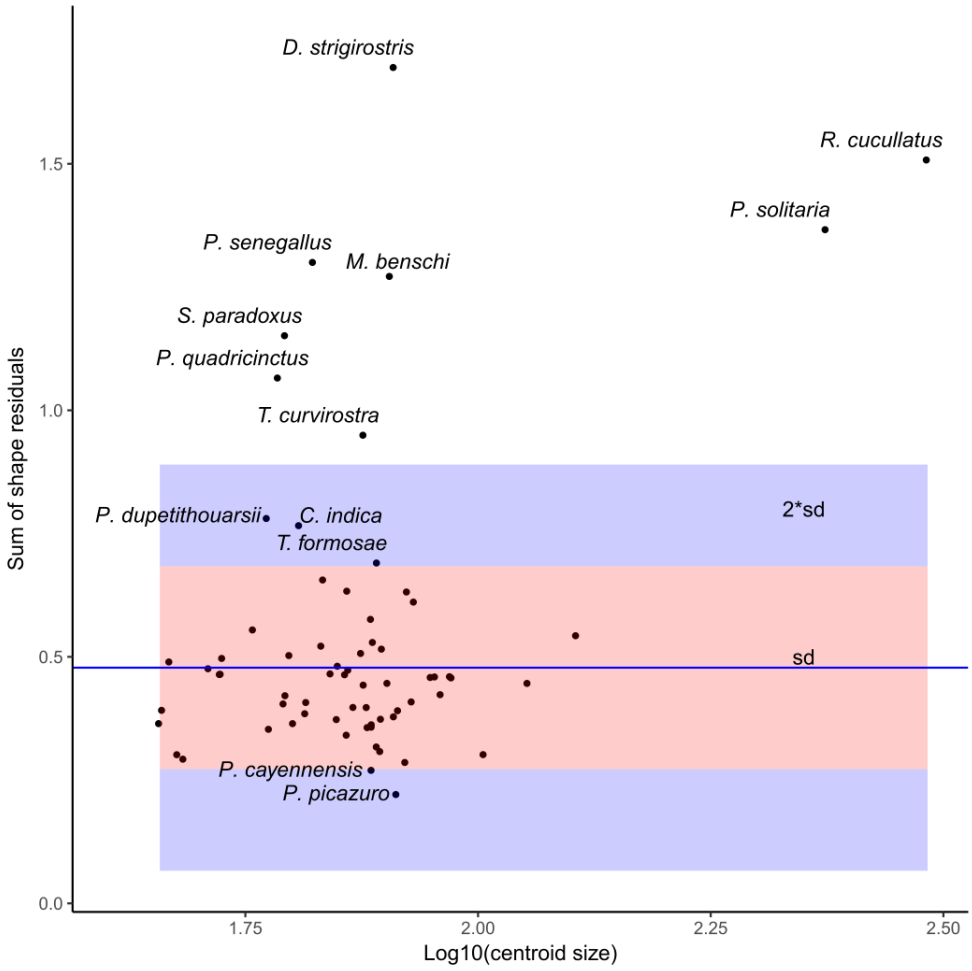


Figure 2.4. Shape outliers. Sum of shape residuals plotted against the centroid size. Blue line is the mean of SSR, red band indicate one standard deviation of the Columbiform-nP SSR, blue band indicates 2 standard deviations of the Columbiform-nP SSR. All Pteroclidiformes and Mesitornithiformes fall outside the confidence interval as Raphus, Pezophaps, and D. strigirostirs.

Deviations of skull shapes of eight species from allometric predictions fall beyond two standard deviations from the mean SSR, using the Columbiform-nP multi-D.pgls model coefficients (Figure 2.4). These species have shapes that are extremely different to those predicted by allometry. All non-columbiforms fall in this category (three Pteroclidiformes plus *Monias*). Several columbiforms also have unusual skull shapes: *Treron curvirostra*, *Didunculus strigirostris*, *Pezophaps*, and *Raphus*. *Ptilinopus dupetithouarsii*, *Chalcophaps*

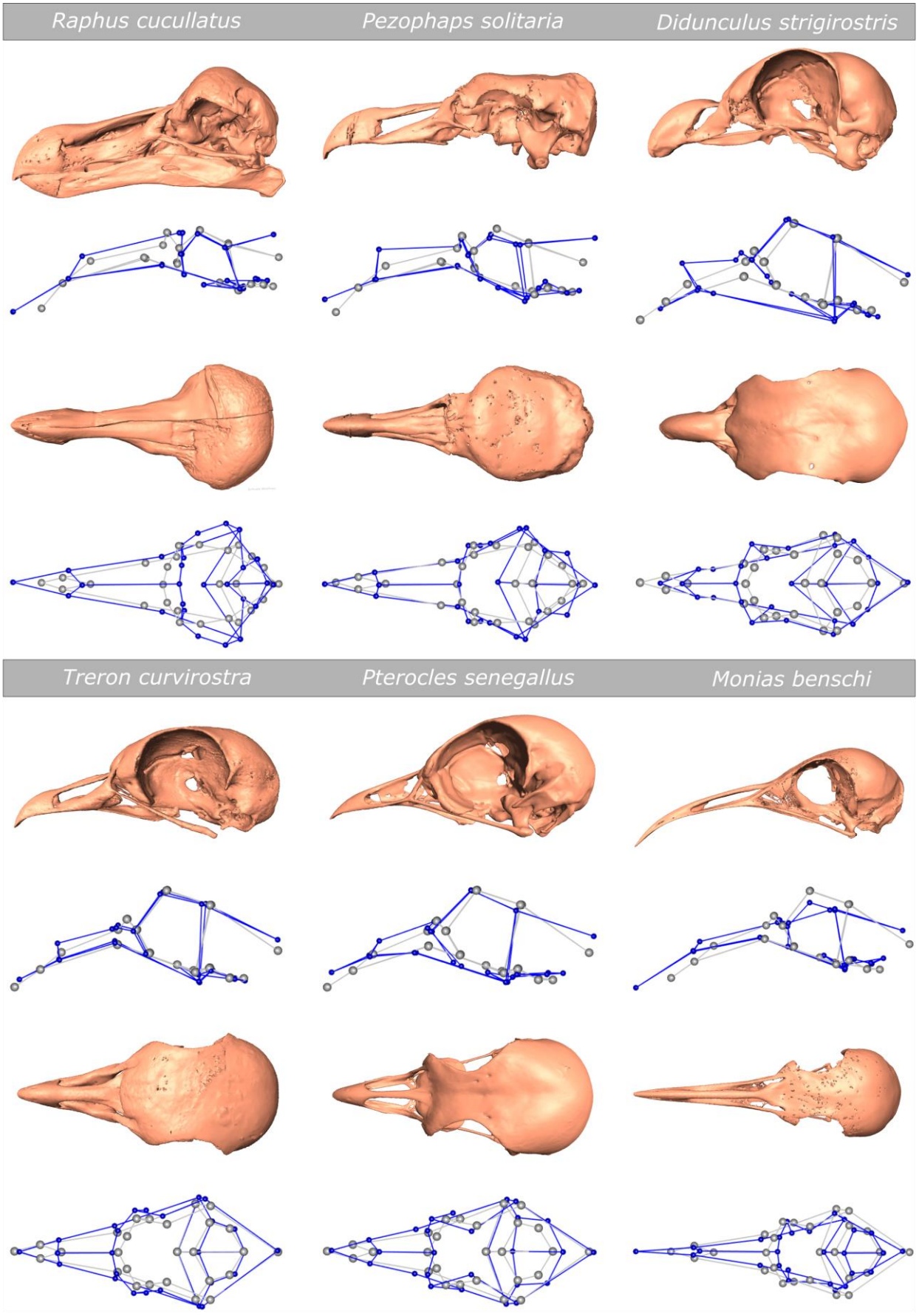

Raphus cucullatus
Pezophaps solitaria
Didunculus strigirostris
Treron curvirostra
Pterocles senegallus
Monias benschi

Figure 2.5. Shape outliers (real and predicted shape), whose sum of shape residuals falls more beyond two standard deviations of the Columbiformes-nP sample. Figure shows the predicted shapes in the allometric model of Columbiformes-nP: Empirical landmarks (Blue) versus expected shapes (Grey). Figure also shows the three-dimensional models of the specimens.

indica and *Treron formosae* also have shapes that vary from the mean by at least one standard deviation, while *Patagioenas picazuro* and *Patagioenas cayennensis* fall on the other side of the distribution being more similar to the expected allometric model than other pigeons.

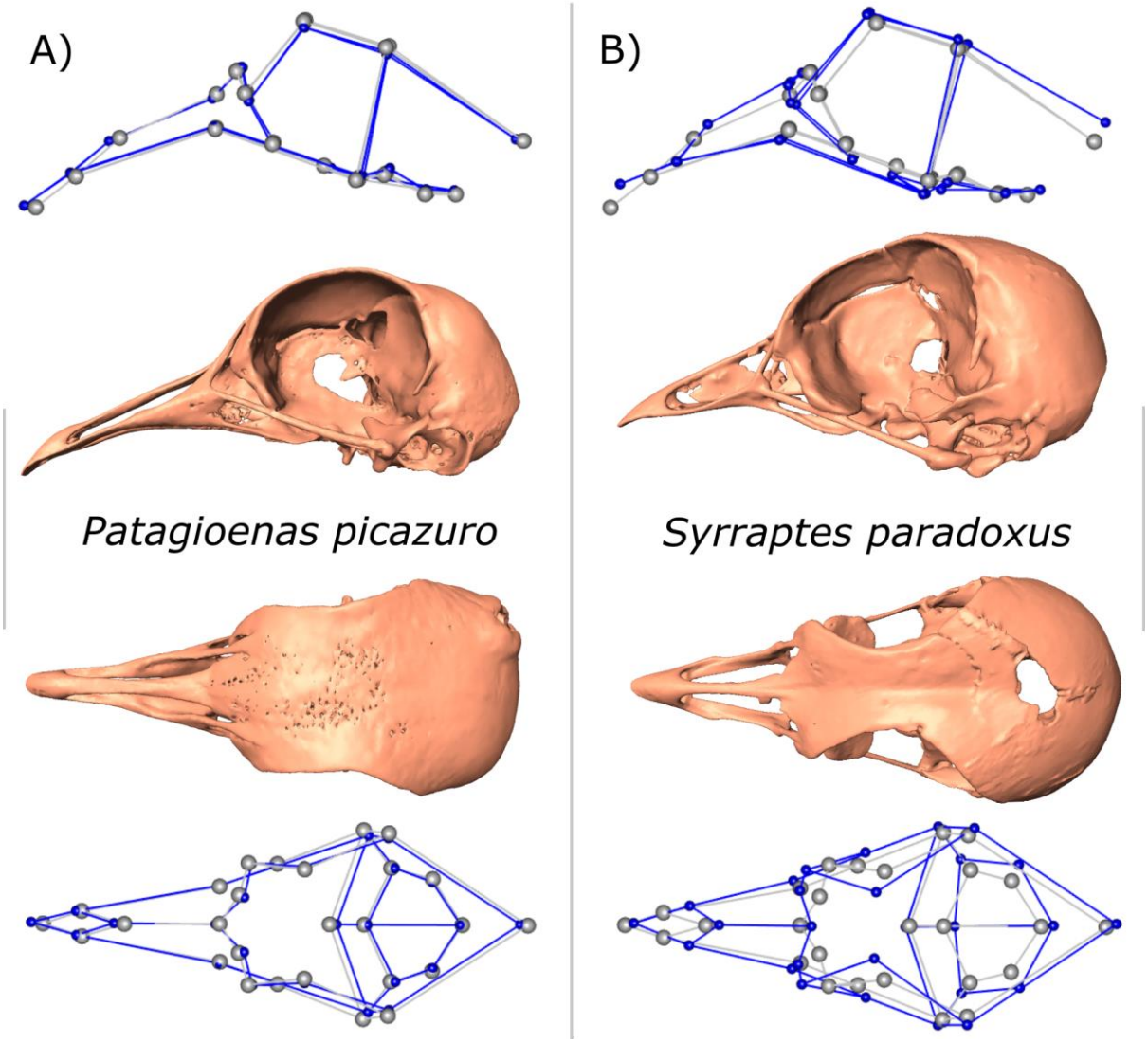


Figure 2.6. Shape of heterochronic Pteroclidiformes. Comparison of the mean Columbiform and skull shape (grey) and the empirical landmark constellations (blue) of a columbiform close to the mean shape (*Patagioenas picazuro*) and a pteroclidiform (*Syrrhaptes paradoxus*). Pteroclidiformes present a short straight rostrum that is shorter than the braincase, the frontal bone is narrow between the orbits, and large orbits.

Visualisation of the skull shapes of these outliers indicate how they differ from allometric expectations (Figure 2.5). *Pezophaps* and *Raphus* appear to follow the allometric shape-change of the reduction of the skull vault and orbit size. However, the expansion of the lateralmost parts of the frontal goes far beyond the allometric expectation. Also, both species show exaggerated features, such as a dorsoventrally deeper rostrum. *D. strigirostris* exhibits an anteroposteriorly shorter rostrum and a mediolaterally broader braincase than expected. *Treron curvirostra* presents a broader braincase and taller rostrum than expected. The braincase of *Syrrhaptes paradoxus* is dorsoventrally expanded beyond the expectation with a anteroposteriorly shorter rostrum than expected. These features resemble the skull expected for a smaller-sized pigeon skull (Figure 2.6). Finally, *Monias* exhibits a skull that is flattened laterally, possesses a comparatively smaller braincase and a longer and more curved rostrum than expected.

Heterochrony in skull shape versus size

The skull shape predicted a higher centroid size for *Monias* than the empirical centroid size (168mm versus 81mm), and a lower centroid size than the empirical centroid size for *Didunculus* (74mm versus 81mm), *Pezophaps* (17cm versus 24 cm), and two pteroclidiforms: *Syrrhaptes paradoxus* (44mm versus 62mm) and *Pterocles senegallus* (61mm versus 52mm). These predicted centroid sizes fall outside of the 95% confidence intervals of the ols models (Figure 2.6, Table 2.3). Centroid size for other outliers like *Treron*

curvirostra differed from 75mm to 86mm, while that of *Chalcophaps indica* differed from 64mm to 82mm. Similar patterns are evident for predicted body mass versus empirical body mass. However, predicted body mass estimates for all pteroclidiforms were lower than empirical body masses, and *Raphus* presented a higher predicted than empirical body mass. These three taxa fell outside the 95% confidence interval of the ols model.

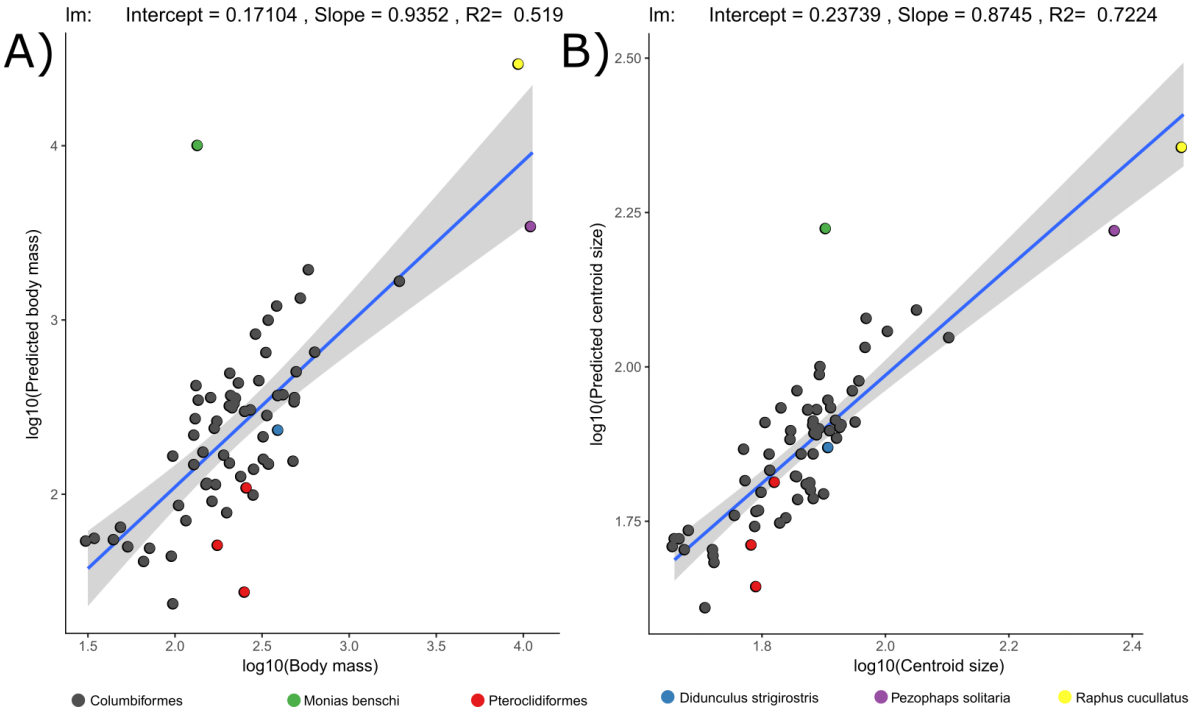


Figure 2.7. Linear model fit for the empirical and predicted sizes using the mean linear D.pgls model coefficients of 200 phylogenies. A) body mass and B) centroid size. While Pteroclidiformes predicted body mass and centroid size is lower than their empirical one, Monias presents the opposite. The size predictions for the dodo and the Rodrigues solitaire are closer to their empirical values.

When the predicted and empirical sizes are fitted in ols models (Figure 2.7), the slopes obtained are lower than one (0.87 for centroid size and 0.94 for body mass). The R^2 is 0.72 for centroid size and 0.52 for the body mass. The overall residuals are smaller for the centroid size model than for the body mass ols model. The species for which heterochonic shape minimized more than 10% of the sum squared residuals (SSR%, Table 2.3) are 13 in

the centroid size model and 17 in the body mass model (12 spp. coincide between models). The direction of heterochrony (paedomorphosis or peramorphosis) was consistent in both models (centroid size and body mass). Paedomorphic species which showed improvement in both models are (Table 2.3): *Syrrhaptes paradoxus*, *Phaps histrionica*, *Ocyphaps lophotes*, *Metriopelia melanoptera*, *Columba rupestris*, *Columba oenas*, *Columba palumbus*, and *Columba livia*. Paedomorphic species which showed improvement in one model are *Phaps chalcoptera* (body mass) and *Columba guinea* (body mass).

Table 2.3. Predicted size and improvement in shape prediction obtained by using heterochronic size in the allometric model. The sum of squared residuals (SSR) was used as the metric of improvement in shape prediction. The percentage of improvement in the sum of squared residuals (SSR %) was calculated as the empirical size SSR – predicted (heterochronic) size SSR, divided by the empirical SSR.

Species	Mass	Predicted mass	Csize	Predicted Csize	SSR % (Csize)	SSR % (Mass)
Alectroenas pulcherrima	165	366	68.3	86.3	4.88	3.61
Alectroenas madagascariensis	173	244	84.0	77.1	2.31	0.47
Aplopelia larvata	155	116	62.8	58.9	1.22	1.33
Claravis pretiosa	68	42	53.0	49.8	0.83	1.75
Columba pulchricollis	330	218	77.0	72.7	2.18	4.95
Columba rupestris	246	129	76.2	63.5	17.61	11.98
Columba vitiensis	353	1018	93.5	108.2	3.53	10.50
Columbina cruziana	50	66	48.3	54.7	11.59	3.10
Columbina passerina	35	57	45.9	53.0	5.31	2.86
Drepanoptila holosericea	215	376	72.5	92.0	9.21	6.05
Ectopistes migratorius	299	847	79.0	100.7	4.60	5.04
Gallicolumba luzonica	196	171	65.5	68.4	0.40	0.27
Geotrygon mystacea	211	328	76.9	80.9	0.17	2.90
Metriopelia ceciliae	55	51	46.7	53.0	1.64	0.18
Patagioenas speciosa	259	305	78.7	79.9	0.09	1.84
Patagioenas nigrirostris	176	116	63.4	63.0	0.07	6.12
Patagioenas plumbea	179	268	70.6	76.7	6.33	7.82
Phaps chalcoptera	331	162	72.4	66.8	5.73	14.67
Phaps histrionica	289	101	72.7	61.3	14.29	23.51
Pterocles senegallus	264	111	66.6	65.4	0.00	1.82
Syrrhaptes paradoxus	257	28	62.1	44.3	12.21	21.89
Treron formosae	140	354	78.0	85.8	1.45	3.75
Columba arquatrix	400	376	83.7	82.4	0.07	0.39

Patagioenas fasciata	343	664	78.8	97.7	19.18	14.18
Columba guinea	352	153	75.0	64.9	9.09	13.37
Patagioenas picazuro	279	311	81.9	79.3	2.29	1.01
Patagioenas squamosa	312	458	82.2	86.4	0.31	1.52
Columba trocaz	511	515	89.1	92.0	0.03	0.00
Columbina talpacoti	46	56	45.5	51.5	4.12	0.46
Geopelia cuneata	32	55	47.6	50.9	2.91	8.06
Geophaps plumifera	98	45	53.2	48.5	3.47	9.10
Geotrygon versicolor	225	339	77.2	78.5	0.12	1.99
Hemiphaga novaeseelandiae	653	667	91.3	95.5	0.80	0.03
Leptotila rufaxilla	157	118	68.0	56.2	2.98	0.81
Leucosarcia melanoleuca	429	380	85.0	80.3	0.92	1.01
Macropygia unchall	168	93	62.2	58.7	0.75	3.18
Ocyphaps lophotes	204	80	69.6	57.3	17.35	22.11
Phapitreron leucotis	108	88	57.4	57.8	0.04	0.87
Petrophassa albipennis	132	151	59.7	65.8	6.99	1.04
Ptilinopus dupetithouarsii	100	169	59.4	74.0	5.58	3.17
Starnoenas cyanocephala	219	320	70.8	79.3	1.77	2.29
Streptopelia turtur	132	223	65.3	72.7	2.01	3.82
Turtur tympanistria	74	50	52.9	50.9	0.53	1.54
Zenaida macroura	119	72	61.9	55.5	7.16	6.73
Caloenas nicobarica	540	1362	101.6	114.8	11.33	20.39
Chalcophaps indica	136	429	64.3	81.8	1.94	5.18
Columba oenas	291	142	76.1	65.3	11.94	13.47
Columba palumbus	490	158	80.1	62.6	12.87	17.07
Didunculus strigirostris	400	238	81.3	74.5	0.17	0.45
Ducula pacifica	395	1227	93.8	120.5	15.38	18.07
Goura cristata	2000	1703	127.7	112.2	2.83	0.37
Pezophaps solitaria	11300	3507	236.7	167.1	2.30	1.63
Phaps elegans	212	154	72.1	66.9	1.62	1.62
Pterocles quadricinctus	180	52	61.1	51.8	2.56	7.34
Treron curvirostra	135	277	75.5	85.6	0.71	2.98
Patagioenas cayennensis	229	363	77.0	82.2	4.62	12.79
Patagioenas leucocephala	238	444	75.5	85.8	6.30	9.17
Patagioenas maculosa	347	289	78.0	78.1	0.01	1.98
Lopholaimus antarcticus	497	346	85.5	81.1	1.06	2.32
Metriopelia melanoptera	100	24	51.4	41.0	13.93	23.00
Otidiphaps nobilis	500	366	90.1	81.9	4.63	3.49
Turacoena manadensis	213	505	81.4	88.8	2.40	7.13
Ducula goliath	600	1983	113.2	124.3	8.03	24.66
Streptopelia decaocto	149	178	73.6	72.7	0.15	0.75
Monias benschi	138	10244	80.5	168.5	26.06	33.56
Raphus cucullatus	9600	30000	304.1	228.1	-5.15	3.05
Columba livia	355	152	77.0	61.6	16.90	17.05

Peramorphic species which showed improvement in both models (Table 2.3) are *Monias benschi*, *Caloenas nicobarica*, *Ducula pacifica*, and *Patagioenas fasciata*. Peramorphic species which showed improvement in one model are *Columba vitiensis* (body mass), *Columbina cruziana* (centroid size), *Patagioenas cayennensis* (body mass), and *Ducula goliath* (body mass). The heterochronic analysis proposed here is capable of identifying the taxa which present clear heterochronic shape and separates them from the species for which regular allometric hypothesis would suffice.

Finally, I performed a series of distance-based pgls models taking heterochronic size as the independent variable (Table 2.4). I found that both allometry and heterochrony are significant variables that can explain the skull shape (P(median)= 0.001, (interquartile range)= 0.001-0.001). Heterochrony (R^2(median)= 0.15, (interquartile range)= 0.14-0.18) can explain more of the sample (columbiforms excluding Raphini) variation than allometry (R^2(median)= 0.1, (interquartile range)= 0.09-0.12). When both variables were taken into account, considering allometric size before heterochronic size (shape = allometry + heterochrony), both allometry (R^2(median)= 0.1, (interquartile range)= 0.09-0.12) and heterochrony (R^2(median)= 0.08, (interquartile range)= 0.07-0.1) were significant (P(median)= 0.001, (interquartile range)= 0.001-0.001). However, when heterochronic size was considered before allometric size only heterochrony was significant (R^2(median)= 0.15, (interquartile range)= 0.14-0.18; P(median)= 0.001, (interquartile range)= 0.001-0.001) and allometry became non-significant (R^2(median)= 0.02, (interquartile range)= 0.01-0.03; P(median)= 0.142, (interquartile range)= 0.026-0.302). Overall these results were expected

because heterochrony is estimated by reducing the sum of squared residuals. However, heterochrony provides independent information when taken into account after allometry.

Table 2.4. Phylogenetic generalized least squares models (median values across 500 phylogenies) explaining skull shape of Columbiformes (excluding Raphus and Pezophaps). Median values are marked with $\bar{x}$. Percentage of significant models across 500 phylogenies is marked as Signif. Significant variables (median P) are marked with *, significant variables which were significant in more than 85% of the phylogenies are marked with *.

Skull shape ~ single explanatory variable												
	Df	F ($\bar{x}$)	Z ($\bar{x}$)	R2 ($\bar{x}$)	R2 (Q2)	R (Q4)	P ($\bar{x}$)	P (Q2)	P (Q4)	*Signif* (%)		
Allometry	1	6.29	4.38	0.1	0.09	0.12	0.001	0.001	0.001	98.2	*	*
Heterochrony	1	10.8	5.58	0.15	0.14	0.18	0.001	0.001	0.001	100	*	*
Skull shape ~ two explanatory variables												
	Df	F ($\bar{x}$)	Z ($\bar{x}$)	R2 ($\bar{x}$)	R2 (Q2)	R (Q4)	P ($\bar{x}$)	P (Q2)	P (Q4)	*Signif* (%)		
Allometry	1	6.8	4.55	0.1	0.09	0.12	0.001	0.001	0.001	98.4		
Heterochrony	1	5.59	4.38	0.08	0.07	0.1	0.001	0.001	0.001	99.8	*	*
Heterochrony	1	10.92	5.6	0.15	0.14	0.18	0.001	0.001	0.001	100		
Allometry	1	1.19	1.08	0.02	0.01	0.03	0.142	0.026	0.302	30.2		

Discussion

Allometry of head size against body size

Raphus and *Monias* bear larger skulls than expected based on their body mass, while most Pteroclidiformes have smaller skulls than expected. The head size of *Pezophaps* falls within the 95% confidence interval of allometric predictions. AIC favours phylogenetic generalized least squares over ordinary least squares models (Table 2.1). For Columbimorphae the ordinary least squares slope was 0.295 and the mean value for the phylogenetic generalized least squares model was 0.285 (sd= 0.00), these values show negative allometry of head size in relation to body mass (Figure 2.1) compared to an expectation under isometry based on purely geometrical scaling of 0.33 (Gould, 1966). Raphini are influential datapoints with large body sizes. The slope is less steep, although still consistent with negative allometry, when they are excluded (ols slope= 0.263; pgls slope(mean)= 0.252, (sd)= 0.00). Negative allometry of skull size may be widespread among tetrapods and similar slopes have been indirectly obtained for rodents (Fitch, 2000; 0.277), theropods (Therrien and Henderson, 2007; at least .278) and can be inferred from rotational inertia studies in therapods and quadrupedal archosaurs (Henderson and Snively, 2004). Allometry is indirectly calculated when the authors tried to predict body size from skull size. Median λ values show that the phylogenetic signal in the relationship between head size and body mass is greatest (λ(median) = 0.68, range= 0.60-0.74) when Columbimorphae are analysed together (i.e. Columbiformes, plus Pteroclidiformes, plus Mesitornithiformes) than for Columbiformes analysed alone (λ(median) = 0.33, (range)=0.16-0.44). λ is slightly greater when the Raphini are excluded (Columbiformes-nP sample; λ(median)= 0.42, (range)=0.29-0.55). The results of analyses using body mass should be interpreted with caution because the body mass

values could be influenced by the uncertainty of the weight estimation of Raphini (Livezey, 1993) and by the use of species mean body mass values instead of individual body mass.

Allometry of skull shape against size

Distance-based regression models indicate significant relationships between skull shape and size using the non-phylogenetic method (D.ols; $P<0.001$). Using the phylogenetic method (D.pgls; Table 2.2), analyses were significant on average for Columbimorphae (centroid size: P(mean)= 0.04; body mass: P(mean)= 0.017) and for Columbiformes (centroid size: P(mean)= 0.039; body mass: P(mean)= 0.017) except for the sample that excluded the Raphini (centroid size and body mass: P(mean)= 0.079) . This analysis shows that skull shape is influenced by skull centroid size (even when phylogeny and phylogenetic uncertainty considered), evidenced by non-negligible mean R^2 values (11.4 to 15.9%). Significance and R^2 (centroid size: D.ols: R^2 = 0.152; D.pgls: R^2(mean)= 0.114, (sd)=0.071) are lowest when Raphini are excluded from the sample.

The identified allometric shape changes are biologically meaningful/correct for all samples. The difference between the R^2 values obtained by Columbiformes and Columbiformes-nP is expected because the allometric models tend to explain less variance of a sample when the size range is reduced excluding the largest specimens in the sample (*Pezophaps* centroid size= 23 cm; *Raphus* centroid size= 30 cm). In datasets with small size ranges, the allometric analysis can mistake other PCs of shape as an allometric component (Mitteroecker *et al.*, 2004; Klingenberg, 2016). This is because the form analyses expect the highest variation in the sample to be size (Mitteroecker *et al.*, 2004; Klingenberg, 2016).

Skull centroid size was a better predictor of skull shape than mean species body mass in all models. This may result from the decoupling of head size and body mass caused by negative allometry of head size (described above). This would indicate that the size of a structure is a better predictor of its shape than the size of the whole animal. The decoupling of body mass from skull shape justifies focusing the discussion on the role of the centroid size in skull shape.

I found evidence for low variation of skull shape among Columbimorphae. Allometry explains only a mean of 11.4% (sd=7.1%; centroid size) of the skull shape variation in columbiforms (Table 2.2). Comparisons of the sum of absolute shape residuals among taxa indicate that the discrepancy between empirical skull shape, and that predicted by allometry, are greatest in the outgroups (Pteroclidiformes and Mesitornithiformes), in Raphini, and in two other columbiforms (*Didunculus strigirostris* and *Treron curvirostra*).

Heterochrony in columbiform evolution

It is generally accepted that in a multi-species sample the allometric patterns identify the "evolutionary allometry" that describe the common variation in all species due to size change, and not the allometric variation within a particular species (Mitteroecker *et al.*, 2004; Adams, 2014). In line with evolutionary allometry is the evolutionary definition of heterochrony, which is the change in rates and timing of developmental process due to the interplay between size, shape and age. (Gould, 1977; Klingenberg, 1998; Mitteroecker, Gunza and Bookstein, 2005). These changes, which are measurable only at a species level as ontogenetic trajectories, can influence and direct the morphological variation among related taxa over evolutionary time (Klingenberg, 1998; Mitteroecker, Gunza and Bookstein,

2005). These changes are possibly related to the patterns of covariation found in the additive genetic matrix and reflected in the phenotype and manifesting as evolutionary lines of least resistance (Lande, 1979; Schluter, 1996; Marroig and Cheverud, 2005, 2010). In this multidimensional theoretical framework, I implemented a test for heterochrony that show that heterochrony plays a significant role in the explaining patterns of phenotypic evolution in Columbiformes.

The proposed heterochronic test uses shape to predict size based on the inter-specific allometric model and evaluates the extent to which this predicted 'heterochronic' size improves the proportion of shape variance explained by the allometric model (Table 2.3). Predicted skull sizes based on skull shape tended to be lower than the empirical ones as the size increases (ordinary least squares [i.e. non-phylogenetic] centroid size slope = 0.876, [compared to 1.0 expected under isometric]; Figure 2.7).

Heterochronic changes are good for describing some shape changes in shape outliers of Columbimorphae, such as paedomorphosis in Pteroclidiformes and peramorphosis in Mesitornithiformes. However, columbiform shape outliers (*Raphus*, *Pezophaps*, *Didunculus*, *Treron*) do not match predictions of the heterochronic hypothesis.

Heterochrony can explain more than 8% (distance-based pgls R^2 median) of the unexplained variation after allometry in the columbiforms (Table 2.4). However, heterochrony improved the shape prediction in more than 10% in 18 species of the sample (13 spp. for centroid size and 17 spp. for body mass; Table 2.3). These 18 species which have strong evidence of heterochrony are not the same as the identified shape outliers of the allometric model (Figure 2.4 and 2.5). The peramorphic species identified are mostly

frugivorous: frugivorous mostly arboreal foraging species (*Patagioenas cayennensis*, *Ducula goliath*, *Ducula pacifica*, and *Columba vitiensis*), a frugivorous terrestrial foraging species (*Caloenas nicobarica*), a frugivorous generalist forager (*Patagioenas fasciata*), a granivorous ground forager (*Columbina cruziana*) and an insectivorous ground forager (Monias benschi).

The identified paedomorphic species are mostly granivorous ground foragers: *Syrrhaptes paradoxus*, *Phaps chalcoptera*, *Phaps histrionica*, *Ocyphaps lophotes*, *Metriopelia melanoptera*, *Columba guinea*, *Columba rupestris*, and *Columba livia* (wild diet; Hoyo *et al.*, 2017). The other identified paedomorphic species have generalist diets and foraging habits: *Columba oenas*, *Columba palumbus*, and *Columba livia* (diet in urban populations; Spennemann and Watson, 2017).

Distribution likely influences the skull shape in Columbiformes

I found that all outliers whose shape could not be satisfactorily explained by allometry or described by heterochrony (Raphini, *Didunculus, Treron*, *Ptilinopus dupetithouarsii*, and *Chalcophaps indica*) are insular taxa with frugivorous diets (although *C. indica* inhabits both continents and islands and has a more generalist diet which includes seeds and live prey). Island distribution can accelerate evolutionary rates though ecological release or other factors (Van Valen, 1965; Millien, 2006; Parent and Crespi, 2009; Presgraves and Glor, 2010; Tokita *et al.*, 2016). I further examine the influence of distribution (type and area in km^2) in Chapter Three.

An unexpected result was that most paedomorphic species are distributed on continents while peramorphic species are distributed on both continents and islands. The apparent

relationship between heterochrony and distribution could suggests that heterochrony and evolution in the lines of least evolutionary resistance (allometry [Schluter, 1996; Marroig and Cheverud, 2005] and heterochrony) is a prominent mechanism for the morphological evolution in areas where the niche is constrained by competition (Hardin, 1960; Millien, 2006; Bolnick *et al.*, 2010; Mahler *et al.*, 2010). The statistical appraisal of the relationship between heterochrony and distribution opens a new exiting avenue for future research.

Influence of allometry and heterochrony on the outlier skull shape

Shape change visualization was used to show that a good way to avoid the overfitting of the allometric models towards the distinct skull shape of Raphini was to exclude this clade from shape prediction (Figures 2.2 and 2.3). Visualization of the shape changes was performed using the mean coefficients of the multi-phylogeny distance-based phylogenetic generalized least squares model of the columbiform sample excluding the Raphini.

Pteroclidiformes

Several pieces of information provide convincing evidence of paedomorphosis in Pteroclidiformes: (1) in an allometric model, the skull shape is relatively far from the one expected for a pigeon of their size, and close to the one of the smallest columbiforms (Table S2.5); (2) they have a short straight rostrum that is shorter than the braincase, the frontal bone is narrow between the orbits (Figure 2.6 and 2.7); (3) The range of centroid sizes (61 to 67 mm) is more constrained and near the mean values of the total range of centroid sizes (46 to 236 mm) of Columbiformes (Table S2.5); (4) two pteroclidiforms (*Syrrhaptes paradoxus* and *Pterocles quadricinctus*) presented predicted centroid sizes much smaller than the empirical ones (Table 2.3, Figure 2.7); (5) heterochronic (predicted) size greatly

improves the shape prediction in one pteroclidiform (centroid size: 12%; Table 2.3); (6) predicted body masses for all pteroclidiforms are much lower than the reported size range of the species (Table S2.6); and (7) the head size of pteroclidiforms seem to be smaller than the one expected for their body sizes (Figure 2.1). The common allometric analysis suggested that pteroclidiforms follow a similar but parallel allometric path to columbiforms (conservative RSC; Appendix One).

Monias benschi

I found convincing evidence of peramorphosis in *Monias*: (1) the shape of *Monias* seem to be similar to the expected shape of a large pigeon (10 kg; Figure 2.1, Table 2.3); (2) predicted centroid size (16 cm) is the double of the empirical centroid size (Table 2.3); (3) the predicted centroid size falls outside the 95% confidence interval of the ordinary least squares model of empirical versus predicted size (Figure 2.7); (4) the improvement in shape prediction obtained when the heterochronic (predicted) size was used was the highest improvement for all species in the sample (26% centroid size); (5) the predicted body size for this species was an order of magnitude larger than the reported body mass and double the centroid size; and (6) *Monias* presents a larger head than the one expected for a Columbimorphae of its size (Figure 2.1).

Despite the evidence presented above, it is necessary to note that *Monias* is the only mesitornitform included in the analysed sample. The results presented here for *Monias* must be analysed with caution because it is not possible to compare the allometric trajectory of a cloud of points to a single point from the standpoint of the multivariate heterochrony (Mitteroecker, Gunza and Bookstein, 2005). To further test my heterochronic

hypothesis it would be necessary to obtain a large sample of individuals and species of Mesitornithiformes. These individuals were not included in the sample because the sampling aimed to be comparative across Columbimorphae. The sampling of this depauperate clade (3 spp.) and the evaluation of its ontogenetic and allometric trajectories (Mitteroecker *et al.*, 2004; Mitteroecker, Gunza and Bookstein, 2005) is an exciting new avenue of research.

Nonetheless, if the detected heterochronic patterns of *Monias* are correct, this would have remarkable implications for the interpretation of the evolution of Columbimorphae as a whole. Mesitornithiformes are the sister taxa of Pteroclidiformes, and they together are the sister clade to Columbiformes (Jetz *et al.*, 2012; Prum *et al.*, 2015; Soares *et al.*, 2016). My findings suggest that ancestral shape variation was similar to the present day columbiform variation. Two different hypotheses about the changes in allometry can be proposed. First, from this basal group, a highly variable clade diverged and was the ancestor of both Mesitornithiformes and Pteroclidiformes. Second, Mesitornithiformes and Pteroclidiformes might form part of an unknown diverse clade with an overall morphological range similar to extant Columbiformes. Mesitornithiformes and Pteroclidiformes would represent the only surviving clades, representing only the morphological extremes of paedomorphosis and peramorphosis. The second proposal could be supported by the current distribution of the clade and by the fact these are species-poor clades compared with Columbiformes. Pteroclidiformes is represented by 16 species with desertic adaptations distributed in Africa, Madagascar, the Middle East, India, and the south of Europe, while Mesitornithiformes are only represented by three species, all distributed in Madagascar.

The Raphini

The shape changes identified in the allometric model can explain some of the unusual aspects of skull shape in Raphini (Figure 2.2). Shape changes like the dorsoventral compression of the rostrum, lateral expansion of the frontal, reduction of the orbits, and enlargement of the rostrum compared with the braincase were predicted for large pigeons even when these species were excluded from the analysis (Figure 2.2C). However, the identified allometric shape changes did not explain some aspects of the empirical shapes of Raphini. The shape changes present in the skulls of *Raphus* and *Pezophaps* that are not predicted by the pgls model of the Columbiform-nP sample are: (1) dorsoventrally taller beaks (versus dorsoventrally narrow beaks); (2) anteriorly expanded rostra with less curved beaks (versus expanded rostra presenting a ventral curvature in the midsagittal plane); (3) lower basicranial flexion than expected *i.e.*, alignment of rostrum and the base of the braincase in a straight axis (versus crania with high basicranial flexion); and (4) the prominent mediolateral expansion of the orbital rim (versus skulls with similar expansion to the mean shape).

Pezophaps showed little evidence of paedomorphosis: the predicted centroid size was much lower (16.7cm) than the empirical centroid size (23.6cm), falling outside the 95% confidence interval (Table 2.3, Figure 2.7). However, the following suggest that heterochrony does not play a major role in accounting for the skull shape of *Pezophaps*: (1) heterochronic centroid size only improved the shape prediction in 2.3% (Table 2.3); (2) overall the skull shape is similar to the allometric prediction for a Columbimorphae of that size (Figure 2.5); and (3) the head size of *Pezophaps* falls within the 95% CI showing the

head size of this species is what could be expected for a Columbimorphae of that size (Figure 2.1).

Raphus also showed conflicting heterochronic evidence: (1) predicted centroid size (23cm) was lower than empirical centroid size (30cm); (2) heterochronic centroid size did not improve the shape prediction (-5.5%; Table 2.3); (3) the predicted centroid size falls within the 95% confidence interval of the linear model (Figure 2.7); and (4) the head size of the dodo was larger than the one expected for a Columbimorphae of their size (Figure 2.1).

Treron curvirostra

The skull shape of *T. curvirostra* cannot be explained by allometry or heterochrony, highlighting the necessity of different explanatory variables for this species. *T. curvirostra* shows a skull that is broader laterally than expected, with a dorsoventrally taller rostrum in the midsagittal plane than expected. Heterochronic centroid size barely improved the shape prediction (0.71%; Table 2.3).

Didunculus strigirostris

Besides the genus *Treron*, *D. strigirostris* is the only other pigeon that can tear food items (Goodwin, 1983). *Didunculus* can also use its beak to open *Dysoxylum* spp. (wild mahogany tree; Hoyo *et al.*, 2017) seeds in a similar way to parrots. This feeding adaptation seems to be a more likely explanation for most of *Didunculus* skull shape than allometry. However, *D. strigirostris* was the most disparate species in the sample: (1) it was the species with the largest sum of squared residuals (Figure 2.5), presenting higher values than any other Columbimorphae; (2) it presents a robust skull with a short robust dorsoventrally expanded rostrum that differs substantially from the predicted shape for a pigeon of that size (Figure

2.5); (3) observing that this pigeon presents larger orbits and a shorter rostrum than expected could suggest some paedomorphosis has taken place in this species; (4) the predicted centroid size (7.5 cm) was lower than empirical centroid size (8.1cm; Table 2.3). However, heterochronic centroid size did not improve the shape prediction much (0.17% for centroid size); (5) the head size of *Didunculus* fell within the expected size for a columbiform of its size (Figure 2.1C); and (6) the predicted centroid size was lower than the empirical one, falling outside the 95% confidence interval.

Allometry and heterochrony are not enough to explain the "strange" skull of the Raphini

The Raphini have historically been characterised morphologically as the most eccentric columbiforms (Owen, 1866; Livezey, 1993; Shapiro *et al.*, 2002; Claessens, Meijer and Hume, 2015). Historically, heterochrony has been proposed as a mechanism that could explain some of the features of the raphine skull (Livezey, 1993; and was suggested for other structures by Owen, 1866). Furthermore, a series of recent publications highlight that development constraints (such as allometry and modularity) seem to be leading factors in morphological evolution in bird crania (Bright *et al.*, 2016; Cooney *et al.*, 2017; Young *et al.*, 2017). Therefore, I expected to find evidence that allometry and heterochrony satisfactorily explained the skull morphology of *Raphus* and *Pezophaps*. Another reason to expect these taxa following allometry and heterochrony is given by the theory of lines of least evolutionary resistance in which recently diverging species are expected to follow closely the lines of least evolutionary resistance (Lande, 1979; Schluter, 1996; Marroig and Cheverud, 2005). These lines of least evolutionary resistance are a by-product of the

correlation of characters in the phenotypic and genotypic matrix and are identifiable as the largest axis of variation in a sample (Lande, 1979; Marroig and Cheverud, 2005) which is often related to overall size changes (Lande, 1979; Schluter, 1996; Marroig and Cheverud, 2005, 2010). Contrary to my initial expectations, allometry and heterochrony do not satisfactorily explain some aspects of the skull shape in Raphini. I found that *Pezophaps* follows the allometric expectations of shape and size more closely than *Raphus*. Raphini showed some evidence of heterochrony but the use heterochronic size did not improved the shape prediction for these species (However, see discussion about size prediction and its implications for the "fat" dodo hypothesis; Appendix One).

Morphological disparity of Raphidae

It is necessary to highlight the high morphological diversity of the Raphidae clade which includes *Raphus*, *Pezophaps*, *Goura*, *Didunculus*, and *Caloenas* (Shapiro *et al.*, 2002; Pereira *et al.*, 2007; Soares *et al.*, 2016) and likely also *Otidiphaps* and *Trugon* (Pereira *et al.*, 2007; Lapiedra *et al.*, 2013). Raphidae therefore includes three of the most conspicuous outliers in terms of skull shape among columbiforms (*Didunculus* and the Raphini). Raphidae also includes *Goura cristata* which is the largest extant pigeon (2000g), and two other large pigeons: *Trugon terrestris* (400g) and *Otidiphaps nobilis* (500g). This clade also includes fossil species like *Caloenas maculata* (of uncertain geographic provenance; Heupink, Van Grouw and Lambert, 2014) and the flightless, dodo-sized *Natunaornis gigoura* of Fiji (Worthy, 2001). Raphidae has clearly produced highly divergent morphologies compared with other pigeons. However, the developmental constraints

(allometry and heterochrony) of other columbiforms are not enough to account for the morphological evolution of these species.

Age of divergence

The age of divergence of Raphini is key to interpret the morphological disparity of this group (Shapiro *et al.*, 2002; Pereira *et al.*, 2007; Soares *et al.*, 2016). Molecular evidence suggests that the distinct morphology of *Raphus* and *Pezophaps* probably evolved in the last 13.1mya (9.5–17.3mya; Soares *et al.* (2016). However, Mauritius emerged 6.8 to 7.8mya and Rodrigues emerged 1.5mya (Shapiro *et al.*, 2002). These geological dates would suggest that the ancestor of *Raphus* and *Pezophaps* was able to fly thus suggesting that most of the morphological disparity of the Raphini (or at least *Pezophaps*) was acquired in the last 1.5 million years. However, a stepping-stone dispersal could account for an older date of morphological diversification through flightlessness (Shapiro *et al.*, 2002). In this comparatively short time, the Raphines seem to have been able to obtain a distinct morphology by escaping the constraints marked by allometry and heterochrony in columbiforms. These constraints seem to be present in most pigeons and might have been conserved from the origin of crown Columbiformes in the Eocene (30-45mya; Pereira *et al.*, 2007) or late Oligocene-Miocene (18.9–31.3mya, Soares *et al.*, 2016).

Ecomorphology and the skull shape in Columbiformes

Diversification of feeding mode has been historically contemplated as a driver of morphological evolution (Darwin, 1859; Herrel *et al.*, 2005; Foster, Podos and Hendry, 2008; Slater and Van Valkenburgh, 2009; Dumont *et al.*, 2014; Gill *et al.*, 2014) in an adaptationist program (Mayr, 1983). The columbiform outliers (*Treron curvirostra* and

Didunculus strigirostris, *Pezophaps*, and *Raphus*) seem to share some characters consistent with evolutionary divergence in feeding strategies influencing the skull shape, and resulting in a robust, tall rostra, with possibly increased bending strength in *Pezophaps*, *Didunculus* and *Treron* (Owen, 1866; Livezey, 1993; Dicker, Pennock and Shigley, 2003; Martínez-Gómez *et al.*, 2009; Tanner *et al.*, 2010; Tseng, 2013). Increased bending resistance due to a change of material distribution is a well-known phenomenon in engineering (Dicker, Pennock and Shigley, 2003), and these structural properties have been characterized in biological structures like skulls (Cuff and Rayfield, 2013). *Didunculus* is the only pigeon capable of opening seeds, while pigeons in the *Treron* genus are the only pigeons capable of cutting large fruit into smaller chunks (Goodwin, 1983; Hoyo *et al.*, 2017). Other taxa that fell outside one standard deviation of the SSR (*Ptilinopus dupetithouarsii* and *Treron formosae)* also eat exclusively fruit.

Therefore, my results suggest that dietary factors like main food item or foraging might be correlated with an important adaptive component of shape evolution in Columbiformes. The importance of ecomorphology in morphological evolution has been downplayed by recent publications that focus on the role of development and modularity in morphological evolution (Bright *et al.*, 2016; Cooney *et al.*, 2017; Young *et al.*, 2017). Even when development is taken into account in the form of allometry and heterochrony, I found circumstantial evidence that diet might have an important effect on morphological evolution. A statistical appraisal of the role of ecomorphology in the columbiform skull shape evolution is provided in Chapter Three while taking in account modularity.

Ecomorphology and the skull shape of Raphini

The skull shape of the Raphini, especially the dodo, has been hypothesized to be related to the inclusion of animals in the diet (Owen, 1866; Livezey, 1993). These hypotheses state that animals would be included in the diet of Raphini sporadically and as supplement of their diets of fallen fruit and seeds, with bulbs also hypothesized to be used as a food resources by these obligate ground dwelling birds (Owen, 1866; Goodwin, 1983; Livezey, 1993; Angst, Buffetaut and Abourachid, 2011). I noted that Raphini shows some morphological similarities to other fruit eating outliers (*T. curvirostra* and *Didunculus*). These similarities could suggest an agreement with classical hypothesis of Raphini which argue for these animals feeding on fallen fruit on the forest ground (Hachisuka, 1953 in Livezey, 1993). Further evaluation of the biomechanical performance of the skull shape in Raphini (Chapter Three) is needed to assess if the biomechanical performance of these species corresponds to a frugivorous diet or to live prey consumption.

Conclusions

Allometry of head size against body size

- *Raphus* and *Monias* present larger skulls than expected based on their body mass
- Most Pteroclidiformes have smaller skulls than expected.
- The head size of *Pezophaps* falls within the 95% confidence interval of allometric predictions.
- Negative allometry of head size in relation to body mass is present in all samples.
- The phylogenetic signal (λ) in the relationship between head size and body mass is greater in Columbimorphae than for Columbiformes.

Allometry of skull shape against size

- The relation between skull shape and size using the non-phylogenetic method is significant. If phylogeny is taken into account, the relation is only significant for Columbimorphae and for Columbiformes but not for the sample excluding Raphini.
- Nevertheless, skull shape is influenced by skull centroid size, evidenced by non-negligible mean R^2 values (even in the sample excluding Raphini).
- The non-significance of the allometric shape changes, when excluding Raphini form the sample, is likely an artefact provoked by the removal of the largest centroid sizes from the sample.
- Skull centroid size was a better predictor of skull shape than mean species body mass.
- There is evidence of low variation of skull shape among Columbimorphae.
- Allometry explains only a mean of 11.4% of shape variation in Columbiformes.
- Outliers from the allometric model are Pteroclidiformes, Mesitornithiformes, Raphini, and in two other columbiforms (*Didunculus strigirostris* and *Treron curvirostra*).

Heterochrony in columbiform evolution

- A new test for heterochrony based on the size prediction using shape is implemented.
- Heterochrony plays a significant role in the phenotypic evolutionary patterns observed in Columbimorphae.
- Heterochronic changes are good for describing some shape outliers such as paedomorphosis in Pteroclidiformes and peramorphosis in Mesitornithiformes.
- Columbiform shape outliers (*Raphus*, *Pezophaps*, *Didunculus*, *Treron*) do not match predictions of the heterochronic hypothesis.
- Heterochrony can explain more than 8% of the unexplained variation after allometry in the columbiforms.
- Heterochrony improved the shape prediction in more than 10% in 18 species of the sample (13 spp. for centroid size and 17 spp. for body mass).
- The identified peramorphic species are mostly frugivorous.
- The identified paedomorphic species are mostly granivorous ground foragers.
- Most paedomorphic species are distributed on continents while peramorphic species are distributed on both continents and islands.
- The apparent relationship between heterochrony and distribution could suggest that heterochrony is a prominent mechanism for the morphological evolution in areas where the niche is constrained by competition.

Skull shape, allometry and heterochrony of outlier species

- **Pteroclidiformes** show strong evidence of paedomorphosis.
- Common allometric analysis suggested that Pteroclidiformes follow a similar but parallel allometric path to columbiforms (Appendix One).
- ***Monias*** show strong evidence of peramorphosis.

- The allometric model (of the sample excluding Raphini) can account for some of the unusual aspects of skull shape in **Raphini:** dorsoventral compression of the rostrum, lateral expansion of the frontal, reduction of the orbits, and enlargement of the rostrum compared with the braincase.
- Unusual aspects of skull shape in **Raphini** that are not accounted by allometry are: dorsoventrally taller beaks; anteriorly expanded rostra with less curved beaks; lower basicranial flexion than expected; and the prominent mediolateral expansion of the orbital rim.
- Heterochrony does not play a major role in accounting for the skull shape of Raphini.
- The skull shape of ***Treron curvirostra*** cannot be explained by allometry or heterochrony. This species shows a skull that is broader laterally than expected, with a dorsoventrally taller rostrum in the midsagittal plane than expected.
- ***Didunculus strigirostris*** was the most disparate species in the sample. It presents a robust skull with a short robust dorsoventrally expanded rostrum that differs substantially from the predicted shape for a pigeon of that size.

Diet and skull shape

- The outliers whose shape could not be satisfactorily explained by allometry or described by heterochrony (Raphini, *Didunculus, Treron*, *Ptilinopus dupetithouarsii*, and *Chalcophaps indica*) are all fruit eaters except for *C. indica*.
- The columbiform outliers (*Treron* and *Didunculus*, and the Raphini) exhibit robust, tall rostra, which suggests an increased bending resistance and an adaptation to similar feeding strategies.

- *Didunculus* is the only pigeon capable of opening seeds (of the wild mahogany tree), while *Didunculus* and pigeons in the *Treron* genus are the only pigeons capable of cutting large fruit into smaller chunks.
- Even when development (allometry and heterochrony) is considered, diet might have had an important effect on morphological evolution.
- Other feeding strategies (diet which includes animal matter, crabs or roots) could also influence the shape of the skull in Raphini.

The "strange" skull of Raphini and the high morphological diversity of Raphinae

- I found a high morphological diversity of the Raphidae clade which includes *Raphus*, *Pezophaps*, *Goura*, *Didunculus*, and *Caloenas*.
- Raphidae has produced highly divergent morphologies compared with other pigeons. It includes three of the identified outliers in terms of skull shape among columbiforms (*Didunculus* and the Raphini). Raphidae also includes *Goura cristata* which is the largest extant pigeon and *Natunaornis gigoura* (another dodo-sized species).
- The developmental constraints (allometry and heterochrony) of other columbiforms are not enough to account for the morphological evolution of these species.
- Adaptation to ecomorphological factors (such as main foraging/main diet and live prey consumption) is likely to have played a major role in the morphological evolution of these species.

Mass prediction and its significance for the "fat" dodo (Appendix One)

- The predicted body mass was 30kg. However, I do not argue for a "fat" dodo because the calculated heterochronic size did not improve the shape prediction in this species.

Supplementary material (S2)

Supplementary figures

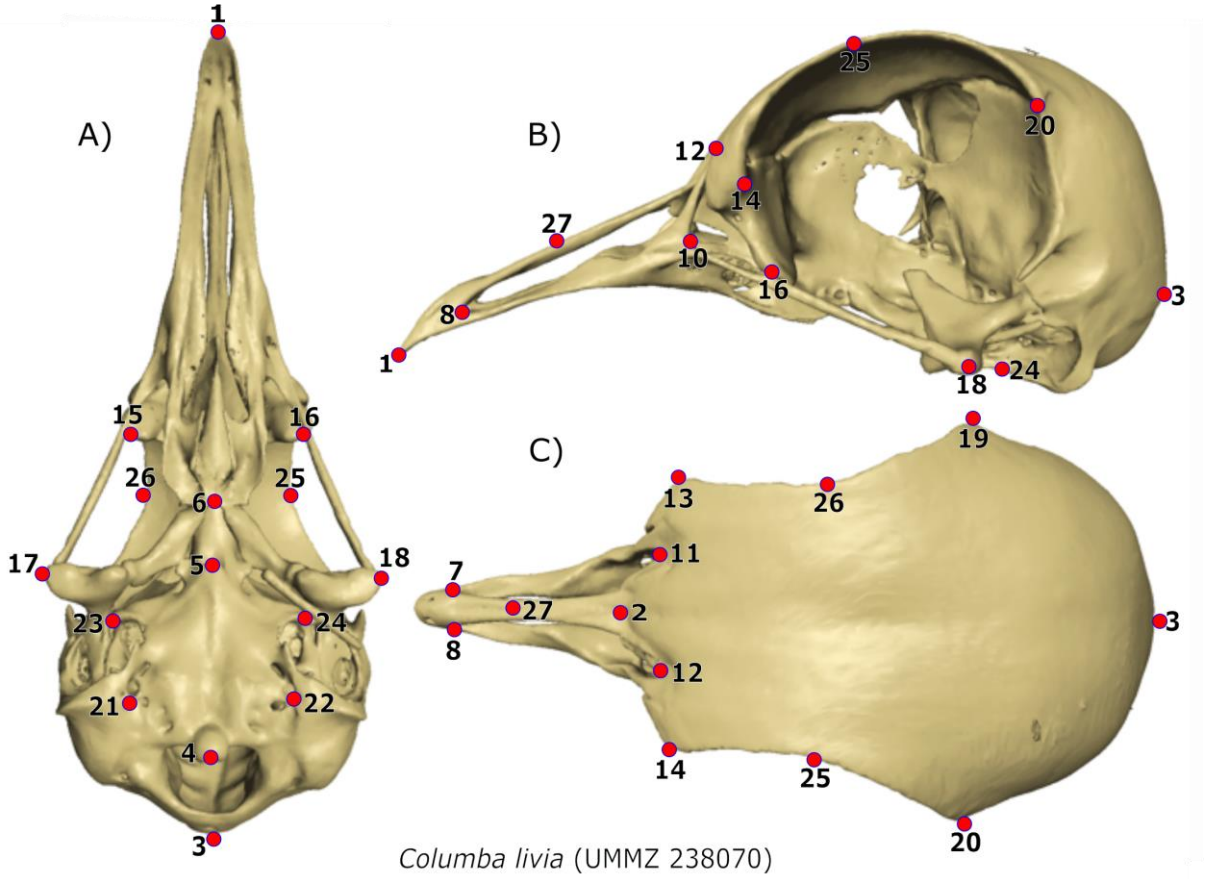


Figure S2.1. The 27 landmarks used in this study displayed in *Columba livia* (UMMZ 238070). A) ventral view; B) left lateral view; C) dorsal view. Landmarks 1 to 24 are type I landmarks, landmarks 25-27 are Type II landmarks. Anatomical description of the landmarks can be found in Table S2.3.

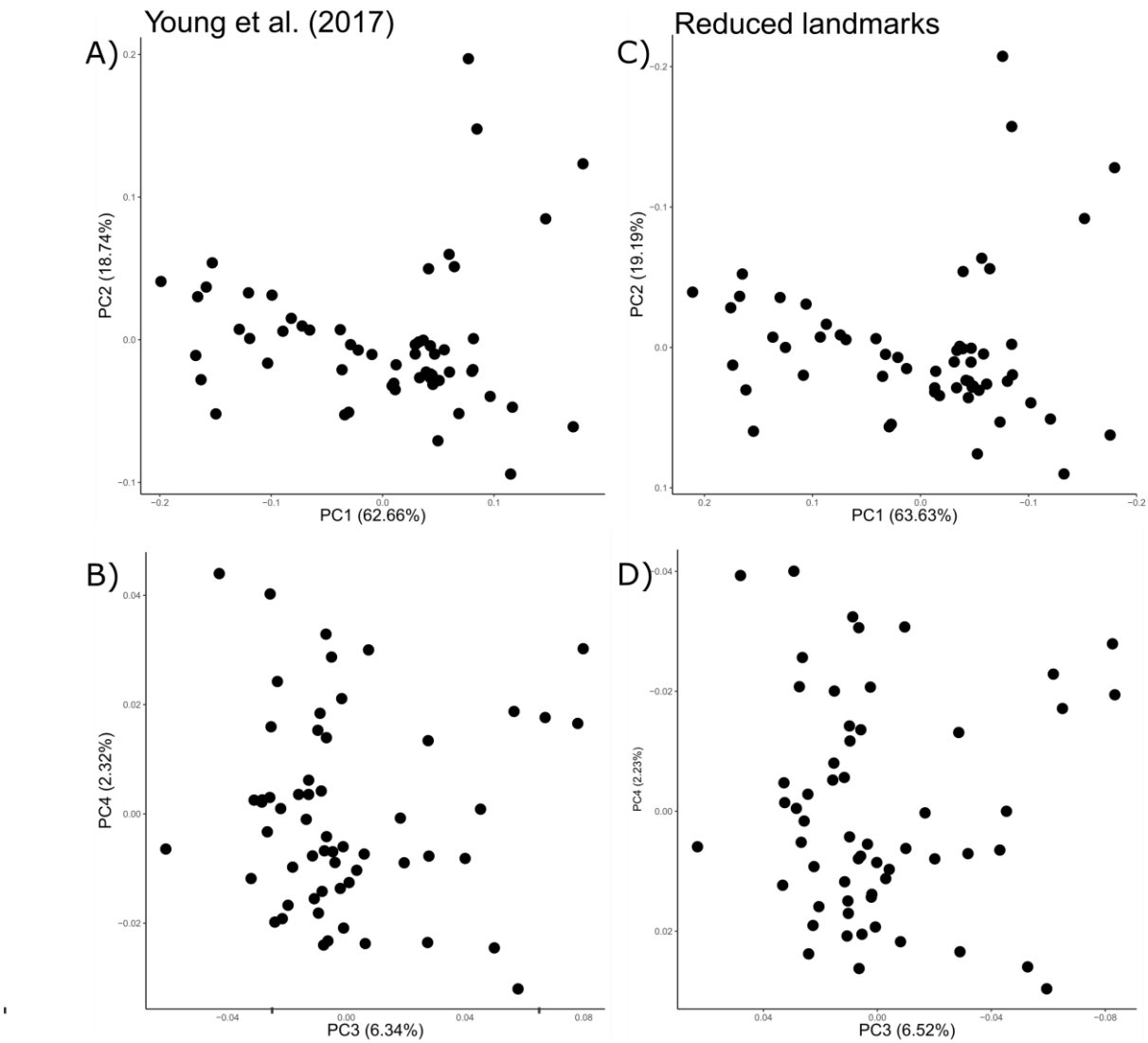


Figure S2.2. Differences in the ordination obtained for Young et al. (2017) when the original landmark system is used versus the reduced landmark system used in this chapter. Variation explained by each PC axis and the ordination of data points seems to remain stable in the first three PCs: 88% of variation in original landmarks and or 89% of variation of reduced landmarks.

Supplementary Tables

Table S2.1. Dodo and Rodrigues solitaire mass estimates. Augmented from (van Heteren et al., 2017)

Study	Comparative sample (number of species)	Elements	Measurement	Dodo mass in kg (sample size)	Solitaire mass in kg (sample size)	Remarks
Campbell and Marcus (1992)	All birds (387)	F	Circumference	13.2–16.4 (3)		
Livezey (1993)	Columbidae (187)	F	Length	Male: 10.6 (7)	13.9 (6)	"Flighted" model
				Female: 8.6 (8)	8.7 (19)	
				Male: 15.9 (7)	20.9 (6)	50% addition to correct for flightlessness or fat condition
				Female: 12.9 (8)	13.1 (19)	
				Male: 21.2 (7)	27.8 (6)	100% addition to correct for flightlessness and fat condition
				Female: 17.2 (8)	17.4 (19)	
Kitchener (1993)	Columbidae (32)	F, TT, TMT	Length, diameter	10.6–17.5 (29 F, 32 TT, 26 TMT)		
Angst, Buffetaut and Abourachid (2011a)	All birds (323)	F, TT, TMT	Length	10.5 (25 F, 27 TT, 30 TMT)		Based on the regression of Zeffer, Johansson and Marmbebro (2003)
Louchart and Mourer-Chauviré (2011)	All birds (387)	F	Circumference	11.7–15.4 (3)		Based on the regressions of Campbell and Marcus (1992)
	Heavy terrestrial birds	F	Circumference	9.5–12.3 (3)		
Heteren et al. (2017)	Columbidae, Galloanserae, Tinamiformes and Ratites (53)	F	Circumference	All birds: 14.1 (174)		Based on 174 dodo femora and regressions with Campbell and Marcus dataset.
				Heavy bodied: 13.6 (174)		
				Flightless: 12.4		
Brassey et al. (2016)	Columbifomes (20)	All	Convex hull	10.8-14 (3)		Three complete composite skeletons

Table S2.2. Specimens in the sample, missing landmarks, and missing landmarks after reflection

Specimen	Origin and Date	Specimen ID	n LM missing	which LM?	missing after reflection	which LM?
Lopholaimus antarcticus	NHMUK May 2016	BMNH 1864.12.20.9	0		0	
Columba leucocephala	NHMUK May 2016	BMNH S/1952.2.393	0		0	
Turacoena manadensis	NHMUK May 2016	BMNH 1871.9.13.1	1	7	0	
Metriopelia melanoptera	NHMUK May 2016	BMNH 1871.10.20.4	0		0	
Columba picazuro	NHMUK May 2016	BMNH 1898.10.1.1	2	5 &17	1	5
Columba trocaz	NHMUK May 2016	BMNH 1937.11.2.2	0		0	
Columba squamosa	NHMUK May 2016	BMNH 1898.7.10.1	1	18	0	
Phapitreron leucotis	NHMUK May 2016	BMNH 1903.7.27.1	0		0	
Columba maculosa	NHMUK May 2016	BMNH 1859.7.30.14	0		0	
Leucosarcia melanoleuca	NHMUK May 2016	BMNH 1861.8.21.2	0		0	
Columbina talpacoti	NHMUK May 2016	BMNH S/1974.11.11	2	1 & 8	1	1
Turtur tympanistria	NHMUK May 2016	BMNH S/1975.45.8	0		0	
Geophaps plumifera	NHMUK May 2016	BMNH S/1973.71.13	0		0	
Geopelia cuneata	NHMUK May 2016	BMNH S/1981.93.8	0		0	
Columba cayennensis	NHMUK May 2016	BMNH 1868.9.12.6	0		0	

Starnoenas cyanocephala	NHMUK May 2016	BMNH 1863.12.28.7	1	16	0	
Leptotila rufaxilla	NHMUK May 2016	BMNH 1903.12.20.248	0		0	
Macropygia unchall	NHMUK May 2016	BMNH 1871.7.21.9	0		0	
Ptilinopus dupetithouarsii	NHMUK May 2016	*BMNH S/1975.9.3	0		0	
Petrophassa albipennis	NHMUK May 2016	BMNH S/1969.4.14	1	11	0	
Zenaida macroura	NHMUK May 2016	BMNH S/1984.77.44	0		0	
Columba guinea	NHMUK May 2016	BMNH S/2007.116.1	0		0	
Ocyphaps lophotes	NHMUK May 2016	BMNH S/1964.1.26	0		0	
Streptopelia turtur	NHMUK May 2016	BMNH S/1984.100.11	0		0	
Columba arquatrix	NHMUK May 2016	BMNH S/2011.20.1	0		0	
Geotrygon versicolor	NHMUK May 2016	BMNH S/2016.9.2	0		0	
Hemiphaga novaeseelandiae	NHMUK May 2016	BMNH S/2002.46.6	1	3	1	3
Columba fasciata	NHMUK May 2016	BMNH S/1952.2.395	0		0	
Ducula pacifica	Tempo	UMZC 409.B	0		0	
Goura cristata	Tempo	UMZC 413.B1	1	24	0	
Treron curvirostra	Tempo	UMZC 413	1	17	0	
Chalcophaps chrysochlora	Tempo	UMZC 413.C	0		0	
Caloenas nicobarica	Tempo	UMZC 412.A	0		0	
Columba palumbus	Tempo	UMZC 409.A	1	17	0	
Columba oenas	Tempo	UMZC 410.A	0		0	
Columba livia	Tempo	NMS (not registered)	4	8, 10, 17 & 18	2	17 &18

Alectroenas madagascariensis	Tempo	UMZC 413.E	1	7	0	
Phaps elegans	Tempo	UMZC 410.C	0		0	
Pezophaps solitaria	Tempo	UMZC 415.R	5	13, 14, 15,16 & 21	4	13, 14, 15 & 16
Caloenas nicobarica	Tempo	FMNH 314877	0		0	
Didunculus strigirostris	Tempo	FMNH 23504	0		0	
Pterocles quadricinctus	Tempo	FMNH 319937	0		0	
Phaps histrionica	Michigan March 2017	UMMZ 214189	0		0	
Columba vitiensis	Michigan March 2017	UMMZ 210708	0		0	
Columba livia	Michigan March 2017	UMMZ 215474	0		0	
Alectroenas madagascariensis	Michigan March 2017	UMMZ 208400	0		0	
Columba pulchricollis	Michigan March 2017	UMMZ 220498	0		0	
Treron formosae	Michigan March 2017	UMMZ 225081	0		0	
Gallicolumba luzonica	Michigan March 2017	UMMZ 235306	0		0	
Alectroenas pulcherrimus	Michigan March 2017	UMMZ 210346	0		0	
Columba rupestris	Michigan March 2017	UMMZ 215432	0		0	
Drepanoptila holosericea	Michigan March 2017	UMMZ 223764	1	3	1	3
Oena capensis	Michigan March 2017	UMMZ 235234	0		0	
Turtur tympanistria	Michigan March 2017	UMMZ 212646	0		0	
Phaps chalcoptera	Michigan March 2017	UMMZ 209794	1	16	0	
Columbina passerina	Michigan March 2017	UMMZ 233651	0		0	
Otidiphaps nobilis	Michigan March 2017	UMMZ 237888	5	1, 6, 7, 8 & 16	4	1, 6, 7 & 8

Metriopelia ceciliae	Michigan March 2017	UMMZ 156824	0		0	
Pterocles senegallus	Michigan March 2017	UMMZ 205885	0		0	
Geotrygon mystacea	Michigan March 2017	UMMZ 156110	0		0	
Columbina cruziana	Michigan March 2017	UMMZ 156825	1	17	0	
Ectopistes migratorius	Michigan March 2017	UMMZ 243571	0		0	
Patagioenas nigrirostris	Michigan March 2017	UMMZ 153079	0		0	
Aplopelia larvata simplex	Michigan March 2017	UMMZ 219821	0		0	
Patagioenas plumbea	Michigan March 2017	UMMZ 208486	0		0	
Patagioenas speciosa	Michigan March 2017	UMMZ 157625	0		0	
Syrrhaptes paradoxus	Michigan March 2017	UMMZ 215431	0		0	
Claravis pretiosa	Michigan March 2017	UMMZ 133700	1	17	0	
Columba livia 1	Michigan March 2017	UMMZ 205123	0		0	
Columba livia 2	Michigan March 2017	UMMZ 116231	0		0	
Columba livia 3	Michigan March 2017	UMMZ 238070	0		0	
Columba livia 4	Michigan March 2017	UMMZ 157172	0		0	
Columba livia 5	Michigan March 2017	UMMZ 243415	1	6	1	6
Columba livia 6	Michigan March 2017	UMMZ 157056	1	2	1	2
Columba livia 7	Michigan March 2017	UMMZ 227912	0		0	
Columba livia 8	Michigan March 2017	UMMZ 204121	0		0	
Columba livia 9	Michigan March 2017	UMMZ 220242	0		0	
Columba livia 10	Michigan March 2017	UMMZ 152906	2	2 & 17	1	2

Wild rock pigeon (*C. livia*)	NHMUK July 2016	BMNH 1868.2.19.5	1	15	0
Columba arquatrix	Michigan July 2017	UMMZ 208297	0		0
Columba livia 11	Michigan July 2018	UMMZ 135838	0		0
Columba livia 12	Michigan July 2019	UMMZ 201088	0		0
Columba livia 13	Michigan July 2020	UMMZ 204600	0		0
Columba livia 14	Michigan July 2021	UMMZ 206018	0		0
Columba livia 15	Michigan July 2022	UMMZ 215474	0		0
Columba livia 16	Michigan July 2023	UMMZ 221772	1	18	0
Columba livia 17	Michigan July 2024	UMMZ 223737	0		0
Columba palumbus 2	Michigan July 2025	UMMZ 207549	0		0
Ducula goliath	Michigan July 2026	UMMZ 220840	0		0
Hemiphaga novaeseelandiae 2	Michigan July 2027	UMMZ 213100	0		0
Patagioenas picazuro 2	Michigan July 2028	UMMZ 227488	0		0
Patagioenas squamosa 2	Michigan July 2029	UMMZ 228336	0		0
Streptopelia decaocto	Michigan July 2030	UMMZ 224843	0		0
Monias benschi	Tempo	BMNH 1924.11.29.1	0		0
Raphus cucullatus	Tempo	OUMNH ZC11605	8	21, 27, 33, 39, 45, 51, 57 &78	0

Table S2.3. Landmark description and equivalence to Young *et al.* (2017)

Landmark	Location	Description	Young
1	Midline	Distalmost tip of premaxilla	2
2	Midline	Midline point cranial hinge	1
3	Midline	Tip of Occipital crest	3
4	Midline	Anterior midline of the foramen magnum	23
5	Midline	Anterior midline point of basicranium	24
6	Midline	Midline point between vomer and pterygoid	19
7	Bilateral	Nasal distal contact (right)	27
8	Bilateral	Nasal distal contact (left)	30
9	Bilateral	Maxilla-nasal contact with jugal (right)	10
10	Bilateral	Maxilla-nasal contact with jugal (left)	9
11	Bilateral	Contact between nasal and frontal (right)	18
12	Bilateral	Contact between nasal and frontal (left)	17
13	Bilateral	Lateral contact between lacrimal and frontal (right)	14
14	Bilateral	Lateral contact between lacrimal and frontal (left)	13
15	Bilateral	Inferior and lateralmost point of lacrimal (right)	12
16	Bilateral	Inferior and lateralmost point of lacrimal (left)	11
17	Bilateral	Lateral point on jugal (right)	5
18	Bilateral	Lateral point on jugal (left)	4
19	Bilateral	Posterior orbital rim, frontal and postorbital contact (right)	20
20	Bilateral	Posterior orbital rim, frontal and postorbital contact (left)	28
21	Bilateral	Lateral Basioccipital contact with Exoccipital (right)	26
22	Bilateral	Lateral Basioccipital contact with Exoccipital (left)	25
23	Bilateral	Basioccipital and Quadrate (right)	32
24	Bilateral	Basioccipital and Quadrate (left)	31
25	Bilateral	Brain Orbital margin, midpoint between (14) and (20) (left)	15
26	Bilateral	Brain Orbital margin, midpoint between (13) and (19) (right)	16
27	Midline	Face Midpoint between (1) and (2)	8

Table S2.4. Missing landmark characterization

Original landmarks 45 (1.75%) missing landmarks in the sample				
Specimen	Specimen ID	N missing	Which	Reason
Pezophaps solitaria	UMZC 415.R	5	13, 14, 15,16 & 21	Broken skull base
Otidiphaps nobilis	UMMZ 237888	5	1, 6, 7, 8 & 16	Broken rostrum
Columba livia	NMS (not registered)	4	8, 10, 17 & 18	Broken tip
Columba picazuro	BMNH 1898.10.1.1	2	5 &17	Broken anterior midline point of basicranium, bended zygomatic arch
Columbina talpacoti	BMNH S/1974.11.11	2	1 & 8	Broken tip
Columba livia 10	UMMZ 152906	2	2 & 17	Hole in cranial hinge, right zygomatic arch broken
Turacoena manadensis	BMNH 1871.9.13.1	1	7	Right nasal contact broken
Columba squamosa	BMNH 1898.7.10.1	1	18	Left zygomatic arch broken
Starnoenas cyanocephala	BMNH 1863.12.28.7	1	16	Left Inferior and lateralmost point of lacrimal broken
Petrophassa albipennis	BMNH S/1969.4.14	1	11	Left contact between nasal and frontal difficult to locate

Hemiphaga novaeseelandiae	BMNH S/2002.46.6	1	3	Tip of occipital crest missing
Goura cristata	UMZC 413.B1	1	24	Left basioccipital and quadrate difficult to locate
Treron curvirostra	UMZC 413	1	17	Right zygomatic arch broken
Columba palumbus	UMZC 409.A	1	17	Right zygomatic arch broken
Alectroenas madagascariensis	UMZC 413.E	1	7	Right nasal contact broken
Drepanoptila holosericea	UMMZ 223764	1	3	Tip of occipital crest missing
Phaps chalcoptera	UMMZ 209794	1	16	Left Inferior and lateralmost point of lacrimal broken
Columbina cruziana	UMMZ 156825	1	17	Right zygomatic arch broken
Claravis pretiosa	UMMZ 133700	1	17	Right zygomatic arch broken
Columba livia 5	UMMZ 243415	1	6	Broken palate
Columba livia 6	UMMZ 157056	1	2	Hole in cranial hinge
Wild rock pigeon (*C. livia*)	BMNH 1868.2.19.5	1	15	Broken right lacrimal
Columba livia 16	UMMZ 221772	1	18	Left zygomatic arch broken
Raphus cucullatus	OUMNH ZC11605	8	21, 27, 33, 39, 45, 51, 57 &78	Right hand side of specimen is covered in soft tissue
After reflecting paired landmarks 17 (.66%) landmarks missing in the sample				
Pezophaps solitaria	UMZC 415.R	4	13, 14, 15 & 16	Broken skull base
Otidiphaps nobilis	UMMZ 237888	4	1, 6, 7 & 8	Broken rostrum
Columba livia	NMS (not registered)	2	17 &18	Broken tip
Columba picazuro	BMNH 1898.10.1.1	1	5	Broken anterior midline point of basicranium

Columbina talpacoti	BMNH S/1974.11.11	1	1	Broken tip
Hemiphaga novaeseelandiae	BMNH S/2002.46.6	1	3	Tip of occipital crest missing
Drepanoptila holosericea	UMMZ 223764	1	3	Tip of occipital crest missing
Columba livia 5	UMMZ 243415	1	6	Broken palate
Columba livia 6	UMMZ 157056	1	2	Hole in cranial hinge
Columba livia 10	UMMZ 152906	1	2	Hole in cranial hinge

Table S2.5. Centroid size and body mass range in Columbiformes and Pteroclidiformes

	Centroid size (mm)			Body mass (g)		
	Min	Mean	Max	Min	Mean	Max
Columbiformes	45.6	75.4	236.0	31.6	417.6	9600.0
Columbiformes-nP	45.6	72.9	127.7	31.6	274.1	2000.0
Pteroclidiformes	61.1	63.3	66.6	180.0	233.5	263.5

Table S2.6. Empirical, predicted, and reported species mass. Highlighted cells fall within the range of reported mass for the species. * indicates minimum and maximum values taken from means of males and females and not from raw data.

	Body mass		Dunning 2008		
	Empirical	Predicted	Min	Max	From mean
Alectroenas madagascariensis	173.00	244.00	113	210	
Alectroenas pulcherrimus	165.00	366.00	161	169	
Aplopelia larvata	155.00	116.00	147	163	
Caloenas nicobarica	540.00	1362.00	460	675	
Chalcophaps indica	136.00	429.00	120	172	
Claravis pretiosa	68.00	42.00	41	103	
Columba arquatrix	400.00	376.00	226	489	
Columba guinea	352.00	153.00	307	371	
Columba livia	354.50	152.00	340	369	*
Columba oenas	291.00	142.00	254	334	
Columba palumbus	490.00	158.00	284	614	
Columba pulchricollis	330.00	218.00			
Columba rupestris	245.50	129.00	180	262	
Columba trocaz	511.00	515.00	390	520	
Columba vitiensis	353.00	1018.00	268	415	
Columbina cruziana	50.10	66.00	43.8	52.1	
Columbina passerina	35.40	57.00	27	39	
Columbina talpacoti	45.60	56.00	35.5	56.5	
Didunculus strigirostris	400.00	238.00			

Drepanoptila holosericea	215.00	376.00	210	220	
Ducula goliath	600.00	1983.00			
Ducula pacifica	395.00	1227.00	370	420	
Ectopistes migratorius	298.50	847.00	256	341	
Gallicolumba luzonica	196.00	171.00	181	204	
Geopelia cuneata	31.60	55.00	24	39	
Geophaps plumifera	98.10	45.00	84	124	
Geotrygon mystacea	211.00	328.00	138	256	
Geotrygon versicolor	225.00	339.00			
Goura cristata	2000.00	1703.00			
Hemiphaga novaeseelandiae	653.00	667.00	510	795	
Leptotila rufaxilla	157.00	118.00	131	183	
Leucosarcia melanoleuca	429.00	380.00	220	500	
Lopholaimus antarcticus	497.00	346.00			
Macropygia unchall	168.00	93.00	153	180	
Metriopelia ceciliae	55.10	51.00	49	59.8	
Metriopelia melanoptera	100.00	24.00	100	100	
Monias benschi	138.00	10244.00	112	172	
Ocyphaps lophotes	204.00	80.00	142	260	
Otidiphaps nobilis	500.00	366.00			
Patagioenas cayennensis	229.00	363.00	197	254	
Patagioenas fasciata	342.50	664.00	226	460	
Patagioenas leucocephala	238.00	444.00	230	253	*
Patagioenas maculosa	347.00	289.00	308	345	
Patagioenas nigrirostris	176.00	116.00	128	236	
Patagioenas picazuro	279.00	311.00	210	402	
Patagioenas plumbea	179.00	268.00	155	206	
Patagioenas speciosa	258.50	305.00	255	262	*
Patagioenas squamosa	312.00	458.00	235	388	
Petrophassa albipennis	132.00	151.00	130	178	
Pezophaps solitaria	11300.00	3507.00	8700	27800	
Phapitreron leucotis	108.00	88.00	89.3	136	
Phaps chalcoptera	331.00	162.00	250	450	
Phaps elegans	211.50	154.00	162	260	
Phaps histrionica	289.00	101.00	235	355	

Pterocles quadricinctus	180.00	52.00	160	200	*
Pterocles senegallus	263.50	111.00	255	280	
Ptilinopus dupetithouarsii	100.00	169.00	90	100	
Raphus cucullatus	9600.00	30000.00	8600	21200	
Starnoenas cyanocephala	219.00	320.00	200	242	
Streptopelia decaocto	149.00	178.00	113	184	
Streptopelia turtur	132.00	223.00	85	170	
Syrrhaptes paradoxus	257.00	28.00	180	300	
Treron curvirostra	134.50	277.00	112	161	
Treron formosae	140.00	354.00			
Turacoena manadensis	212.50	505.00	172	253	
Turtur tympanistria	73.60	50.00	54	89	
Zenaida macroura	119.00	72.00	115	123	*

Chapter Three. Ecological factors and their relationship with skull shape in Columbiformes.

Abstract

Columbiformes are an ecologically diverse and speciose clade of non-passerine birds. The skull shape of columbiform species like the dodo (*Raphus cucullatus*), the Rodrigues solitaire (*Pezophaps solitaria*), the tooth-billed pigeon (*Didunculus strigirostris*) and the thick-billed green pigeon (*Treron curvirostria*) are not adequately explained either by allometry or heterochrony. In this chapter, I aim to find the ecological and biomechanical factors that might explain the unexplained variance in the columbiform skull. My results show that patterns of integration and modularity do not explain variation of columbiform skulls adequately. I found that feeding behaviour factors explain both skull shape and inferred biomechanical performance. The results suggest that classical Darwinian evolution with selection towards adaptive peaks (frugivory or granivory) has taken place during the evolution of Columbiformes. I finally argue for the recognition of an adaptive radiation in Raphinae (which includes *Didunculus*, *Pezophaps*, *Raphus* and others). This adaptive radiation might be comparable, in terms of morphological disparity, to other remarkable bird adaptive radiations like the Galapagos finches (Geospizinae), Hawaiian honeycreepers (Drepanidinae), and Madagascan vangas (Vangidae) albeit happening in several distant islands. A new classification of pigeon feeding behaviour, the use of phylomorphospace visualization of feeding (diet and foraging) evolution, and the assessment of the biomechanical landscape of Columbiformes are reported.

Introduction

Why is morphology expected to covary with other factors?

Different species, even closely related ones, often show different morphologies (MacArthur, 1958; Herrel *et al.*, 2005; Jønsson *et al.*, 2012; Tokita *et al.*, 2016). How are these different morphologies obtained and what is the role of ecological factors in this morphological differentiation? In a pure adaptationist framework, organisms interact with the physical world through their bodies (Niklas, 1994; Langerhans and Reznick, 2010; Tseng and Flynn, 2015) and natural selection favours the fittest individuals (Darwin, 1859). Natural selection causes gradual change over generations (Darwin, 1859). However, natural selection is not uniform across time and space because it depends on different and changing biotic and abiotic factors (Arnold, 1983). Over evolutionary time, differences in direction and intensity of natural selection lead species to undergo phenotypic divergence, and, if populations are reproductively isolated, the differences in direction and intensity of natural selection can lead to speciation (Darwin, 1859; Mayr, 1983; Foster, Podos and Hendry, 2008; Kodandaramaiah, 2009). Furthermore, species with completely identical characteristics cannot coexist because one of the species would be competitively excluded (Hardin, 1960). As geographical space is limited, similar species often coexist in space because they utilise slightly different resources (MacArthur, 1958; Diamond, 1973), e.g., by spreading through time, canopy space, food item size. If different resources and different foraging strategies exist, then different performance optima for each strategy might emerge (Niklas, 1994; Tokita *et al.*, 2016). These different optima, over evolutionary time, might also change the phenotypic mean of the species because any small change that maximises the outcome (feeding efficiency) will provide a fitness advantage (Hardin, 1960).

Accounting for a multitude of factors affecting shape (and the interplay between them) is necessary to correctly assess the evolution of the skull shape in a comparative framework. These factors include not only the quantitative data on skull shape itself, but also ecological, biomechanical, and biogeographical factors.

This research chapter deals with the general question of how the columbiform (see below) morphology covaries among species in relation to different ecological traits and biomechanical variables. Developmental constraints (Klingenberg, 2008; Goswami and Polly, 2010; Bright *et al.*, 2016; Cooney *et al.*, 2017; Felice and Goswami, 2017; Young *et al.*, 2017) might also be at play in the columbiform skull. I therefore test the modularity and integration of the columbiform skull and ultimately assess the effect of the covariation of skull modules with the ecological and biomechanical variables.

Columbiformes

Columbiformes are a biologically and ecologically diverse clade of non-passerine birds. Columbiformes comprises a single family (Columbidae) which encompasses more than 300 species that are distributed in every continent except Antarctica and the driest parts of Africa and Eurasia (Goodwin, 1983; Gibbs, Barnes and Cox, 2010; Hoyo *et al.*, 2017). Pigeons and doves diverged from sandgrouses in the late Oligocene around 24.7 Mya (Soares *et al.*, 2016). One of the most morphologically diverse clades nested in Columbidae contains the genera *Didunculus*, *Goura*, *Caloenas*, *Pezophaps* and *Raphus* (Shapiro *et al.*, 2002). Less well-known members of this clade are inferred from more fragmentary fossil remains: the extinct flighted *Caloenas maculata* (of uncertain biogeographic affinity to Oceania; Heupink, Van Grouw and Lambert, 2014) and the flightless, dodo-sized *Natunaornis gigoura* of Fiji

(Worthy, 2001). The placement of Raphinae within Columbidae has been supported with molecular and morphological evidence (Shapiro *et al.*, 2002; Janoo, 2005; Heupink, Van Grouw and Lambert, 2014; Soares *et al.*, 2016). The species in this clade form part of the Indo-Pacific clade of Columbidae (Soares *et al.*, 2016) and will be referred to as Raphinae. The dodo (*Raphus cucullatus)* and the Rodrigues solitaire (*Pezophaps solitaria)* are the two species that have been traditionally considered to deviate most from other columbiform shape and had been placed in their own family (Raphidae), outside Columbidae but inside Columbiformes. However, *Raphus* and *Pezophaps* are placed within Columbidae (Janoo, 2005). *Pezophaps* and *Raphus* will be hereby referred as to Raphini.

I have previously demonstrated that allometry and heterochrony play an important role in explaining the skull shape variation in Columbiformes. However, allometry explains only 11% of the skull shape variation in this group and some pigeon skull shapes deviate substantially from those expected purely due to allometry (Chapter Two). These species were detected as outliers in the allometric model. Furthermore, the skull shape of other outliers like *Monias* and the Pteroclidiformes could be explained by heterochrony however, some outliers were impervious to either allometric or heterochronic explanations. Some of the most extreme examples of these species are the dodo, the Rodrigues solitaire, the Samoan tooth-billed pigeon (*Didunculus strigirostris*), and the thick-billed green pigeon (*Treron curvirostra*).

Some factor, other than allometric and heterochronic changes could be hypothesized to explain the unexplained variation in columbiform skull shape. Here I try to explain the unexplained variation of the skull shape in Columbiformes by analysing the correlation of

shape with factors like diet, foraging, biomechanics, centroid size, body mass, and distribution. As these factors might correlate differently with different parts of the skull (modules), the integration and modularity of the columbiform skull will also be analysed.

Historically, one factor proposed to explain the skull shape has been the adaptation to different feeding strategies. These adaptations have been proposed to explain the shape diversity of the avian skull, for example in different bird groups like Galapagos finches (Geospizinae: Darwin, 1859; Foster, Podos, and Hendry, 2008), Hawaiian honeycreepers (Drepanidinae: Tokita *et al.*, 2016) and Madagascan vangas (Vangidae: Jønsson et al., 2012). However, recent studies have found that beak shape is mainly determined by size and integration instead of the expected dietary factors (Bright *et al.*, 2016). This poses the question of whether dietary or feeding factors would explain some of the unexplained variation in Columbiformes.

Form-function links have been previously suggested to explain the shape of pigeon bills. Goodwin (1983) noted that in pigeons, bills range from robust/stout and hooked to thin with a slightly hooked point. The relative size and shape of the bill should be correlated to food or foraging strategy. For example thin bills "are characteristic of species known to feed largely on small seeds and are, presumably, the most efficacious for picking up such small objects" (Goodwin, 1983). Martínez-Gómez et al., (2017) noted that the elongated but slightly down curved bill of the Galapagos dove (*Zenaida galapagoensis*) is used as a digging tool (as in the similarly shaped bill of the Impeyan pheasant (*Lophura impeyanus*). The bill of *Treron curvirostra* has also been noted to be much shorter and stubbier than that in other members of the genus (Martínez-Gómez *et al.*, 2009). Feeding explanations have

been proposed to explain the peculiar skull shape of the dodo, *Raphus* (Livezey, 1993), which include the complex kinematics that could allow the inclusion of animal matter like crustaceans and molluscs in the diet (Claessens, Meijer and Hume, 2015).

Feral pigeons (all street pigeons) are descendants of domesticated pigeons that escaped captivity (Johnston, 1992). Feral pigeons lost the exaggerated traits of domestic fancy pigeons or the particular phenotype of domestic homers (Darwin, 1868; Johnston, 1992; Johnston and Janinga, 1995) and have returned to phenotypes closer to the one of wild *C. livia* at least twice: once in the old world and another time in America (Johnston, 1992). Despite feral pigeons have returned to phenotypes closet to wild *C. livia*, some of the skeletal characters of feral pigeons still resemble their domestic ancestors, for example in their disproportionally long tarsus (Sol, 2008).

The return to phenotypes like the one of wild *C. livia* by feral pigeons under natural selection could imply that functional constraints for diet might determine the "wild" skull morphology. In fact, Darwin (1868) noted that some domestic pigeon breeds with extreme morphologies can only feed because of human intervention, also pointing to the constraints imposed by function to form (Darwin, 1868; Young *et al.*, 2017). However, at least one skull measurement (absolute bill length) appears to be uncorrelated with foraging strategies in feral *C. livia* (Sol, 2008). It has also been noted that columbiform body size often reflects dietary preferences in pigeons: small fruit-doves (*Ptilinopus spp.*) feed on small fruit, medium-sized doves on medium-sized fruit and large doves (*Ducula spp.*) tend to feed on large fruit (Diamond, 1973). However, at least in feral pigeons the body mass is not significantly associated with foraging strategy (Sol, 2008).

Traditionally, the foraging strategies of Columbiformes (Goodwin, 1983; Gibbs, Barnes and Cox, 2010) have been classified in three broad categories: frugivorous, granivorous or an intermediate state between the two of them. Another factor that could explain the variation of skull shape in Columbiformes could be the foraging strategy of this group because different foraging habits might have different requirements. As with diet, the foraging strategies of these group have been classified in three broad categories: ground (terrestrial) foraging, arboreal foraging and an intermediate state of both of them (Goodwin, 1983; Gibbs, Barnes and Cox, 2010). Both, diet and foraging, classifications form part of the feeding behaviour and might fail to accurately reflect the broad scope of pigeon feeding ecology by themselves.

The importance of taking both feeding and foraging into account when classifying the pigeon feeding behaviour comes from the competitive exclusion principle which states that "complete competitors cannot coexist" (Hardin, 1960). It has been noted that morphologically or phylogenetically similar species, that should compete for the same resources may avoid this competition by segregating in different axes: space, diet, body size, time of activity or foraging strategy (MacArthur, 1958; Diamond, 1973). It has also been noted that pigeons possibly segregate similar diets by foraging across different canopy levels (Hume, 2011). Here, I propose a new classification of pigeon feeding strategies, which takes both feeding and foraging into account, and discuss the evolution of these strategies in Appendix Two.

Biomechanical performance

Biomechanical performance and the shape of skeletal structures are interconnected (Dicker, Pennock and Shigley, 2003; McGhee, 2012; Cuff and Rayfield, 2013; Tseng, 2013; Taylor and Thomas, 2014). Biomechanical performance is a consequence of the skull shape. However, if biomechanical performance is the most proximate target of natural selection, then biomechanical performance could be a principle factor that could explain the skull shape (Tseng, 2013). Biomechanical performance is usually regarded as a proxy for feeding behaviour and can readily be calculated when the skull shapes are modelled as simple machines, (*e.g.*, levers) from which key functional attributes (e.g. mechanical advantage) can be calculated. This study explores the link between the skull shape of Columbiformes and a variety of functional traits. These functional traits might be related to different aspects of feeding and foraging: (1) food processing can be related to mechanical advantage (Tanner *et al.*, 2010; Tseng, 2013; Dumont *et al.*, 2014) and bite force (Demes and Creel, 1988; Herrel *et al.*, 2005; Dollion *et al.*, 2017). (2) Maximum food item size can be related to mouth opening size (Diamond, 1973; Emerson and Radinsky, 1980; Wheelwright, 1985; Andersson, Norman and Werdelin, 2011; Dehling *et al.*, 2016). (3) The ability to cut fruits or open seeds can be related to bending resistance of the rostrum (Cuff and Rayfield, 2013; Tseng, 2013; Gill *et al.*, 2014). (4) Different foraging strategies might require different visual acuity, which can be related to differences in eye size (Brooke *et al.*, 1999; Garamszegi, Møller and Erritzøe, 2002).

When shape is characterized, such as in a geometric morphometrics framework, it is possible to simulate theoretical shapes within the resulting morphospace that are not

represented in the empirical sample. When the biomechanical performance is calculated for all of the shapes in the morphospace (theoretical and real), it is possible to add the performance to the morphospace as a an additional dimension (Niklas, 1997, 1999, 2004; Tseng, 2013). This approach would allow the construction of a functional morphospace that is a particular case of a "fitness landscape" (Niklas, 1994; Petkov, 2015). Some people have argued in favour of the "fitness landscape" metaphor (Niklas, 1994, 1997; McGhee, 2012; Petkov, 2015), in which biomechanical performance is the dimension of the data that represents the fitness of a particular shape, assuming that a good biomechanical performance is related with the reproductive output (= fitness) of individuals (Niklas, 1994; McGhee, 2012). The problem of measuring "fitness" in terms of comparatively few biological tasks assumed to contribute to fitness in an independent and equal manner is acknowledged (Niklas, 1994). However, the use of this framework allows biomechanical factors to build upon other concepts integrated in it (Petkov, 2015) like the principle of frustration (Niklas, 1994, 1997, 2004; Marshall, 2006). This principle states that different tasks can have different optimizations, so the attempts to become optimized in multiple tasks is frustrated by the intrinsic differences in optimal solutions for different tasks. Here I calculate the performance of different biomechanical characters across the morphospace of pigeon skull shape. I will use this performance to produce a biomechanical landscape and taking concepts from the "fitness landscape" method into account to explain the observed distribution of pigeon species shape in the biomechanical landscape.

It is easy to consider the correlation of shape, feeding and biomechanics, and the relationship between these variables is commonly considered in comparative evolutionary analyses (Rayfield, 2007; Tanner *et al.*, 2010; Cuff and Rayfield, 2013; Tseng, 2013; Taylor

and Thomas, 2014; Tseng and Flynn, 2015; Dollion *et al.*, 2017; Martinez *et al.*, 2018). However, other factors like geographic distribution could also be linked to the shape of structures of an organism. Island distributions have been related to both peculiar morphological changes associated with insular taxa as well as prolific adaptive radiations resulting from the colonization of isolated habitats (Millien, 2006; Harmon *et al.*, 2010; Presgraves and Glor, 2010). The globally distributed Columbiformes include many oceanic islands and every continent except Antarctica. Therefore, factors such as geographic range size and distribution type (i.e., insular or continental) could be related to the skull shape because they might act as proxies of competition, ecological opportunity and ecological release. (Van Valen, 1965; Millien, 2006; Parent and Crespi, 2009; Bolnick *et al.*, 2010). I take these factors into account when examining the morphological diversity of pigeon skulls because it could be expected that island distributed taxa to be more morphologically diverse than continental taxa.

Integration and modularity

The concepts of integration and modularity, in a geometric morphometrics framework, refer to the amount of covariation between landmarks in a structure that is hypothesized to present different sub-sections or modules (Klingenberg, 2014; Adams, 2016). Integration and modularity are located at opposite ends of a spectrum: integration refers to a system in which traits tend to vary jointly, with landmarks across all the structure (in different 'modules') being highly correlated with one another. Modularity refers to the opposite case when most joint variation (covariation) is concentrated within certain regions of a structure (modules). Finally, in the midpoint of this spectrum lays the null hypothesis of random

covariance across landmarks both between and within modules (Adams and Felice, 2014; Klingenberg, 2014; Bookstein, 2015; Adams, 2016). Integration is generally thought to be more substantial in regions that form a "functional matrix": a coherent anatomical domain balancing diverse functional criteria that persists over a growth trajectory (Bookstein, 2015). This functional matrix seems also the most likely place to find the frustration principle defined by Marshall (2006). It is possible to imagine that different modules of the skull (*e.g.*, braincase and rostrum) may show different patterns of correlation to factors that explain the shape variation in Columbiformes. Patterns of integration in the skull of *Columba livia* have been previously investigated (Young *et al.*, 2017). However, the integration and modularity in *Columba livia* were not tested in a phylogenetic context and the results for one species might not be transferrable to all Columbiformes. I aim to re-test the role of modularity and integration in my columbiform sample and to relate different ecological factors with the different modules of the columbiform skull.

In summary, this chapter will test how the skull shape of Columbiformes has been influenced by: (1) ecological factors (diet and foraging), (2) biomechanical factors (performance), and (3) distribution (type and area in km^2) and (body mass). I analyse the influence of these factors on skull shape while considering and exploring the possible modular nature of the skull into account. This chapter tests a series of adaptationist and developmental theories of the pigeon skull, which might shed light into the heated debate of the nature of phenotypical evolution, i.e., adaptation versus development.

Methods

Sample

I analysed the same specimens used in Chapter Two. For biomechanical evaluation of the species in the sample I used the Procrustes aligned coordinates. The aligned landmarks are useful to avoid biasing my biomechanical characters with the intrinsic biomechanical performance differences of differently sized objects. For all other statistical analysis of shape, I used the regression residuals of allometric models. I use these residuals to account for shape variation that is free from the allometric shape changes identified in Columbiformes (Chapter Two). The residuals were obtained using the mean coefficients of 200 distance-based phylogenetic generalized least squares models (Adams, 2014) of skull shape versus centroid size. The mean coefficients were used to account for both phylogeny and phylogenetic uncertainty.

Phylogeny

As in the previous chapter, I used a sample of 5,000 phylogenetic trees of the species in my sample from the global phylogeny of birds (https://birdtree.org/; Jetz *et al.*, 2012) based on the Hackett *et al.*, (2008) backbone. Three species in my sample were missing from the phylogenetic trees (*Raphus cucullatus*, *Pezophaps solitaria* and *Ectopistes migratorius*); these three species were added to the trees using the `bind.tree` function of phytools (Revell, 2012). The species were added at half of the branch length of their sister taxa. The sister taxon specified for *P. solitaria* was *Caloenas nicobarica* (Soares *et al.*, 2016), *P. solitaria* was then used as sister taxa to *R. cucullatus*, and *E. migratorius* was placed as sister to the genus *Patagioenas* (Johnson *et al.*, 2010). To avoid the possible influence of using

consensus trees instead of source trees I obtained a sample of 500 phylogenetic trees out of the broader sample 5,000 trees. I performed all phylogeny-dependent analysis across these 500 trees in order to incorporate both phylogenetic information and phylogenetic uncertainty into my results.

Size

I used the same two proxies for size that were used in Chapter Two. First, the mean body mass (Table S3.1) of all species was obtained from the *Handbook of Avian Body Masses* (Dunning and John, 2008) except for those of *Pezophaps* and the *Raphus* which were obtained from the mean of both sexes using the lowest body mass estimates of Livezey (1993). Lower estimates were chosen because modern body mass estimates of *Raphus* recover similar values to the lower-mid estimates from Livezey (Angst, Buffetaut and Abourachid, 2011; Louchart and Mourer-Chauviré, 2011; Brassey *et al.*, 2016; van Heteren *et al.*, 2017). However, unlike Livezey (1993), other studies did not estimate the body mass of *Pezophaps*. Second, I used skull centroid size as a second proxy of size. This was done to surpass problems like the mismatch of allometry identified by the mean species body mass or by the actual centroid size of sampled specimens, which was addressed in Chapter Two. I have also previously demonstrated, using R^2 values, that shape is better explained by skull centroid size than by the mean body masses reported in the literature. I will evaluate how biomechanics and feeding correlate with both size measurements because different information might be provided by the centroid size and body mass.

Distribution

I classified each species according to its distribution type using information from the distribution maps of the Data Zone of Birdlife international (BirdLife International, 2018). The distributions were classified as "Insular", "Continental" or "Both" (Table S3.1). The threshold chosen for this classification was based on the size of the landmass in which the species lives. If the distribution was in land masses as large as Australia (7,692,000km^2), this was classified as continental. Distributions in smaller landmasses were taken as Insular (even if the distributions ranged along a large number of islands (*e.g.*, Antilles, Malaysian archipelago). The classification of both insular and continental together only applied to five species (*Chalcophaps indica*, *Columba livia*, *Patagioenas leucocephala*, *Phaps elegans*, and *Treron curvirostra*) in which a large proportion of the distribution was found in islands and a significant portion was in a large landmass. Information about the range distribution size (measured in km^2) was also obtained from the Data Zone of BirdLife International, 2018.

Feeding behaviour (diet plus foraging)

To obtain detailed information about the feeding behaviour of sampled species, I reviewed the *Handbook of the Birds of the World* (Del Hoyo *et al.*, 2004) and scored a character matrix of species by food item described in the text: fruit, berries, flowers, grains, buds, leaves, seeds, snails, insects, shoots, acorns, root crops, large nuts, mostly fruit, mostly grains, drupes, grubs, aerial tubers, and mostly nuts or acorns (using a binary, presence/absence classification). I aimed to obtain most information provided by the text. The other scored characters were the foraging preference (terrestrial, mostly terrestrial, arboreal, mostly arboreal). I decided to include the variables of mostly arboreal, mostly terrestrial, mostly

grains, and mostly fruits because these characters are recorded in the Handbook of the Birds of the World (2017), and these variables might help to distinguish between sporadic and regular feeding behaviour in pigeons. When little information was available, photos and videos of the foraging birds were searched and reviewed online from HBW live (Hoyo *et al.*, 2017), YouTube (www.youtube.com) and Google image searches (www.google.co.uk). Previous feeding classifications have been mostly anecdotical (Goodwin, 1983; Gibbs, Barnes and Cox, 2010; Hoyo *et al.*, 2017), classifying the pigeons and doves broadly by the food ingested (fruit, seeds or both) and by the foraging surface used (terrestrial, arboreal or both). This classification is appropriate in the sense that it describes the spectrum of strategies used by Columbiformes. However, a classification that takes in account all known information of each species is necessary. This new classification should also be produced by a mathematical algorithm to be as objective and repeatable as possible.

To obtain a comprehensive classification of feeding strategies, the feeding matrix was subjected to a cluster analysis using the R (R Core Team, 2015) function `hclust` using both the complete and average linkage of a binary distance (`dist`) matrix (Figure S3.1; Table 3.1). The number of significant clusters was tested via permutation (Clarke, Somerfield and Gorley, 2008) using the `simprof` function of the Clustsig package (Whitaker and Christman, 2014) (Figure S3.2). The same distance matrix was analysed using a principal coordinates analysis (PCO) to obtain a block of continuous data that could be compared to geometric morphometric data using multivariate statistical methods (Rohlf, Corti and Olmstead, 2000; MacLeod, 2007; Collyer, Sekora and Adams, 2015; Benson *et al.*, 2017). To visualize the PCO, I produced plots for each of the four most important PCO axes against

the distinct feeding characters and coloured the points according to the presence-absence of each of the feeding strategies in the sampled species (Figures 3.1 and S3.3). I also produced a plot similar to a phylomorphospace (Sidlauskas, 2008) but I replaced the usual morphological principal components with the feeding PCO axis, thus creating a "phylofeedingspace" to visualize how phylogenetic relations distribute in this feeding space (Figure A2.1). To assess the ancestral feeding and evolutionary changes in feeding in Columbiformes (Appendix Two), I performed an ancestral character reconstruction (Pagel, 1994; Paradis, Claude and Strimmer, 2004). To perform this ancestral character reconstruction, I used an equal rates of evolution model with the function `ace` of the ape package (Paradis, Claude and Strimmer, 2004) in R (R Core Team, 2015). The identified feeding clusters (from the complete linkage algorithm) were used as character states in the ancestral character reconstruction (ACR). The ACR was performed on a randomly selected phylogeny (Figure A2.2).

Biomechanical performance

I decided to evaluate a third multivariate block of information related to the theoretical biomechanical performance of the pigeon skull (Table S3.3). Landmarks used to evaluate the biomechanical performance were the same as in Chapter Two, except for the addition of two new landmarks. These landmarks are paired (left/right) Type I landmarks located at the tip of the *processus oticus* (Figure S3.4: landmarks 28 and 29). These landmarks were added to capture the eye size more accurately (see below). Size influences some biomechanical attributes. However, as I was aiming to study the performance of different shapes and not different forms (shape + size: Klingenberg, 2016), biomechanical

performance was evaluated using the Procrustes superimposed landmarks to discard the influence of size. This allowed evaluation of the differences in performance related to skull shape changes. This also allowed me to compare the performance of different shapes directly (Appendix Three).

Size was not considered when biomechanical performance was calculated. Geometric morphometrics often describes shapes imbedded in a Kendall shape space (Kendall, 1984) by projecting them to a plane (Adams and Otárola-Castillo, 2013; Klingenberg, 2016). The shape coordinates need to be Procrustes aligned (without the influence of position, size and rotation) to be imbedded in the Kendall space (Gower, 1975; Rohlf and Slice, 1990; Klingenberg, 2016). Arguably, size could have been included in my biomechanical analysis adding the size as a new column to the Procrustes aligned coordinates (Mitteroecker *et al.*, 2004; Klingenberg, 2016). However, this would transform the tangent plane to the Kendall shape space by adding volume to it (form space), complicating both the shape description and representation of shapes. A second way to include size in the analysis would be to calculate the biomechanical performance on the raw coordinates of each species. However, that approach would prevent the simulation of shapes not included in the empirical sample.

Biomechanical variables

I will now describe the biomechanical variables that were analysed in this chapter. Detailed results and discussion of these variables are provided in Appendix Three:

Mechanical advantage

Mechanical advantage (MA) is one of the most studied biomechanical measurements (Trinkaus and Villemeur, 1991; Tanner *et al.*, 2010; Tseng, 2013; Dumont *et al.*, 2014).

Mechanical advantage has been used to assess changes in feeding through ontogenetic trajectories (Tanner *et al.*, 2010), climbs of performance peaks in fitness (biomechanical) landscapes over time (Tseng, 2013), and to identify adaptive optima in morphospace (Dumont *et al.*, 2014). The mechanical advantage of a mechanism is the instantaneous ratio of the output force to the input force (Dicker, Pennock and Shigley, 2003). For a lever, mechanical advantage depends on the ratio of the perpendicular distance from the fulcrum of the input force (Fi) to that of the output force (Fo). Pigeon jaws are examples of third-class levers (Figure S3.4), this type of lever does not provide a positive mechanical advantage (i.e., the system sacrifices force to increase velocity) so any input force will be smaller than the output force at the jaw tip. To calculate the mechanical advantage, I followed several steps. (1) I obtained the position of the lever fulcrum: the midpoint between the lateral points of the jugal bones (landmarks 17 and 18). (2) I calculated the distalmost point where the jaw muscles could input any force: the midpoint between the lacrimal landmarks (15 and 16). (3) To measure the input distance (Di), the distance from the fulcrum to effort point was calculated. (4) To measure the output distance (Do) the distance from the fulcrum to the distalmost tip of premaxilla (landmark 1) was calculated. (5) The MA was then calculated as:

$$MA = \frac{Di}{Do} \tag{3. 1}$$

Input force

The input force (Fi) of the skull in this lever analogy is given by the cross-sectional area of the masticatory muscles, in the case of pigeons this muscle is the *adductor mandibulae* and

is delimited anteriorly by the lacrimal bone. I calculated Fi in two ways: (1) The cross-sectional area of the adductor muscles was calculated as the sum of the areas of two triangles (Ma and Ma', Figure S3.4) defined by landmarks 6, 18 and 6 for the right muscle and landmarks 17, 17 and 6 for the left muscle respectively. (2) I obtained the centroid size of the Ma and Ma' triangles using the function `gpagen` of Geomorph (Adams and Otárola-Castillo, 2013). I selected the muscle centroid size as the input force proxy to be used in most analyses because patterns recovered by both proxies were similar. The model assumes that lacrimal bone represented an anterior barrier for muscle fibres. As with all other biomechanical performance characters Procrustes coordinates were used to calculate the performance, this means that the calculated performances are relative performances to other shapes imbedded in the same Kendall shape space (Kendall, 1984; Klingenberg, 2016).

Bite force

Although mechanical advantage is a common biomechanical character in the literature, its relevance is somewhat limited in isolation. This is because the transmission and application of forces is function of both mechanical advantage and properties of relevant muscle. For example, an extension of basic mechanical advantage when information about muscle area or the actual values measured in-vivo is available is bite force. Bite force has been calculated either by classical measurements (Demes and Creel, 1988; Herrel *et al.*, 2005) or in a geometric morphometric setting (Dollion *et al.*, 2017). In the lever analogy the bite force is equal to the output force (Fo). Bite force is dependant of both Fi and MA. Output force is important for bird not only as a mean of cutting a food item (which species in the genus *Treron* do), but also for the manipulation of objects. This manipulation can be either

soft like picking a grain from a surface or forceful like unplugging fruits from plants, retaining live animal prey, opening seeds or even cutting food items into smaller pieces. My model assumes that the skull is not kinetic. Fo was calculated with next formula:

$$Fo = \frac{Fi * Di}{Do}$$

(3. 2)

Velocity of bite (mouth closure)

The velocity (Vel) with which the mouth closes could also be important in some feeding scenarios in which live prey can escape. Some pigeons supplement their diet with animals like adult insects, grubs, and snails. (Goodwin, 1983; Hoyo *et al.*, 2017) . The velocity with which such a lever closes is given by the inverse of the mechanical advantage:

$$Vel = \frac{Fi * Do}{Di}$$

(3. 3)

Maximum gape (mouth opening)

In contrast to these metrics that principally reflect food processing, mouth opening size is feeding-related trait that correlates with food item size (Emerson and Radinsky, 1980; Andersson, Norman and Werdelin, 2011). Intuition suggests that this biomechanical character would be important to pigeons because most species swallow food items whole (Goodwin, 1983; Gibbs, Barnes and Cox, 2010) and mouth opening (Mo) represents a physical constraint on the maximum size of an item that they can manipulate and ingest. In fact, the size of pigeons is correlated to the size of fruit they consume (Diamond, 1973).

It could be expected that pigeons feeding from large items (fruits) would present a larger gape than pigeons feeding on small seeds. An arbitrary angle of 45 degrees was used to calculate the couth opening. The calculation of Mo assumes: (1) that the length from the distalmost tip of the premaxilla to the fulcrum of the jaw was equal to the distance of the dentary symphysis to the fulcrum. The similarity in these lengths is something I have observed myself while manipulating columbiform skulls. (2) That the skull is not kinetic, and (3) that all the pigeons in the sample can open their mouths to 45° without their muscles stretching beyond their working range. The arbitrary angle chosen should not affect the comparative results across the morphospace (see below). However, because the lack of empiric measurements of maximum angle of gape in pigeons, caution should be taken when interpreting the mouth opening results. Mo was calculated using the formula:

$$Mo = Do * Sin(45°)$$

(3. 4)

Bending resistance of the rostrum

Bending resistance is also an important biomechanical character because some manipulations of food item can produce stresses and strains that could injure the animal while biting. Bending resistance can be calculated using classical beam theory (Dicker, Pennock and Shigley, 2003; Cuff and Rayfield, 2013) or sophisticated engineering techniques like finite element analysis (Tseng, 2013; Gill *et al.*, 2014). The bending resistance can be related to the feeding of pigeons that are able to cut fruits or open seeds (genus *Didunculus* and *Treron*: (Goodwin, 1983; Gibbs, Barnes and Cox, 2010; Hoyo *et al.*, 2017) (Goodwin, 1983; Gibbs, Barnes and Cox, 2010; Hoyo *et al.*, 2017). Bending resistance

can be calculated for a beam by obtaining the second moment of area or moment of inertia. Moment of inertia is a geometrical property of an area which reflects how its matter is distributed with regard to an arbitrary axis (Dicker, Pennock and Shigley, 2003). The information provided by my landmark system prevents the accurate calculation of the moment of inertia because of the lack of information about the distribution of bone mass in the skull. The calculation of the second moment of area is possible for the skulls in the sample. However, this would not be possible for all other theoretical forms in the morphospace. Furthermore, it would be possible to warp (deform) a 3D mesh to target theoretical morphologies around the morphospace in a similar fashion to Tseng and Flynn (2015) and then calculate the second moment of area from these models. However, to ensure the mesh deformations were valid, a higher density of semilandmarks on the surface of rostrum bones would be needed. As the landmark system used here does not include these landmarks, it is impossible to calculate the second moment of area directly.

To obtain a proxy for the bending resistance of the skull shape, I decided to approximate the moment of inertia behaviour with the available information. As a rule of thumb, structures are more resistant to bending when their mass is distributed further away from the centroid of the structure (e.g., a tube versus a rod of the same material and mass). Following this reasoning I approximate the moment of inertia by calculating the centroid size of a triangle lying on a perpendicular plane to the rostrum in the middle of the beak (Iprox). To calculate Iprox I followed the next steps (Figure S3.4): (1) I calculated the midpoint (A) of landmarks 9 and 10. (2) I calculated the midpoint (B) between landmarks 7 and 8. (3) I found the vector AB. (4) I found a vector from landmark 27 to the point A (AL27). (5) I projected the vector AL27 in the vector AB to find the projected position of landmark

27 (27’). (6) I found vectors that united the nasal distal contact and the maxilla-nasal contact with jugal on both sides of the skull (vectors L8L10 and L7L7). (7) I projected 27’ into vectors L8L10 and L9L10 to obtain points 27’’ and 27’’’. (8) I obtained Iprox using the function `gpagen` of Geomorph (Adams and Otárola-Castillo, 2013) to obtain the centroid size of the triangle delimited by landmarks 27’, 27’’, and 27’’’.

Three other measurements were taken as an approximation to the second moment of inertia: (1) the dorsoventral height at mid-length of the rostrum was calculated as the distance between landmark 27 and 27’ and accounts for resistance to bending in only the vertical plane. (2) Mediolateral width at mid-length of the rostrum was calculated as the distance between landmarks 27’’ and 27’’’ and accounts for the resistance to bending in the horizontal plane. Finally (3), the moment of mass can be determined for a lever when the length of the lever is available. This moment of mass represents the bending resistance given by the shape and material arrangement but taking in account the length of the structure. To approximate this structural property, I obtained out moment of mass proxy (I3d) I used the formula:

$$I3d = \frac{Iprox}{Dlever}$$

(3. 5)

Where Dlever is the lever length, calculated as the distance between the midpoint between the nasal contacts (landmarks 7 and 8) and the midpoint between the maxilla-nasal contacts (landmarks 9 and 10). I chose to use this distance instead of the output distance (Do) because it represents a portion of the rostrum that most resemble a beam, thus conforming to the moment of inertia expectations (Dicker, Pennock and Shigley, 2003).

Eye size

Different prey and foraging strategies may require different visual acuity, specifically in taxa that mainly feed on small seeds or on live prey. (Brooke *et al.*, 1999; Garamszegi, Møller and Erritzøe, 2002). Different feeding behaviours of pigeons may require different visual acuities although previous studies have find eye size in pigeons to scale uniformly with body mass (eye size = mass$^{0.631}$: Brooke et al., 1999). I used `gpagen` function to calculate the total eye centroid size as the sum of the right and left eye centroid sizes (landmarks 15,13,26, 29 and 28, and 16, 14, 25, 20 and 29 respectively: Figure S3.4). Landmarks 28 and 29 are the two extra landmarks (*processus oticus*). These landmarks were only used for the eye size calculation and not in any other analysis of the chapter. Eye centroid sizes were calculated using the Procrustes aligned coordinates

Simulation and visualization of biomechanical performance across the morphospace

Columbiform skull shape was summarized using a principal component analysis (Figures A3.1 to A3.4). I used Geomorphs's function `plotTangentSpace` to evaluate the principal components (PC) of shape. I also aimed to visualize how biomechanical performance changed across this morphospace. To achieve this, I evaluated the biomechanical performance across a uniform distribution of theoretical morphologies represented in the morphospace following several steps: (1) I identified the minimum and maximum values of specimens on all PC axes of the sample, these values were then multiplied by 1.05 so that the range of theoretical morphologies was slightly larger than the range of the empirical sample. (2) I obtained a vector of 100, equally-spaced values between these maximum and minimum values. (3) I obtained a matrix of dimension 100^2 that represented all possible combinations between these two 100 element vectors (used

as two principal component axes). (4) I obtained theoretical morphologies by multiplying the values of each row of the matrix for the eigenvalues. (5) I calculated all the biomechanical proxies (as described above) for these morphologies in the first four PC axis. I decided to analyse the first four principal components because they account for most of the sample variation (56.2%) and subsequent axes account for small proportions of the variation. To visualize this functional morphospace, I added the calculated biomechanical performance using contour lines to plots of combinations of pairs of principal components, these principal components described different aspects of the columbiform shape variation (Figures A3.1 to A3.4).

Ecological and biomechanical factors correlation with skull shape

To evaluate the correlation of skull shape with multidimensional factors, such as (PCO-transformed) feeding and biomechanics, I used a two-block partial least squares approach (Rohlf, Corti and Olmstead, 2000; MacLeod, 2007; Collyer, Sekora and Adams, 2015; Adams, 2016). I compared feeding and biomechanics data blocks against the columbiform allometric residuals of shape and against themselves. Two-block partial least squares evaluates the correspondence between the most correlated variables (salient variables) between two different data blocks without assuming any dependence of one set of variables over another one (Rohlf, Corti and Olmstead, 2000; MacLeod, 2007; Collyer, Sekora and Adams, 2015; Adams, 2016). It does this by constructing pairs of composite axes from linear combinations of the original variables (in a similar manner to principal component analysis; PCA). Each pair of latent variables corresponds to a PLS dimension

that maximises the covariance between the two data blocks (Rohlf, Corti and Olmstead, 2000; Benson *et al.*, 2017).

While other kinds of analysis (e.g. PCA) use a correlation matrix that is composed of four submatrices:

Diagram 1. Example of a correlation matrix composition

R^{11}: Block A	R^{12}: Cross correlation AB
R^{21}: Cross correlation AB	R^{22}: Block B

Two-block PLS only examines one of the correlation submatrices because one of the correlation submatrices is simply the transpose of the other one: R^{12}=t R^{21}. The problem of using only the cross-correlation matrix R^{12} is that this matrix is neither symmetrical nor square, so it becomes impossible to obtain the eigenvalues by standard eigenanalysis. Because of this, the correlation matrix is analysed via single value decomposition (Rohlf, Corti and Olmstead, 2000; MacLeod, 2007). Two-block PLS summarizes the correlation between the two data blocks in the single values of the single value decomposition (PLS dimensions). Eigenvalues can be obtained by squaring the single values. The percentage of correlation explained by a dimension (pair of complex axes) can be obtained simply by calculating the percentage of the sum of eigenvalues that the eigenvalue associated with that PLS dimension represents. Statistical significance of the correlation patterns can be assessed by comparing the two-block PLS correlation (PLS_{corr}) against permutated data (Adams and Felice, 2014). Any significant PLS dimension can be further analysed, for example by assessing the loadings of the original variables in each PLS dimension in order to identify salient variables (MacLeod, 2007; Adams and Felice, 2014; Benson *et al.*, 2017).

As in the case of PCA, where the data points can be projected to each principal component axis, each of the data blocks can be projected into these PLS dimensions, producing the PLS scores. PLS scores of both blocks (XScores and YScores) can be plotted to visually examine how the data blocks correlate with each other across PLS dimensions (Figures 3.2A-B, 3.3A-B, S3.5, and S3.7). Other possibility is retro-transforming an arbitrary value (*e.g.*, max and min XScores of shape) into the original data space, thus allowing to interpret shape changes in the sample along a PLS dimension. I modified the Geomorph's (Adams and Otárola-Castillo, 2013) `shape.predictor` function to interpret shape changes along the important PLS dimensions (Figures 3.2C-D, 3.3C-D).

I performed an ordinary two-block PLS to analyse how the skull shape (residuals after allometry regression) and modules (rostrum and braincase; Supplementary material S3) covary with the feeding and biomechanical data blocks (Table 3.3) using Geomorph's function `two.b.pls`. I decided to also test the covariation between blocks in a phylogenetic framework by performing a phylogenetic two-block PLS using Geomorph's `phylo.integration`. The ordinary and the phylogenetic two-block PLS analyses ask different questions: (1) the two-block PLS asks if the morphology (skull or modules) of the pigeons in the sample correlates with the other traits (feeding or biomechanics) of those pigeons. The correlation identified by the ordinary two-block PLS can be caused by independent evolution or the traits. (2) the phylogenetic two-block PLS asks if evolutionary changes in the pigeon shape (skull or modules) reconstructed along the phylogeny correlate with evolutionary changes in other traits (feeding or biomechanics) reconstructed along the phylogeny. The phylogenetic implementations ask if there is linked evolution of characters due to form-function relationships.

I performed the phylogenetic analysis over 500 randomly chosen phylogenies from Jetz et al. (2012). `two.b.pls` and `phylo.integration` functions also perform a permutation test to avoid spurious correlations arising from the multi-dimensional nature of the analysis. I summarized the results of this analysis over the 500 different runs and obtained by obtaining mean values of interest (Table 3.3). I calculated the percentage of variation explained by each of the models, while the number of dimensions is equal to the number of columns in the input data block with the fewest columns: feeding data block (19 variables).

As first dimensions contain most of the variation in all analyses (at least 82% in PLS dimension one, and at least 95% for the cumulative variation for PLS dimension one and two), Table S3.4 only shows the first four dimensions for each analysis. I also obtained the eigenvectors of the first two PLS dimensions, which summarize the loadings of the original variables in each dimension. However, as most variation (56% of the relative corrected eigenvalue in PCO1 to PCO4) is represented by the first PCO axes in the feeding block, I only included the first eight axes (71% of the relative corrected eigenvalue) in Table 3.4. Finally, the loadings of variables in the first dimension of biomechanics and feeding were obtained (Table 3.5). To visualize the shape changes I predicted the shape for the maximum and minimum shape scores for the first two PLS dimensions. Since the residuals for the allometric multi-phylogeny pgls were used as the shape data block in the two-block PLS: the predicted shape was difficult to interpret because it only showed the unexplained variation of the sample, similar to plotting the shape residuals in 3D space. To be able to properly visualize the PLS shape changes, I added the mean shape of the sample to each of

the predicted shapes. This mean shape + predicted residuals are shown in (Figures 3.2C-D, 3.3C-D, S3.6, and S3.8).

Interpretation of the two-block PLS has to be accomplished through examination of the PLS dimensions and the visual inspection of shape changes and the amount of correlation between blocks measures by the r_{PLS} coefficients. However, as the PLS results depend on both sample size and number of variables, the direct comparison of the degree of correlation between different datasets (either RV of r_{PLS}) is not possible (Adams and Collyer, 2016). **Hypotheses (or main result interpretation of the two-block PLS:** the r_{PLS} values vary from zero to a value determined by sample size and number of variables. The comparison of correlation between several data blocks can be obtained by comparing the effect size of the different PLS analyses (z-scores). Z-scores can be calculated using the next formula:

$$z = \frac{r - \mu_r}{\sigma_r}$$

(3. 6)

Where μ_r is the expected value of r_{PLS} under the null hypothesis of random correlation (mean of sampling distribution), and σ_r is the standard deviation of the sampling distribution. I calculated the z-scores for all of the two-block PLS analyses (Table 3.3, Figure 3.6) using Geomorph's function `compare.pls` (Adams and Otárola-Castillo, 2013; Adams and Collyer, 2016).

Modularity and integration

I tested the modularity and integration of the rostrum and braincase of the columbiform sample using the modules defined for the pigeon skull by Young (2017) (Table S3.2). I tested the integration between modules using a two-block PLS to obtain the PLS_{corr} between

modules (as described above; Table 3.2). I performed the two-block PLS using Geomorph's functions `integration.test` (Adams and Otárola-Castillo, 2013). To test the modularity in the columbiform skull I used a covariance ratio test (Adams, 2016). To obtain the CR coefficients between modules (Table 3.2). I obtained the CR coefficients using the `modularity.test` function of Geomorph (Adams and Otárola-Castillo, 2013). When only two data blocks are analysed, the `integration.test` function tests the covariation between these two blocks (in this case two shape data blocks) by performing a two-block PLS analysis.

The RV coefficient (Klingenberg, 2009; Goswami and Polly, 2010; Klingenberg and Marugán-Lobón, 2013) permits to test whether the modules defined a priori by the researcher fit the observed covariance matrix than random modules of equal size and number. The RV coefficient tests the degree of covariation between two matrices (Klingenberg, 2009; Klingenberg and Marugán-Lobón, 2013). The RV coefficients are calculated from the square symmetrical covariance matrix:

$$RV = \frac{trace(R^{12}R^{21})}{\sqrt{trace(R^{11}R^{11})trace(R^{22}R^{22})}}$$

(3. 7)

This expression takes values between zero and one and represents the amount of covariation between modules scaled by the covariation within modules (Klingenberg, 2009; Adams, 2016). This RV coefficient is evaluated via permutation of landmarks between modules in order to evaluate the obtained correlations against the null hypothesis of random correlation (Klingenberg, 2009). However, it has been shown that the RV coefficient is highly affected by sample size (number of specimens) and number of variables

(number of landmarks; Adams, 2016). The solution to the problems of RV coefficients is to change the formula replacing the diagonal values of the covariance matrices within modules (R^{11} and R^{22}) with zeros (R_*^{11} and R_*^{22}) thus calculating the covariance ratio (CR: Adams, 2016):

$$CR = \frac{trace(R^{12}R^{21})}{\sqrt{trace(R_*^{11}R_*^{11})trace(R_*^{22}R_*^{22})}}$$

(3. 8)

The CR numerator is the same as in the RV coefficient. The denominator is the sum of squared covariation within modules **minus** the variation in each trait dimension. What this ensures is that CR denominator, unlike RV, only takes in account the covariation within modules and not the variation in each dimension. This makes CR a measurement of covariation between modules relative to the squared covariation within them (not the total amount of covariation). **Hypotheses of the covariance ratio:** CR can take values equal to or greater than zero. CR values of one represent random covariation between and within modules. CR values higher than one describe higher covariation between than within modules (integration). Finally values between zero and one represent larger variation within than between modules (modularity).

Finally, as a different metric I evaluated the integration of the skull and modules against the null hypothesis of self-similarity (Bookstein, 2015). Self-similarity is tested by estimating the parameter α that is the slope of a regression between the log partial warp variance against the log bending energy of the partial warps. This is done in a deflation setting which allows the local bending energy to be estimated taking in account the geometrical size differences thus making the bending energy comparable at different scales. **Hypotheses of**

the self-similarity: The calculated slope can take different values being -1 the expected slope for the null hypothesis of self-similarity (meaning that the sample shows no interpretable structure at any spatial scale). Slopes with higher absolute values point to structures being integrated (meaning the sample shows patterns at large spatial scales: between all landmarks) while slopes with lower absolute values point to structures being disintegrated (meaning most variation happens in small spatial scales: modules). However, this approach does not take in account the phylogenetic information. I evaluated the integration against the null hypothesis of self-similarity using Geomorph's (Adams and Otárola-Castillo, 2013) function `global.integration` (Table 3.2).

Variables that explain skull shape (distance-based regression)

Numerical variables

Two-block PLS does not assume any explanatory power of one block over the other data block. It is therefore useful as an exploratory analysis in which the variables that covary strongly and are putatively most useful for predicting patterns in the other data block (salient variables) can be identified (Rohlf, Corti and Olmstead, 2000; MacLeod, 2007). To test the explanatory power of the salient variables I used the distance-based linear regression approach (Adams, 2014). Here, as in Chapter Two, two approaches were used: (1) distance-based linear regression (D.lm) using Geomorph's function `procD.lm` and (2) multi-phylogeny distance based partial least squares (multi-D.pgls) applying Geomorph's function `procD.pgls` across 500 random phylogenies. I tried to explain the unexplained variation after allometric regression using several ecological factors: body mass, centroid size, distribution type, distribution area, feeding clusters, salient feeding PCO axes, diet and

foraging types and biomechanical PLS Scores of the first two PLS dimensions (YScores of the two-block PLS, as biomechanics and feeding were always used as the Y block in the two-block PLS). To obtain a summary of the biomechanical characters, I decided to use the PLS scores because they are a summary of all salient biomechanical characters. As biomechanical characters are calculated regionally in the skull, they might explain most of the shape variation if they are used together as explanatory variables in a regression setting.

Categorical variables

I included several categorical variables that could explain the skull shape in columbiforms: First, a variable of the assigned significant clusters identified by the average linkage algorithm (ClusterGAve). Second, new variables that summarize some of the binary data-matrix into more comprehensive variables were analysed: FruitDB was a binary variable that accounted for pigeons that ate fruits, drupes or berries; LivePrey was also a binary variable that accounted for all pigeons that ate insects, molluscs or larvae; Greens was binary and accounted for pigeons consuming leaves, buds or flowers; NutsRoots was binary and accounted for pigeons eating nuts, acorns or tubers (generally hard food items; GrainsOrSeeds was also binary accounting for pigeons eating grains or seeds. I also included the classical categorical classification of diet (MostDiet: frugivorous, granivorous or both) and foraging (MostForage: arboreal, terrestrial or both).

Distance-based regression methods have the caveat of not having an implementation of AIC. This can make overfitting of the models difficult to account for. Because of this, z-scores, R^2 and P values were used to choose the best models.

Finally, I explored which variables might explain the biomechanical characters of the columbiform skull (Table 3.7). I took PLS biomechanical dimension one and two as a summary of all my biomechanical characters. I evaluated these PLS dimensions against all other non-shape non-biomechanical variables using the ordinary linear least squares regression (ols) and phylogenetic generalized least squares (pgls). Pgls was performed using the `gls` function from the package nlme (Pinheiro and Bates, 2010). I fitted Pagel's lambda (λ: Pagel, 1999) "manually" by selecting the maximum likelihood gls model after evaluating it using the `corPagel` function on a series of possible lambda values (sequence from 0 to 1 by increments of 0.01). This implementation was computationally demanding so I implemented the analysis in a multi-core setting using the `parLapply` function of the "parallel" package.

As these ordinary least squares regressions were not distance-based, I was able to choose the best models by estimating the AIC of each proposed model. I picked the best model by selecting the model with the minimum AIC value and evaluated which of the other models were likely to minimize the loss of information by applying the formula:

$$P_{info} = e^{\frac{AIC_{min} - AIC_i}{2}} \quad (3.9)$$

Results

Cluster analyses of feeding (diet and foraging)

The simulation test identified a different number of significant feeding clusters when different hierarchical clustering algorithms were used (Figure S3.2; Table 3.1): Average linkage obtained eight significant clusters while complete linkage obtained seven significant clusters. Both linkage algorithms produce two coherent main clusters (Figure S3.1): "M1" a cluster of mostly arboreal and frugivorous pigeons, and "M2" a cluster of mostly terrestrial feeders. For the main cluster "M2", the only difference between linkage algorithms is that sometimes one large cluster of species is divided into two smaller clusters. However, all species included in the large cluster are included in the smaller clusters. Complete linkage cluster "BC" was recovered as clusters B and C by the average linkage, and average linkage cluster DE was recovered as clusters D and E by the complete linkage. These congruent clusters are referred with upper case letters (Table 3.1). For the main cluster "M1", the identified clusters by each algorithm were more variable and did not exhibit an exact correspondence between algorithms albeit similarities were noted (see below). These non-congruent clusters are referred with lower case letters (Table 3.1). The clusters produced by the complete linkage algorithm were used in subsequent interpretation of analysis. The clusters produced by the average linkage algorithm were used in the linear regression setting (see below).

Table 3.1. Feeding clustering of Columbiformes using average and complete linkage algorithms. Equivalent clusters are coloured. Cluster 1 and Cluster 2 show the correspondence between the significant clusters obtained using average or complete linkage algorithms. Clusters in lower case show cluster unique to each analysis. Clusters in upper case are correspondent between analyses (green = complete concordance, yellow is concordance between species albeit in separate clusters).

Species	Average	Cluster 1	Cluster 2	Complete
Raphus cucullatus	1	A	A	6
Caloenas nicobarica	1			6
Pezophaps solitaria	1			6
Columba oenas	2	B	BC	4
Patagioenas picazuro	2			4
Columba palumbus	2			4
Patagioenas fasciata	4	C		4
Macropygia unchall	4			4
Goura cristata	3	DE	D	7
Columbina passerina	3			7
Gallicolumba luzonica	3			7
Turtur tympanistria	3			7
Leucosarcia melanoleuca	3			7
Chalcophaps indica	3			7
Streptopelia turtur	3			7
Streptopelia decaocto	3			7
Aplopelia larvata	3			7
Otidiphaps nobilis	3			7
Patagioenas maculosa	3		E	5
Starnoenas cyanocephala	3			5
Geotrygon mystacea	3			5
Geotrygon versicolor	3			5
Metriopelia melanoptera	3			5
Petrophassa albipennis	3			5
Columbina cruziana	3			5
Metriopelia ceciliae	3			5
Leptotila rufaxilla	3			5
Claravis pretiosa	3			5
Phaps elegans	3			5
Phaps histrionica	3			5
Geophaps plumifera	3			5
Geopelia cuneata	3			5
Phaps chalcoptera	3			5
Ocyphaps lophotes	3			5
Columba rupestris	3			5
Columba guinea	3			5
Columba livia	3			5
Columbina talpacoti	3			5

Zenaida macroura	3			5
Hemiphaga novaeseelandiae	8			3
Ducula pacifica	8			3
Patagioenas squamosa	8	i		3
Ducula goliath	8		f	3
Columba trocaz	6	j		3
Treron curvirostra	6			3
Patagioenas leucocephala	7			3
Didunculus strigirostris	7			2
Phapitreron leucotis	7			2
Patagioenas plumbea	7			2
Treron formosae	7			2
Alectroenas madagascariensis	7		g	2
Patagioenas speciosa	7			2
Patagioenas cayennensis	7	k		2
Turacoena manadensis	7			2
Drepanoptila holosericea	7			2
Lopholaimus antarcticus	7			2
Alectroenas pulcherrimus	7			1
Columba pulchricollis	7			1
Patagioenas nigrirostris	7			1
Ptilinopus dupetithouarsii	7		h	1
Ectopistes migratorius	5			1
Columba vitiensis	5	l		1
Columba arquatrix	5			1

Complete linkage clusters

For the main cluster “M1”, complete linkage identified three feeding sub-clusters (Figure S3.1): “h” and “f” are clades of generalist mostly arboreal feeders that can also forage on the ground. Cluster “h” complements their frugivorous diet with seeds and insects and includes species like *Alectroenas pulcherrimus*, *Columba pulchricollis*, *Patagioenas nigrirostris*, *Ptilinopus dupetithouarsii*, *Ectopistes migratorius*, *Columba vitiensis*, and *Columba arquatrix*. Cluster “f” complements their diet with other plant matter like leaves and includes species like *Hemiphaga novaeseelandiae*, *Ducula pacifica*, *Patagioenas squamosa*, *Ducula goliath*, *Columba trocaz*, *Treron curvirostra*, and *Patagioenas*

leucocephala. Cluster "g" contains species that are mainly exclusively frugivorous and exclusive arboreal foragers like *Didunculus strigirostris*, *Phapitreron leucotis*, *Patagioenas plumbea*, *Treron formosae*, *Alectroenas madagascariensis*, *Patagioenas speciosa*, *Patagioenas cayennensis*, *Turacoena manadensis*, *Drepanoptila holosericea*, and *Lopholaimus antarcticus*.

For the main cluster "M2" (mostly terrestrial foraging), complete linkage found four significant sub-clades: the cluster "BC" is a generalist group that can also forage in trees and feeds on seeds, invertebrates, berries, and green plant matter. This cluster contains species like *Columba oenas*, *Patagioenas picazuro*, *Columba palumbus*, *Patagioenas fasciata*, and *Macropygia unchall*. Cluster "A" is mostly frugivorous and forages exclusively on the ground, this cluster includes *Raphus cucullatus*, *Caloenas nicobarica*, and *Pezophaps solitaria*. Cluster "D" includes mostly granivorous species that sometimes include fruits on their diet like: *Goura cristata*, *Columbina passerina*, *Gallicolumba luzonica*, *Turtur tympanistria*, *Leucosarcia melanoleuca*, *Chalcophaps indica*, *Streptopelia turtur*, *Streptopelia decaocto*, *Aplopelia larvata*, and *Otidiphaps nobilis*. Finally, cluster "E" represents mostly granivorous, exclusive terrestrial foragers like *Patagioenas maculosa*, *Starnoenas cyanocephala*, *Geotrygon mystacea*, *Geotrygon versicolor*, *Metriopelia melanoptera*, *Petrophassa albipennis*, *Columbina cruziana*, *Metriopelia ceciliae*, *Leptotila rufaxilla*, *Claravis pretiosa*, *Phaps elegans*, *Phaps histrionica*, *Geophaps plumifera*, *Geopelia cuneata*, *Phaps chalcoptera*, *Ocyphaps lophotes*, *Columba rupestris*, *Columba guinea*, *Columba livia*, *Columbina talpacoti,* and *Zenaida macroura*.

Average linkage clusters

The average clustering algorithm identified two main clusters: “M1” of mostly arboreal and “M2” a cluster of mostly terrestrial foragers. These two main clusters were consistent with the ones identified by complete linkage results (Table 3.1). For the main cluster “M2”: cluster “A” was recovered by both average and complete linkage algorithms while cluster “BC” of the complete linkage was recovered as two separate clusters (“B” and “C”) by the average linkage algorithm. Clusters “D” and “E” from the complete linkage were recovered as a single cluster “DE” by the average linkage. For the mostly arboreal foraging main cluster “M1”, four sub-clades were recovered by the average linkage instead of three clades recovered by the complete linkage algorithm. Average linkage clusters “i” and “j” broadly correspond to cluster “f” of the complete linkage except for the exclusion of *Patagioenas leucocephala*. Cluster “i" contains species like *Hemiphaga novaeseelandiae*, *Ducula pacifica*, *Patagioenas squamosa*, and *Ducula goliath* that eat more plant matter like leaves and flowers than cluster “j”. “j” includes species like *Columba trocaz* and *Treron curvirostra*. Average cluster “k” includes most of the mainly terrestrial foraging, mostly granivorous species identified by the complete linkage algorithm (clusters “g”, “h”, and *Patagioenas leucocephala)*. Finally, average cluster “l” includes *Ectopistes migratorius*, *Columba vitiensis*, and *Columba arquatrix*.

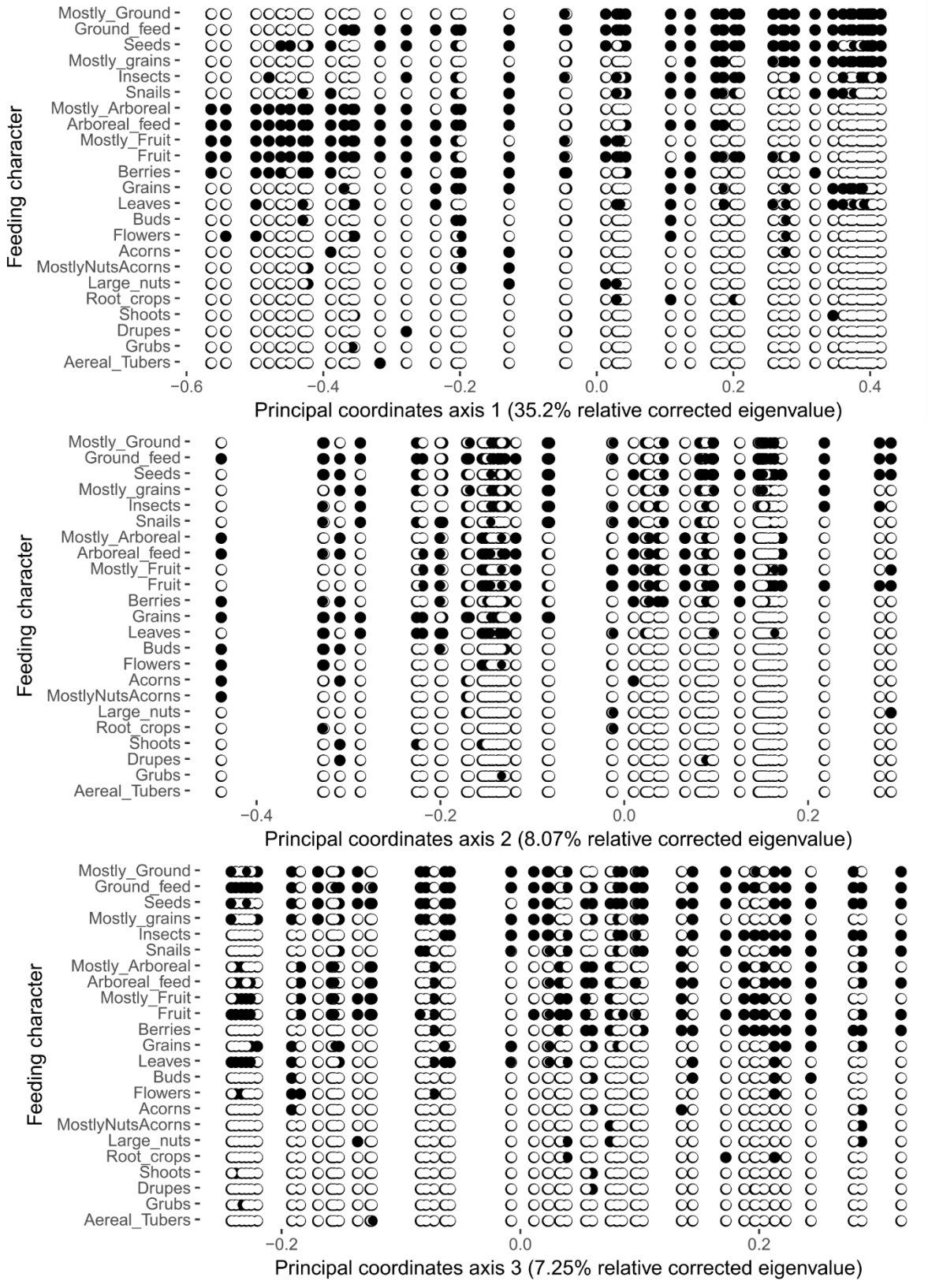


Figure 3.1. First, three principal coordinates (PCO) axes plotted against the binary feeding characters. Each column of circles represents a species. Black circles represent the presence of a feeding trait, and white circles represent the absence of the trait for that species. This figure allows one to assess patterns of feeding characters on the PCO axes.

Principal coordinates analysis of feeding behaviour

The first three axes from the principal coordinates analysis (PCO) of the binary distance matrix of the feeding behaviour (Figure 3.1) summarize 50.5% of the feeding variation (35.2, 8.1 and 7.3% respectively). When the feeding characters were plotted against the PCO values (Figure 3.1) it was possible to observe that species with negative PCO1 values feed mostly fruit and berries and foraged in trees. Positive PCO1 values are related to terrestrial foragers with granivorous diets complemented with insects. PCO2 seems to be related less directly with foraging and more with food items. Positive PCO2 values are related to fruit and seed eating and negative values seem to be related to grains, leaves, and buds. Positive PCO3 values are related to diets that include insects, snails and berries and some arboreal feeding. Negative PCO3 are related with seeds, leaves. Interpretations of PCO4–PCO6 are less clear (Figure S3.3) with PCO4 positive values seemingly indicating seeds and grains feeding and negative values to fruits.

Phylogeny and feeding behaviour ("Phylofeedingspace")

Detailed results for the phylofeedingspace are provided in Appendix Two. When the phylogeny is plotted against PCO1 and PCO2 (Figure A2.1B) it was possible to observe that the genera *Columba* and *Patagioenas* (Columbini) occupy large parts of the feeding space. However, neither *Patagioenas* nor Columba have invaded the obligate terrestrial feeding of cluster "A" (central PCO1 values and highly positive PCO2 values). Figure A2.1A shows that most of the other clades present more restricted feeding behaviours and occupy discrete parts of the feeding space. When the phylofeedingspace constructed with PCO3 and PCO4 is constructed (Figure A2.1) the Columbini also occupied the largest part of the

feeding space. The other clades do not present such a discrete distribution in the feeding space as in PCO1 and PCO2.

Biomechanics

The detailed results (and discussion) for the biomechanical landscape are provided in the Appendix Three. The principal component analysis of all 29 Procrustes aligned landmarks of the sample showed that the first six principal components summarize 80% of the shape variation in the sample (32,4%, 23.1%, 9.2%, 6%, 5.2%, and 4.3% respectively; Figures A3.1 to A3.4). The analysis of patterns in the biomechanical landscape pointed out for PC1 and PC2 are the biomechanical dimensions that seem to be more closely related to the feeding behaviour clusters: when the performance of different biomechanical characters is plotted against the first two principal components of shape (56% of the sample variation), it is possible to observe the non-linear patterns of performance across morphospace. Principal components three and four (Figures A3.3 and A3.4) summarize 15.2% of the sample variation (9.2 and 6% respectively). It was difficult to identify visually a clear correlation between the biomechanical performance and the significant feeding clusters in Figures A3.3 and A3.4. In subsequent paragraphs, I will report the results of the biomechanical performance landscape focussing on **PC1 and PC2**.

For the **input force** (muscle centroid size; Figure A3.1E), *Raphus*, *Pezophaps* and *Didunculus* seem to be the taxa with skull shapes that present larger muscle areas (these taxa were assigned to clusters “A” and “g”). *Treron*, *Ducula pacifica*, *Ptilinopus*, and *Alectroenas* present the second highest muscle size (from clusters “f”, “g”, and “h”). Most other columbiform species present lower values of input force. The lowest muscle areas were

obtained for *Chalcophaps Geotrygon*, *Aplopelia*, *Leptotila* and *Turtur* (from clusters "E" and "D"). For the **mechanical advantage** (Figure A3.2D), the taxon with higher mechanical advantage is *Didunculus* while *Treron curvirostra* and *Pezophaps* exhibit the second highest mechanical advantage values (clusters "g", "A", and "f"). *Raphus* shares the third highest mechanical advantage values with *Treron formosae*, Drepanoptila, Alectroenas and Ptilinopus (clusters "A", "g", and "h"). The **effort distance** (Figure A3.2E) and **output force** (Figure A3.1A) follow a similar pattern than the mechanical advantage.

For PC1 versus PC2, taxa with higher values of **output distance** (Do) and mouth **opening** (Mo; Figure A3.1B) are *Raphus*, followed by *Pezophaps* and *Treron*, *Ptilinopus*, *Ducula*, *Hemiphaga*, *Goura*, *Caloenas*, *Columba vitiensis*, and *Columba trocaz* (clusters "A", "f", "g", "h", and "D"). For **velocity of bite** (Figure A3.2C), *Raphus* shows the highest bite velocity, followed by *Pezophaps* and a group composed by *Didunculus*, *Treron*, *Ducula* and *Goura* (clusters "A", "g", "f", and "D"). The Raphini present the smallest **eye sizes** (Figures A3.1F), while pigeons like *Metriopelia*, *Columbina passerina*, *Claravis*, *Turtur*, and *Leptotila rufaxilla* are characterized by large eye sizes (clusters "E" and "D").

For the **dorsoventral height (thickness) at mid length of the rostra** (Figure A3.2A), the pigeons with thickest rostra are the Raphini, followed by *Didunculus*, *Treron* and *Ptilinopus* (clusters "A", "g", "f", and "h"). For the proxy for the **moment of area** (Figure A3.1C) follows a similar pattern to rostrum thickness, in which highest moment of area is shown by the Raphini, followed by *Treron* and then for a large cluster of pigeons including *Didunculus*. The pigeons with larger **lever length (Dlever)** with respect to other pigeons (Procrustes aligned) in the morphospace, are *Raphus* and *Goura* while the shorter lever is presented by

Didunculus, followed by *Treron* (Figure A3.2B). The **moment of mass** (moment of area accounting for structure length) presents extremely different patterns than those of the moment of area (Figure A3.1D), *Didunculus* is the pigeon with highest moment of mass while the Raphini present similar resistance to bending than other pigeons.

Modularity and integration

Table 3.2. Integration, modularity and global integration in the skull of the comparative sample of Columbiformes. Ordinary and phylogenetic results presented for integration (two-block PLS) and modularity (CR coefficients). Phylogenetic results are the mean and standard deviation of phylogenetic analysis performed across 500 phylogenies to account for phylogenetic uncertainty.

Integration braincase ~ rostra	PLS_{corr}	sd	p	sd
Ordinary	0.880		0.001	
Phylogenetic	0.863	0.039	0.001	0.000
Modularity braincase ~ rostra	CR	sd	P	sd
Ordinary	0.871		0.001	
Phylogenetic	1.029	0.054	0.456	0.320
Global integration	Skull	Rostrum	Braincase	
ordinary	-0.353	-0.491	-0.482	

Integration between braincase and rostrum was calculated using a two-block PLS analyses (Table 3.2). Results indicate a strong and significant integration between these two hypothesized modules (PLS_{corr}= 0.88 and *P*=0.001). When phylogeny was taken in account the covariation was only slightly lower for the ordinary two-block PLS, and remained significant (PLS_{corr}= 0.86 ± 0.039 and *P*= 0.001 ± 0.000). Global integration (Bookstein 2015), which does not take phylogeny into account, was calculated for each of the modules: complete skull (α= -0.353), rostrum (α= -0.491) and braincase (α= -0.482). These values indicate that the columbiform skull is a "disintegrated" structure; most variation happens in small spatial scales or within modules (Bookstein, 2015).

The covariance ratio between different modules (CR coefficient) indicated that modularity is present in the columbiform skull (CR= 0.871, *P*= 0.001) with more variance within modules than between modules. However, when phylogeny was taken into account the proposed modularity is no longer detected. CR value becomes close to 1 (CR= 1.029 ± 0.054), pointing to the null hypothesis of the sample presenting no integration or modularity. This is complemented by the low significance (*P*= 0.456 ± 0.320) of the CR values obtained by proposed modules against random allocation of landmarks in different modules (Adams, 2016). These results altogether indicate that the columbiform skull presents a low degree of modularity and that this structure is mainly integrated with modules that are highly correlated.

Two-block partial least squares

Two-block PLS is an intricate analysis for which multiple parts (significance, correlation, number of significant dimensions, vector loadings, shape changes, and the scores of each data block) need to be considered to interpret it correctly. In this chapter, I performed seven of such analysis: three analyses of shape (skull, rostrum and braincase) versus feeding, three analyses of shape versus biomechanical performance, and one analysis of feeding versus biomechanical performance. For the sake of conciseness, the analyses reported here are the two-block PLS of skull shape versus biomechanical performance and versus feeding, and one analysis of feeding versus biomechanical performance. The detailed results for the modules (rostrum and braincase) are provided in the Supplementary material (S3).

The two-block PLS analyses results are reported as follows: (1) The general covariation and significance of the two "shape versus factors" analyses; (2) the results for the analysis of covariation between skull shape and feeding, including the detailed analysis of two PLS dimensions; (3) the results for the analysis of covariation between skull shape and biomechanics, including the detailed analysis of two PLS dimensions; (4) the results for the analysis of covariation between feeding and biomechanics is reported.

Table 3.3. Two-block partial least squares correlation and significance results. All two-block comparisons were carried out twice: once in an ordinary and once in a phylogenetic setting. A) Shape (skull, rostrum, and braincase) was used as the left data block in the two-block PLS, the right data block was either biomechanical performance or the feeding (diet plus foraging) PCO axes. B) Two-block analyses of feeding (PCO data block) and biomechanical performance data block.

A) Two-block PLS of shape versus feeding and biomechanics								
Module	Method	Blocks	PLS_{corr}	sd	p	sd	Z-score	sd
Skull	ordinary	Shape vs Feeding	0.588		0.003		3.939	0.055
	phylogenetic	Shape vs Feeding	0.755	0.095	0.007	0.012	5.928	0.049
	ordinary	Shape vs Biomechanics	0.857		0.001		5.474	0.087
	phylogenetic	Shape vs Biomechanics	0.808	0.042	0.001	0.001	6.28	0.062
Rostrum	ordinary	Shape vs Feeding	0.575		0.002		3.96	0.058
	phylogenetic	Shape vs Feeding	0.726	0.106	0.006	0.011	6.246	0.047
	ordinary	Shape vs Biomechanics	0.874		0.001		6.128	0.086
	phylogenetic	Shape vs Biomechanics	0.831	0.039	0.001	0	7.457	0.06
Braincase	ordinary	Shape vs Feeding	0.525		0.009		2.997	0.055
	phylogenetic	Shape vs Feeding	0.669	0.121	0.045	0.068	4.257	0.052
	ordinary	Shape vs Biomechanics	0.746		0.004		4.406	0.086
	phylogenetic	Shape vs Biomechanics	0.709	0.065	0.009	0.005	5.012	0.064
B) Two-block PLS of feeding versus biomechanics								
	Method	Blocks	PLS_{corr}	sd	p	sd	Z-score	sd
	ordinary	Feeding vs Biomechanics	0.531		0.01		3.412	0.063
	phylogenetic	Feeding vs Biomechanics	0.575	0.133	0.095	0.119	3.167	0.062

The general covariation and significance

In all analyses (Table S3.4), PLS dimension one explained more than 82% of the covariation between data blocks, PLS dimension two explained between 4% and 13% of the correlation, with subsequent dimensions explaining little covariation (maximum of 3.2%). PLS dimension one accounted for a higher proportion of the covariation between skull shape and feeding (90.39%) than with biomechanical performance (82.07%). PLS dimension two only explained more than 10% of the covariation when biomechanical performance was compared with the skull shape (13%).

Table 3.4. PLS vectors (from the phylogenetic two-block PLS analysis) of the right block data (biomechanical performance or feeding PCO). Each vector shows the loadings of the original variables in each of the first two PLS dimensions (at least 95% of the identified covariance). Left data block in all analysis was shape (skull, rostrum or braincase), The left PLS vectors of loadings are not shown because the landmark data is easier to identify by projecting shape changes. Only the loadings of the first eight feeding PCO axes are shown because they represent most feeding variation (71% of the relative corrected eigenvalue vectors).

	Skull		Rostrum		Braincase	
Block vs Shape	Dim. 1	Dim. 2	Dim. 1	Dim. 2	Dim. 1	Dim. 2
PCO 1	-0.1	-0.01	-0.09	-0.02	-0.34	0.08
PCO 2	0.05	0.13	0.04	0.18	0.02	0
PCO 3	-0.01	-0.04	-0.02	-0.07	-0.21	-0.06
PCO 4	0.02	0.01	0.01	0.01	0.09	-0.04
PCO 5	0	0.01	0	0.03	-0.01	-0.02
PCO 6	0	0.02	0	0.04	0.22	0.04
PCO 7	0.03	0.07	0.03	0.09	0.05	0
PCO 8	0	-0.02	0	-0.02	0.16	-0.01
…	…	…	…	…	…	…
Input distance	-0.1	-0.01	-0.11	0	0.13	0.03
Output distance	-0.09	0	-0.02	-0.05	0.14	-0.17
Mouth opening	-0.09	0	-0.02	-0.05	0.14	-0.17
Rostrum height	-0.28	-0.04	-0.14	-0.16	0.55	-0.18
Lever length	0.53	0.02	0.6	-0.02	-0.26	-0.38
Rostrum width	-0.16	0	-0.11	-0.04	0.2	-0.1
Muscle centroid size	-0.12	-0.01	-0.1	-0.03	0.14	-0.05
Eye centroid size	-0.04	-0.01	-0.09	0.02	-0.09	0.21

Shape versus feeding (two-block PLS results)

Covariation and Significance

The overall skull shape block showed a moderate and significant covariation with feeding (PLS_{corr} = 0.588; *P*=0.003; Table 3.3). When phylogeny was considered, the correlation was higher and significant, albeit significance was lower than for the ordinary analysis (PLS_{corr} = 0.755, sd= 0.095; *P*= 0.007, sd= 0.012).

PLS dimension one (feeding)

Salient variables

The loadings of the PLS vector in PLS dimension one (Table 3.4), were used to identify the salient or useful feeding variables. Vector loadings indicate that PCO1 is the most salient to predict shape in PLS dimension one. The salience of PCO1 for the covariation with the skull is -0.1.

Feeding traits in PLS dimension one

When the binary feeding characters were plotted against the feeding YScore in dimension one (89 to 91% of covariation: Figures 3.4 and S3.9) it was possible to differentiate two clusters of feeding characters in the dataset: one cluster (negative YScores) with terrestrial or mostly terrestrial foraging pigeons that feed mostly with seeds, grains, insects and snails. This cluster can also feed on larger grains and leaves. The second identified cluster (positive YScores) includes arboreal or mostly arboreal foraging pigeons that feed on fruits and berries. The identified clusters were more conspicuous when the rostrum and braincase modules were examined separately (Figure S3.9).

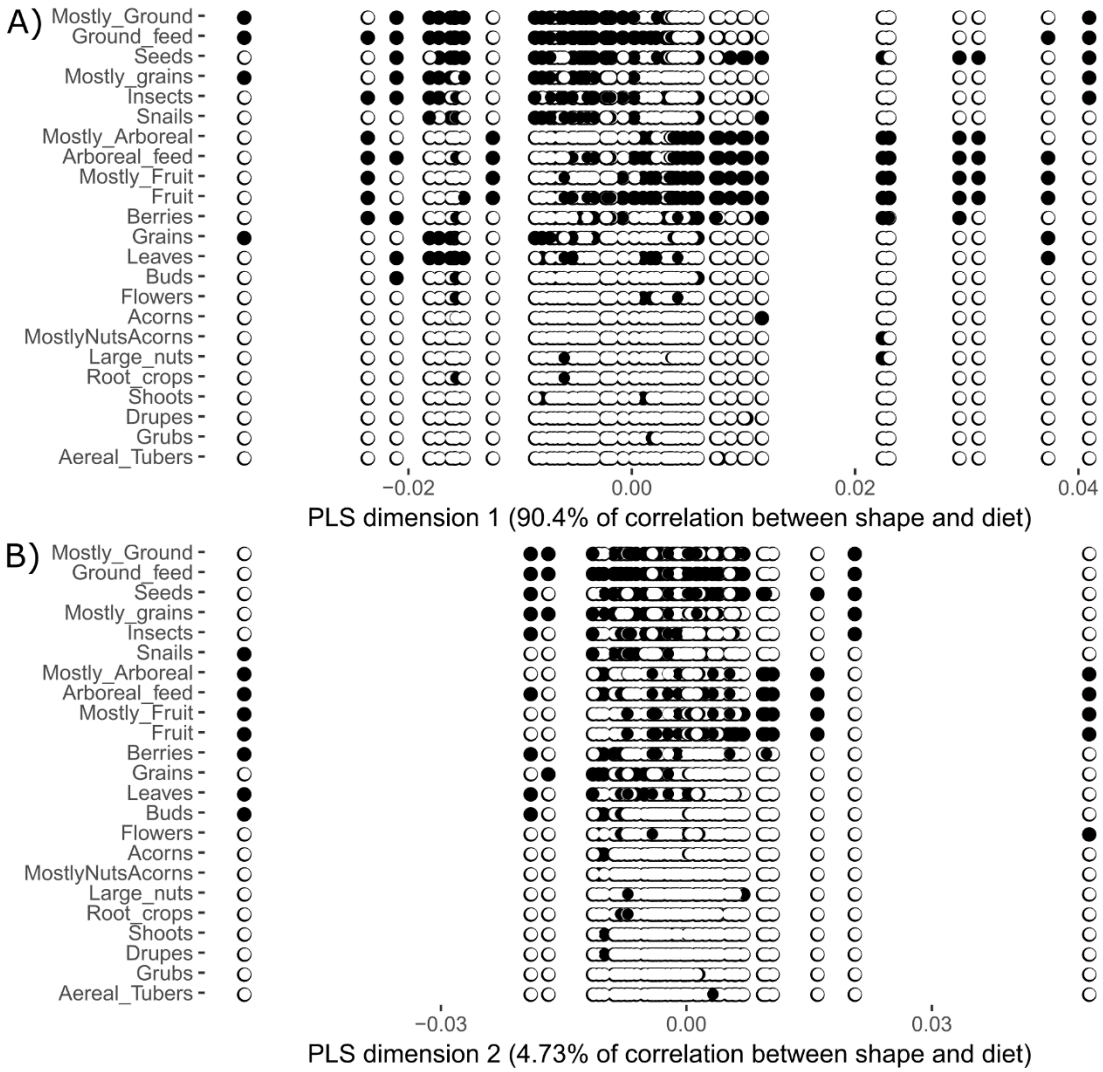


Figure 3.4. Feeding PLS scores (YScores) in PLS dimension one (A) and two (B). Each column of circles represents a species in the sample. Black circles represent presence of the feeding trait, and white circles represent absence of that feeding trait.

Shape changes

To assess the shape changes associated with the feeding traits I examined the predicted shapes of the XScores in dimension one (Figures 3.2C-D and S3.6). The minimum shape score (XScore) obtained was related with a long, slender rostrum and frontals, these changes were associated with terrestrial and granivorous traits. The maximum XScore

value was related with a dorsoventrally high, short rostrum, and a mediolaterally expanded braincase. These changes were related to the frugivorous and arboreal traits.

PLS scores of shape and diet

The comparison between the PLS scores of feeding block (Figures 3.2 and S3.5) revealed that the covariation between the scores of shape and feeding is conspicuous in PLS dimension one of the complete skull. *Phaps elegans*, *Columba trocaz*, and *Patagioenas plumbea* (clusters "E", "f", and "g") were the pigeons with highest scores and the lowest scores were obtained by *Phaps histrionica*, *Patagioenas nigrirostris*, *Patagioenas picazuro* (clusters "E", "h", and "BC").

PLS dimension two (feeding)

Salient variables

In PLS dimension two (Table 3.4), PCO2 seems to be the most salient feeding variable in dimension two for the complete skull (0.13) and rostrum (0.18). PCO2 is negligible for the correlation of the braincase in dimension two (-0.004).

Feeding traits in PLS dimension two

When the binary feeding variables were plotted against feeding YScores of dimension two (4.45% to 4.73% of the covariance; Figures 3.4 and S3.10), it was challenging to identify clusters in the data. However, terrestrial granivorous pigeons have constrained YScores towards central values, while the arboreal frugivorous pigeons show a wider YScore range.

Shape changes

In the second PLS dimension (Figures 3.3C and S3.8), the feeding block shows shape changes in the skull and rostrum, but not in the braincase. A similar pattern of shape changes than the ones identified in dimension one was obtained for the skull and rostrum. High XScores values are related to dorsoventrally taller, anteroposteriorly shorter rostrums with anterolaterally expanded frontals and posterolateral expanded braincases and basicrania.

PLS scores of shape and feeding

When PLS scores of shape and diet in dimension 2 were compared (Figures 3.3A and S3.7) for the complete skull, high feeding YScores were obtained by *Patagioenas leucocephala*, *Phaps elegans*, and *Patagioenas plumbea* ("f", "E", and "g") while low feeding values were obtained by *Phaps histrionica*, *Patagioenas picazuro*, *Patagioenas squamosa* ("E", "BC", and "f").

Shape versus biomechanics (two-block PLS results)

Covariation and significance

The covariation and significance (Table 3.3) were higher for skull shape and biomechanical performance (PLS_{corr} = 0.857; *P*=0.001) than for skull shape and feeding. In the phylogenetic setting the covariation between shape and biomechanics remained high and significant (PLS_{corr} = 0.808, sd= 0.042; *P*= 0.001, sd= 0.001).

PLS dimension one (biomechanics)

Salient variables

For the biomechanical performance in dimension one (82% to 85% of the covariance; Table 3.4), the lever length (Dlever) is the most salient variable for the skull (0.53). The second most salient variable for the skull is the rostrum height (-0.28). The rostrum width presents a salience of -0.16 for the complete skull while the muscle centroid size (-0.12) and the input distance (-0.1) are also salient.

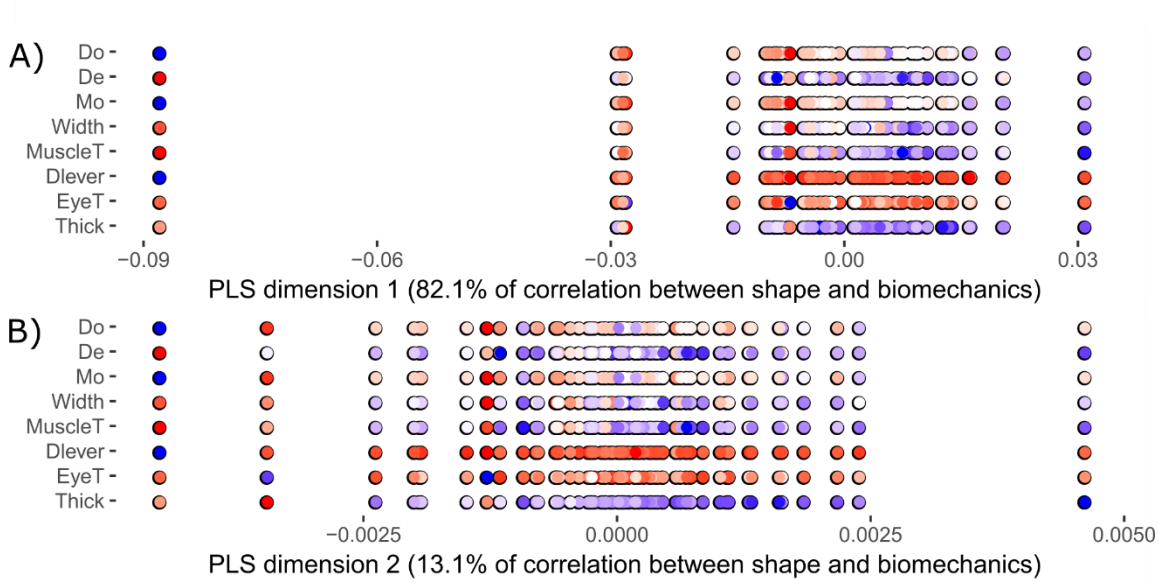


Figure 3.5. Standardized biomechanical characters versus PLS scores in dimension one (A) and two (B) for each species in the dataset. Each column of circles represents a species in the sample, and intensity of the colour marks the comparative performance.

Biomechanical performance in PLS dimension one

The PLS biomechanical dimension one accounted for 82% of the covariation with complete skull shape (Table S3.4). When the original biomechanical variables are plotted against the biomechanical YScores in dimension one, some general patterns can be identified (Figures 3.5A and S3.11). For higher YScores values there is a: decrease in output distance, mouth opening, rostrum width, muscle centroid size, and rostrum thickness. Lever length

increases with higher YScore values of dimension one while eye centroid size and input distance show no clear patterns.

I identified one outlier in the skull and rostrum modules (*Didunculus*; Figure S3.11). This outlier presents high values of input distance, rostrum width and thickness, and muscle area. *Didunculus* also presents remarkable low values of output distance, mouth opening, and lever length. In the braincase module, Didunculus and *Pezophaps* are outliers, but they present extremely different biomechanical properties because *Pezophaps* presents high values of output distance, mouth opening, and lever length. *Pezophaps* also presents average values of rostrum width, muscle area, and input distance and presents low values of eye centroid size.

Shape changes

In dimension one (82 to 85% of the covariation; Table S3.4), the shape changes obtained for the skull in the biomechanical block were similar to the ones obtained for the feeding block. However, these changes were more prominent for the biomechanical performance block (Figures 3.2D and S3.6). These shape changes were: (1) low XScores have long, slender rostra and frontals. (2) high XScores have a dorsoventrally high, anteroposteriorly short rostrum, and a mediolaterally expanded braincase.

PLS scores of shape and biomechanics

The distribution of species scores across the PLS dimension is different in the biomechanical block than in the feeding block. The percentage of covariance in dimension one of biomechanics is lower than in feeding dimension one (Figure 3.2B, S3.5). In this biomechanical dimension one, it was easier to identify scores related to arboreal

frugivorous species: low scores in the skull and the rostrum and high scores in the braincase module. Higher values in the complete skull were identified for *Phaps elegans*, *Patagioenas squamosa*, and *Caloenas nicobarica* (clusters "E", "f", and "A"), while low values were obtained by *Didunculus strigirostris*, *Patagioenas nigrirostris*, *Pezophaps solitaria*, *Treron curvirostra* (frugivorous clusters "g", "h", "A", and "f").

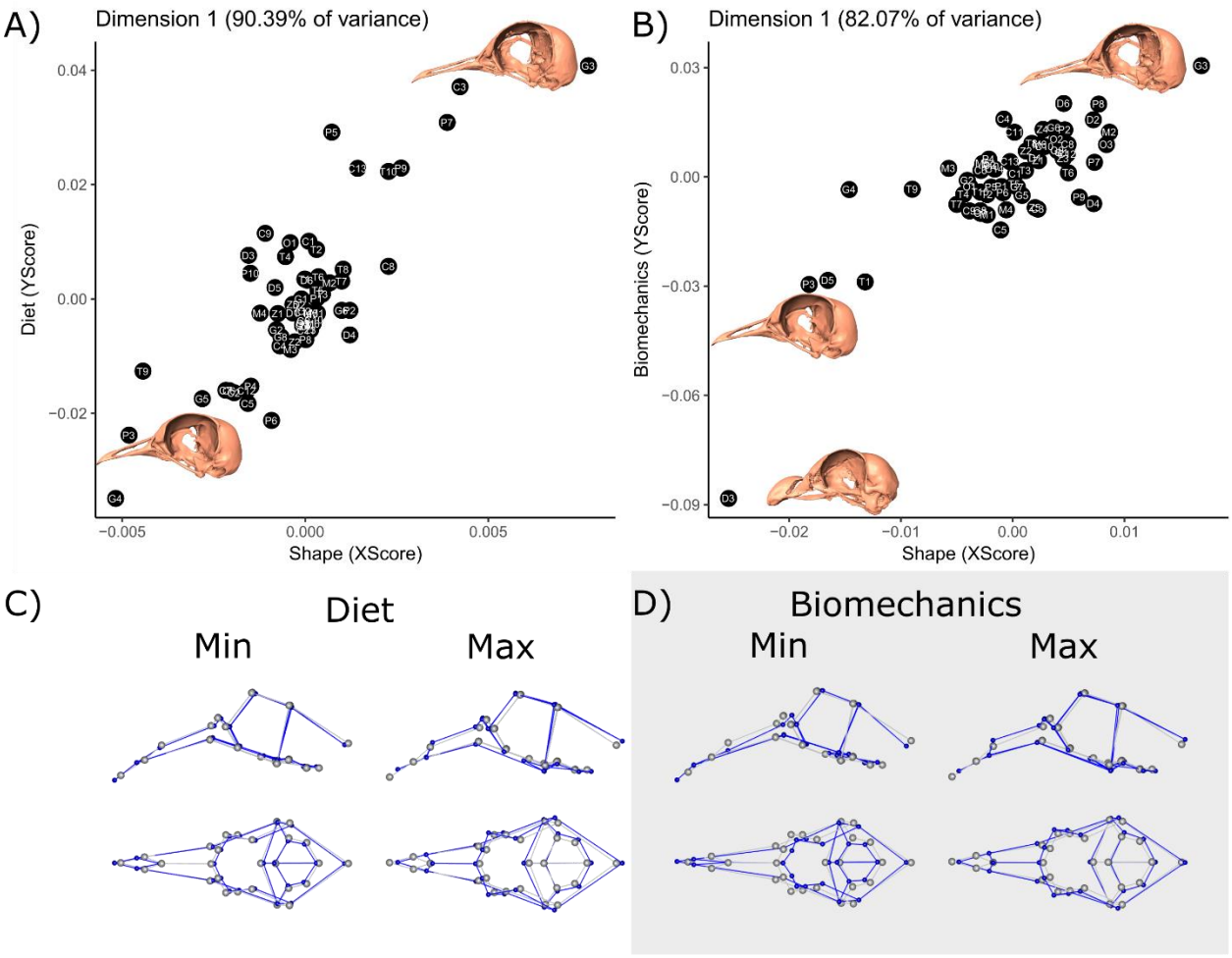


Figure 3.2. PLS dimension one. A) Shape (XScores) versus other diet block (YScores). B) Shape (XScores) versus other biomechanical performance block. Legend as in Figure A3.1. Three-dimensional models of species with extreme values exemplify the empirical skull shape variation along the first PLS dimension. C) and D) Predicted shapes for the maximum and minimum values of XScores in the PLS dimension one. Patterns recovered by the biomechanical and feeding blocks against shape are congruent overall however the degree of shape change is different. Legend: Leucosarcia melanoleuca (G1), Ocyphaps lophotes (G2), Phaps elegans (G3), Phaps histrionica (G4), Phaps chalcoptera (G5), Petrophassa albipennis (G6), Geopelia cuneata (G7), Geophaps plumifera (G8), Gallicolumba luzonica (G9), Phapitreron leucotis (O1), Treron curvirostra (T1), Treron

formosae (T2), Hemiphaga novaeseelandiae (T3), Lopholaimus antarcticus (T4), Ducula pacifica (T5), Ducula goliath (T6), Ptilinopus dupetithouarsii (T7), Drepanoptila holosericea (T8), Alectroenas madagascariensis (T9), Alectroenas pulcherrimus (T10), Caloenas nicobarica (D6), Pezophaps (D5), Raphus (D4), Didunculus (D3), Goura cristata (D2), Otidiphaps nobilis (D1), Turtur tympanistria (O2), Chalcophaps indica (O3), Geotrygon versicolor (Z5), Starnoenas cyanocephala (Z4), Geotrygon mystacea (Z3), Zenaida macroura (Z2), Leptotila rufaxilla (Z1), Patagioenas speciosa (P10), P. leucocephala (P9), P. squamosa (P8), P. plumbea (P7), P. picazuro (P6), P. cayennensis (P5), P. maculosa (P4), P. nigrirostris (P3), P. fasciata (P2), Ectopistes migratorius (P1), Columba arquatrix (C1), C. guinea (C2), C. trocaz (C3), C. rupestris (C4), C. livia (C5), C. oenas (C6), C. palumbus (C7), C. vitiensis (C8), C. pulchricollis (C9), Streptopelia turtur (C10), Streptopelia decaocto (C11), Aplopelia larvata (C12), Turacoena manadensis (C13), Macropygia unchall (C14), Columbina cruziana (M1), Columbina passerina (M2), Columbina talpacoti (M3), Metriopelia melanoptera (M4), Metriopelia ceciliae (M5), and Claravis pretiosa (M6).

PLS dimension two (biomechanics)

Salient variables

For the overall skull shape in the second PLS dimension, salience is low for all variables (Table 3.4). For the rostrum module, rostrum depth is salient (-0.16). An unexpected result was that several proxies are salient for braincase shape correlation in dimension 2: output distance (-0.17), mouth opening (-0.17), rostrum depth (-0.18), lever length (-0.38), rostrum width (-0.1), and eye centroid size (0.21). These results were surprising because several of these variables are located in the rostrum module (Supplementary material S3).

Biomechanical performance in PLS dimension two

In dimension two, patterns are less clear for the complete skull (Figures 3.5B and S3.12). I identified outliers for the complete skull: two negative outliers *Didunculus* and *Pezophaps* and one positive outlier *Phaps histrionica*.

Shape changes

In the second PLS dimension (which explains 4 to 13% of correlation) there are conspicuous differences between the shape changes predicted in the diet and biomechanical blocks (Figures 3.3C-D and S3.8). Shape changes were identified in the braincase module but not in the complete skull or rostrum module (Supplementary material S3, Figure S3.8).

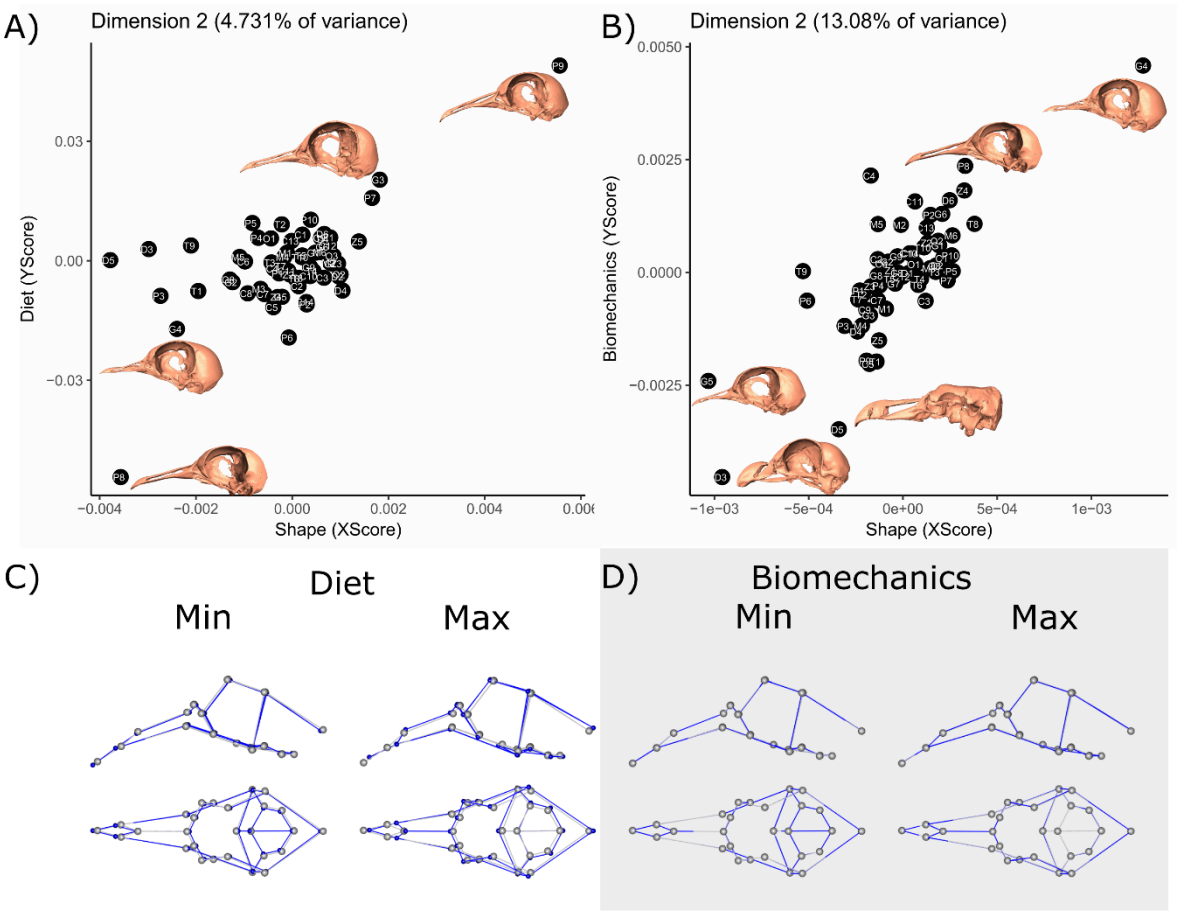


Figure 3.3. PLS dimension two. A) Shape (XScores) versus other diet block (YScores). B) Shape (XScores) versus other biomechanical performance block. Legend as in Figure 3.2. Three-dimensional models of species with extreme values exemplify the empirical skull shape variation along the first PLS dimension. C) and D) Predicted shapes for the maximum and minimum values of XScores in the PLS dimension two. PLS dimension 2 shape changes were identified differentially when evaluating the biomechanical and feeding data blocks. PLS dimension 2 captures important shape changes for the complete skull while, the biomechanical data block does not capture important shape changes in the skull. Figure S3.6 and S3.8 show that PLS dimension 2 captures shape changes for the complete skull and the rostrum module while, in the biomechanical data block only captures important shape changes in the braincase module.

PLS scores of shape and biomechanics

In PLS dimension two, for the biomechanical data block versus complete skull shape (Figure 3.3B), high values were obtained by *Phaps histrionica*, *Patagioenas squamosa*, *Columba rupestris*, and *Starnoenas cyanocephala* ("E" and "f"), while *Didunculus*, *Pezophaps*, *Phaps chalcoptera* ("g", "A", and "E") presented the lowest YScores values.

The overall two-block PLS results showed that the covariance of shape with feeding was higher than the covariance with biomechanical performance. For the feeding block, clear patterns were identified only for the first PLS dimension. The shape changes in both dimensions are similar for the skull and rostrum (Supplementary material S3). For the biomechanical performance block, both dimensions showed patterns related to diet. The shape changes, in dimension one, were similar to the ones of the feeding block. In dimension two most shape changes happened in the braincase (Supplementary material S3).

Two-block partial least squares of feeding versus biomechanical performance

Covariation and significance

The covariation between feeding and biomechanical performance was moderate (Table 3.3) and presented a lower statistical support than any of the other analysis in an ordinary setting (PLS_{corr}= 0.531; *P*= 0.010). When phylogeny was taken into account, the covariation was also moderate, but non-significant (PLS_{corr} = 0.575, sd= 0.133; *P*=0.095, sd= 0.119).

Salient variables

When the feeding and biomechanical performance were analysed in a two-block PLS (Table 3.5), the salient variables in the first dimension of the biomechanical block were: rostrum dept (0.49), rostrum width (0.13), and effort distance (0.13). In dimension 2 the salient variables were rostrum depth (-0.16) and lever length (-0.15). For the feeding block in dimension one, the most salient axes were: PCO4 (-0.34), PCO1 (-0.21), PCO7 (0.17), PCO8 (-0.13), and PCO3 (-0.12). In dimension 2 the most salient axes were: PCO4 (0.13) and PCO1 (-0.11).

Table 3.5. PLS vectors of the phylogenetic two-block PLS analysis of diet versus biomechanical blocks in the first two PLS dimensions (at least 94% of the covariation between blocks). Each vector shows the loadings of the original variables in the PLS dimensions. A) shows the loadings for the right PLS vector, and B) shows the loadings for the left PLS vector.

A) PLS vectors for the biomechanical block		
Variable	Dim. 1	Dim. 2
Input distance	0.13	0.03
Output distance	0.06	-0.01
Mouth opening	0.06	-0.01
Rostrum height	0.49	-0.16
Lever length	0.04	-0.15
Rostrum width	0.13	0.07
Muscle centroid size	0.09	0.01
Eye centroid size	-0.02	-0.01
B) PLS vectors for the feeding block		
Variable	Dim. 1	Dim. 2
PCO 1	-0.21	-0.11
PCO 2	0.03	-0.05
PCO 3	-0.12	0.04
PCO 4	-0.34	0.13
PCO 5	0.08	-0.03
PCO 6	0.08	-0.01
PCO 7	0.17	-0.03
PCO 8	-0.13	0.04
PCO 9	0.08	-0.07
PCO 10	0.04	-0.04
PCO 11	0.01	-0.02

PCO 12	0.03	-0.04
PCO 13	0.07	-0.03
PCO 14	-0.01	-0.03
PCO 15	-0.07	0
PCO 16	-0.02	0.02
PCO 17	-0.03	0.01
PCO 18	0.05	-0.02
PCO 19	0.01	0.01

Three-way comparison between feeding, shape, and biomechanical blocks (z-scores)

The statistical comparison between different two-block PLS analyses, like the ones presented here for different modules, needs to be done taking in account the differences between sample sizes and number of variables (Adams and Collyer, 2016). I obtained the effect size of different analyses (z-scores: Table 3.3, Figure 3.6). For ordinary two-block PLS, larger effect sizes were obtained by analyses comparing shape against biomechanical performance (z-scores feeding = 3.00 to 3.96 versus z-scores biomechanics = 4.26 to 6.25). For phylogenetic analyses, larger effect sizes still occurred in the biomechanical blocks (z-scores = 5.01 to 7.46) but the difference against feeding blocks was smaller (z-scores=4.26 to 6.25). Overall, the effect of diet and biomechanics is larger in the rostrum shape (z-scores = 6.25 and 7.46) than the skull shape (z-scores = 5.93 and 6.28) and the braincase shape (z-scores = 4.26 and 5.01). Finally, the effect sizes of diet against biomechanical blocks are lower (z-scores = 3.412 and 3.167; Figure 3.6). The effect sizes of diet versus biomechanical blocks are similar in an ordinary or phylogenetic setting. These results indicate that, in a phylogenetic setting, biomechanics has a larger effect on skull and braincase shape, while

both feeding, and biomechanical data blocks have a similar effect size in the rostrum shape module.

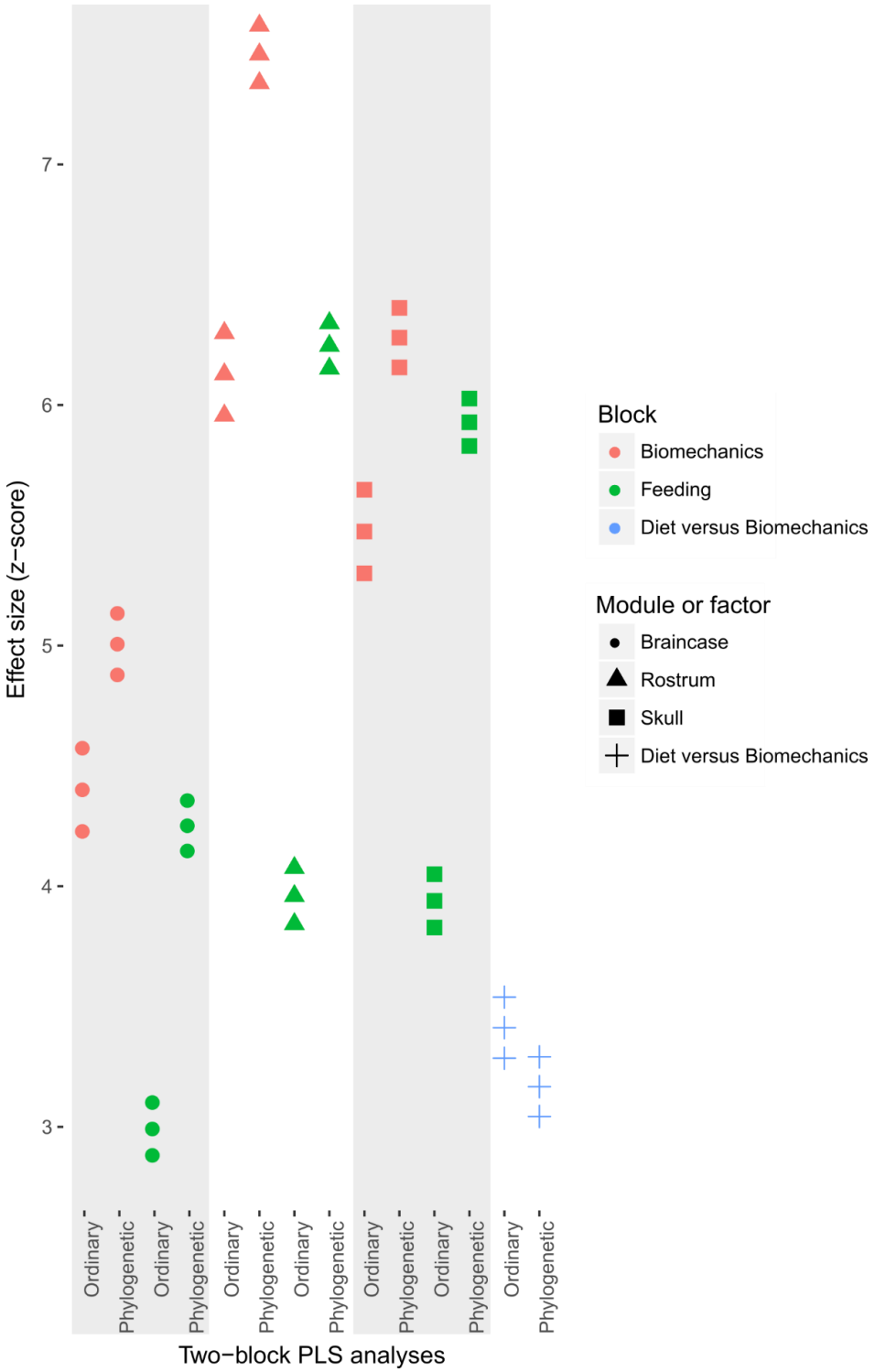


Figure 3.6. Z-scores of all two-block PLS analyses. Upper and lower dots indicate the two standard deviations confidence interval. Correlation is consistently higher in the phylogenetic framework

when shape is compared with other data blocks. Also, correlation between data blocks with shape is higher when within the modules than in the complete skull.

Factors explaining shape (regression setting)

Distance-based ordinary least squares regression

Complete skull

The salient variables identified by the two-block partial least squares were used to try to explain skull and module shape (Tables 3.6, S3.5, S3.6). I identified that only a small number of variables are significant to explain skull shape in a regression setting (Table 3.6). The significant variables identified by the D.ols were: centroid size (*P*= 0.001), mass (*P*= 0.001), biomechanics PLS dimensions one (*P*= 0.001) and two (*P*= 0.002), all biomechanical characters (*P*= 0.001), feeding PCO1 (*P*= 0.001), and PCO3 (*P*= 0.043). Some of the categorical variables were significant: significant clusters from the average clustering algorithm (*P*= 0.001), frugivorous or granivorous (*P*= 0.004), live prey (*P*= 0.001), green plant matter (*P*= 0.008), and terrestrial or arboreal foragers (*P*= 0.044). While most of these significant variables explained less than 10% of the variation in the sample, biomechanical PLS-dimension one (R^2= 18%) and most biomechanical characters explained more than 10% of the unexplained variation: input distance (R^2= 13%), lever length (R^2= 26.5%), output distance (R^2= 11%), mouth opening (R^2= 11%), muscle area (R^2= 17%), rostrum depth (R^2= 13%) and width (R^2= 12%). For the categorical variables, the significant clusters explained a large amount of the variation (R^2= 27.5%).

Modules

Detailed results for the factors explaining module shape are provides in Supplementary material (S3). For the rostrum module the D.ols identified 18 significant variables (Table

S3.5). Seventeen significant variables that explain the shape of the braincase module were identified (Table S3.6).

Table 3.6. Results for the ordinary least squares (ols) and phylogenetic generalized least squares models of skull shape versus candidate explanatory variables. A series of pairwise regressions were performed to try to explain the skull shape (independent variable). The candidate explanatory variables were either untested ecological variables or variables previously identified as salient variables in the two-block PLS.

	Distance-based ordinary least squares			Distance-based phylogenetic generalized least squares					
Skull shape~	Z	Rsq	Pr(>F)	Z	Z.sd	Rsq	Rsq.sd	Pr(>F)	Pr(>F).sd
landmass area	-1.249	0.007	0.896	-1.145	0.741	0.048	0.096	0.820	0.198
Csize	**3.505**	0.091	**0.001**	2.561	1.066	0.079	0.075	0.054	0.120
Body mass	**3.209**	0.075	**0.001**	2.172	0.764	0.053	0.068	0.051	0.106
Distribution	0.335	0.034	0.359	-0.926	0.534	0.096	0.111	0.809	0.185
BiomechD1	**4.690**	**0.180**	**0.001**	1.323	0.509	**0.146**	0.117	0.125	0.098
BiomechD2	**3.017**	0.068	**0.002**	-0.615	0.581	0.082	0.111	0.694	0.204
De	**4.467**	**0.135**	**0.001**	1.985	0.944	0.073	0.087	0.082	0.124
Dlever	**5.554**	**0.265**	**0.001**	**4.313**	1.346	**0.218**	0.091	**0.010**	0.030
Do	**4.025**	**0.111**	**0.001**	1.289	0.507	**0.122**	0.095	0.133	0.090
EyeT	**3.714**	0.096	**0.001**	2.102	0.980	**0.120**	0.112	0.074	0.109
Mo	**4.025**	**0.111**	**0.001**	1.289	0.507	**0.122**	0.095	0.133	0.090
MuscleT	**5.124**	**0.170**	**0.001**	2.167	0.897	**0.101**	0.085	0.063	0.111
Thick	**4.072**	**0.134**	**0.001**	1.852	0.803	0.081	0.061	0.085	0.135
Width	**4.355**	**0.124**	**0.001**	1.444	0.572	0.091	0.105	0.109	0.102
FoodD1	0.255	0.016	0.385	-0.058	0.524	**0.112**	0.139	0.502	0.193
FoodD2	-1.395	0.006	0.950	-0.860	0.335	0.065	0.093	0.822	0.130
PCO1	**3.385**	0.069	**0.001**	0.507	0.417	0.049	0.071	0.303	0.137
PCO2	0.808	0.021	0.208	-0.445	0.478	0.057	0.099	0.652	0.177
PCO3	1.705	0.031	**0.046**	-0.322	0.708	0.083	0.120	0.602	0.237
PCO6	0.756	0.021	0.232	-0.170	0.617	0.090	0.113	0.551	0.216
PCO8	0.062	0.015	0.458	-0.166	0.569	0.084	0.129	0.538	0.214
ClusterGAve	**3.647**	**0.275**	**0.001**	-0.324	0.237	**0.172**	0.070	0.596	0.100
FruitDB	0.236	0.016	0.391	0.048	0.382	0.021	0.039	0.447	0.151
GrainsOrSeeds	0.815	0.021	0.198	0.446	0.653	0.058	0.102	0.343	0.180
Greens	2.503	0.043	**0.008**	0.473	0.410	0.057	0.092	0.315	0.141
LivePrey	**3.723**	0.072	**0.001**	0.076	0.646	0.090	0.116	0.462	0.217
MostDiet	2.988	0.090	**0.004**	0.590	0.278	0.059	0.050	0.275	0.085
MostForage	2.518	0.095	**0.044**	0.804	0.371	0.076	0.069	0.204	0.090
NutsRoots	0.479	0.018	0.318	0.566	0.273	0.055	0.087	0.283	0.083

Factors explaining shape (phylogenetic regression setting)

When the phylogeny and phylogenetic uncertainty were taken in account, only the lever length (biomechanical character) was found to be significant for explaining the skull shape (*P*= 0.01; Table 3.6). However, this result might be expected because this variable was measured directly from the Procrustes aligned coordinates, although other biomechanical traits measured from the same coordinates were non-significant. Despite being non-significant, some variables still presented non-negligible R^2 values: PLS biomechanics dimension one (R^2= 14.6%), lever length (R^2= 21.8%), output distance (R^2= 12.2%), eye size (R^2= 12%), mouth opening (R^2= 12.2%), muscle area (R^2= 10.1%), PLS feeding dimension one (R^2= 11.2%), and the significant average clusters (R^2= 17.2%).

For the rostrum module the lever length was also the only significant variable (*P*= 0.006). However, nine variables presented correlations higher than 10% (Table S3.5). PLS biomechanical dimension one (R^2= 16.7%), lever length (R^2= 27.5%), output distance (R^2= 13%), eye size (R^2= 11.1%), mouth opening (R^2= 13%), muscle area (R^2= 10.4%), and PLS feeding dimension one (R^2= 11.4%). Categorical variables with high correlation were the significant clusters (R^2= 18.4%) and the distribution type (R^2= 10.2%).

For the braincase module in a phylogenetic framework I identified one significant variable (Table S3.6): lever length (*P*= 0.048). Only seven variables presented correlations with shape larger than 10%: PLS biomechanical dimension one (R^2= 10.7%), lever length (R^2= 11.7%), output distance (R^2= 10.7%), eye size (R^2= 13.3%), mouth opening (R^2= 10.7%), PLS feeding dimension one (R^2= 10.8%), and the categorical significant clusters (R^2= 15.3%).

From these significant variables, only two presented high effect sizes: lever length (z-scores= 2.7) and eye size (z-scores= 2.2).

Factors explaining biomechanical performance (regression setting)

Finally, I evaluated what variables could explain the biomechanical properties of the columbiform skull (summarized by PLS biomechanical dimensions; Table 3.5). I found no phylogenetic signal (λ= 0) in the correlation between biomechanics and any evaluated factors, this makes the phylogenetic generalized least squares results identical to the ordinary least squares results (Table 3.7). For the linear model, PLS biomechanical dimension one was not explained in a significant manner ($P < 0.05$) by any variable (Table 3.7). The largest correlation was obtained by the significant clusters of diet (R^2= 20%). AIC values obtained by all the variables ranged between -342.93 and -338.16. The model with minimum AIC value was obtained by the categorical variable of frugivorous versus granivorous. I also identified other models that are at least 40% more likely to minimize the information loss: feeding PCO1 (P_{info}= 86.3%), PCO3 (P_{info}=75.2%), significant clusters (P_{info}=48.8%), live prey consumption (P_{info}=98.2%), main foraging strategy (P_{info}=62.3%), and the consumption of nuts and roots (P_{info}=61.1%).

Table 3.7. Results for the ordinary least squares (ols) and phylogenetic generalized least squares models of biomechanical performance versus a series of candidate explanatory variables (ecological and feeding). The XScores (PLS XScores of the two-block PLS analysis of skull shape versus biomechanical performance) were used as a summary of the overall biomechanical performance. The first two PLS Xscores in the first two dimensions were used as independent variables. A series of pairwise regressions were performed to try to explain the biomechanical performance (independent variable).

Model	Ordinary least squares			Phylogenetic generalized least squares		
PLS biomechanic dim 1	AICval	R2	pVal	AICm	Lambda	Minimization of information loss
mass	-340.971	0.025	0.218	-340.971	0.000	38%
Csize	-340.503	0.017	0.302	-340.503	0.000	30%
Area	-339.568	0.003	0.683	-339.568	0.000	19%
Distribution	-338.157	0.012	0.695	-338.157	0.000	9%
FoodD1	-339.526	0.002	0.722	-339.526	0.000	18%
FoodD2	-339.463	0.001	0.796	-339.463	0.000	18%
PCO1	-342.632	0.050	0.078	-342.632	0.000	**86%**
PCO2	-339.394	0.000	0.982	-339.394	0.000	17%
PCO3	-342.357	0.046	0.092	-342.357	0.000	**75%**
PCO6	-340.122	0.011	0.403	-340.122	0.000	25%
PCO8	-339.435	0.001	0.843	-339.435	0.000	17%
ClusterGAve	-341.493	**0.201**	0.076	-341.493	0.000	**49%**
FruitDB	-339.994	0.009	0.448	-339.994	0.000	23%
GrainsOrSeeds	-339.394	0.000	0.999	-339.394	0.000	17%
Greens	-339.397	0.000	0.956	-339.397	0.000	17%
LifePrey	-342.890	0.054	0.067	-342.890	0.000	**98%**
MostDiet	-342.927	0.084	0.072	-342.927	0.000	**100%**
MostForage	-341.981	0.070	0.113	-341.981	0.000	**62%**
NutsRoots	-341.941	0.040	0.118	-341.941	0.000	**61%**
PLS biomechanic dim 2~	AICval	R2	pVal	AICm	Lambdam	Minimization of information loss
mass	-654.198	0.075	**0.030**	-654.198	0.000	**70%**
Area	-650.847	0.024	0.224	-650.847	0.000	13%
Csize	-653.844	0.069	0.037	-653.844	0.000	**58%**
Distribution	-654.595	**0.109**	**0.031**	-654.595	0.000	**85%**
FoodD1	-651.492	0.034	0.147	-651.492	0.000	18%
FoodD2	-654.922	0.085	**0.020**	-654.922	0.000	**100%**
PCO1	-650.312	0.016	0.326	-650.312	0.000	10%
PCO2	-650.290	0.015	0.331	-650.290	0.000	10%
PCO3	-650.222	0.014	0.349	-650.222	0.000	10%
PCO6	-649.535	0.004	0.639	-649.535	0.000	7%
PCO8	-650.261	0.015	0.338	-650.261	0.000	10%
ClusterGAve	-646.117	**0.131**	0.330	-646.117	0.000	1%
FruitDB	-649.978	0.011	0.422	-649.978	0.000	8%
GrainsOrSeeds	-649.309	0.000	0.961	-649.309	0.000	6%
Greens	-650.249	0.015	0.341	-650.249	0.000	10%
LifePrey	-649.387	0.001	0.782	-649.387	0.000	6%
MostDiet	-650.549	0.050	0.214	-650.549	0.000	11%

MostForage	-648.330	0.016	0.614	-648.330	0.000	4%
NutsRoots	-650.035	0.011	0.403	-650.035	0.000	9%

For PLS biomechanical dimension two, I found three significant variables: mass (*P*= 0.03), distribution type (*P*=0.031), and the PLS feeding dimension two (*P*= 0.02). Variables with R^2 values higher than 10% were the significant feeding clusters (R^2= 13.1%) and the distribution type (R^2= 10.9%). AIC values of different models ranged between -654.92 and -646.12. The model with minimum AIC value was obtained by the feeding dimension two. However, I identified other models that are at least 40% more likely to minimize the information loss: mass (P_{info}= 69.6%), centroid size (P_{info}= 58.3%), and distribution type (P_{info}= 84.9).

Discussion

Diet classification of Pigeons

I propose a new classification of pigeon feeding behaviour based on diet and foraging. This new classification defined between seven and eight pigeon clusters. However, as this new classification is not the main objective of this chapter and it is not related to geometric morphometrics I discuss these results and the feeding evolution of Columbiformes in detail in Appendix Two. The new classification recovers the Raphini, along with *Caloenas nicobarica*, as members of a distinctive terrestrial frugivorous clade (cluster "A") and not only as a particular cases of the standard pigeon classifications: "*R. cucullatus* and *P. solitaria* are considered most simply to be 'obligate,' perhaps specialized, members of the terrestrial group." (Livezey, 1993).

Feeding evolution (phylofeedingspace)

Detailed discussion of the feeding evolution in columbiforms is provided in Appendix Two. The matter of the evolution of feeding behaviour in Columbiformes has not been considered with enough detail in the literature (Goodwin, 1983; Janoo, 2005; Gibbs, Barnes and Cox, 2010). One noticeably exception is Lapiedra *et al.* (2013) who found terrestrial foraging to be the ancestral foraging strategy in columbiforms. Little attention has been paid towards possible ancestral states and the putative feeding behaviour (diet and foraging) convergence of some distantly related pigeon groups (Figure A2.1A): (1) granivory of some *Columba* and *Patagioenas*, and Claravinae, Zenaidini or Turturini, or (2) the frugivory of some *Columba* and *Patagioenas*, and species of the, hereby called, "fruit

pigeons" (*Alectroenas*, *Drepanoptila*, *Ptilinopus*, *Ducula*, *Lopholaimus*, *Hemiphaga*, and *Treron*).

Terrestrial foraging behaviour is the likely ancestral condition in Columbiformes (Figure A2.1 and A2.2). This agrees with the assessment made by Lapiedra *et al.* (2013). Columbiformes have occupied other regions (besides the ancestral terrestrial granivory) of the feeding space at least three times (Figure A2.2): (1) by *Columba* and *Patagioenas* around 29 to 25 million years ago (mya) (Late Rupelian to Early Aquitanian; Oligocene to Early Miocene), (2) by Raphinae around 34 mya (Middle Rupelian; Oligocene) and (3) by "fruit pigeons" around 30 mya (Rupelian; Oligocene).

Biomechanical landscape

The biomechanical landscape approach allowed me to assess the species distribution in the performance space (based on shape alone). A detailed discussion of the biomechanical landscape and its implications for the natural history of Raphini is provided in Appendix Three. From which the first two principal components of shape (55% of the sample variation) are related to the feeding behaviour classification proposed here. I detected biomechanical performance differences related to diet in pigeons with a conservative shape (closer to the mean shape of the sample), I noted that frugivorous species (Cluster M1; "fruit pigeons", frugivorous Columbini, and Raphinae) show higher biomechanical performance than granivorous species. This high performance corresponded to large muscle area and high mechanical advantage. These frugivorous species skull shapes also showed high resistance to bending (high rostrum thickness and moments of area and mass).

The granivorous species show slender rostra, large eye sizes, and small mouth openings that close at high velocity. The granivorous species also show low mechanical advantages and low output forces with small muscle areas and low bending resistance (moments of area and mass). For PC3 and 4 (15.2% of sample variation), only muscle area and lever length seem to be related with any feeding strategies (ancestral granivorous diet, Appendix Two). *Didunculus* is the pigeon with a skull shape that presents a higher bending resistance and output force, this species also presents relatively large eye sizes, unlike the Raphini.

The skull shape of the Raphini, especially the dodo, has been hypothesized to be related to the inclusion of animals in the diet (Owen, 1866; Livezey, 1993). The biomechanical performance of the skull shape in Raphini, compared to that of other pigeons, seems to contradict some of the feeding behaviour hypotheses. Raphini do exhibit the highest bite velocity of the sampled species which could suggest the inclusion of animal matter in the diet. However, Raphini exhibit the smallest comparative eye size which could indicate low visual acuity. The bending resistance (moment of mass) of Raphini is similar to the one of *Treron curvirostra* or other "fruit pigeons". Furthermore, Raphini exhibit the largest mouth opening of the sample which might be related to the consumption of large fruits (Diamond, 1973; Emerson and Radinsky, 1980; Andersson, Norman and Werdelin, 2011). Overall these results support the classical view of feeding behaviour in Raphini (mainly fallen fruit on the forest ground; Owen 1866; Livezey 1993).

Modularity and integration

The only assessment of modularity and integration in the columbiform skull for feral and domestic *Columba livia* was done by Young et al. (2016), the authors reported both a strong

shape integration in feral pigeons (PLScorr = 0.845, *P*= 0.030) and domestic pigeons (PLScorr = 0.978, *P*= 0.001). However, they obtained CR values showed evidence of weak integration for feral pigeons (CR = 0.868, *P*= 0.010) and showed evidence of random covariation between and within modules for domestic pigeons (CR = 1.029, *P*= 0.010). While these results were compared with the ones obtained by a comparative sample of birds, they were not done in a comparative phylogenetic framework.

This research took the logical step of comparing the modularity and integration of *C. livia* with a closely related clade (i.e., Columbiformes). The analysis of the comparative sample, which took into account the phylogeny and phylogenetic uncertainty, found similar patterns of integration between the rostrum and the braincase (PLScorr = 0.86; sd= 0.039; *P*= 0.001). However, I found the CR values of Columbiformes were non-significant and close to 1 (CR= 1.029; sd= 0.054; *P*= 0.456 ± 0.320), which agrees with the domestic pigeon results from Young et al. (2016). The self-similarity, which does not take phylogeny into account, for the complete skull pointed towards most variation happening in small spatial scales (α= -0.353), these results suggest that modularity exists but is not strong in the columbiform skull.

From these results, I argue that it is not desirable to directly compare the modularity and integration patterns of one species with broader taxonomic groups. Modularity seems to be weak and non-significant, which is not a clear pattern that can be compared across taxonomic levels (feral and domestic *C. livia*, Columbiformes and all birds). On the other hand, the detected strong integration of the skull might not reflect similar developmental constraints, but the constraints expected from a functional matrix, a structure which

balances different functional criteria that persist over a growth which is expected to be an integrated structure (Bookstein 2015).

Correlation between shape and biomechanics

I found that PLS dimension one represents most of the correlation between shape and both biomechanics and diet. When I interpreted the minimum and maximum values of the feeding PLS dimension one, there was a good concordance with the two main feeding clusters proposed (terrestrial granivorous and frugivorous tree foraging pigeons). I identified shape changes related to these PLS dimensions to be concordant with previous theories of pigeon form/shape correlation (Diamond, 1973; Goodwin, 1983). I found long slender rostra are related with granivory while thicker braincases with laterally expanded frontals and thick rostra in the midsagittal plane are related to frugivory. These same shape changes were detected on the rostrum module. However, these changes were more difficult to see in the braincase.

Correlation of biomechanics on shape and diet

Biomechanics and shape are correlated, this result was expected because biomechanical factors are calculated from the shape. However, the diet and biomechanical data are independent, and I decided to discuss the correlation between these factors further. Based on the observed patterns of species distribution in the biomechanical landscape, a high correlation between biomechanics and diet was expected. However, my results showed that the lowest correlation between blocks was obtained between diet and biomechanics, this correlation was also non-significant (PLScorr = 0.575 ± 0.133 and *P*=0.095 ± 0.119). Overall the two-block PLS analysis allowed me to explore large amounts of variables

simultaneously and find salient variables. I further tested these salient or important variables in a regression setting.

Factors that explain skull and module shape

Accounting for phylogeny and phylogenetic uncertainty significantly diminished the number of significant variables. For the skull and both modules (rostrum and braincase), the only significant variable that explains skull shape was the lever length. Lever length was directly measured from the Procrustes aligned skulls. As lever length is expected to be correlated with skull length, it was anticipated that it would explain skull shape. However, lever length explaining braincase shape was an unforeseen result. Because of the possible circular reasoning of the biomechanics in shape, I will only discuss the non-biomechanical variables that presented high correlation with the skull shape in a phylogenetic regression setting. For continuous variables, only the PLS feeding dimension one was highly correlated with the shape of the complete skull (11.2%), rostrum module (11.4%), and braincase module (10.8%). For the categorical variables, only the significant clusters from the average linkage algorithms explained a high proportion of the shape of the skull (17.2%), rostrum module (18.4%) and braincase module (R2= 15.3%). Overall these results add to previous sections of this research in supporting the influence of feeding behaviour on shape.

Factors that explain biomechanics

Our results suggest again that biomechanics presents a non-negligible correlation with feeding clusters. The skull biomechanics is correlated with the significant clusters in both PLS dimensions. This correlation, along with the best AIC model being the categorical variable "frugivorous versus granivorous" for dimension one (82% correlation) supports the

fact that these two feeding strategies show different biomechanical requirements. Also, live prey consumption and the feeding PCO1 and PCO3 presented models which might fit the shape data better. All of the variables explaining biomechanics are related to feeding behaviour. The biomechanical dimension one contrasts with biomechanical dimension two (13% of correlation), in which non-feeding factors seem to be important for predicting biomechanics. Besides the feeding clusters, the distribution type also presented high correlation with biomechanics. The AIC values showed that, besides feeding PLS dimension two, three significant variables produce models that could fit the biomechanical data well and reduce information loss (Table 3.7): size (body mass and centroid size) and distribution type. Biomechanics might be expected to correlate with size (body or centroid size) because lager pigeons consume larger food items (Diamond, 1973). As I demonstrated in this chapter, the consumption of large food items like fruits requires a higher biomechanical performance (bending resistance, input force, mechanical advantage). The performance in my analyses was calculated on the size-free Procrustes aligned coordinates (although these coordinates are not free from allometric size). Noticeably, the correlation between biomechanics and size was found even in the Procrustes aligned coordinates.

Our results show that biomechanics is not entirely explained by feeding behaviour. However, diet is recovered as a highly important continuous or categorical variable that explains biomechanics. The detected amount of correlation is non-negligible and is larger than the one obtained for allometry in Chapter Two (11%). These findings show that the different biomechanical performance needed for processing different food resources has significantly shaped the columbiform skull. Thus, my research supports a Darwinian (Darwin, 1859) view of skull shape evolution in Columbiformes. However, I acknowledge

that these results suggest an interplay between function and development rather than absolute adaptationist (Mayr, 1983) or developmental/non dietary (Bright *et al.*, 2016) controls of columbiform evolution. The importance of other factors in skull shape is shown in biomechanical PLS dimension two were, besides diet, other factors like size and distribution could explain the shape of the columbiform skull.

The results also show the effects of the principle of frustration (Marshall, 2006) working on the functional matrix (Bookstein, 2015) of the columbiform skull. Again, the balancing between, sometimes contradictory, functions can obscure the relationship between shape and function. However, the ecological diversity in Columbiformes allowed me to detect such interactions in the columbiform skull.

Effect of feeding behaviour and biomechanics on skull shape, evidence for a columbiform adaptive radiation

The findings suggest that biomechanics has a higher effect on the skull and module shape than feeding. However, this result can be expected because biomechanics was calculated from the shape data. What these findings highlight is the fact that the covariation between biomechanics and shape is higher in the rostrum and lower in the braincase. This pattern was similar for the feeding data, which suggests that the rostra of birds are indeed subjected to higher selection pressures than the braincase module. The selection is towards different biomechanical performances required by different diets. These results contrast with the view of non-dietary factors controlling for most of the shape that has been proposed for other birds (Bright *et al.*, 2016).

I find evidence for both Darwinian (natural selection; Darwin, 1859) and Simpsonian (quantum evolution; Simpson, 1944) views of evolution. Bright et al. (2017) found evidence for phenotypical discontinuities on the avian beak phenotype coming rapid increases in rates of evolution, supporting a "quantum evolution model", i.e., changes occur unpredictably across phylogeny. Bright et al. (2017) characterized the shift of evolutionary rates changes as follows: (1) High evolutionary rates at the base of the tree (Quantum evolution) in Phoenicopteridae, Musophagidae, Pelecanidae and Caprimulgiformes. (2) Quantum leaps associated with subsequent low rates likely because of evolutionary constraints (Pelecanidae and Ciconiidae). (3) Quantum leaps towards already occupied morphospace (Hirundidae), and (4) Quantum leaps to a new area of the morphospace which is then expanded (Trochilidae). (5) Some of the highest evolutionary rates correspond to island or archipelago radiations (Madagascan vangas, Galapagos finches, and Hawaiian honeycreepers).

In light of my findings, the *Columba* and *Patagioenas* clade is an example of (3) a quantum leap towards an already occupied morphospace (by other pigeons) while the Raphinae are an example of a classical island or archipelago radiation which has been able to invade a new part of the feeding space (and morphospace) which was previously unoccupied.

Furthermore, changes in rates of evolution in Columbiformes were detected but not discussed by Bright et al. (2017). Two steam-stem branch evolutionary rates in columbiforms supported whole-clade shifts in evolutionary rates, while a terminal branch with high rates of evolution was also detected (putatively *Didunculus*). Their mega-evolutionary morphospace characterization showed one columbiform species that was

plotted away from the other columbiforms in the sample. I made an average cluster of the Euclidean distances between species reported by Bright et al. (2017). When the nine highest clusters of the 2,000 species sample, *Didunculus* was included within a cluster nine of 318 species, from mainly five orders: Passeriformes (102 spp.), Psittaciformes (75 spp.), Accipitriformes (61 spp.), Galliformes (35 spp.), and Strigiformes (18 spp.). When the next highest cluster was recovered (cluster 10), *Didunculus* was placed in a small cluster of 6 species: four Accipitriformes (*Chondrohierax uncinatus*, *Helicolestes hamatus*, *Pithecophaga jefferyi*, and *Rostrhamus sociabilis*) and one species of Passeriformes (*Pseudonestor xanthophrys*). The fact that this small cluster was recovered as one of the first ten highest clusters in a 2,000 species sample shows the uniqueness of the beak shape of *Didunculus*. Even though the closest species to *Didunculus* in the morphospace do not share the same feeding behaviour (cluster 10), these results open a new avenue of research for evolutionary convergence between this group and other birds with similar diets (e.g., some Passeriformes and Psittaciformes of cluster 9).

The results also highlight the possible underestimation of the evolutionary rates in Columbiformes by Bright et al. (2017). These authors acknowledged that their evolutionary rates were influenced by the omission of some fossil/extinct taxa in their sample (Cooney *et al.*, 2017; Mitchell, 2019). I argue that if *Pezophaps*, *Raphus*, and *Treron curvirostra* were included in the evolutionary rates analysis from Bright et al. (2017), the analysis would likely show high evolutionary rates shift in the Raphinae clade. This high shift in evolutionary rates might be comparable to other remarkable bird adaptive radiations (Madagascan vangas, Galapagos finches, and Hawaiian honeycreepers). The proposed adaptive radiation in Raphines is another avenue of research that would benefit from further testing on a

larger sample of Columbiformes. This sample should also include Pteroclidiformes (sister clade) that also showed a terminal branch with high rates of evolution in Bright et al. (2017) analyses.

Conclusions

Main text

Modularity and integration

- I found similar patterns of integration between the rostrum and the braincase to the ones published by Young *et. al* (2017).
- Modularity is weak and non-significant. It should not be compared across taxonomic levels (feral and domestic *C. livia*, Columbiformes and all birds).
- The self-similarity, which does not take phylogeny into account, for the complete skull suggested that weak modularity exists in the columbiform skull.
- The relatively strong integration of the skull reflects the constraints expected from a functional matrix but might not reflect similar developmental constraints.
- Patterns of integration and modularity do not explain variation of columbiform skulls adequately.

Correlation between shape and biomechanics

- Most of the correlation between shape and both biomechanics and diet happens in by PLS dimension one.
- Shape changes related to PLS dimensions are concordant with previous theories of pigeon form/shape correlation (Diamond, 1973; Goodwin, 1983).
- Long slender rostra are related with granivory while thicker braincases with laterally expanded frontals, and thick rostra in the midsagittal plane are related to frugivory.
- The shape changes found on the complete skull are similar to those on the rostum module but are less noticeable in the braincase.

Correlation of biomechanics on diet

- Diet and biomechanics have the lowest correlation between blocks. The correlation was non-significant.

Factors that explain skull and module shape

- Phylogeny and phylogenetic uncertainty significantly diminished the number of significant variables explaining shape.
- The only significant biomechanical variable that explains skull shape was the lever length (on skull and both modules).
- Lever length being a significant variable to explain the braincase module shape was unexpected.
- The PLS feeding dimension one was highly correlated with the shape of the skull and modules (rostrum and braincase).
- The significant feeding clusters explained a high proportion of the shape of the skull and modules.

Factors that explain biomechanics

- Biomechanics presents a non-negligible correlation with feeding clusters.
- The skull biomechanics is correlated with the significant clusters in both PLS dimensions.
- The best model (AIC) was the categorical variable "frugivorous versus granivorous" for dimension one. Frugivory and granivory seem to require different biomechanical performances.
- Models which considered live prey consumption or feeding PCO1 or PCO3 might fit the shape data better.
- All variables explaining biomechanics are related to feeding behaviour.

- Non-feeding factors predict biomechanics in biomechanical dimension two: distribution type and size (body mass and centroid size).
- Feeding is a non-negligible highly important continuous or categorical variable that explains biomechanics.
- The overall results support a Darwinian view of skull shape evolution in Columbiformes.

Effect of feeding behaviour and biomechanics on skull shape

- The rostra of birds might be subjected to higher selection pressures than the braincase module. The covariation between shape and other factors (feeding and biomechanics) is higher in the rostrum and lower in the braincase.
- These results disagree with the view of non-dietary factors controlling for most of the shape that has been proposed for other birds (Bright *et al.*, 2016).
- Columbiformes show both Darwinian (natural selection) and Simpsonian (quantum evolution) evolution.
- *Columba* and *Patagioenas* are an example of a quantum leap towards an already occupied morphospace (by other pigeons).
- Raphinae is an example of a classical island or archipelago radiation which has been able to invade a new, previously unoccupied, part of the feeding space (and morphospace).
- Using data from Bright *et al.* (2017), *Didunculus* was clustered along four accipitriforms and one species of passeriform. This placement shows the uniqueness of the beak shape of *Didunculus* among pigeons.
- There is an apparent morphological evolutionary convergence between *Didunculus* and other birds with similar diets (e.g., some Passeriformes and Psittaciformes).

- I propose that if the evolutionary rates analysis from Bright et al. (2017) had included *Pezophaps*, *Raphus*, and *Treron curvirostra* then Columbiformes and Raphinae would likely show evidence of shifts towards high evolutionary rates.

Appendix Two. Columbiform feeding (diet and foraging) classification

- I propose a new classification of pigeon feeding (diet and foraging) which divides pigeon diets into 7 or 8 clusters.
- *Pezophaps* and *Raphus* are recovered along *Caloenas nicobarica* in this feeding classification.
- Granivorous terrestrial foraging is the likely ancestral feeding behaviour in Columbiformes.
- I proposed the use of the phylomorphospace for the visualization of feeding evolution.
- Clades of columbiforms have occupied other parts of the feeding space at least three times: (1) *Columba* and *Patagioenas* 29 to 25 million years ago, (2) by Raphinae 34 million years ago and (3) by "fruit pigeons" 30 million years ago.

Appendix Three. Biomechanical landscape

- Biomechanical landscape was a useful framework to distinguish biomechanical differences between different feeding strategies based on shape alone.
- The species with distinct biomechanical performance are the pigeons with distinctive morphology (*Pezophaps*, *Raphus*, *Didunculus*, and *Treron curvirostra*).
- In Pigeons closer to the mean shape of the sample, frugivorous species (Cluster M1) show larger muscle area, higher mechanical advantage, and higher resistance to bending than granivorous species.

- The granivorous species show slender rostra, large eye sizes, small mouth openings that close at high velocity, low mechanical advantages, and low output forces with small muscle areas and low bending resistance.
- *Didunculus* is the pigeon with a skull shape that presents a higher bending resistance and output force.
- The Raphini showed the highest velocity of bite, largest mouth opening, and smallest eye sizes. However, the bending resistance of Raphini was similar to “fruit pigeons”
- The performance of the skull does not support the animal consumption hypothesis in Raphini.

Supplementary material (S3)

Detailed results for the two-block PLS of skull and modules vs feeding and biomechanics

Because of the complexity of the two-block PLS analyses I decided to report only the results of the complete skull in Chapter Three. In this supplement I report the results of the complete skull and compare them with the results obtained by each skull module (rostrum and braincase). The results are reported as follows: (1) The general covariation and significance of the six shape analyses; (2) the results for the analysis of covariation between shape (skull and modules) and feeding, including the detailed analysis of two PLS dimensions; (3) the results for the analysis of covariation between shape (skull and modules) and biomechanics, including the detailed analysis of two PLS dimensions.

The general covariation and significance

In all analyses (Table S3.4), PLS dimension one explained more than 82% of the covariation between data blocks, PLS dimension two explained between 4% and 13% of the correlation, with subsequent dimensions explaining little covariation (maximum of 3.2%). PLS dimension one accounted for a higher proportion of the covariation between shape and feeding (89.4% to 91.6%) than with biomechanical performance (82.07% to 85.3%).

For the rostrum module (Table S3.4), PLS dimension one also accounted for a higher covariation proportion of shape against feeding (91.6%) and biomechanics (82.5%) than the complete skull (90.39% and 82.1% respectively). Finally, for the braincase module, PLS dimension one accounted for less of the covariation with feeding (89.4%) but more with biomechanical performance (85.3%). PLS dimension two only explained more than 10% of

the covariation when biomechanical performance was compared with the skull shape (13%) and with the rostrum module.

Shape versus feeding (two-block PLS results)

Covariation and Significance

The overall skull shape block presented a moderate and significant covariation with feeding (PLS_{corr} = 0.588; *P*=0.003; Table 3.3). When phylogeny was considered, the correlation was higher and significant, albeit significance was lower than for the ordinary analysis (PLS_{corr} = 0.755, sd= 0.095; *P*= 0.007, sd= 0.012).

The covariation of the rostrum shape and feeding (Table 3.3) was similar to that of the complete skull (PLS_{corr} =0.575; *P*=0.002). When phylogeny was taken into account the covariation was higher (PLS_{corr} = 0.726, sd= 0.106; *P*=0.006, sd= 0.011). The covariation of braincase shape and feeding was moderate with lower statistical support than the other modules (PLS_{corr} =0.525; *P*=0.009). When the phylogeny was taken into account, the covariation was higher (PLS_{corr}= 0.669 ± 0.121 and *P*=0.045 ± 0.068).

PLS dimension one (feeding)

Salient variables

The loadings of the PLS vector in PLS dimension one (Table 3.4), were used to identify the salient or useful feeding variables. Vector loadings indicate that PCO1 is the most salient to predict shape in PLS dimension one. The salience of PCO1 for the covariation with the skull is -0.1, PCO1 is lower for the rostrum shape (-0.09) than for the braincase (-0.34). For the braincase module, PCO3 (-0.21) and PCO6 (0.22) present a high salience.

Feeding traits in PLS dimension one

When the binary feeding characters were plotted against the feeding YScore in dimension one (89 to 91% of covariation: Figures 3.4 and S3.9) it was possible to differentiate two clusters of feeding characters in the dataset: one cluster (negative YScores) with terrestrial or mostly terrestrial foraging pigeons that feed mostly with seeds, grains, insects and snails. This cluster can also feed on larger grains and leaves. The second identified cluster (positive YScores) includes arboreal or mostly arboreal foraging pigeons that feed on fruits and berries. The identified clusters were more compact and conspicuous when the rostrum and braincase modules were examined separately (Figure S3.9).

Shape changes

To assess the shape changes associated with the feeding traits I examined the predicted shapes of the XScores in dimension one (Figures 3.2C-D and S3.6). The minimum shape score (XScore) obtained was related with a long, slender rostrum and frontals, these changes were associated with terrestrial and granivorous traits. The maximum XScore value was related with a dorsoventrally high, short rostrum, and a mediolaterally expanded braincase. These changes were related to the frugivorous and arboreal traits.

For the rostrum module (Figure S3.6), the same shape changes leading to a shorter taller beak and anteriorly expanded frontals at high PLS XScore values were identified. For the braincase at high XScore values (related with terrestrial frugivorous feeding), I identified a shape change that marks the lateral contraction and dorsoventral compression of the module and the ventral displacement of the tip of the occipital crest.

PLS scores of shape and diet

The comparison between the PLS scores of feeding block (Figures 3.2 and S3.5) revealed that the covariation between the scores of shape and feeding is conspicuous in PLS dimension one (skull and rostrum). *Phaps elegans*, *Columba trocaz*, and *Patagioenas plumbea* (clusters "E", "f", and "g") were the pigeons with highest scores and the lowest scores were obtained by *Phaps histrionica*, *Patagioenas nigrirostris*, *Patagioenas picazuro* (clusters "E", "h", and "BC").

For the rostrum module (Figure S3.5) the highest diet YScores were obtained by *Columba trocaz*, *Phaps elegans* and *Patagioenas plumbea* (clusters "f", "E", and "g"), while low values were obtained by *Phaps histrionica*, *Patagioenas nigrirostris*, *Patagioenas picazuro* (clusters "E", "h", and "BC"). For the braincase module the highest values were obtained by *Patagioenas leucocephala*, *Patagioenas cayennensis*, and *Patagioenas speciosa* (frugivorous arboreal clusters "f" and "g"), while lowest values were obtained by *Patagioenas picazuro*, *Patagioenas squamosa* and *Patagioenas maculosa* (clusters "BC", "f", and "E").

PLS dimension two (feeding)

Salient variables

In PLS dimension two (Table 3.4), PCO2 seems to be the most salient feeding variable in dimension two for the rostrum (0.18) and the skull (0.13). PCO2 is negligible for the correlation of the braincase in dimension two (-0.004).

Feeding traits in PLS dimension two

When the binary feeding variables were plotted against feeding YScores of dimension two (4.45% to 4.73% of the covariance; Figures 3.4 and S3.10), it was challenging to identify

clusters in the data. However, terrestrial granivorous pigeons have constrained YScores towards central values, while the arboreal frugivorous pigeons show a wider YScore range.

Shape changes

In the second PLS dimension (Figures 3.3C and S3.8), the feeding block shows shape changes in the skull and rostrum, but not in the braincase. A similar pattern of shape changes than the ones identified in dimension one was obtained for the skull and rostrum. High XScores values are related to dorsoventrally taller, anteroposteriorly shorter rostrums with anterolaterally expanded frontals and posterolateral expanded braincases and basicrania. However, unlike in dimension one, the tip of the occipital crest position is dorsally higher in the midsagittal plane and the braincase becomes dorsally taller.

PLS scores of shape and feeding

When PLS scores of shape and diet in dimension 2 were compared (Figures 3.3A and S3.7) for the complete skull, high feeding YScores were obtained by *Patagioenas leucocephala*, *Phaps elegans*, and *Patagioenas plumbea* ("f", "E", and "g") while low feeding values were obtained by *Phaps histrionica*, *Patagioenas picazuro*, *Patagioenas squamosa* ("E", "BC", and "f"). For the rostrum module high values were obtained by *Patagioenas leucocephala*, *Patagioenas plumbea*, and *Phaps elegans* ("f", "g", and "E") while low values were obtained by *Patagioenas squamosa*, *Patagioenas picazuro* and *Phaps histrionica* ("f", "BC", and "E"). For the braincase module high feeding values were obtained by *Patagioenas maculosa*, *Columbina talpacoti*, *Phaps histrionica*, *Columba livia* (all from cluster "E") while low values were obtained by *Patagioenas cayennensis*, *Patagioenas squamosa*, *Columbina passerina*, and *Alectroenas pulcherrimus* ("g", "f", "D", and "h").

Shape versus biomechanics (two-block PLS results)

Covariation and significance

The covariation and significance (Table 3.3) were higher for skull shape and biomechanical performance (PLS_{corr} = 0.857; *P*=0.001) than for skull shape and feeding. In the phylogenetic setting the covariation between shape and biomechanics remained high and significant (PLS_{corr} = 0.808, sd= 0.042; *P*= 0.001, sd= 0.001).

The rostrum shape showed a stronger covariation (Table 3.3) with biomechanical performance (PLS_{corr} =0.874, *P*=0.001) than the skull shape. When phylogeny was taken into account, the covariation of rostrum shape and biomechanical features remained high and significant (PLS_{corr} =0.831, sd= 0.039; *P*=0.001, sd= 0.000). The covariation between braincase shape and biomechanical performance was lower and less significant (PLS_{corr} = 0.746; *P*= 0.004). When the phylogeny was taken into account the covariation was lower and less significant, albeit still significant (PLS_{corr} =0.709, sd= 0.065; *P*=0.009, sd= 0.005).

PLS dimension one (biomechanics)

Salient variables

For the biomechanical performance in dimension one (82% to 85% of the covariance; Table 3.4), the lever length (Dlever) is the most salient variable for the skull (0.53), and rostrum (0.6) while the loading of this variable is lower and negative for the braincase shape (-0.26). The second most salient variable for the skull is the rostrum height (-0.28) this is less salient for the rostrum (-0.14) and highly salient for braincase shape (0.55). The rostrum width presents a salience of -0.16 for the complete skull, while the salience for the rostrum module is lower (-0.11) and higher for the braincase (0.2). The muscle centroid size is also

salient for the skull (-0.12) and the braincase (0.14), while the salience of this variable is lower for the rostrum (-0.1). The input distance is also salient for the skull (-0.1), rostrum (-0.11) and braincase (0.13).

Biomechanical performance in PLS dimension one

The PLS biomechanical dimension one accounted for 82% of the covariation with complete skull shape (Table S3.4). When the original biomechanical variables are plotted against the biomechanical YScores in dimension one, some general patterns can be identified (Figures 3.5A and S3.11). For higher YScores values there is a: decrease in output distance, mouth opening, rostrum width, muscle centroid size, and rostrum thickness. Lever length increases with higher YScore values of dimension one while eye centroid size and input distance show no clear patterns. Similar patterns were found for the rostrum module except that rostrum thickness stops showing an evident decrease towards higher YScores values (Figure S3.11). Finally, for the braincase module the patterns found were comparatively different, towards high YScore values I identified the increase of most biomechanical characters: output distance, mouth opening, rostrum width, muscle area, and rostrum thickness while other biomechanical proxies show no clear patterns (Figure S3.11).

I identified one outlier in the skull and rostrum modules (*Didunculus*; Figure S3.11). This outlier presents high values of input distance, rostrum width and thickness, and muscle area. *Didunculus* also presents remarkable low values of output distance, mouth opening, and lever length. In the braincase module, Didunculus and *Pezophaps* are outliers, but they present extremely different biomechanical properties because *Pezophaps* presents high

values of output distance, mouth opening, and lever length. *Pezophaps* also presents average values of rostrum width, muscle area, and input distance and presents low values of eye centroid size.

Shape changes

In dimension one (82 to 85% of the covariation; Table S3.4), the shape changes obtained for the skull in the biomechanical block were similar to the ones obtained for the feeding block. However, these changes were more prominent for the biomechanical performance block (Figures 3.2D and S3.6). These shape changes were: (1) low XScores have long, slender rostra and frontals. (2) high XScores have a dorsoventrally high, anteroposteriorly short rostrum, and a mediolaterally expanded braincase.

For the rostrum, the same shape changes (Figure S3.6) leading to a shorter taller beak and anteriorly expanded frontals at high PLS XScore values were identified. For the braincase module at high XScore values, I noted the lateral contraction and dorsoventral compression of the module, and the ventral displacement of the tip of the occipital crest in the midsagittal plane. A shape change only observed when shape-biomechanics covariation is analysed, is a remarkable posterolateral contraction of the basicranium.

PLS scores of shape and biomechanics

The distribution of species scores across the PLS dimension is different in the biomechanical block than in the feeding block. The percentage of covariance in dimension one of biomechanics is lower than in feeding dimension one (Figure 3.2B, S3.5). In this biomechanical dimension one, it was easier to identify scores related to arboreal frugivorous species: low scores in the skull and the rostrum and high scores in the braincase

module. Higher values in the skull module were identified for *Phaps elegans*, *Patagioenas squamosa*, and *Caloenas nicobarica* (clusters "E", "f", and "A"), while low values were obtained by *Didunculus strigirostris*, *Patagioenas nigrirostris*, *Pezophaps solitaria*, *Treron curvirostra* (frugivorous clusters "g", "h", "A", and "f"). The rostrum module the pigeons with high values are *Phaps elegans*, *Goura cristata*, and *Patagioenas squamosa* (clusters "E", "D", and "f") while low values were obtained by *Didunculus strigirostris*, *Patagioenas nigrirostris*, and *Treron curvirostra* (frugivorous arboreal clusters "g", "h", and "f"). Finally, for the braincase module high biomechanical PLS scores were obtained by *Didunculus*, *Pezophaps* and *Treron curvirostra* (frugivorous clusters "g", "A", and "f"), while low values were obtained by *Columba rupestris*, *Phaps histrionica*, *Caloenas nicobarica*, and *Patagioenas squamosa* (clusters "E", "A", and "f").

PLS dimension two (biomechanics)

Salient variables

For the overall skull shape in the second PLS dimension, salience is low for all variables (Table 3.4). For the rostrum module, rostrum depth is salient (-0.16). An unexpected result was that several proxies are salient for braincase shape correlation in dimension 2: output distance (-0.17), mouth opening (-0.17), rostrum depth (-0.18), lever length (-0.38), rostrum width (-0.1), and eye centroid size (0.21). These results were surprising because several of these variables are located in the rostrum module.

Biomechanical performance in PLS dimension two

In dimension two, patterns are less clear for the complete skull (Figures 3.8B and S3.12). When the biomechanical characters were plotted against the YScores of the rostrum

module in PLS dimension two: some patterns were identified. Towards high YScore values, there is a decrease in rostrum thickness, muscle size, rostrum width and input distance. For the braincase module, a decrease in thickness and width is also detected towards high YScore values. I identified outliers for the complete skull: two negative outliers *Didunculus* and *Pezophaps* and one positive outlier *Phaps histrionica*. I identified *Pezophaps* as one outlier in the rostrum module. For the braincase module, I identified an outlier cluster (*Raphus*, Pezophaps, *Patagioenas leucocephala* and *Columba trocaz*) close to negative values and one positive outlier (*Didunculus*).

Shape changes

In the second PLS dimension (which explains 4 to 13% of correlation) there are conspicuous differences between the shape changes predicted in the diet and biomechanical blocks (Figures 3.3C-D and S3.8). Shape changes were identified in the braincase module but not in the complete skull or rostrum module. High XScores values have similar shapes to the ones found in dimension one for the same module. Identified shape changes are the posterior-lateral compression of both the skull roof and the basicranium, and the comparatively lower position of the tip of the occipital crest in the midsagittal plane.

PLS scores of shape and biomechanics

In PLS dimension two, for the braincase module in the second PSL dimension (Figure S3.7) high values were obtained by *Didunculus*, *Caloenas*, *Columba rupestris*, *Patagioenas squamosa*, and *Alectroenas madagascariensis* (“g”, “A”, “E”, and “f”) while low values were obtained by *Raphus*, *Patagioenas leucocephala*, *Columba trocaz*, and *Pezophaps* (“A” and

"f"). For the biomechanical data block versus complete skull shape (Figure 3.3B), high values were obtained by *Phaps histrionica*, *Patagioenas squamosa*, *Columba rupestris*, and *Starnoenas cyanocephala* ("E" and "f"), while *Didunculus*, *Pezophaps*, *Phaps chalcoptera* ("g", "A", and "E") presented the lowest YScores values. For the rostrum module, pigeons with high biomechanical values were *Phaps histrionica*, *Columba rupestris*, *Patagioenas squamosa*, *Caloenas nicobarica* ("E", "f" and "A"), while low values were obtained by *Raphus*, *Pezophaps*, *Patagioenas leucocephala*, *Columba trocaz, and Columba livia* ("A", "f", and "E").

The overall two-block PLS results showed that the covariance of shape with feeding was higher than the covariance with biomechanical performance. For the feeding block, clear patterns were identified only for the first PLS dimension. The shape changes in both dimensions are similar for the skull and rostrum. For the biomechanical performance block, both dimensions showed patterns related to diet. The shape changes, in dimension one, were similar to the ones of the feeding block. In dimension two most shape changes happened in the braincase.

Two-block partial least squares of feeding versus biomechanical performance

Covariation and significance

The covariation between feeding and biomechanical performance was moderate (Table 3.3) and presented a lower statistical support than any of the other analysis in an ordinary setting (PLS_{corr}= 0.531; *P*= 0.010). When phylogeny was taken into account, the covariation was also moderate, but non-significant (PLS_{corr} = 0.575, sd= 0.133; *P*=0.095, sd= 0.119).

Salient variables

When the feeding and biomechanical performance were analysed in a two-block PLS (Table 3.5), the salient variables in the first dimension of the biomechanical block were: rostrum dept (0.49), rostrum width (0.13), and effort distance (0.13). In dimension 2 the salient variables were rostrum depth (-0.16) and lever length (-0.15). For the feeding block in dimension one, the most salient axes were: PCO4 (-0.34), PCO1 (-0.21), PCO7 (0.17), PCO8 (-0.13), and PCO3 (-0.12). In dimension 2 the most salient axes were: PCO4 (0.13) and PCO1 (-0.11).

Factors explaining module shape (ordinary regression setting)

Rostrum module

For the rostrum module the D.ols identified 18 significant variables (Table S3.5): centroid size (*P*= 0.007), mass (*P*= 0.01), PLS biomechanical dimension one (*P*= 0.001) and two (*P*= 0.004), input distance (*P*= 0.001), lever length (*P*= 0.001), output distance (*P*= 0.001), eye size (*P*= 0.002), mouth opening (*P*= 0.001), muscle area (*P*= 0.001), rostrum depth (*P*= 0.003), rostrum width (*P*= 0.001), and feeding PCO1 (*P*= 0.001). D.ols also identified significant categorical variables: significant clusters (*P*= 0.003), green plant matter (*P*= 0.007), live prey (*P*= 0.001), Fruit or grain eaters (*P*= 0.002), and terrestrial or arboreal foragers (*P*= 0.021). Only 11 of those significant variables accounted for more than 10% of the unexplained variation. All the important continuous variables were biomechanical variables: PLS biomechanical dimension one (R^2= 21.4%), input distance (R^2= 16.4%), lever length (R^2= 35.2%), output distance (R^2= 11.7%) mouth opening (R^2= 11.7%), muscle area (R^2= 19%), rostrum depth (R^2= 12%) and width (R^2= 12%). The categorical variables with correlations

higher than 10% were the significant clusters (R^2= 27.8%), main feeding strategy (R^2= 10.5%), and main foraging strategy (R^2= 11.6%).

Braincase module

Seventeen significant variables that explain the shape of the braincase module were identified (Table S3.6): centroid size (*P*= 0.001) and body mass (*P*= 0.001), PLS biomechanical dimension one (*P*= 0.001) and two (*P*= 0.006), input distance (*P*= 0.001), lever length (*P*= 0.002), output distance (*P*= 0.001), eye size (*P*= 0.001), mouth opening (*P*= 0.001), muscle size (*P*= 0.001), rostrum depth (*P*= 0.001), rostrum width (*P*= 0.001), and the feeding PCO1 (*P*= 0.016). I identified some significant categorical variables: significant clusters (*P*= 0.003), green plant matter consumers (*P*= 0.032), live prey consumers (*P*= 0.004) and grain versus fruits (*P*= 0.025). Ten of the significant variables explained more than 10% of the unexplained variation: centroid size (R^2= 11.7%), PLS biomechanical dimension one (R^2= 12.1%), lever length (R^2= 11.8%), output distance (R^2= 10%), eye size (R^2= 12%), mouth opening (R^2= 10%), muscle size (R^2= 13.7%), rostrum depth (R^2= 15.9%), rostrum width (R^2= 13.1%), and the categorical significant clusters (R^2= 27%). Input distance is the only significant variable that presents a low correlation (R^2= 8.5%) but large effect size (R^2= 3.352).

Supplementary figures

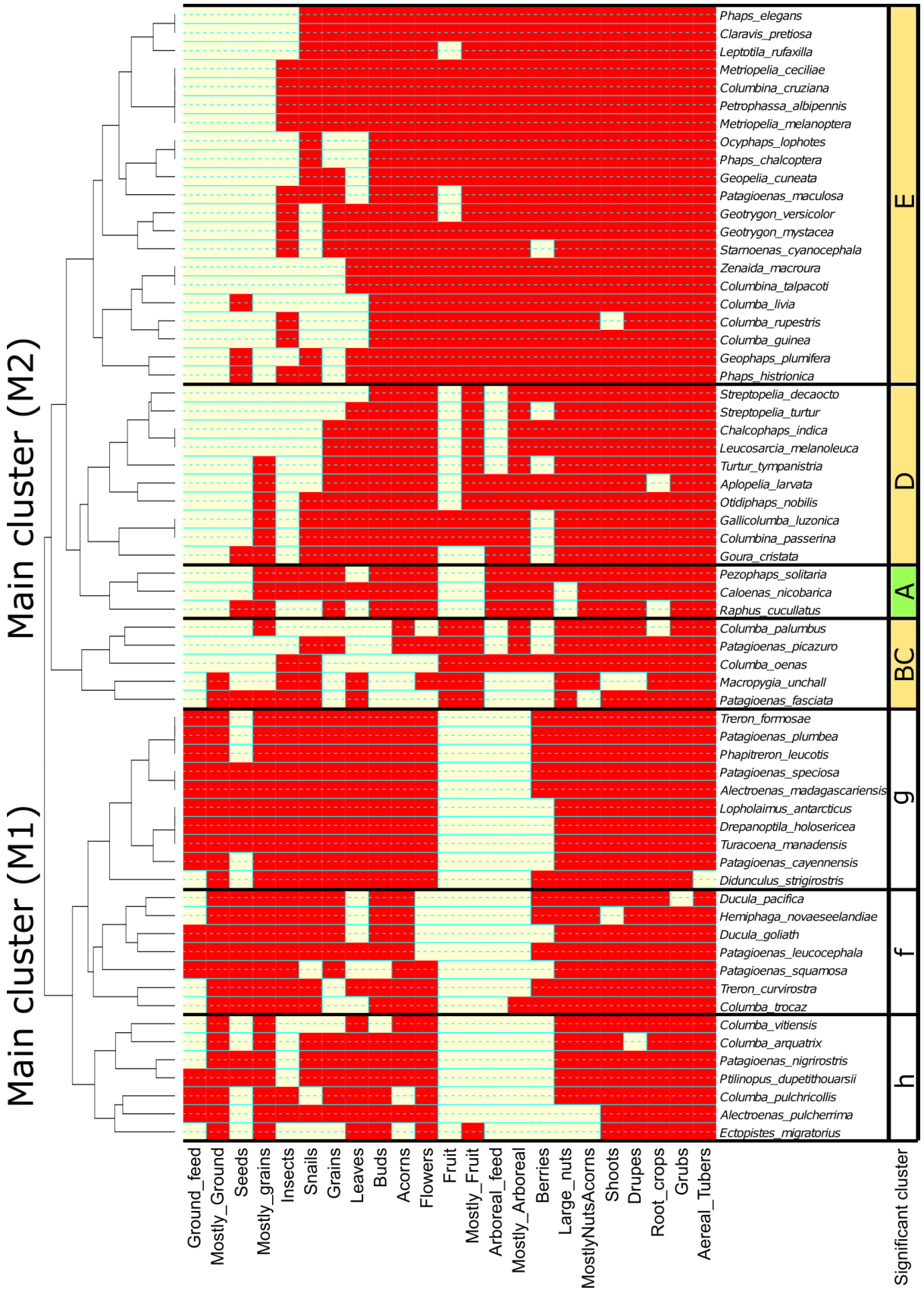


Figure S3.1. Complete linkage clustering of the feeding behaviour (diet and foraging) in Columbiformes. Significant clusters identified by the complete linkage clustering: green colour indicates completely coincident clusters (cluster “A”), yellow colour indicates clusters that were consistent by species but were subdivided into smaller clusters by the other algorithm (clusters “BC”, “D”, and “E”). The clusters “h”, “f”, and “g” are given in lower case because they not recovered by the average linkage algorithm. Main clusters M1 and M2 are consistent in both methods of clustering. Main cluster M1 is a mostly arboreal foraging group while the main cluster M2 is a mostly terrestrial foraging group. The interplay in food items (which includes items other than fruit and grains) and foraging strategies makes the feeding ecology of Columbiformes more complicated than previously assessed.

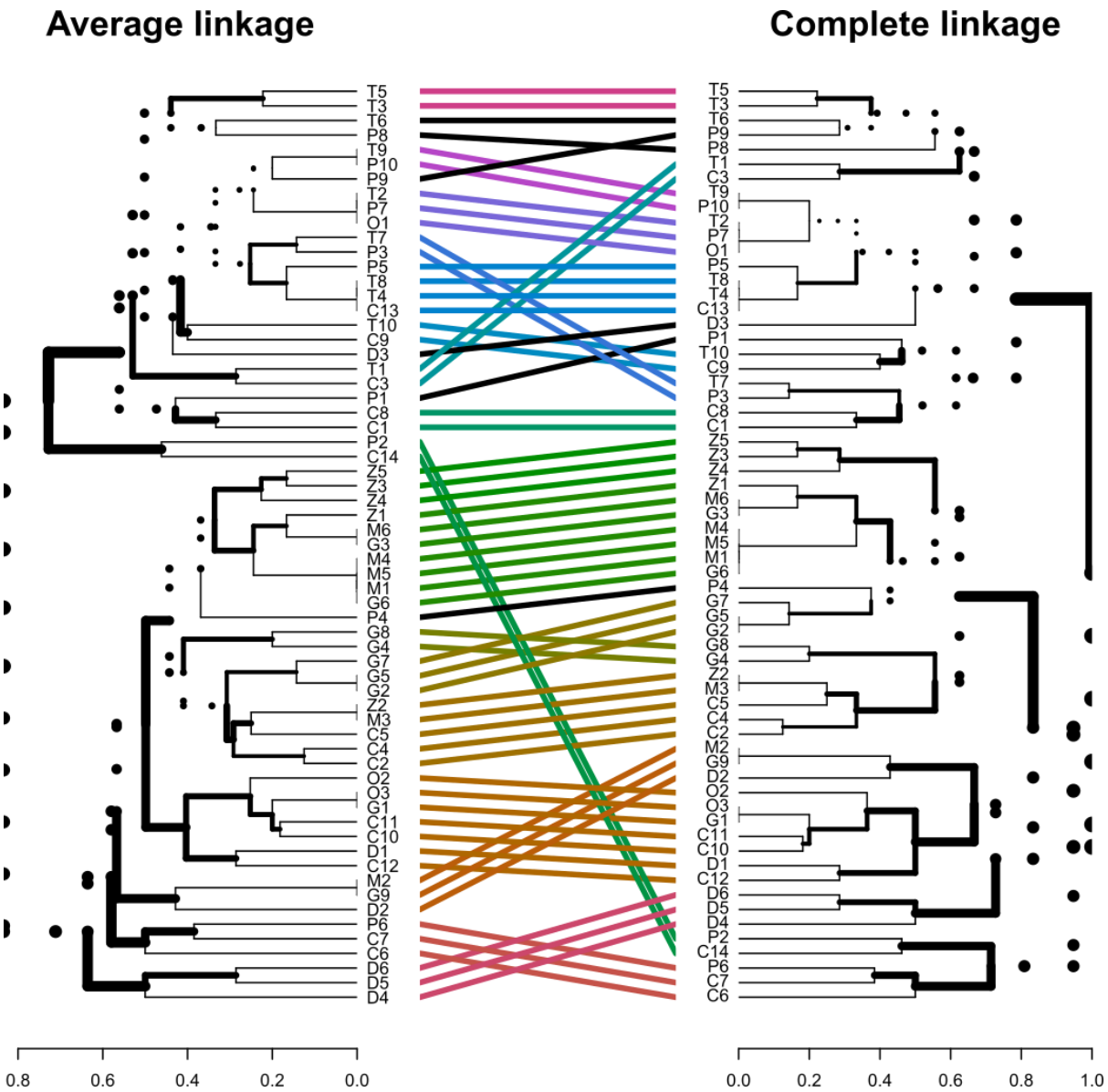
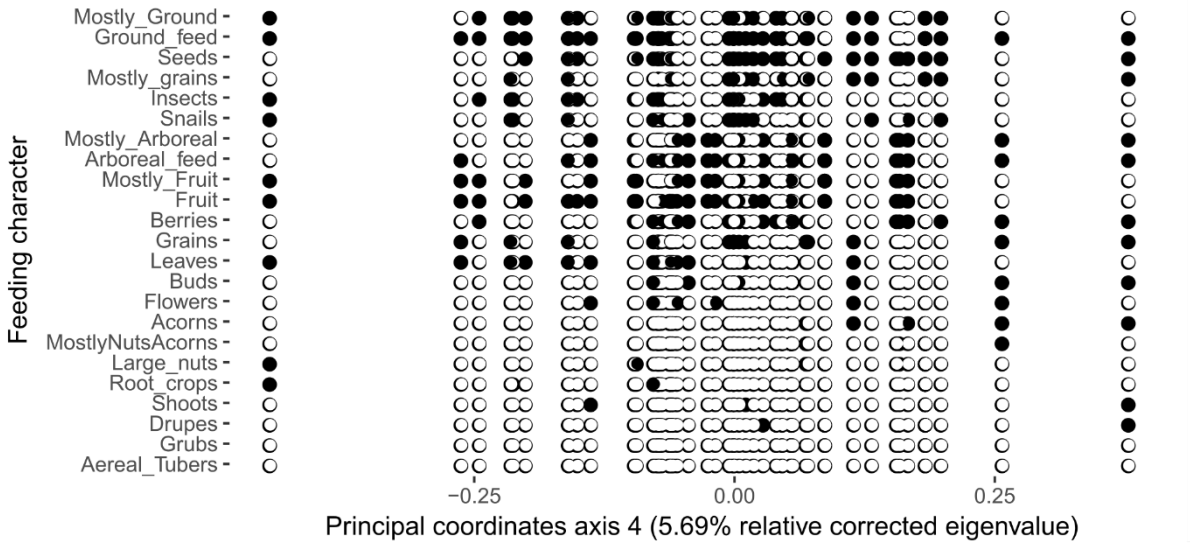
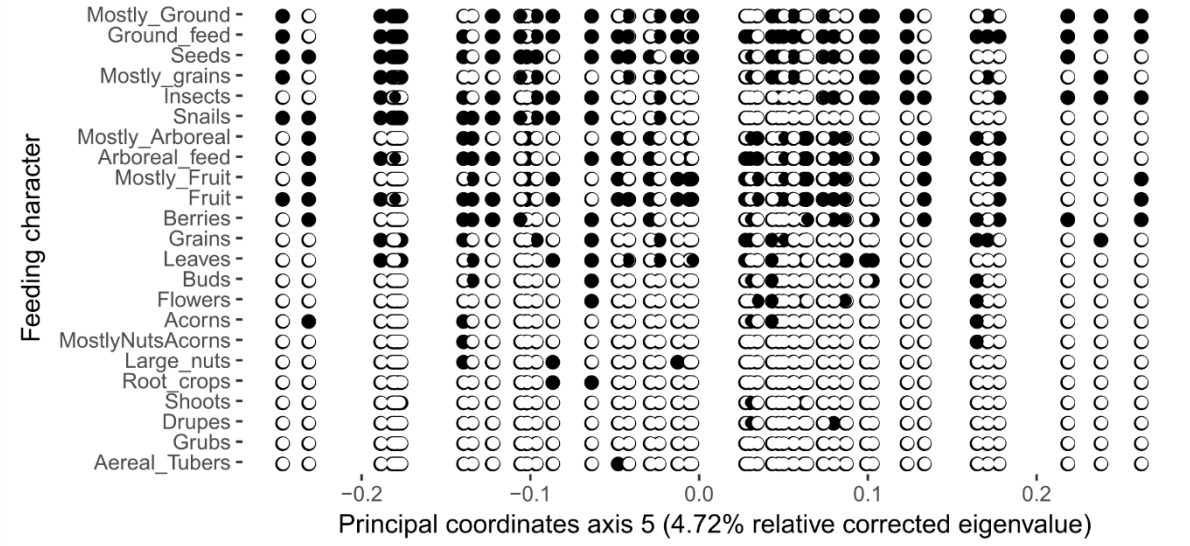


Figure S3.2. Tanglegram showing the differences in clustering when using complete linkage or average linkage algorithms. The figure shows that overall similar clusters were obtained by both clustering algorithms. Legend: Leucosarcia melanoleuca (G1), Ocyphaps lophotes (G2), Phaps elegans (G3), Phaps histrionica (G4), Phaps chalcoptera (G5), Petrophassa albipennis (G6), Geopelia cuneata (G7), Geophaps plumifera (G8), Gallicolumba luzonica (G9), Phapitreron leucotis (O1), Treron curvirostra (T1), Treron formosae (T2), Hemiphaga novaeseelandiae (T3), Lopholaimus antarcticus (T4), Ducula pacifica (T5), Ducula goliath (T6), Ptilinopus dupetithouarsii (T7), Drepanoptila holosericea (T8), Alectroenas madagascariensis (T9), Alectroenas pulcherrimus (T10), Caloenas nicobarica (D6), Pezophaps (D5), Raphus (D4), Didunculus (D3), Goura cristata (D2), Otidiphaps nobilis (D1), Turtur tympanistria (O2), Chalcophaps indica (O3), Geotrygon versicolor (Z5), Starnoenas cyanocephala (Z4), Geotrygon mystacea (Z3), Zenaida macroura (Z2), Leptotila rufaxilla (Z1), Patagioenas speciosa (P10), P. leucocephala (P9), P. squamosa (P8), P. plumbea (P7), P. picazuro (P6), P. cayennensis (P5), P. maculosa (P4), P. nigrirostris (P3), P. fasciata (P2), Ectopistes migratorius (P1), Columba arquatrix (C1), C. guinea (C2), C. trocaz (C3), C. rupestris (C4), C. livia (C5), C. oenas (C6), C. palumbus (C7), C. vitiensis (C8), C. pulchricollis (C9), Streptopelia turtur (C10), Streptopelia decaocto (C11), Aplopelia larvata (C12), Turacoena manadensis (C13), Macropygia

unchall (C14), Columbina cruziana (M1), Columbina passerina (M2), Columbina talpacoti (M3), Metriopelia melanoptera (M4), Metriopelia ceciliae (M5), and Claravis pretiosa (M6).


Feeding character
Mostly_Ground
Ground_feed
Seeds
Mostly_grains
Insects
Snails
Mostly_Arboreal
Arboreal_feed
Mostly_Fruit
Fruit
Berries
Grains
Leaves
Buds
Flowers
Acorns
MostlyNutsAcorns
Large_nuts
Root_crops
Shoots
Drupes
Grubs
Aereal_Tubers
−0.25
0.00
0.25
Principal coordinates axis 4 (5.69% relative corrected eigenvalue)


Feeding character
Mostly_Ground
Ground_feed
Seeds
Mostly_grains
Insects
Snails
Mostly_Arboreal
Arboreal_feed
Mostly_Fruit
Fruit
Berries
Grains
Leaves
Buds
Flowers
Acorns
MostlyNutsAcorns
Large_nuts
Root_crops
Shoots
Drupes
Grubs
Aereal_Tubers
−0.2
−0.1
0.0
0.1
0.2
Principal coordinates axis 5 (4.72% relative corrected eigenvalue)

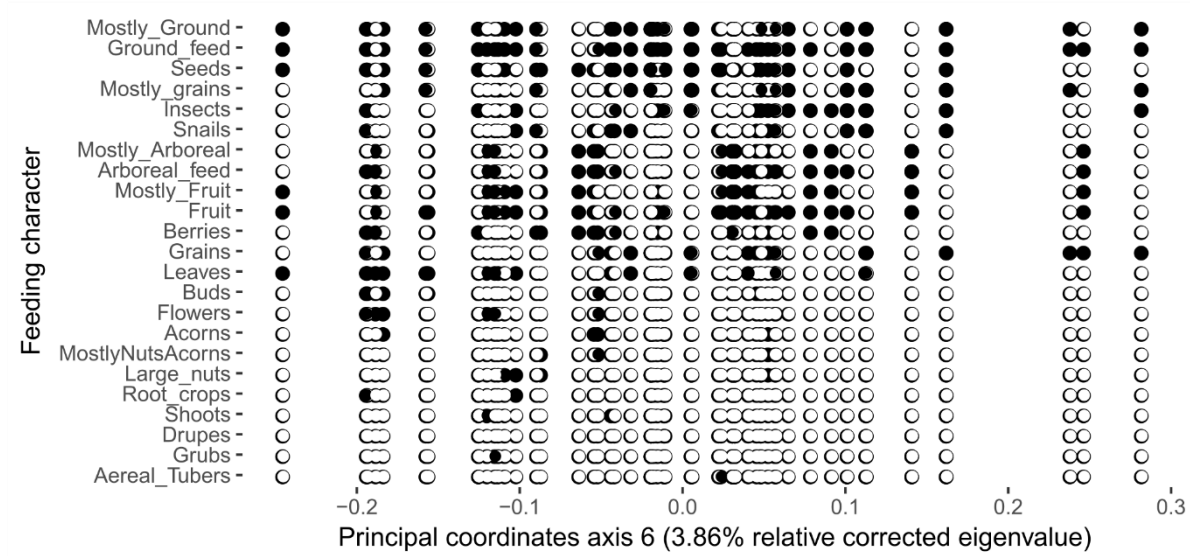

Feeding character
Mostly_Ground
Ground_feed
Seeds
Mostly_grains
Insects
Snails
Mostly_Arboreal
Arboreal_feed
Mostly_Fruit
Fruit
Berries
Grains
Leaves
Buds
Flowers
Acorns
MostlyNutsAcorns
Large_nuts
Root_crops
Shoots
Drupes
Grubs
Aereal_Tubers
−0.2
−0.1
0.0
0.1
0.2
0.3
Principal coordinates axis 6 (3.86% relative corrected eigenvalue)

Figure S3.3. Principal coordinates axes (3-6) plotted against the binary feeding characters. Each column of circles represents a species. Black circles represent the presence of a feeding trait, and white circles represent the absence of the trait for that species. This figure allows one to assess patterns of feeding characters on the PCO axes

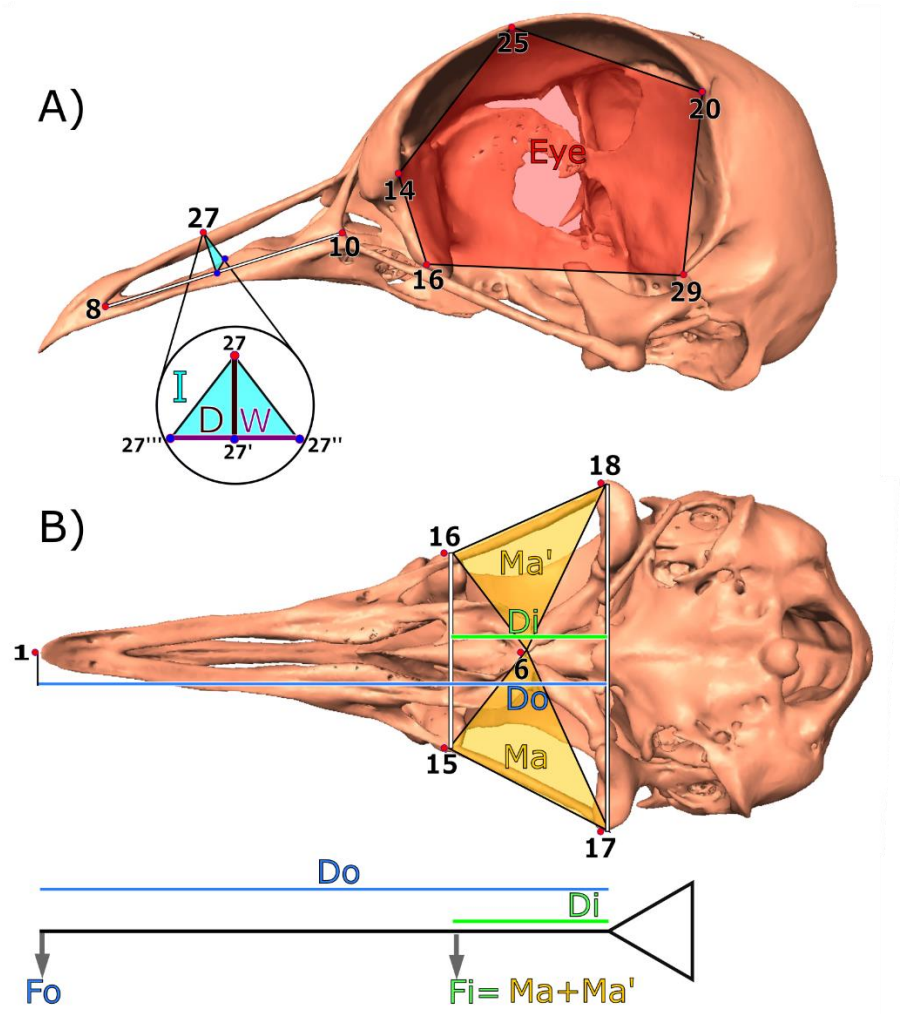


Figure S3.4. Biomechanical model of pigeon skull as a simple machine. Biomechanical characters obtained by comparing the pigeon skull to a third-degree lever. A) lateral view and B) ventral view. Numbers show the landmarks used to calculate the biomechanical performance. D) Dorsoventral height at mid-length of the rostrum; W) Mediolateral width at mid length of the rostrum; I) moment of area as the centroid of landmarks 27, 27', and 27''; Ma) Muscle area; Do) Output distance; Di, Input distance; Fo) output force, and Fi) Input force.

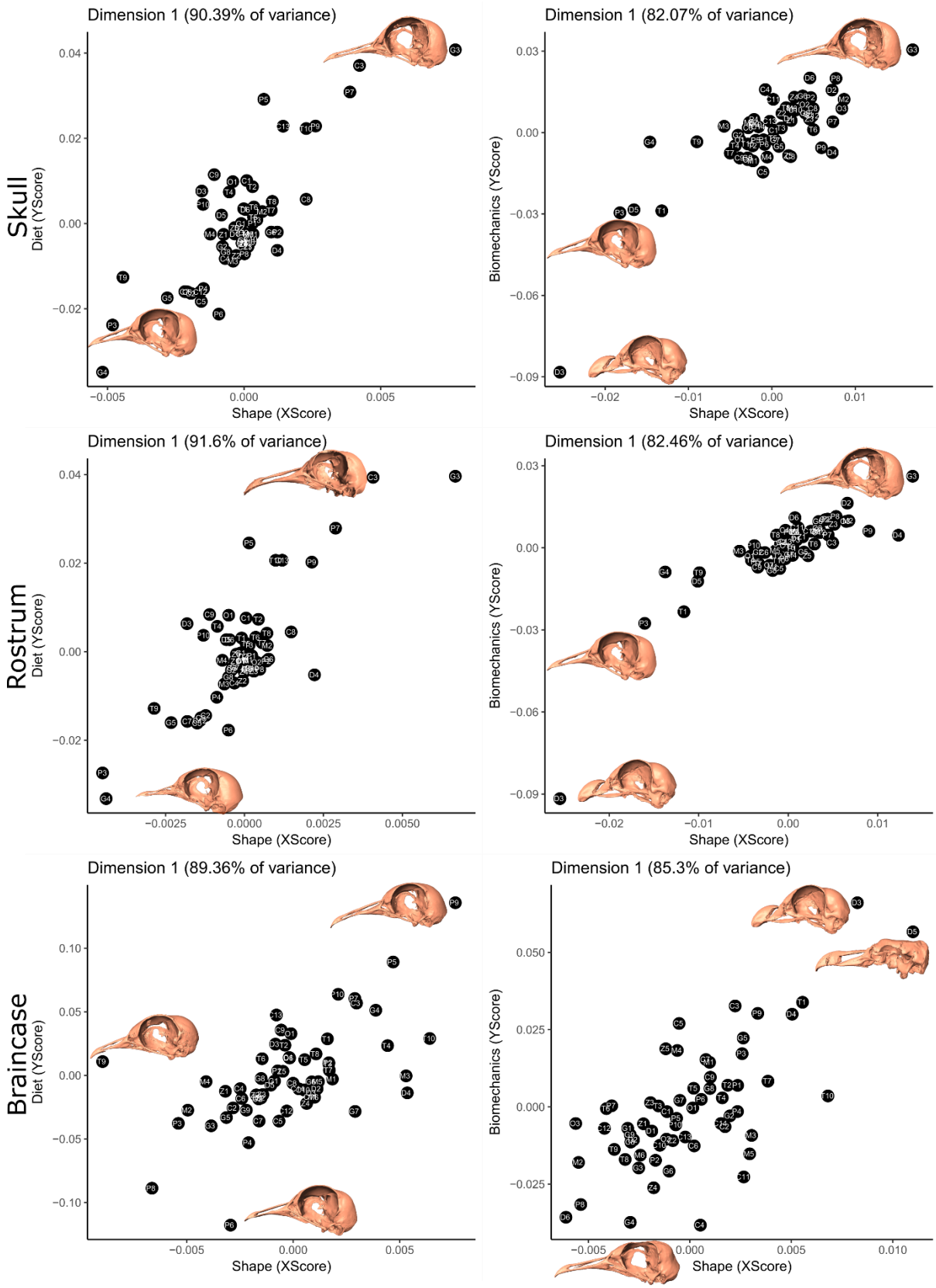


Figure S3.5. PLS dimension one, shape (XScores) versus other data blocks (YScores). Three dimensional models of species with extreme values exemplify the shape variation along the first PLS dimension. Legend as in Figure S3.2.

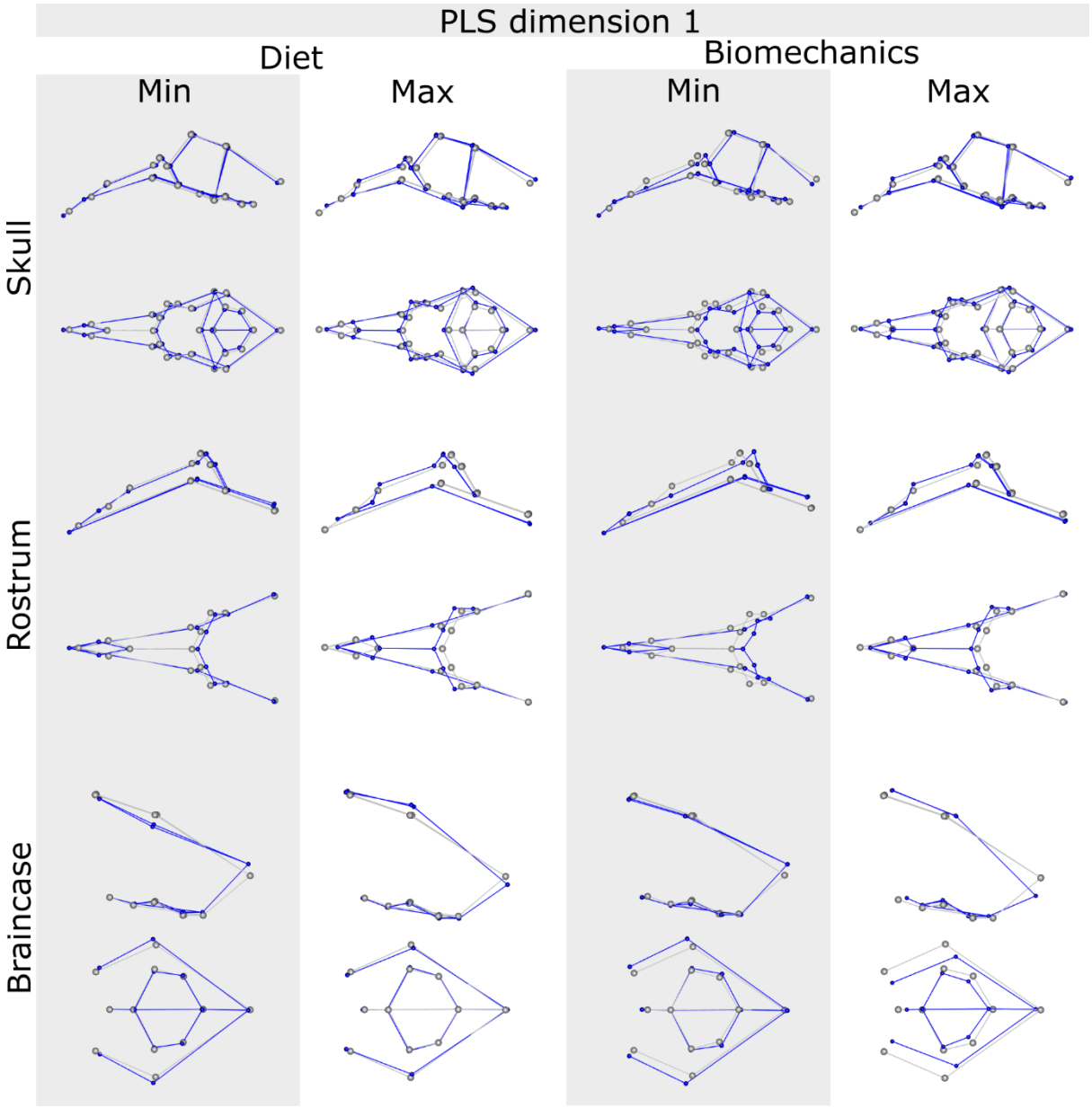


Figure S3.6. Predicted shapes for the maximum and minimum values of XScores in the PLS dimension one. Patterns recovered by the biomechanical and feeding blocks against shape are congruent overall however the degree of shape change is different. Braincase module shows the larger change degree difference between the two modules evaluated.

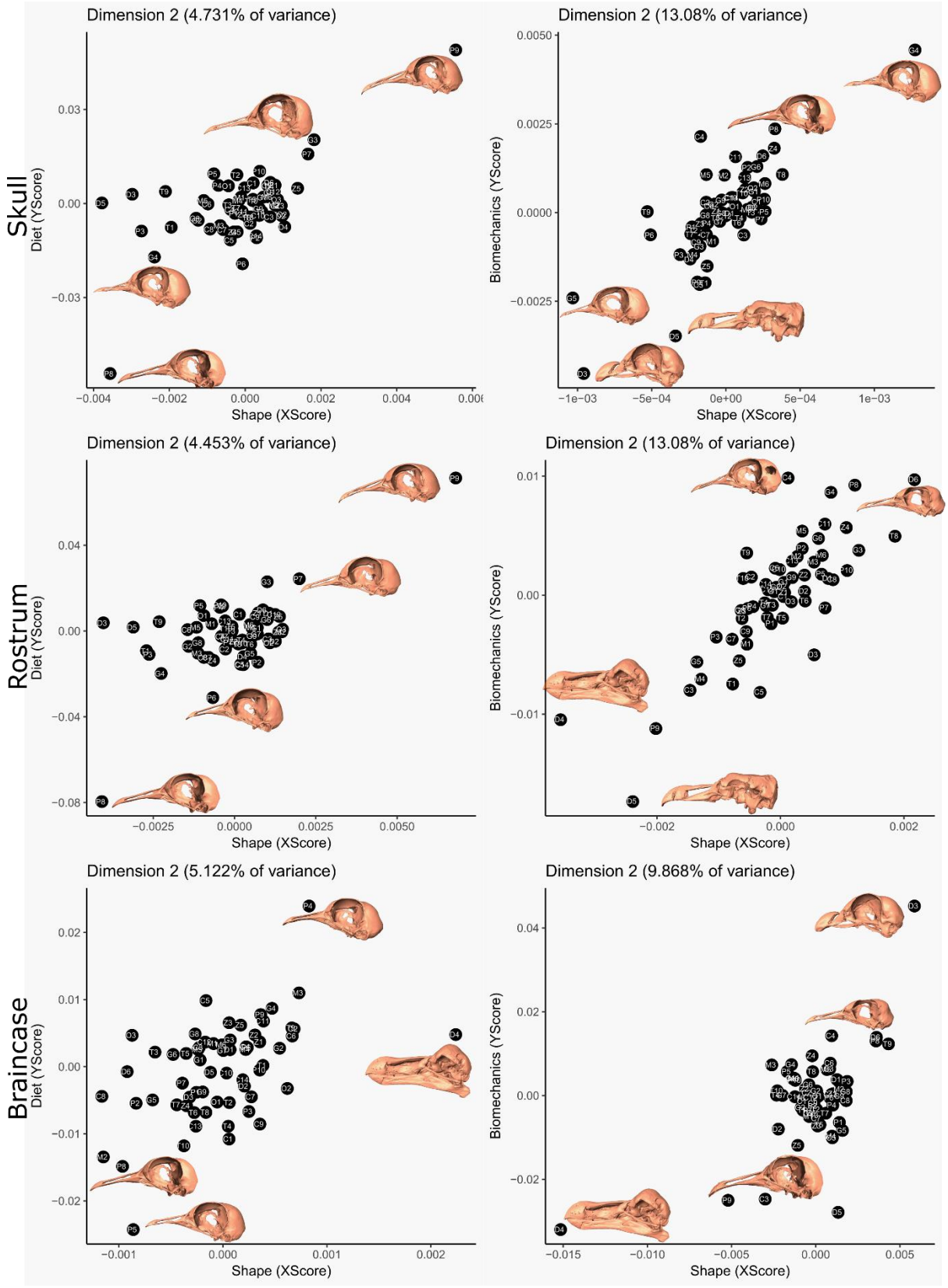


Figure S3.7. PLS Shape (XScores) versus other data blocks (YScores), PLS dimension two. Three dimensional models of species with extreme values exemplify the shape variation along the PLS dimension. Legend as in Figure S3.2.

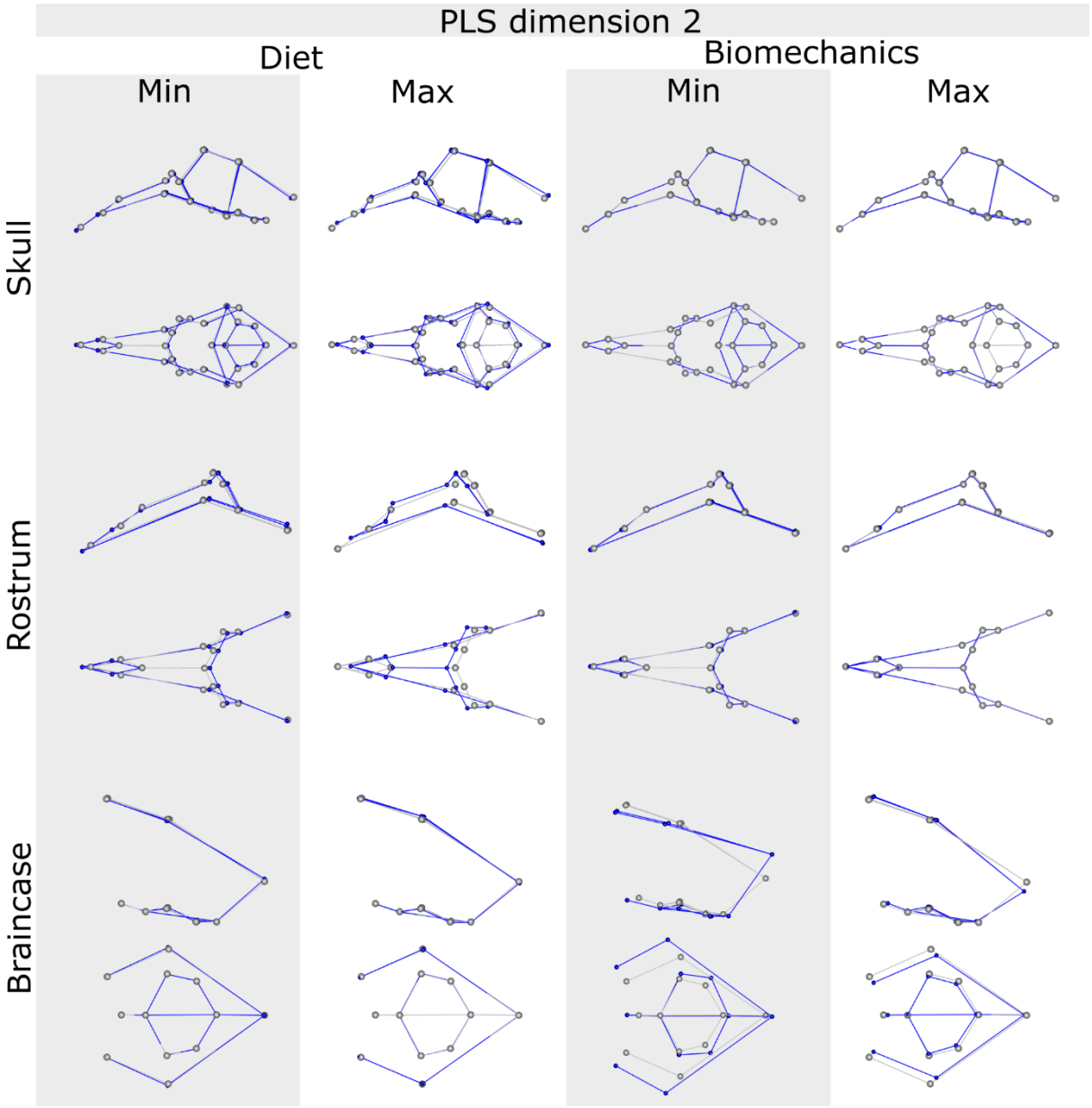


Figure S3.8. Predicted shapes for the maximum and minimum values of XScores in the PLS dimension two. PLS dimension 2 shape changes were identified differentially when evaluating the biomechanical and feeding data blocks. PLS dimension 2 captures important shape changes for the complete skull and the rostrum module while, in the biomechanical data block only captures important shape changes in the braincase module.

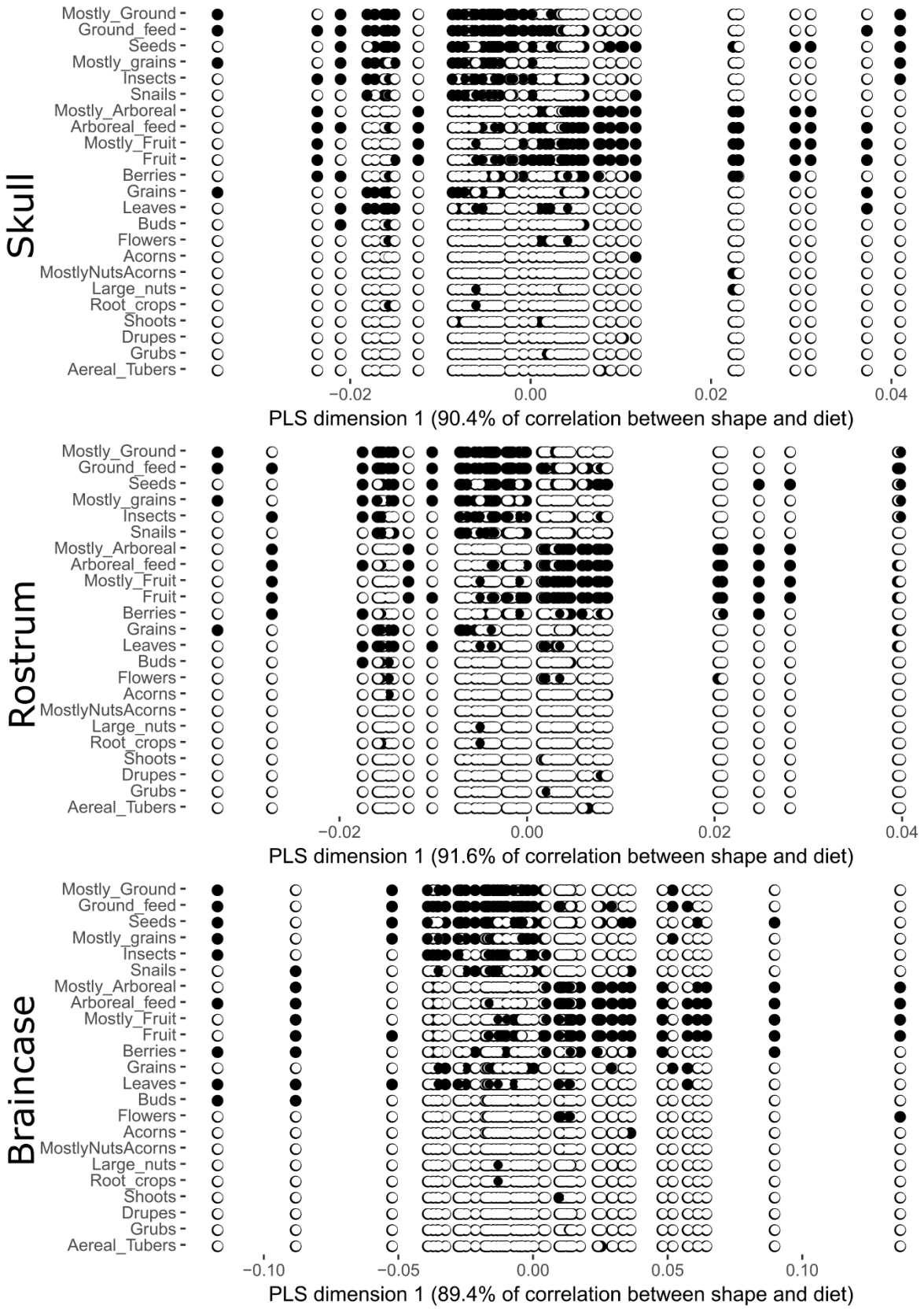


Figure S3.9. Feeding PLS scores (YScores) in PLS dimension one. Each column of circles represents a species in the sample. Black circles represent presence of the feeding trait, and white circles represent absence of that feeding trait. Two clear clusters of feeding strategies can be observed.

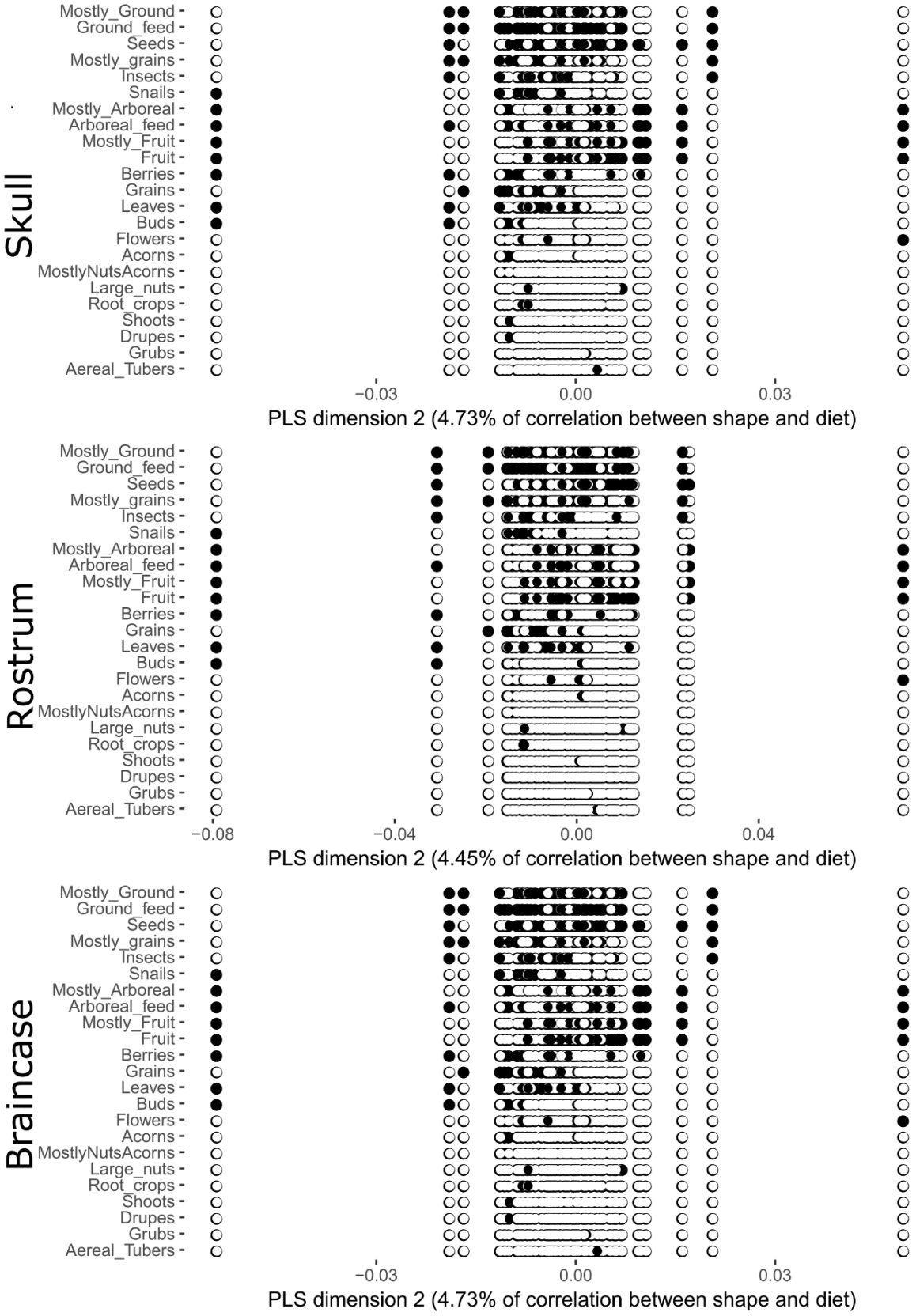


Figure S3.10. Feeding PLS scores (YScores) in PLS dimension two. Each column of circles represents a species in the sample. Black circles represent presence of the feeding trait, and white circles represent absence of that feeding trait.

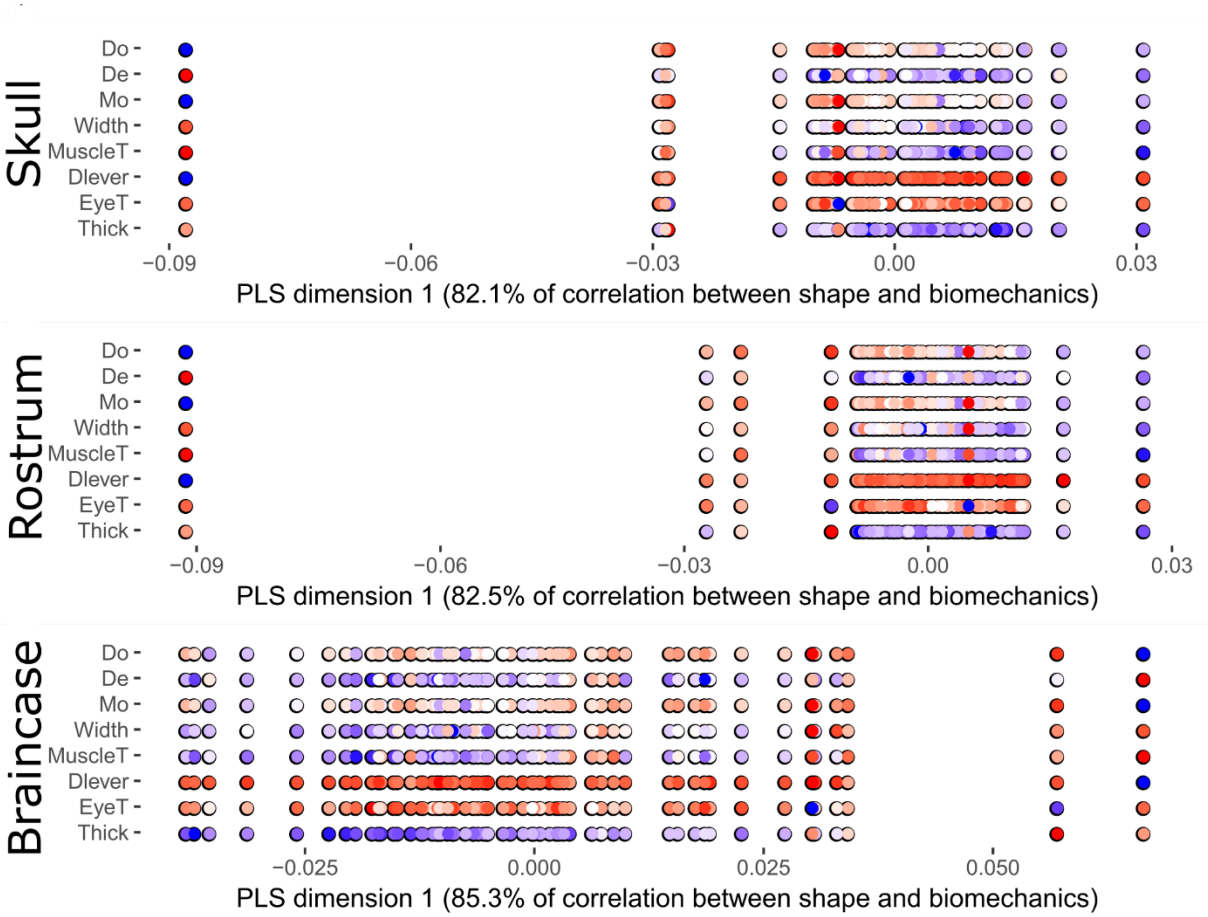


Figure S3.11. Standardized biomechanical characters versus PLS dimension one scores (YScores) for each species in the dataset. Each column of circles represents a species in the sample, and the intensity of the colour marks the comparative performance.

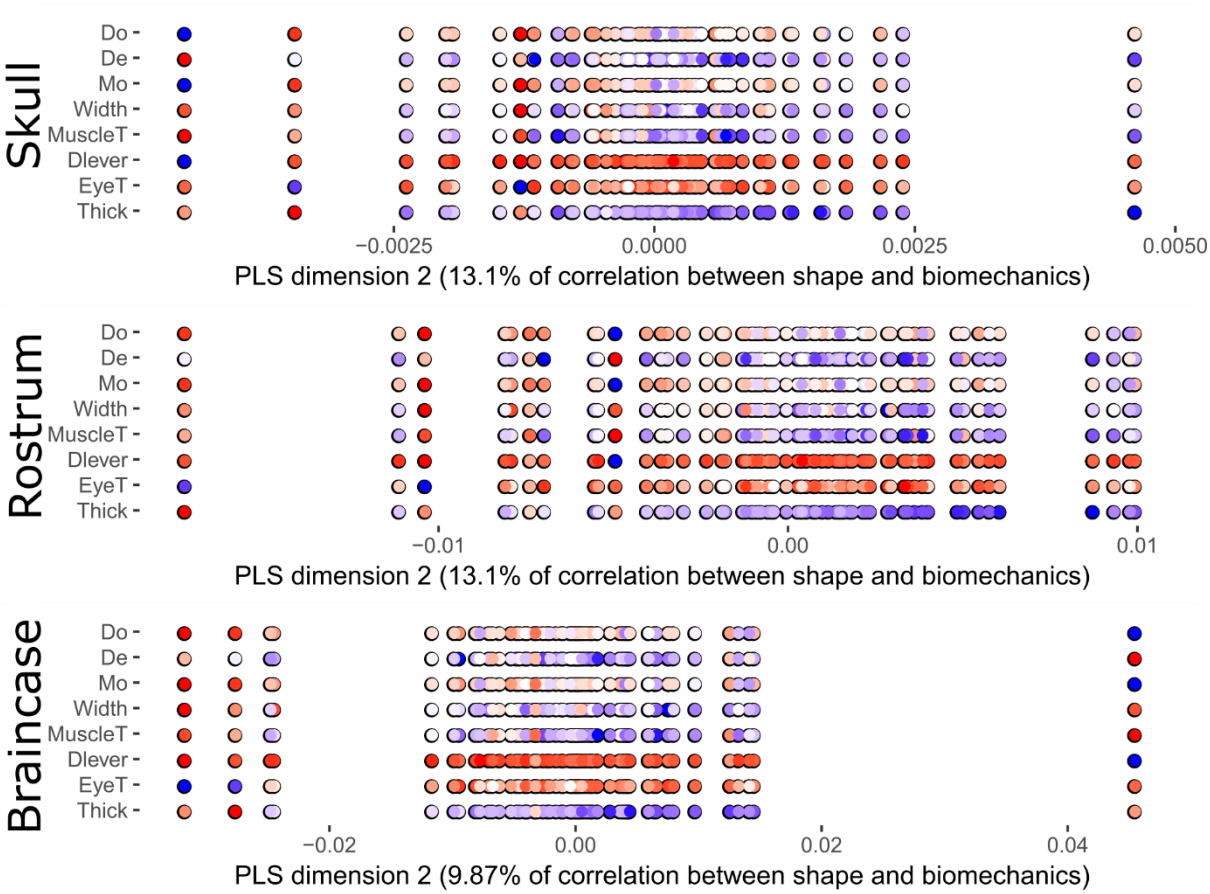


Figure S3.12. Standardized biomechanical characters versus PLS dimension two scores for each species in the dataset. Each column of circles represents a species in the sample, and intensity of the colour marks the comparative performance.

Supplementary tables

Table S3.1. Ecological indicators, other than feeding behaviour, collected for the sample. Distribution type, distribution area in km2, and mean body mass for the species.

Species	Area (km_2)	Mean body mass (g)	Distribution	Where
Alectroenas madagascariensis	522000	173	Island	Madagascar
Alectroenas pulcherrimus	7300	165	Island	Seychelles
Aplopelia larvata	20200000	155	Continental	Sub-Saharan Africa
Caloenas nicobarica	16200000	540	Island	Malay Archipelago
Chalcophaps indica	21300000	136	Both	Asia and Malay Archipelago
Claravis pretiosa	18900000	68	Continental	Meso and South America
Columba arquatrix	11100000	400	Continental	Sub-Saharan Africa
Columba guinea	25600000	352	Continental	Sub-Saharan Africa
Columba livia	61000000	354.5	Both	Europe, Africa, and Asia Minor
Columba oenas	21400000	291	Continental	Europe, and Asia minor
Columba palumbus	31800000	490	Continental	Europe, Malaysia, and Asia Minor
Columba pulchricollis	2990000	330	Continental	Asia
Columba rupestris	17800000	245.5	Continental	Asia
Columba trocaz	390	511	Island	Funchal
Columba vitiensis	18200000	353	Island	Malay Archipelago
Columbina cruziana	1240000	50.1	Continental	South America
Columbina passerina	23600000	35.4	Continental	North, South America and Caribbean
Columbina talpacoti	24100000	45.6	Continental	North and South America
Didunculus strigirostris	2900	400	Island	Samoa

Drepanoptila holosericea	22600	215	Island	New Caledonia
Ducula goliath	22700	600	Island	New Caledonia
Ducula pacifica	11000000	395	Island	Papua New Guinea
Ectopistes migratorius	9000000	298.5	Continental	North America
Gallicolumba luzonica	212000	196	Island	Manila
Geopelia cuneata	7860000	31.6	Continental	Australia
Geophaps plumifera	2590000	98.1	Continental	Australia
Geotrygon mystacea	164000	211	Island	Caribbean
Geotrygon versicolor	13500	225	Island	Jamaica
Goura cristata	216000	2000	Island	Papua
Hemiphaga novaeseelandiae	669000	653	Island	New Zealand
Leptotila rufaxilla	14300000	157	Continental	South America
Leucosarcia melanoleuca	1010000	429	Continental	Australia
Lopholaimus antarcticus	1240000	497	Continental	Australia
Macropygia unchall	12900000	168	Continental	Thailand and Indonesia
Metriopelia ceciliae	918000	55.1	Continental	South America
Metriopelia melanoptera	5720000	100	Continental	South America
Ocyphaps lophotes	8790000	204	Continental	Australia
Otidiphaps nobilis	514000	500	Island	Papua New Guinea
Patagioenas cayennensis	18700000	229	Continental	Mesoamerica and South America
Patagioenas fasciata	5680000	342.5	Continental	North America
Patagioenas leucocephala	3470000	238	Both	Caribbean
Patagioenas maculosa	3960000	347	Continental	South America
Patagioenas nigrirostris	1160000	176	Continental	Mesoamerica
Patagioenas picazuro	7020000	279	Continental	South America
Patagioenas plumbea	12700000	179	Continental	South America
Patagioenas speciosa	16900000	258.5	Continental	Mesoamerica and South America
Patagioenas squamosa	1730000	312	Island	Caribbean

Petrophassa albipennis	312000	132	Continental	Australia
Pezophaps solitaria	108	11300	Island	Rodrigues
Phapitreron leucotis	251000	108	Island	Philippines
Phaps chalcoptera	10300000	331	Continental	Australia
Phaps elegans	4520000	211.5	Both	Tasmania and Australia
Phaps histrionica	4830000	289	Continental	Australia
Ptilinopus dupetithouarsii	14700	100	Island	Marquesas
Raphus cucullatus	2000	9600	Island	Mauritius
Starnoenas cyanocephala	198000	219	Island	Cuba
Streptopelia decaocto	93400000	149	Continental	Europe, North Africa, Asia Minor, India, and Mongolia
Streptopelia turtur	36000000	132	Continental	Europe and Africa
Treron curvirostra	9970000	134.5	Both	Thailand and Indonesia
Treron formosae	101000	140	Island	Taiwan
Turacoena manadensis	529000	212.5	Island	Indonesia
Turtur tympanistria	19700000	73.6	Continental	Sub-Saharan Africa
Zenaida macroura	23700000	119	Continental	North and Central America

Table S3.2. Landmarks system and assigned modules. The correspondence to the landmark number used by Young et al. (2017) are shown.

Landmark	Module	Description	Location	Young
1	Rostrum	Distalmost tip of premaxilla	Midline	2
2	Rostrum	Midline point cranial hinge	Midline	1
3	Braincase	Tip of occipital crest	Midline	3
4	Braincase	Anterior midline of the foramen magnum	Midline	23
5	Braincase	Anterior midline point of basicranium	Midline	24
6	Braincase	Midline point between vomer and pterygoid	Midline	19
7	Rostrum	Nasal distal contact (right)	Bilateral	27
8	Rostrum	Nasal distal contact (left)	Bilateral	30
9	Rostrum	Maxilla-nasal contact with jugal (right)	Bilateral	10
10	Rostrum	Maxilla-nasal contact with jugal (left)	Bilateral	9
11	Rostrum	Contact between nasal and frontal (right)	Bilateral	18
12	Rostrum	Contact between nasal and frontal (left)	Bilateral	17
13	Rostrum	Lateral contact between lacrimal and frontal (right)	Bilateral	14
14	Rostrum	Lateral contact between lacrimal and frontal (left)	Bilateral	13
15	Rostrum	Inferior and lateralmost point of lacrimal (right)	Bilateral	12
16	Rostrum	Inferior and lateralmost point of lacrimal (left)	Bilateral	11
17	Rostrum	Lateral point on jugal (right)	Bilateral	5
18	Rostrum	Lateral point on jugal (left)	Bilateral	4
19	Braincase	Posterior orbital rim, frontal and postorbital contact (right)	Bilateral	20
20	Braincase	Posterior orbital rim, frontal and postorbital contact (left)	Bilateral	28
21	Braincase	Lateral basioccipital contact with exoccipital (right)	Bilateral	26
22	Braincase	Lateral basioccipital contact with exoccipital (left)	Bilateral	25
23	Braincase	Basioccipital and quadrate (right)	Bilateral	32
24	Braincase	Basioccipital and quadrate (left)	Bilateral	31
25	Braincase	Orbital margin, midpoint between (14) and (20) (left)	Bilateral	15
26	Braincase	Orbital margin, midpoint between (13) and (19) (right)	Bilateral	16
27	Rostrum	Midpoint between (1) and (2)	Midline	8
28	Braincase	Distalmost point of the *processus oticus* (right)	Bilateral	NA
29	Braincase	Distalmost point of the *processus oticus* (left)	Bilateral	NA

Table S3.3. Biomechanical performance calculated on the Procrustes aligned coordinates. Effort distance (Fe); muscle area (MusT); effort distance (De); output distance (Do); mechanical advantage (MA); output force (Fo); mouth opening (Mo); velocity of bite (Vel); rostrum thickness (Thick); centroid size of the rostrum ad mid-length (Ics); lever length (Dlever); moment of area (Bend); and eye size (EyeT).

Species	Fe	MusT	De	Do	MA	Fo	Mo	Vel	Thick	Ics	Dlever	Bend	EyeT
Alectroenas pulcherrimus	0.017	0.282	0.147	0.131	1.123	0.019	0.093	0.015	0.018	0.039	0.156	0.249	0.374
Alectroenas madagascariensis	0.017	0.282	0.148	0.128	1.151	0.020	0.091	0.015	0.017	0.036	0.155	0.233	0.412
Aplopelia larvata	0.013	0.246	0.123	0.118	1.046	0.014	0.083	0.012	0.022	0.039	0.229	0.171	0.415
Claravis pretiosa	0.010	0.221	0.096	0.119	0.809	0.008	0.084	0.012	0.019	0.036	0.196	0.186	0.426
Columba pulchricollis	0.012	0.239	0.109	0.124	0.883	0.011	0.088	0.014	0.026	0.045	0.200	0.224	0.367
Columba rupestris	0.012	0.244	0.117	0.125	0.933	0.011	0.089	0.013	0.019	0.037	0.203	0.182	0.396
Columba vitiensis	0.012	0.242	0.115	0.121	0.950	0.012	0.085	0.013	0.022	0.042	0.213	0.197	0.346
Columbina cruziana	0.011	0.236	0.104	0.128	0.815	0.009	0.090	0.014	0.028	0.043	0.180	0.237	0.400
Columbina passerina	0.010	0.218	0.094	0.119	0.790	0.008	0.084	0.012	0.020	0.037	0.199	0.184	0.439
Drepanoptila holosericea	0.015	0.272	0.150	0.114	1.322	0.020	0.080	0.012	0.017	0.039	0.178	0.217	0.362
Ectopistes migratorius	0.014	0.260	0.136	0.120	1.134	0.016	0.085	0.013	0.026	0.046	0.223	0.205	0.373
Gallicolumba luzonica	0.013	0.245	0.127	0.115	1.103	0.014	0.082	0.011	0.022	0.039	0.215	0.183	0.415
Geotrygon mystacea	0.013	0.245	0.120	0.122	0.987	0.012	0.086	0.013	0.026	0.039	0.235	0.165	0.394
Metriopelia ceciliae	0.012	0.245	0.115	0.128	0.900	0.011	0.090	0.013	0.018	0.043	0.184	0.232	0.421
Patagioenas speciosa	0.013	0.250	0.132	0.111	1.184	0.016	0.079	0.011	0.023	0.042	0.215	0.194	0.385
Patagioenas nigrirostris	0.014	0.254	0.124	0.126	0.988	0.013	0.089	0.014	0.026	0.045	0.178	0.251	0.401
Patagioenas plumbea	0.014	0.252	0.126	0.121	1.041	0.014	0.085	0.013	0.025	0.041	0.211	0.195	0.376
Phaps chalcoptera	0.012	0.242	0.118	0.122	0.971	0.012	0.086	0.013	0.021	0.039	0.213	0.184	0.420
Phaps histrionica	0.011	0.225	0.098	0.120	0.814	0.009	0.085	0.013	0.015	0.038	0.195	0.196	0.390
Treron formosae	0.015	0.269	0.139	0.123	1.130	0.017	0.087	0.014	0.031	0.052	0.174	0.301	0.383
Columba arquatrix	0.013	0.246	0.122	0.118	1.032	0.013	0.083	0.013	0.024	0.042	0.214	0.198	0.365
Patagioenas fasciata	0.014	0.259	0.133	0.123	1.080	0.015	0.087	0.013	0.018	0.039	0.230	0.171	0.353

Columba guinea	0.013	0.247	0.119	0.122	0.980	0.013	0.086	0.013	0.022	0.042	0.215	0.196	0.396
Patagioenas picazuro	0.013	0.247	0.125	0.117	1.067	0.014	0.083	0.012	0.024	0.042	0.202	0.209	0.382
Patagioenas squamosa	0.011	0.229	0.115	0.109	1.055	0.012	0.077	0.011	0.022	0.042	0.226	0.188	0.370
Columba trocaz	0.013	0.251	0.116	0.130	0.894	0.012	0.092	0.015	0.031	0.056	0.228	0.248	0.346
Columbina talpacoti	0.011	0.233	0.107	0.121	0.890	0.010	0.085	0.013	0.020	0.033	0.185	0.178	0.426
Geopelia cuneata	0.012	0.243	0.118	0.123	0.957	0.012	0.087	0.013	0.023	0.040	0.193	0.210	0.431
Geophaps plumifera	0.010	0.228	0.096	0.124	0.776	0.008	0.088	0.013	0.023	0.050	0.175	0.285	0.429
Geotrygon versicolor	0.014	0.254	0.131	0.120	1.089	0.015	0.085	0.012	0.030	0.045	0.234	0.193	0.383
Hemiphaga novaeseelandiae	0.015	0.264	0.136	0.122	1.117	0.017	0.086	0.013	0.025	0.043	0.197	0.217	0.350
Leptotila rufaxilla	0.011	0.228	0.107	0.117	0.913	0.010	0.083	0.012	0.025	0.037	0.214	0.172	0.421
Leucosarcia melanoleuca	0.012	0.240	0.120	0.117	1.024	0.012	0.083	0.012	0.020	0.045	0.217	0.205	0.371
Macropygia unchall	0.013	0.243	0.110	0.123	0.891	0.011	0.087	0.014	0.020	0.042	0.209	0.202	0.385
Ocyphaps lophotes	0.012	0.236	0.109	0.123	0.884	0.010	0.087	0.013	0.020	0.042	0.190	0.221	0.415
Phapitreron leucotis	0.014	0.257	0.130	0.122	1.060	0.015	0.086	0.013	0.023	0.049	0.185	0.267	0.402
Petrophassa albipennis	0.011	0.232	0.110	0.119	0.919	0.010	0.084	0.012	0.016	0.036	0.210	0.170	0.389
Ptilinopus dupetithouarsii	0.017	0.290	0.156	0.129	1.207	0.021	0.091	0.014	0.023	0.045	0.174	0.258	0.356
Starnoenas cyanocephala	0.011	0.234	0.117	0.115	1.021	0.011	0.081	0.011	0.019	0.036	0.212	0.171	0.411
Streptopelia turtur	0.010	0.221	0.101	0.115	0.873	0.009	0.082	0.012	0.020	0.034	0.211	0.161	0.382
Turtur tympanistria	0.011	0.223	0.099	0.118	0.837	0.009	0.083	0.013	0.025	0.040	0.224	0.180	0.420
Zenaida macroura	0.010	0.215	0.094	0.117	0.808	0.008	0.083	0.012	0.023	0.038	0.213	0.178	0.414
Caloenas nicobarica	0.013	0.252	0.139	0.105	1.316	0.017	0.074	0.010	0.023	0.040	0.208	0.193	0.344
Chalcophaps indica	0.012	0.239	0.121	0.116	1.046	0.012	0.082	0.011	0.027	0.038	0.233	0.165	0.417
Columba oenas	0.012	0.241	0.118	0.120	0.979	0.012	0.085	0.013	0.021	0.040	0.205	0.198	0.413
Columba palumbus	0.014	0.259	0.127	0.129	0.983	0.014	0.091	0.014	0.028	0.045	0.209	0.215	0.382
Didunculus strigirostris	0.014	0.305	0.191	0.093	2.049	0.028	0.066	0.007	0.051	0.065	0.039	1.645	0.412
Ducula pacifica	0.016	0.277	0.152	0.119	1.271	0.020	0.084	0.012	0.027	0.045	0.201	0.225	0.337
Goura cristata	0.012	0.245	0.132	0.107	1.238	0.015	0.076	0.010	0.027	0.041	0.245	0.168	0.352
Pezophaps solitaria	0.015	0.276	0.130	0.142	0.915	0.014	0.100	0.016	0.074	0.076	0.212	0.360	0.269

Phaps elegans	0.010	0.216	0.105	0.107	0.985	0.010	0.076	0.010	0.018	0.034	0.215	0.160	0.410
Treron curvirostra	0.018	0.291	0.149	0.135	1.107	0.020	0.095	0.016	0.040	0.054	0.145	0.373	0.373
Patagioenas cayennensis	0.013	0.242	0.122	0.116	1.059	0.013	0.082	0.012	0.023	0.043	0.196	0.218	0.383
Patagioenas leucocephala	0.012	0.240	0.111	0.124	0.895	0.011	0.087	0.014	0.028	0.043	0.230	0.187	0.357
Patagioenas maculosa	0.012	0.240	0.123	0.111	1.104	0.014	0.079	0.011	0.026	0.042	0.214	0.194	0.384
Lopholaimus antarcticus	0.015	0.266	0.133	0.123	1.082	0.016	0.087	0.014	0.025	0.046	0.182	0.251	0.388
Metriopelia melanoptera	0.010	0.228	0.092	0.131	0.705	0.007	0.093	0.014	0.030	0.044	0.191	0.232	0.430
Otidiphaps nobilis	0.011	0.229	0.122	0.102	1.190	0.013	0.072	0.009	0.026	0.040	0.193	0.208	0.392
Turacoena manadensis	0.013	0.243	0.116	0.120	0.968	0.012	0.085	0.013	0.018	0.045	0.210	0.215	0.364
Ducula goliath	0.013	0.248	0.132	0.113	1.167	0.015	0.080	0.011	0.027	0.042	0.191	0.221	0.337
Streptopelia decaocto	0.011	0.235	0.112	0.120	0.934	0.011	0.085	0.012	0.016	0.038	0.215	0.177	0.377
Raphus cucullatus	0.015	0.297	0.151	0.144	1.048	0.016	0.102	0.014	0.053	0.068	0.245	0.278	0.258
Columba livia	0.013	0.247	0.122	0.122	1.005	0.013	0.086	0.013	0.026	0.043	0.209	0.207	0.396

Table S3.4. Proportion of the covariation between blocks explained by the first four PLS dimensions. Results for all the multi-phylogeny two-block PLS analyses of shape data blocks (skull, rostrum or braincase) versus feeding or biomechanical performance data blocks. % of variance was calculated by squaring the eigenvalues and obtaining the percentage of the sum of eigenvalues. Only four dimensions are reported because these dimensions explain most (at least 98%) of the covariation.

Module	Multi-phylogeny two-block PLS	Dim.	Sing.Val.	Eigenvalue	Var. (%)	Cum.Var. (%)
Skull	Shape-Feeding	1	1.30E-03	1.68E-06	90.39	90.39
Skull	Shape-Feeding	2	2.96E-04	8.78E-08	4.73	95.12
Skull	Shape-Feeding	3	1.89E-04	3.59E-08	1.93	97.06
Skull	Shape-Feeding	4	1.47E-04	2.15E-08	1.16	98.21
…	…	…	…	…	…	…
Skull	Shape-Biomechanics	1	3.75E-04	1.41E-07	82.07	82.07
Skull	Shape-Biomechanics	2	1.50E-04	2.24E-08	13.08	95.16
Skull	Shape-Biomechanics	3	7.14E-05	5.09E-09	2.97	98.13
Skull	Shape-Biomechanics	4	4.27E-05	1.83E-09	1.06	99.19
…	…	…	…	…	…	…
Rostrum	Shape-Feeding	1	1.09E-03	1.20E-06	91.60	91.60
Rostrum	Shape-Feeding	2	2.41E-04	5.81E-08	4.45	96.05
Rostrum	Shape-Feeding	3	1.50E-04	2.24E-08	1.72	97.77
Rostrum	Shape-Feeding	4	1.12E-04	1.26E-08	0.96	98.73
…	…	…	…	…	…	…
Rostrum	Shape-Biomechanics	1	3.22E-04	1.04E-07	82.46	82.46
Rostrum	Shape-Biomechanics	2	1.28E-04	1.65E-08	13.08	95.55
Rostrum	Shape-Biomechanics	3	5.92E-05	3.50E-09	2.78	98.33
Rostrum	Shape-Biomechanics	4	3.59E-05	1.29E-09	1.02	99.35
…	…	…	…	…	…	…
Braincase	Shape-Feeding	1	7.02E-04	4.92E-07	89.36	89.36
Braincase	Shape-Feeding	2	1.68E-04	2.82E-08	5.12	94.48
Braincase	Shape-Feeding	3	1.13E-04	1.27E-08	2.30	96.79
Braincase	Shape-Feeding	4	9.11E-05	8.31E-09	1.51	98.29
…	…	…	…	…	…	…
Braincase	Shape-Biomechanics	1	1.98E-04	3.94E-08	85.30	85.30
Braincase	Shape-Biomechanics	2	6.75E-05	4.56E-09	9.87	95.16
Braincase	Shape-Biomechanics	3	3.72E-05	1.38E-09	3.00	98.16
Braincase	Shape-Biomechanics	4	2.23E-05	4.97E-10	1.08	99.24
…	…	…	…	…	…	…

Table S3.5. Results for the ordinary least squares (ols) and phylogenetic generalized least squares models of rostrum shape versus candidate explanatory variables. A series of pairwise regressions were performed to try to explain the rostrum shape (independent variable).

	Distance-based ordinary least squares			Distance-based phylogenetic generalized least squares					
Skull shape~	Z	Rsq	Pr..F.	Z	Z.sd	Rsq	Rsq.sd	Pr(>F)	Pr(>F).sd
Area	-0.645	0.009	0.731	-0.971	0.816	0.052	0.102	0.770	0.228
Csize	2.919	0.075	**0.007**	2.467	0.957	0.084	0.078	0.051	0.112
mass	2.594	0.061	**0.010**	1.919	0.680	0.052	0.070	0.062	0.108
Distribution	0.635	0.039	0.249	-0.727	0.574	**0.102**	0.118	0.748	0.200
BiomechD1	**4.620**	**0.214**	**0.001**	1.524	0.488	**0.167**	0.123	0.092	0.083
BiomechD2	2.861	0.073	**0.004**	-0.262	0.555	0.093	0.118	0.578	0.202
De	**4.395**	**0.164**	**0.001**	2.201	0.870	0.086	0.090	0.057	0.095
Dlever	**5.671**	**0.352**	**0.001**	**4.415**	1.218	**0.275**	0.091	**0.006**	0.019
Do	**3.750**	**0.117**	**0.001**	1.351	0.456	**0.130**	0.099	0.120	0.078
EyeT	**3.094**	0.081	**0.002**	1.747	0.916	**0.111**	0.113	0.106	0.145
Mo	**3.750**	**0.117**	**0.001**	1.351	0.456	**0.130**	0.099	0.120	0.078
MuscleT	**4.846**	**0.190**	**0.001**	2.047	0.732	**0.104**	0.090	0.057	0.086
Thick	**3.568**	**0.120**	**0.003**	1.748	0.684	0.082	0.064	0.082	0.120
Width	**3.830**	**0.120**	**0.001**	1.412	0.517	0.094	0.107	0.110	0.102
FoodD1	0.192	0.015	0.417	-0.004	0.584	**0.114**	0.144	0.491	0.206
FoodD2	-1.315	0.005	0.931	-0.688	0.352	0.067	0.095	0.753	0.134
PCO1	**3.424**	0.086	**0.001**	0.840	0.498	0.058	0.075	0.217	0.145
PCO2	0.727	0.020	0.238	-0.382	0.484	0.058	0.103	0.633	0.177
PCO3	1.619	0.033	0.051	-0.072	0.690	0.089	0.124	0.523	0.230
PCO6	1.120	0.026	0.128	0.077	0.646	0.099	0.120	0.469	0.215
PCO8	-0.280	0.012	0.605	-0.172	0.682	0.085	0.134	0.548	0.240
ClusterGAve	**3.361**	**0.278**	**0.003**	-0.128	0.252	**0.184**	0.077	0.514	0.102
FruitDB	**0.366**	0.017	0.360	-0.385	0.485	0.018	0.043	0.629	0.178
GrainsOrSeeds	**0.387**	0.017	0.343	0.243	0.539	0.054	0.103	0.400	0.172
Greens	2.462	0.048	**0.007**	0.822	0.415	0.069	0.101	0.220	0.115
LivePrey	**3.598**	0.084	**0.001**	0.288	0.673	0.099	0.122	0.397	0.211
MostDiet	**3.134**	**0.105**	**0.002**	0.651	0.315	0.062	0.057	0.261	0.094
MostForage	**2.765**	**0.116**	**0.021**	1.096	0.393	0.091	0.076	0.151	0.077
NutsRoots	0.365	0.017	0.359	0.724	0.279	0.058	0.085	0.238	0.081

Table S3.6. Results for the ordinary least squares (ols) and phylogenetic generalized least squares models of braincase shape versus candidate explanatory variables. A series of pairwise regressions were performed to try to explain the braincase shape (independent variable).

	Distance-based ordinary least squares			Distance-based phylogenetic generalized least squares					
Skull shape~	Rsq	Z	Pr..F.	Z	Z.sd	Rsq	Rsq.sd	Pr(>F)	Pr(>F).sd
Area	0.004	-2.141	0.984	-1.106	0.583	0.042	0.081	0.829	0.142
Csize	**0.117**	**3.651**	**0.001**	2.150	1.057	0.071	0.070	0.080	0.160
mass	0.097	**3.460**	**0.001**	2.088	0.807	0.055	0.063	0.058	0.139
Distribution	0.027	-0.321	0.621	-1.056	0.403	0.086	0.097	0.845	0.111
BiomechD1	**0.121**	**3.712**	**0.001**	0.651	0.462	**0.107**	0.104	0.275	0.143
BiomechD2	0.060	2.592	**0.006**	-1.074	0.520	0.062	0.098	0.829	0.133
De	0.085	**3.352**	**0.001**	0.939	0.799	0.049	0.078	0.235	0.220
Dlever	**0.118**	**3.692**	**0.002**	2.740	1.162	**0.117**	0.087	**0.048**	0.109
Do	**0.100**	**3.604**	**0.001**	0.982	0.578	**0.107**	0.089	0.196	0.149
EyeT	**0.120**	**3.822**	**0.001**	2.203	0.952	**0.133**	0.113	0.062	0.114
Mo	**0.100**	**3.604**	**0.001**	0.982	0.578	**0.107**	0.089	0.196	0.149
MuscleT	**0.137**	**4.308**	**0.001**	1.934	1.035	0.094	0.075	0.100	0.188
Thick	**0.159**	**4.027**	**0.001**	1.694	0.867	0.077	0.056	0.112	0.184
Width	**0.131**	**4.151**	**0.001**	1.200	0.599	0.084	0.101	0.150	0.148
FoodD1	0.018	0.432	0.342	-0.044	0.442	**0.108**	0.131	0.515	0.160
FoodD2	0.006	-1.101	0.878	-0.890	0.269	0.061	0.086	0.821	0.087
PCO1	0.042	2.045	**0.016**	-0.383	0.640	0.034	0.063	0.619	0.188
PCO2	0.022	0.837	0.205	-0.323	0.471	0.056	0.092	0.612	0.161
PCO3	0.028	1.388	0.088	-0.617	0.678	0.070	0.112	0.693	0.203
PCO6	0.012	-0.253	0.607	-0.549	0.644	0.073	0.101	0.673	0.193
PCO8	0.020	0.612	0.266	-0.078	0.469	0.080	0.119	0.514	0.168
ClusterGAve	**0.271**	**3.474**	**0.003**	-0.615	0.297	**0.153**	0.057	0.725	0.104
FruitDB	0.015	0.060	0.473	0.597	0.473	0.027	0.032	0.278	0.166
GrainsOrSeeds	0.028	1.341	0.090	0.715	0.757	0.063	0.101	0.280	0.199
Greens	0.034	1.803	**0.032**	-0.435	0.440	0.034	0.071	0.655	0.146
LivePrey	0.051	2.633	**0.004**	-0.240	0.456	0.075	0.102	0.581	0.164
MostDiet	0.065	1.910	**0.025**	0.428	0.362	0.053	0.036	0.333	0.124
MostForage	0.059	1.450	0.057	0.023	0.397	0.050	0.055	0.468	0.148
NutsRoots	0.020	0.672	0.257	0.208	0.410	0.048	0.090	0.415	0.146

Chapter Four. Artificial and natural selection work on different axes of variation: Examining the phenotypic matrices of wild Columbiformes and domestic and feral *Columba livia*

Abstract

The variation and covariation patterns between characters of the phenotypic matrix contains information about the axes of variation, response to selection, modularity, integration, and evolutionary constraints. These patterns have been proposed to be shared across broad ranges of phylogenetic diversity and different selection modes. However, the validity of these generalizations has not been satisfactorily addressed. Here, I apply several tests (considering and disregarding differences in multidimensional subspaces) to show that the patterns of covariation of domestic pigeons are not shared across ranges of phylogenetic diversity and that artificial selection can exploit new axes of variation. I assessed the similarity of identified patterns of variation in three samples: domestic fancy pigeons (*Columba livia*), feral *C. livia*, and a comparative sample comprising 65 species (77% of the generic diversity) of wild Columbiformes. Low similarity of patterns of variation was found between samples and between selection types (artificial versus natural). I found that domestic fancy pigeons occupy a more substantial proportion of the morphospace than the order Columbiformes; in fact, some specific regions of morphospace are only populated by domesticated or naturally selected pigeons. My results show that the novel shapes seen in domesticated pigeons are not only more extreme forms of the major axes of natural variation in pigeons, but the exploration of novel axes of variation in domestication. My

results also warn against generalizing patterns of variation observed in one species across taxonomic across broad ranges of phylogenetic diversity (multiple phylogenetic lineages).

Introduction

Common pigeons (*Columba livia*) were domesticated around 5,000 (6,000 to 4,000) years ago (Johnston and Janinga, 1995; Sol, 2008; Larson and Fuller, 2014). Pigeons are the first bird that entered a domestic relationship with people from Western Eurasia (Larson and Fuller, 2014). Domestication allowed pigeons to expand their natural habitat range (shore cliffs, open and semi-open environments across Europe, North Africa, and Western Asia ; Johnston, 1992; Gilbert and Shapiro, 2013; Larson and Fuller, 2014) to include a variety of human environments. Based on behavioural evidence, it is thought that pigeons were originally domesticated through the commensal pathway, likely following human associated resources (*e.g.*, food and waste) and in turn being used as a food source by humans (Larson and Fuller, 2014). Evidence of pigeon breeding has been found in Mesopotamia (5,000-4,500 years before present BP; Serjeantson, 2009; Larson and Fuller, 2014) and Egypt (3,000-2,000 years BP; Darwin, 1868; Serjeantson, 2009; Larson and Fuller, 2014). Fragmentary evidence and "speculation about human behaviour" can push back the date of domestication of pigeons to 6,000 to 10,000 years ago (Serjeantson, 2009 pp. 562). However, unequivocal archaeological evidence about pigeon domestication comes from dovecotes. The intensity of management of commensal pigeons increased with the use of dovecotes, which are costume build structures which act as secure nesting and homing spaces for pigeons that allow the collection of droppings (used as fertilizer) and squabs (Atwell, 1996). The oldest dovecote structures are from Roman times (1st century AD: *Anno Domini*; Ashley, Cordell and Mavinic, 2011; altough dovecots made of clay from the Middle East and Egypt are mentioned in Serjeantson, 2009) and Anatolia in the 7th century AD (O'Connor, 2013). Dovecote pigeons which can be considered mainly as commensal

pigeons inhabiting a human made structure and being fed only in the winter months (O'Connor, 2013).

Pigeons are now rarely used for food, having been mainly replaced by the considerably larger chickens (*Gallus gallus*), which were also secondarily selected to regularly lay eggs (Larson and Fuller, 2014; Loog *et al.*, 2017). However, pigeons still produced valuable manure (Ashley, Cordell and Mavinic, 2011; O'Connor, 2013) and the negative correlation between chickens and pigeons is not straightforward in the archaeological record, for example, dovecots become common in Britain from the 11th to 12th century onwards (Sykes, 2007; Serjeantson, 2009) would not be expected because it coincides with the selection a faster onset on egg production in chickens (thyroid-stimulating hormone receptor; Loog *et al.*, 2017). Nevertheless, several distinct breeds of domestic pigeons are still kept for utility (messenger pigeons, racing pigeons, thief pigeons) and for aesthetic reasons ('fancy pigeons') (Darwin, 1868; Martínez-Gómez *et al.*, 2009).

Fancy pigeons and utility pigeons represent yet another increase in management of domestic pigeons in which humans select desired traits and the earliest account of pigeon breeds like Laughers and Spots date from 17th century (Darwin, 1868, pp. 207). Fancy pigeons in particular have obtained a wide range of morphologies, presenting more variation than seen within any other bird species (Price, 2002; Stringham *et al.*, 2012), and were bred and described by Darwin (Darwin, 1859, 1868). Fancy pigeons were fundamental to the construction of the theory of evolution by natural selection, helping Darwin to examine the principles of artificial selection first hand (Darwin, 1859, 1868; Martínez-Gómez *et al.*, 2009; Young *et al.*, 2017). The influence of pigeon breeding in Darwin (1859,

1868) is evident in his analogy between natural selection and artificial selection. In this analogy, natural selection acts like the animal breeder, who selects individuals with a "desirable" trait from the available variation in his sample (fittest individuals), and with the pass of generations, can establish a new breed (species).

Fancy pigeons are an extreme product of aesthetic selection and appear to have been exposed to similarly expansive selective pressures than domestic dogs, which have also been selected for aesthetic reasons producing very disparate morphologies (Drake and Klingenberg, 2010). Fancy pigeons also exhibit patterns of variation similar to dog breeds: modularity and integration between the rostrum and braincase with the main axes of variation representing facial length, cranial flexion, and skull width (Young *et al.*, 2017; However, up to seven modules have been found in bird skull, Felice and Goswami, 2017; however, I found only week evidence of modularity in Chapter Three). Variation in fancy pigeons has also been hypothesised to recapitulate the natural variation across Columbiformes as a whole (Martínez-Gómez *et al.*, 2009). The exaggerated traits of pigeons are reminiscent of traits observed in distantly related wild Columbiformes. However, the majority of these similar traits are convergent mutations rather than evidence of gene flow between *C. livia* and other columbiform species (see below).

There are some records of fertile hybrids between closely related species (Darwin, 1868; Lijtmaer, Mahler and Tubaro, 2003) and the checkered pattern of some pigeons originated as an introgression (from a *C. livia* x *C. guinea* hybrid; Vickrey *et al.*, 2018). However, columbiforms follow Haldane's rule (sterility and inviability appearing first in the heterogametic sex) with inviability of hybrids increasing along with species divergence time

(mean time for total inviability is 6.5 million years; Lijtmaer, Mahler and Tubaro, 2003). Hybrids are, therefore, unlikely to overcome pre and postzygotic barriers (except in *C. oenas* Lijtmaer, Mahler and Tubaro, 2003) and provide new variation to fancy domestic pigeons. Furthermore, the genera that have been recorded to hybridize with *C. livia* are other members of *Columba* or the closely related genus *Streptopelia*, which do not exhibit exaggerated morphologies characteristic of fancy pigeon breeds (Darwin, 1868; Martínez-Gómez *et al.*, 2009). Hybridization is unlikely to have significantly increased the natural variation in the pigeon skull because of the close morphologies of closely related species. This putatively small contribution of variation from interspecific hybridization contrasts with the widespread introgressive capture in dogs (Caniedae), cats (Felidae; Hailer and Leonard 2008; Davis et al. 2015; Li et al. 2016; Gopalakrishnan et al. 2018), chickens (Phasianidae), pigs (Suidae), African cattle (Bovidae), and horses (Equidae; Larson and Fuller 2014).

Remarkably, pigeon breeds do not require a pedigree and are judged solely on the basis of their phenotype, thus, fancy pigeons are not as inbred as purebred dogs (Domyan and Shapiro, 2016). Therefore, the phenotypic diversification of domestic pigeons could be compared with a model of sympatric speciation with limited gene flow rather than an allopatric speciation model in which gene flow is absent. Feral pigeons are domestic pigeons that have become naturalized (Johnston, 1990, 1992; Johnston and Janinga, 1995; Sol, 2008). Descendants of feral pigeons constitute most populations of the synanthropic *C. livia* (Johnston, 1992; Luniak, 2004). The feral pigeons of North America are more closely related to domestic breeds than to European feral pigeons (Johnston, 1992; Stringham *et al.*, 2012). Feral pigeons are subject to natural selection and present overall ancestral traits

(*i.e.*, phenotypes closer to wild *C. livia*; Johnston, 1992); however, some traits in feral pigeons still resemble the ones of their domestic pigeon ancestors (Sol, 2008). For these reasons, the term "feral pigeons" is correctly used to refer to naturalized populations of *C. livia* (Johnston, 1992; Johnston and Janinga, 1995; Sol, 2008; Stringham *et al.*, 2012).

Studies of pigeons and other species have previously been used to compare the extent of phenotypic variation obtained under domestication due to artificial selection to that seen within higher taxonomic groups (Martínez-Gómez *et al.*, 2009; Drake and Klingenberg, 2010; Young *et al.*, 2017). However, I wish to also answer other biological questions relating to recent studies of bird macroevolution. Namely, it has been proposed that the major axes of within-group bill-shape evolution are remarkably consistent (Cooney *et al.*, 2017). It has also been proposed that patterns of variation and covariation in domesticated pigeons are predictive of avian cranial evolution and that these patterns are shared among a broad diversity of vertebrate species (Young *et al.*, 2017). I aim to test the generality of these conclusions by examining the covariation and correlation of the phenotypic matrices of wild Columbiformes and domesticated and feral *Columba livia*. Wherever possible, I do this within an explicitly phylogenetic comparative framework to ask whether the patterns of cranial variation and covariation within domestic *C. livia* are similar to those inferred in feral *C. livia*, and to those inferred along evolutionary lineages among species and genera of Columbiformes.

Darwin stated that the covariation between characters within populations was the "most imperfectly understood" connection between responses to artificial and to natural selection (Darwin, 1859 pp 11-14; Lande, 1979). Understanding covariation and correlation

between characters in evolutionary processes is important because it allows the study of selection and evolutionary constraints. One of the main focuses in the study of covariation and correlation between characters in domestication or evolutionary settings has been the additive genetic matrix (or also phenotypic matrix, see below). The characterization of the matrix structure of the additive genetic covariance matrices can shed light on many different evolutionary questions (Phillips and Arnold, 1999), including the direction of evolution (Schluter, 1996), modularity and integration (Penna *et al.*, 2017), and the estimation of past selection gradients (Boag, 1983; Lande and Arnold, 1983; Grant and Grant, 1995; but see Marroig, Melo and Garcia, 2012). However, it is now generally accepted that phenotypic matrices are similar, and because calculating the phenotypic matrix is more straightforward than obtaining the additive genetic matrix, both matrices are generally regarded as interchangeable in evolutionary studies (Cheverud, 1988; Marroig and Cheverud, 2005, 2010; Aguirre *et al.*, 2014; Hubbe, Melo and Marroig, 2016; Penna *et al.*, 2017). In fact, the phenotypic matrix is often used to replace the additive genetic matrix because the latter is usually impossible to obtain for all taxa studied (Marroig and Cheverud, 2005) or because effective sizes of additive genetic matrices are too small in domestication experiments, and so they produce high uncertainty (Aguirre *et al.*, 2014; Penna *et al.*, 2017).

Lande (1979) proposed a multivariate equation (4.1) that calculates the response to selection by relating the additive genetic matrix to the selection gradient:

$$\Delta z = G ß \qquad (4.1)$$

Where Δ*z* is the response to selection, which depends on the additive genetic matrix (**G**) and the selection gradient (ß). The selection gradient ß is given by the inverse of the phenotypic matrix ($\mathbf{P}^{-1}$) and the selection differential (**S**), which is the covariance between the selected trait and relative "fitness" or direction of selection (Lande, 1979; Hansen and Houle, 2008). This equation (4.1) originally only described the additive genetic matrix, and Lande (1979, pp. 404-405) cautioned against the use of phenotypic matrices as the similar patterns between both could only be superficially similar: "When this is not likely to be true [a marked similarity between the genetic, environmental, and phenotypic covariance patterns], or in the absence of genetic information, reasonable caution should be exercised in any attempt to infer past selective forces from observed evolutionary changes and the phenotypic covariation pattern within population".

One of the most important implications of this equation is that because of the covariance between traits, the response to selection of one trait can be different or even contrary to the selection gradient. The importance of the multivariate evolutionary response equation of Lande (1979) is that it represents the missing link between the study of phenotype and the underlying additive genetic matrices. Lande (1979) also demonstrated that the direction of phenotypic change will not be aligned with the direction of the selection gradient (fitness increase or artificial selection), because the direction will be influenced by both the selection gradient and the covariance matrix. One implication of this is that antagonistic selection (selection that acts against the matrix structure) will take more time to produce phenotypic change than selection aligned with the selection gradient (Lande, 1979; Marroig and Cheverud, 2005, 2010).

Approaches (discussed below) like the lines of least evolutionary resistance (Schluter, 1996; Marroig and Cheverud, 2005), multivariate evolution of additive genetic (**G**) matrices (Aguirre *et al.*, 2014; Penna *et al.*, 2017), and random skewers (Cheverud and Marroig, 2007) are descendants of the seminal work of Lande (1979), because they are heavily based and influenced by the multivariate equation of selection response. In parallel, some multivariate statistical methods have been developed to explore the variance and covariance matrices from a purely mathematical perspective. These techniques are heavily influence by principal components analysis (=eigenvalue decomposition; Krzanowski, 1979, 1993, 2000; Flury, 1988; Schott, 1988; Arnold and Phillips, 1999; Phillips and Arnold, 1999; Shifrin, 2004). One of the most elegant and complete tests for matrix similarity is the common principal components analysis (CPCA) designed by Flury (1988) and implemented in the **G** matrix comparison by Arnold and Phillips (1999) and Phillips and Arnold (1999). CPCA hierarchically tests the range of hypotheses spanning from different to equal matrices: nonrelated matrices < partial common principal components < common principal components < proportionality of variance < equality of matrices. However, this approach suffers from problems with statistical modelling caused by the maximum likelihood estimation of matrices (Krzanowski, 1993) and instability due to problems of sample size (Polly, 2005; Goswami and Polly, 2010). To avoid problems of the CPCA (Flury, 1988; Arnold and Phillips, 1999; Phillips and Arnold, 1999) it is possible to perform analyses of angles (Krzanowski, 1979) and subspaces (Krzanowski, 1993), which are particular cases of the CPCA. All methods quoted so far can be implemented to describe either the **G** matrix or phenotypic matrices (**P** matrix) in the context of domestication, answering a series of descriptive and evolutionary questions: (1) are pigeons under different selection regimes

similar in their overall features?; (2) do different selection regimes change the correlation between skull shape variables?; (3) is the response to selection similar in pigeons that were in different selection regimes?; and (4) are domestic pigeons following the same multivariate direction of greatest genetic variation as Columbiformes, or alternatively has domestication explored new axes of variation?

To answer these evolutionary questions, it would be tempting to characterize the different pigeon sample sets (feral *C. livia*, domestic *C. livia*, and comparative columbiforms) in a naïve way by performing an ordination of the samples (PCA, see below). One could then try to assess these different ordinations by looking at the distribution of points in morphospace, by assessing the size and overlap of the morphological hypervolumes of different samples, or by characterizing the angles, scales, and differences between principal components of the different samples. However, as each sample is imbedded in their own subspace, a direct "naïve" comparison between samples is not possible (Krzanowski, 1979). Here I circumvent this problem by projecting samples into a subspace before assessing the overlap of hypervolumes. I also assessed other evolutionary questions:

An evolutionary question that can be answered is how similar in their overall features pigeons under natural selection are in comparison to pigeons under artificial selection. This is the shared subspaces test (Krzanowski, 1979) and is implemented by comparing the principal components of different samples in a shared subspace. This approach finds the closest vector in both samples and allows for identification of the features that are most similar between samples besides the overall similarity of the samples (Krzanowski, 1979, 1993). I tested the significance of the common subspace results against the results of

randomly permuted data between samples as suggested by Krzanowski (1993). The null hypothesis is that covariation matrices of both samples are equal. The alternative hypothesis is that the samples have higher minimum angles or lower similarities than expected by chance.

Another evolutionary question is whether the correlation between variables is similar between samples of pigeons under different selection regimes. This is the permutational test for correlation matrices (Krzanowski, 1993) and is implemented by comparing the principal components of the correlation matrices of different samples. This test identifies common eigenvectors and eigenvalues or common eigenvectors associated with different eigenvalues in the correlation matrices (Krzanowski, 1993). Significance is tested against the results of randomly permuted data (Krzanowski, 1993). The null hypothesis of the permutational test for correlation matrices is the equality of correlation matrices (eigenvectors and eigenvalues). This test has two alternative hypotheses: the equality of eigenvectors but not of eigenvalues between correlation matrices, and the total inequality of correlation matrices (both eigenvectors and eigenvalues).

Different covariance matrix (for example, product of different selection regimes) respond differentially to the same selection gradient. The similarity of response by two covariance matrices can be used as a proxy for the similarity of structure of these matrices. This is the random skewers method (Cheverud and Marroig, 2007) and is implemented by obtaining the response of different covariance matrices to random selection vectors and measuring the co-linearity of the responses of the two matrices (Cheverud and Marroig, 2007). Significance is measured by comparing the observed vector correlations against the

correlations of random vectors. Significance can be further assessed by permuting the data matrices (Krzanowski, 1993). The null hypothesis is no shared covariance structure between matrices. The alternative hypothesis is that both matrices have a more similar structure than expected by random correlation between vectors. This question is assessed because if natural and artificial selection act on the same axes of variation or if the same constraints apply across birds, one would expect the same response to selection, not only between the Columbiformes and feral *Columba livia*, but also in the domesticated pigeons.

Finally, it is pertinent to test the similarity of samples using a lines of least resistance approach. The lines of least evolutionary resistance (LLER) are the multivariate direction of greatest genetic variation in the genetic or phenotypic matrix and appear either by natural selection or drift (Schluter, 1996; Marroig and Cheverud, 2005). This approach allows me to test the overall response to selection within a sample and to establish if the expectation of phenotypic variation maximization along the LLER holds for several groups under different selection regimes (Marroig and Cheverud, 2005). The LLER approach is implemented in several steps (Schluter, 1996; Marroig and Cheverud, 2005, 2010): (1) finding the direction of greatest variation in a sample (LLER); (2) finding the direction of phenotypic evolution of the species in the sample by comparing them with their ancestor; (3) finding the correlation between 1 and 2; and (4) the amount and pace of phenotypic evolution can be compared with the correlation of evolutionary direction to find overall macroevolutionary trends. Significance of these results is assessed against the results of randomly permuted data (Krzanowski, 1993). The LLER approach is here used to test whether the same constraints apply to artificial and natural selection or if domestic pigeons have surpassed the constraints imposed by the lines of least evolutionary resistance of

Columbiformes. For example, the LLER hypothesis indicates three rules that domesticated pigeons may or may not follow (here I test 1 and 3): (1) Recently diverged populations speciate along LLER; (2) the bias towards LLER is lower in clades that diverge a long time ago compared to recently diverged clades; and (3) phenotypic change is slow or small when selection is not aligned with the line of maximum phenotypic or genetic variation (Marroig and Cheverud, 2005). Overall, because the first principal component or $\mathbf{p}_{max}$ is heavily influenced by size (Marroig and Cheverud, 2005, 2010; Mitteroecker, Gunza and Bookstein, 2005), it is regarded in the LLER approach as a proxy for allometry (Marroig and Cheverud, 2005; however see Mitteroecker, Gunza and Bookstein, 2005). For this reason, if LLER predictions are true, it would imply that change in size (allometry and heterochrony) is the line of least evolutionary resistance. However, Mitteroecker et al. (2005), warned against using PC1 to summarize allometry, the implications of the use of PC1 to describe allometry and heterochrony will be discussed in the light of the reported results.

Methods

To explore the effects of domestication, I compared the sample of 94 Columbiformes from Chapter Two and Three with a sample of 108 domestic pigeons (Table S4.1). The total number of individuals studied was therefore 202. This included a large sample of feral individuals of *Columba livia* (*n*=19; presented in Chapter Two, 18 of which were collected in North America), plus modern and historical specimens of fancy pigeons (*n*=50). The sample of fancy pigeons was extended by adding previously published landmark data (Young *et al.*, 2017; *n*=58) for a total of *n*=108 fancy pigeons. The fancy pigeons obtained in this study come from two sources: specimens collected by Charles Darwin (accessioned at NHMUK Tring; *n* = 26) and a personal research collection of modern fancy pigeons collected by the author (CAEC; *n* = 24).

Micro-computed tomography (µCT) of the Darwin collection specimens was done using a Nikon Metrology HMX ST 225 scanner at the NHMUK. Modern fancy pigeons were prepared at the National Autonomous University of Mexico (UNAM) and were scanned in the Cancer Research Institute (INCAN), Mexico using ALBIRA small animal PET/SPECT/CT imaging system (Sánchez, Orero and Soriano, 2013). The CT scan data were imported and segmented in Materialise Mimics 18.0 (Materialise NV, Belgium) and exported as .stl and .ply files. The .stl files were simplified using the "Quadratic Mesh decimation" method in MeshLab 2016 (Cignoni *et al.*, 2008). These models were imported to the IDAV Landmark Editor (v.3.5; http://graphics.idav.ucdavis.edu/research/EvoMorph) to place 3D landmarks.

Landmarks

I used the same landmark system as in previous chapters to allow comparisons of the fancy pigeon sample with the specimens from previous chapters. The landmark system used in this study consists of 27 three-dimensional coordinates, the first 24 of which are type one landmarks, while the other three are type two landmarks (Landmarks 25-27). These type two landmarks (Bookstein, 1991; MacLeod, 2013a) were calculated by placing a series of semilandmarks describing a curve and then calculating the midpoint of this curve using the R (R Core Team, 2015) package Geomorph (Adams and Otárola-Castillo, 2013). Missing landmarks were present in seven of the Darwin pigeons: three in Barb (BMNH 1868.2.19.10), two in Runt (BMNH 1868.2.19.3) and one in Turbit (BMNH 1868.2.19.19), English frill back (BMNH 1868.2.19.20), Spot (BMNH 1868.2.19.13), Swallow (BMNH 1868.2.19.6), and TurbitXTrumpeteer (BMNH 1868.2.19.12). Missing landmarks were also present in two modern pigeons: Lechuza (CAEC 2015.9.15), and Marchenera (CAEC 2015.9.12). As was done in previous chapters, I reflected bilateral landmarks across the midline to reduce the number of missing landmarks. After reflection only four pigeons had missing landmarks. The pigeons with missing landmarks (Table S4.1) were two of the Darwin pigeons (Barb [BMNH 1868.2.19.10] and Turbit [BMNH 1868.2.19.19]) and two modern fancy pigeons (Lechuza [CAEC 2015.9.15] and Marchenera [CAEC 2015.9.12]). These four missing landmarks were estimated using the `estimate.missing` function from the package Geomorph (Adams and Otárola-Castillo, 2013).

Geometric morphometrics

Shape analysis.

Geometric morphometric analyses were performed in R (R Core Team, 2015) using the package Geomorph (Adams and Otárola-Castillo, 2013). A generalized Procrustes analysis was performed to remove the effects of position, size and rotation from the landmark constellations for each specimen prior to analysis (Gower, 1975; Rohlf and Slice, 1990).

Principal components analysis

Principal components analysis (PCA) is a multivariate statistical method that summarizes the variation in a square, symmetric matrix into orthogonal principal components (PC; Flury, 1988; Krzanowski, 2000). Simply put, the PCA maximizes the information summarized by each PC, so it is expected that each subsequent PC axis will summarize less variation than the previous one. Each one of the axes is orthogonal, which means that each of the axes is mathematically independent (although not biologically independent; see below). Each principal component is an eigenvector (the direction of the linear transformation of the original data) and each eigenvector is associated with an eigenvalue (the scale of the eigenvector). Because of the way the PCA is calculated, PCA is often used to reduce the dimensionality of a dataset, permitting the researcher to visualize the structure of multivariate data by plotting just a few first principal components (Flury, 1988; Krzanowski, 2000).

PCA was used to summarize the variation in the domestic and feral *C. livia* samples because each of the individuals can be considered as an independent data point. However, PCA is not suitable for analysing the comparative sample of Columbiformes because of the shared

history (phylogeny) of the species in the sample (Felsenstein, 1985; Revell, 2009). Whenever possible, phylogenetic principal components analysis (pPCA), which is a statistical procedure that takes into account the phylogeny while calculating the principal components of the sample (Revell, 2009), was used instead.

The phylogeny is taken into account in the pPCA by calculating the matrix **C** of the expected covariances of the data given a phylogenetic tree and a Brownian motion model (Revell, 2009, 2012). By taking the error structure into account (Grafen, 1989), the scores of each of the calculated PC axes will have a phylogenetic correlation of zero, thus being evolutionarily independent (Revell, 2009). Ordinary PCA was used in the naïve comparison of principal components (see below), and the Krzanowski and random skewers tests. However, pPCA was used to assess the overlap of hypervolumes, morphospace occupation, shape changes of each sample and the correlation between phenotypic evolution and the lines of least evolutionary resistance.

Naïve comparison of principal axis of variation (descriptive tests)

The dimensionality of an object can be exemplified by the 3D nature of our world where it is possible, for example, to characterize the position of an object based on x, y and z coordinates. However, it is mathematically convenient and possible to consider a space with more dimensions. One example would be the personal data in a machine learning environment: each person could be characterized by a myriad of information (*e.g.*, height, name, age, nationality, and favourite books). Shape is a multidimensional attribute of objects (i.e., defined by many landmarks). However these data are also highly dimensional not only because each landmark contains three dimensions, but because the number of

variables evaluated (x, y, and z coordinates for each landmark) can be larger than the number of data points (specimens) available (Adams and Felice, 2014; Collyer, Sekora and Adams, 2015; Denton and Adams, 2015; Adams and Collyer, 2018).

I compared the eigenvectors of three subsets: Columbiformes-nP (comparative sample of Columbiformes excluding *Pezophaps solitaria* and *Raphus cucullatus*), feral *Columba livia* and domestic fancy *Columba livia*. **All the following "naïve" comparisons are descriptive, they are not statistical hypothesis tests**. To characterize the phenotypic matrices of different pigeon subsets I used several approaches that help to answer different biological questions:

Overlap of n-dimensional hypervolumes (Ordinary and Phylogenetic PCA)

The size and overlap of *n*-dimensional hypervolumes is common practice in ecology (Blonder *et al.*, 2014; Swanson *et al.*, 2015; Junker *et al.*, 2016). The *n*-dimensional hypervolume was proposed as a way to characterize the niche of different species (Hutchinson, 1957), and the *n*-dimensions have been defined by ecological, environmental or trait variables (Blonder *et al.*, 2014; Swanson *et al.*, 2015; Junker *et al.*, 2016). Here, I quantify the overlap of *n*-dimensional hypervolumes of different samples by using the standard deviation in each PC axis (see below). Although this is not a probabilistic framework (Junker *et al.*, 2016), I argue that this comparison is correct in the standardized Euclidian space produced by a PCA of Procrustes aligned landmarks (Kendall, 1984).

To describe how the morphospace of the domestic fancy pigeons has diverged from the feral pigeons, and from the comparative sample of columbiform species and genera, I calculated the multidimensional centroid coordinates per group and evaluated the overlap

of hypervolumes at different standard deviation values. I calculated hypervolume overlap using two approaches: (1) using the results of the ordinary PCA of the complete sample; and (2) using the phylogenetic PCA of the comparative sample with other samples projected into the pPCA space (Table 4.1). To calculate the centroid coordinates, I obtained the mean value of each of the first 60 principal components per group using the principal component scores. The calculated centroid coordinates are equivalent to the principal component scores that would be obtained by the mean shape of each group projected to the Euclidean principal component space.

I calculated the standard deviation of the PC scores per group and used it to obtain the 68% and 95% confidence intervals (i.e. one and two standard deviations) around the centroid coordinates of each group in each dimension (hypervolumes). I calculated the overlap between these intervals for each dimension. If two groups do not overlap at all, the value for that dimension is zero. However, if both groups overlap completely or if one group is imbedded in the other the value for that dimension will be 1.0. Any partial overlap is calculated as the percentage of the total span of the two groups represented by the overlap of the groups. The calculated overlap can take values from 0 (null overlap between two groups across all dimensions) to **n** (total overlap between two groups; were **n** is the number of dimensions). Finally, to obtain a metric that takes into account the contribution of each principal component, I standardized the overlap by multiplying each dimension overlap by the variance explained by each principal component. The final overlap metric for all dimensions is the sum of standardized overlap and takes a maximum value of one and a minimum of zero (Table 4.1).

Angle comparison (ordinary PCA)

A PCA was performed on the phenotypic matrix of each group. From the eigenvector matrices, the first 20 eigenvectors of each sample were compared between samples. I chose to analyse only a subset of the eigenvectors for two reasons. First, Krzanowski (1993) demonstrated that analysis of a large number of eigenvectors (>*n*/2) is bound to find convergent eigenvectors. Second, most variance is contained in the first eigenvectors of all subsamples: 67% in the first four principal components, 84% in the first seven eigenvectors (Table 4.2, Figure 4.2C), and 96% in the first 20 eigenvectors.

Comparison of the angles of principal components and their eigenvectors is not trivial because each is described by a vector of length 81 (27 landmarks * three dimensions). Because of this high dimensionality, the angles obtained when comparing vectors are not geometrically obvious, unlike dimension two and three where an angle can be interpreted in a straightforward way. The correlation between vectors is the cosine of the angle between vectors. The cosine between two vectors can be calculated as the inner product of those vectors:

$$Correlation = \ cos\ \alpha = \frac{\mathrm{PCn}\ .\ \mathrm{dot}.\ \mathrm{PCn}'}{|\mathrm{PCn}|\ *\ |\mathrm{PCn}'|}$$

(4. 2)

Where PCn is the n^{th} eigenvector of one subset and PCn' is the any eigenvector of the other subset. This angle can be calculated for each combination of eigenvectors (Table S4.2) by repeating the comparison between two blocks containing the number of desired eigenvectors. Because the correlation of vectors is a cosine function, it takes values of such a function and indicates if two vectors are orthogonal (*cos* α = 0) or parallel (*cos* α = 1). The

cosine of α can also yield negative values, with α=-1 indicating a vector with a parallel orientation but exactly opposite direction. It is important to note that all eigenvectors are normalized, so it is possible to directly obtain the correlation and angles between these unit vectors.

Scaling of vectors (ordinary PCA)

Two geometrically obvious mathematical operations that can be performed in a high dimensional space are the division and subtraction of vectors (Shifrin, 2004). Assume a vector ***y*** that is the product of the multiplication of another vector ***x*** and the constant *c*.

$$\boldsymbol{y} = \boldsymbol{x}c \tag{4. 3}$$

When two vectors are in fact running in the same direction but differ only in their scale, it is possible to identify this property by dividing vector ***x*** by vector ***y***. If the result of this division is a new vector containing the repeated constant *c* then it can be stated that two vectors only differ in size. The eigenvector values range between -0.4555813 and 0.4900672. The eigenvectors calculated in R (R Core Team, 2015) use seven decimal places, I decided to round this number to three decimal places before counting the number of repeated elements (Table S4.3) to account for negligible differences between eigenvectors.

Difference between vectors (ordinary PCA)

The subtraction of two vectors gives the distance between each vector in each of the dimensions. In the case of geometric morphometrics, this permits identification of the landmarks and dimensions (x, y, z) in which the two eigenvectors differ the most (Figure S4.2). To obtain this difference, I subtracted the absolute values of the n^{th} eigenvector from

group one from the absolute values of the closest eigenvector in group two. I made the vector subtraction in a pairwise manner between the three samples but chose to only represent the first four eigenvectors (Figure S4.2). The subtraction resulted in an 81-dimensional vector, which I transformed into a 27 * 3 matrix representative of the differences in each dimension of my landmark system. Finally, I obtained the overall difference between landmarks by adding the absolute values for each landmark in all three dimensions (Figure S4.2).

Statistical tests for matrix similarities

Phenotypic matrices contain large amounts of information about past selection, constraints, modularity, integration and response to selection (Lande, 1979; Cheverud and Marroig, 2007; Klingenberg, 2008; Penna *et al.*, 2017). One way of summarizing the information in the phenotypic matrix is to perform a PCA on the matrix covariation or correlation (Krzanowski, 1979, 1993; Penna *et al.*, 2017). When many samples are examined, a natural approach would be to perform a PCA on each sample (Krzanowski, 1979). However, the PCA results of different samples are no longer comparable because each one is embedded in its own subspace (Krzanowski, 1979, 1993, 2000).

Comparing the shape changes associated with principal components of different PCA ordinations can be problematic because of the subspace problem (Krzanowski, 1979, 1993, 2000). Examining the shape changes may suggest a shared structure between samples; however, even shared principal components might be obscured if they are associated with different eigenvalues in different samples (Krzanowski, 1993). It is possible to project all samples into a common subspace. This would allow me to measure overlaps between

hypervolumes (see below) but would prevent me from answering further evolutionary questions about the covariation in each sample. For these reasons, the matrix comparison should be made in a statistical framework for which several analyses have been proposed and are here implemented. **Furthermore, all these tests are evaluated via permutation against the null hypotheses of shares matrix structure.** These analyses are described in turn below.

Krzanowski between groups comparison of principal components (ordinary PCA)

Krzanowski (1979) established a test to compare the principal components of different groups in which the same variables had been measured. Because of the rotation of the PC axes, each group's PC axis will be orientated towards the axis of most variation in the sample. This makes it impossible to visually compare the principal components of several groups because they might seem different but actually form part of the same multivariate subspace. The Krzanowski test allows for the identification of common subspaces. This test examines the congruence between the multidimensional lines described by each eigenvector and allows common linear combinations between samples to be found. These common linear combinations carry biological meaning.

If it is assumed that the same *p* variables have been recorded for groups **A** and **B**, then the original variables in both groups are $x_1, x_2, \ldots, x_p$. When PCA is used in matrices for the groups **A** and **B**, the principal components of these matrices are obtained: $y_{A1}, y_{A2}, \ldots, y_{Ap}$ *and* $y_{B1}, y_{B2}, \ldots, y_{Bp.}$ Each of these principal components has an associated loading $l_{A1}, l_{A2}, \ldots, l_{Ap}$ and $l_{B1}, l_{B2}, \ldots, l_{Bp}$ which have been normalized such as:

$$\sum_{j=1}^{p} l_{Aij}^2 = \sum_{j=1}^{p} l_{Bij}^2 = 1$$

(4. 4)

In a PCA, the original variables $x_1, x_2, \ldots, x_p$ are rotated to capture the most variation in each principal component. Since principal components are orthogonal, each component is not mathematically correlated with previous ones (although they might be biologically correlated; Mitteroecker *et al.*, 2004; Goswami and Polly, 2010; Adams and Collyer, 2017) and the spread of points along subsequent principal components diminishes because each accounts for less variance than the previous ones. The cosine direction of the i^{th} principal component to the axis x_i of the matrix A is given by l_{Aij}, while the cosine direction to axis x_i of the matrix B is given by l_{Bij}.

The Krzanowski test is designed to test a subset of the principal components of each matrix for common linear combinations. The number of *k* principal components in each subset is defined arbitrarily. These *k* components are considered sufficient to explain the variation of the sample. Taking the *k* component of interest, it is possible to obtain the two new matrices **L** and **M** composed of the *k* axes: $y_{A1}, y_{A2}, \ldots, y_{Ak}$ *and* $y_{B1}, y_{B2}, \ldots, y_{Bk}$.

To analyse the new matrices **L** and **M**, it is necessary to first establish the minimum angle between an arbitrary vector **L** and the closest (most parallel) vector in **M**. This is given by:

$$cos^{-1}(\lambda^{0.5})$$

(4. 5)

Where λ_1 is given by the largest eigenvalue produced of **S**:

$$S = LM'L'M$$

(4. 6)

In order to partition the differences between subspaces **A** and **B**, Krzanowski proposed using a_i, which is the eigenvector associated with the eigenvalue λ_i. This eigenvector a_i can be projected into the subspace **A** by:

$$b_{Ai} = L'a_i \ (i = 1, \dots, k)$$

(4. 7)

While it is also possible to find the projection of a_i into the subspace **B** by:

$$b_{Bi} = M'Mb_{Ai}$$

(4. 8)

The angle between the i^{th} pair of vectors b_{Ai} and b_{Bi} can be calculated using equation (4.5). Since Krzanowski proved that the smallest angle between two vectors in **A** and **B** subspaces is given by the largest eigenvalue of **S**, the second highest eigenvalue of **S** would give the second smallest angle between orthogonal vectors of subspaces **A** and **B,** and so forth. This eliminates the necessity to look for different combinations of eigenvectors (Table 4.3).

Since λ_{ij} is the angle between the i^{th} eigenvector of **A** and the j^{th}, the sum of the eigenvalues of **S** (trace of **S**) can be treated as a measurement of overall similarity between subspaces:

$$\sum_{i=1}^{k} \lambda_i = trace\ S = \sum_{i=1}^{k}\sum_{j=1}^{k} cos^2\ \theta_{ij}$$

(4. 9)

The trace of **S** can take values between zero (orthogonal) and *k* (coincident) (Table S4.3). If **A** and **B** share the same subspace in r of the original dimensions, then the first r eigenvalues will present values of one. Finally, the comparison of subspaces **A** and **B** defined by a

different number of principal components $k_A \neq k_B$ is possible by just ignoring any zero eigenvalues.

Since the vectors b_{Ai} and b_{Bi} are in the original *p*-dimensional space, it is possible to find the *k* bisectors between these vectors. These bisectors will be the vectors which are intermediate or closest to both vectors in the original *p*-dimensional space. They can be obtained by:

$$c_i = \{\frac{1}{1 + 3\lambda_i^{0.5}}\}(I + M'M)b_i$$

(4. 10)

Where **I** is a square matrix with *p* dimensions with all non-diagonal elements set to zero. The set of *k* bisectors (c_1, …, c_k) defines the *k*-dimensional subspace closer to **A** and **B** in the original *p* dimensions. As with geometric morphometric regression coefficients and principal component loadings, it is almost impossible to make biological inferences by examining the loadings obtained by all analysed dimensions alone. In the case of my sample, the bisector has a length of 81 (27 landmarks x 3 dimensions), which needs to be summarized in some way to allow an easier visual inspection. I decided to add the absolute values of the three dimensions for each landmark (Figure 4.5) in a similar fashion to the previously discussed difference between vectors (Figure S4.2). Absolute values were used because the bisector lies in the original variable space and the sign of each value in the vector has a real geometrical meaning. Because of the bi-lateral nature of some landmarks, dimension values with different signs might be pointing towards the same geometric transformations (*i.e.*, x-dimension of landmarks in skulls getting more robust laterally

would obtain different signs simply because one side of the skull expands to the right and the other to the left).

To compare the principal components of domestic fancy pigeons against feral *Columba livia* and the comparative columbiform sample, I used a modified version of the `krzanowski.test` function from the package MCMCglmm (Hadfield, 2010). The function was modified to accommodate the results of the PCA performed in Geomorph (Adams and Otárola-Castillo, 2013). I implemented a permutation test with replacement to assess the significance (*P* value; Krzanowski, 1993) of both the angles obtained and the trace of **S** (Figure 4.4). The significance (*P*) value was calculated using a biased estimator (Phipson and Smyth, 2010):

$$P = \frac{b + 1}{m + 1}$$

(4. 11)

Where *b* is the number of permutations with values more or equally extreme to the real data observation and *m* is the total number of permutations. This biased estimation of *P* takes into account that an *n* number of permutations might not be able to recreate all the possible combinations, thus the one added to the numerator and denominator of equation (4.10) lowers the type I error (Phipson and Smyth, 2010). The function `permp` R package statmod (Phipson and Smyth, 2010) provides a development of equation (4.10) that takes into account the replacement nature of the permutation by integrating along the sample size. I also used this `permp` function to calculate the *P* values, however values obtained were practically identical to the ones produced by equation 4.10 (Table 4.3).

I decided to use another approach produced by Krzanowski (1979). This approach is an extension of the previous method but allows for the comparison of multiple subspaces simultaneously by finding the common subspace between all of them. This approach analyses the covariance matrices and is useful because it can highlight common features between all subspaces that could otherwise be overlooked in pairwise comparisons. This approach only requires that the same *p* variables are measured for the *g* groups. Let $L_{(t)}$ be the matrix whose elements are the loadings for the first *n* principal components of the t^{th} group (*t*=1, 2, … *g*). As before it is necessary to find the vector (*b*) that minimize the angle between *b* and the closest vector in the subspace produced by the k principal components of subspace *t*. To find this vector *b*, it is necessary to find the largest eigenvalue of **H** in a similar way to equation (4.6):

$$H = \sum_{t=1}^{g} L_t{}' L_t$$

(4. 12)

It is possible to further analyse the eigenvalues and eigenvectors of **H** to obtain biological meaning, and also the angles between different samples and the common subspace **H** can be obtained. I obtained **H** and the angles between the three pigeon samples using the function `KrzSubspace` of the evolqg R package (Melo *et al.*, 2016). I further performed permutation tests to assess the significance of the minimum angles and eigenvectors (Table 4.3). This method was performed by Aguirre *et al.* (2014) in a Bayesian framework. However, as I did not estimate the phenotypic matrix using a Markov chain Monte Carlo (MCMC) method, I decided that permutation was more suitable to determine the significance of the obtained angles and eigenvalues (see below) of my samples.

Test for correlation of matrices (ordinary PCA; Krzanowski, 1993)

Even if covariance matrices are not equal between populations, they may share the same set of eigenvectors attached to different eigenvalues or in a different order. Krzanowski (1993) proposed to test the equality of eigenvectors and matrices by approximating the correlation matrices using covariance matrices of standardized data (means of 0 and variances of 1; Krzanowski (1993). Pairwise comparisons are made in order to test hypothesis about two populations π_i (i = 1, 2) with correlation matrices Υ_i which can be described by their eigenvalues Δ_i and eigenvector matrix $\mathbf{\Gamma}_i$. I followed Krzanowski (1993) approach to hypothesis formulation:

$$\mathbf{H}_c: \ \mathbf{\Upsilon}_i = \mathbf{\Gamma}\, \Delta_i\, \mathbf{\Gamma}'$$

$$\mathbf{H}_a: \mathbf{\Upsilon}_i \text{ arbitrary}$$

$$\mathbf{H}_0: \mathbf{\Upsilon}_i = \mathbf{\Gamma}\, \Delta\, \mathbf{\Gamma}'$$

Where $\mathbf{H}_0$ is a special case of $\mathbf{H}_c$, were the eigenvectors are the same between populations and the eigenvalues are also identical $\Delta_1 = \Delta_2 = \Delta$. Since the information about the whole populations $\pi_{domestic}$, π_{feral} and $\pi_{comparative}$ is unknown, the parameters were estimated using the analysed samples.

I standardized the three sample matrices of Procrustes aligned landmarks ($\mathbf{X}_{domestic}$, $\mathbf{X}_{feral}$ and $\mathbf{X}_{comparative}$) to obtain variable means of 0 and variances of 1. These standardized matrices ($\mathbf{Y}_1$, $\mathbf{Y}_2$ and $\mathbf{Y}_3$) were obtained by subtracting the column mean from each value and dividing by the standard deviation. Then the covariance matrices $\mathbf{R}_1$, $\mathbf{R}_2$ and $\mathbf{R}_3$ were obtained from the **Y** matrices. These **R** matrices are estimates of the populations $\mathbf{\Upsilon}$ matrices. For each pairwise comparison it is possible to perform a PCA of $\mathbf{R}_i$ to obtain the eigenvector

matrices **A** and **B**. As before, from these **A** and **B** matrices, it is possible to obtain matrices **L** and **M** composed of the *k* columns: y_{A1}, y_{A2}, …, y_{Ak} *and* y_{B1}, y_{B2}, …, y_{Bk}. Where *k* is an (arbitrary) number of principal components or eigenvectors. In this approach, *k* can also be determined by the number of principal components that are considered sufficient to explain the data, however, this number should not exceed $k = (p/2)-1$. Using half of the variables *p* will ensure no distortion is created by coincident eigenvectors (Krzanowski, 1993). If $\mathbf{H}_c$ is true, then both **L** and **M** are estimates of the same **Γ** and the critical angles between the two samples will be low for any *k* (1, …, *p*/2). The minimum angles between subspaces are the inverse cosines of the squared eigenvectors of **S** (equation 4.6, Krzanowski: 1979, 1993).

The hypotheses were tested via permutation. To perform permutations, the standardized matrices $\mathbf{Y}_1$ and $\mathbf{Y}_2$ were united:

$$Y = \left(\frac{Y_1}{Y_2}\right)$$

(4. 13)

From the new matrix **Y**, random rows were taken to obtain two matrices with the same row number as the original $\mathbf{Y}_i$ matrices $\mathbf{Y}_1^{(p)}$ $\mathbf{Y}_2^{(p)}$. I obtained the covariance matrices $\mathbf{R}^{(p)}$ of the $\mathbf{Y}^{(p)}$ matrices and performed a PCA to obtain the same *k* principal component of interest in the matrices $\mathbf{L}^{(p)}$ and $\mathbf{M}^{(p)}$. This permutation was repeated 1000 times for each pairwise comparison to assess significance.

Permutations were used in order to test $\mathbf{H}_c$ against $\mathbf{H}_a$. If $\mathbf{H}_c$ is true, then **L** and **M** both come from the same **Γ** and the angles obtained by $\mathbf{L}^{(p)}$ and $\mathbf{M}^{(p)}$ will be compatible. However, if $\mathbf{H}_a$ is true then $\mathbf{L}^{(p)}$ and $\mathbf{M}^{(p)}$ will be more similar than **L** and **M** and the angles obtained by

permuted data will be smaller than the ones produced by the real data. The trace of **S** (equation 4.9) can be used as a single summary value of the angles between two samples and as the value used to obtain a *P* value through permutations (Krzanowski, 1993; Phipson and Smyth, 2010). If $\mathbf{H}_c$ is true, then it is possible to test $\mathbf{H}_0$ by obtaining μ:

$$\mu = trace[abs(\Delta_1 - \Delta_2)]$$

(4. 14)

μ is a single measurement of the differences between the eigenvalues between the two samples. It is possible to then compare μ with $\mu^{(p)}$ obtained from the permuted data (Krzanowski, 1993) in order to obtain a *P* value (Phipson and Smyth, 2010).

Random skewers (ordinary PCA)

Random skewers (Cheverud and Marroig, 2007) was used to understand the predicted evolutionary response of variance/covariance matrices. This method can be used with additive genetic matrices or with phenotypic matrices because they are similar (Roff, 1995; Marroig and Cheverud, 2005, 2010; Cheverud and Marroig, 2007). This method, as well as the Krzanowski (1979, 1993) methods, are specific implementations of the common principal components approach of Flury (1988), which aims to surpass problems of sample size and multivariate modelling. The common principal components approach offers a complete the hierarchical test of hypotheses (Flury, 1988; Arnold and Phillips, 1999; Phillips and Arnold, 1999). Despite being unable to apply the common principal components, most of the different hypotheses can be tested using other methods: equality of eigenvectors, eigenvalues and common subspaces (Krzanowski, 1979, 1993) and matrix equality is also tested using Random skewers (Figure 4.1; Cheverud and Marroig, 2007).

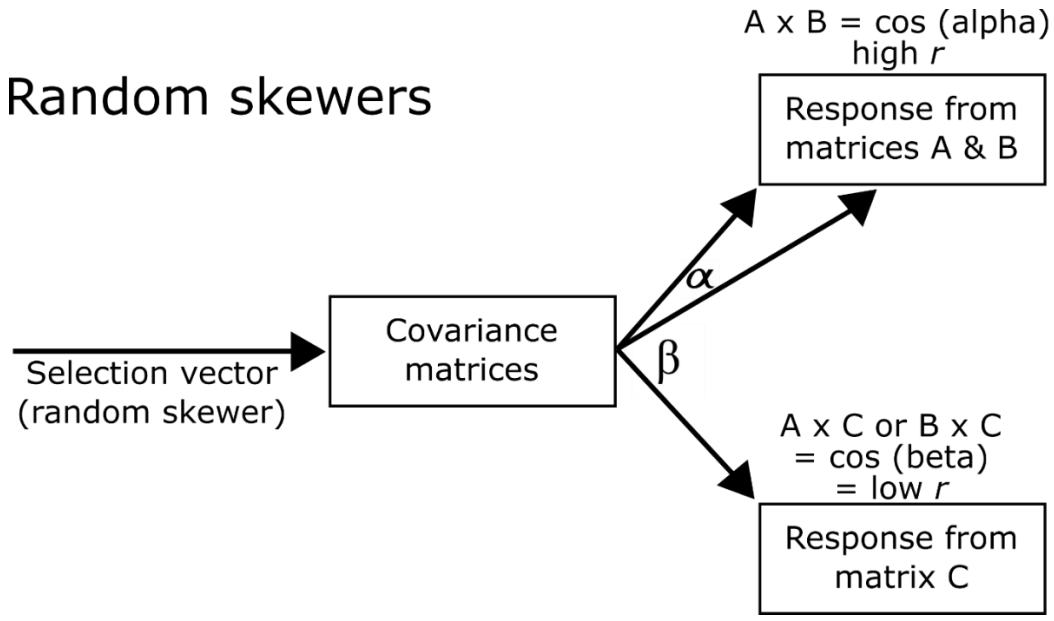


Figure 4.1. Random skewer method for comparison of phenotypic or additive genetic covariance matrices: modified from Cheverud and Marroig (2007). Random selection vectors are repeatedly applied to the covariance matrices and the average correlation between response vectors (cosine of the angle between response vectors) is used as a metric of similarity of evolutionary response. In this figure it is possible to observe that covariance matrices A and B respond similarly to selection vectors while matrix C response to selection is almost orthogonal to both A and B.

The random skewers approach uses a series of random vectors to test the correlation of response of covariance matrices. The matrix response to these random skewers can be interpreted as the similarity of the response (in different matrices) to similar selection pressures. The evolutionary change can be measured in a vector of trait means (Δ*z*), which can be obtained using the following evolutionary response equation (Lande, 1979):

$$\Delta z = \boldsymbol{P}ß$$

(4. 15)

Where **P** is either the phenotypic or additive genetic covariance matrix and ß is the gradient selection vector. ß can be calculated also from the **P** matrix:

$$ß = \boldsymbol{P}^{-1}S$$

(4. 16)

Where S is the selection differential. I used 10,000 random vectors (skewers) applied to each matrix. Each element of the skewers was drawn from a uniform distribution of values between zero and one. These values are assigned a positive or negative sign with 50% probability. Finally, each vector is standardized to a length of one.

Each response vector Δ*z* is recorded. The correlation is measured from these Δ*z* vectors as the co-linearity between responses, measured as the cosine of the angle between vectors with equation (4.2) and 4.17:

$$cos\frac{\Delta z_1 \,.dot.\, \Delta z_2}{\|\Delta z_1\| * \|\Delta z_2\|}$$

(4. 17)

The average value of the correlation of the 10,000 responses is taken as the final similarity metric. Co-linearity can take values from minus one (completely opposite), passing through zero (perpendicular) to one (alignment). Significance is tested in two ways: first, random vector association is tested by comparing the obtained similarities between real matrices with similarities obtained between random vectors (probability; Table 4.6). Second, I also evaluated the probability of these responses by repeating the analysis 1,000 times on randomly row-permuted matrices. The permutation approach tests against the hypothesis of both matrices coming from the same population (P_{perm}: Table 4.6). The latter approach is not commonly used because of the difficulty to account for the data structure (which controls for variation associated with sex and taxonomy). However, my random skewers approach did not account for these factors and did not present these complications. I decided to test both significance tests (random vector association and permutation; Table

4.5). To perform the random skewers analysis, I used the `RandomSkewers` function of the evolqg R package.

Lines of least evolutionary resistance (phylogenetic PCA)

Finally, I propose a modification to the lines of least evolutionary resistance approach (LLER; Lande, 1979; Schluter, 1996; Marroig and Cheverud, 2005, 2010; Hansen and Houle, 2008) to assess the relation between artificial and natural selection. The premise of LLER can be conceptualized as the maximum direction of variation in a covariance matrix, represented as the principal component one of that matrix $\mathbf{p}_{max}$. This $\mathbf{p}_{max}$ is then compared with the phenotypic direction of change (Δz) to obtain a measurement of similarity that can also be compared with the amount of morphological diversification to test hypotheses about the nature of evolution in a group. I base my analysis on the one proposed by Marroig and Cheverud (2005, 2010), however, I have adapted parts of the method to deal with multiple samples that span different subspaces and to include information about the phylogenetic uncertainty across the random sample of 500 phylogenies. Marroig and Cheverud (2005, 2010) analysed LLER in a phylogenetic framework using least squares averages of a GLM model on independent contrasts of pooled within-group covariance matrices (Marroig and Cheverud, 2005). I decided to use a phylogenetic PCA (pPCA) to analyse the comparative sample (excluding *Raphus* and *Pezophaps*) and then project the feral and domestic fancy samples into this pPCA space, effectively translating all samples and variation into the same subspace spanned by the comparative Columbiformes. To test if domestic fancy and feral *C. livia* follow the same LLER as other Columbiformes, I compared the correlation between multivariate direction of greatest phenotypic variation

of the comparative sample ($\mathbf{p}_{max}$) against the phenotypic change direction (Δz) in the three samples using equations (4.2 and 4.17).

The $\mathbf{p}_{max}$ has traditionally been obtained from the results of a single PCA. However, as different samples are being analysed, it is not possible to directly compare the PC1 of the comparative sample with the Δz obtained from PC score values obtained from the PCA of domestic fancy, and feral pigeon samples. There are several problems when comparing the first principal component ($\mathbf{p}_{max}$) from different PC analyses (see Krzanowski subspaces above). A further problem comes from each PCA allocating signs arbitrarily to the first element of the eigenvector. The value of each element in an eigenvector is the amount of correlation between different variables. The sign, although arbitrarily selected, possesses a meaning inside the eigenvector because it signals variables that are positively or negatively correlated. However, this sign can change between different runs of the PCA. If the mean values of the first eigenvector of different phylogenetic PCA analyses was used as a summary statistic for the phylogenetic uncertainty of different topologies, the mean values would be closer to zero than the real values only because of the random flipping of signs. Furthermore, applying a single phylogenetic principal components analysis would be difficult to implement for all the samples due to the lack of phylogenetic information and putative minimal branch lengths of the feral and domestic fancy pigeons (Johnston, 1990, 1992).

Obtaining Δz followed a series of steps. From these PC scores, I calculated the ancestral characters (principal component scores) for all nodes in the phylogeny in a maximum likelihood setting using the `fastAnc` function of the phytools R package (Felsenstein,

1985; Revell, 2012). A similar maximum likelihood estimation of ancestral characters (Schluter *et al.*, 1997) was used by Marroig and Cheverud (2005) which did not take in account the covariation between characters. I acknowledge that ignoring this covariation between two characters can skew the results by ignoring common selective pressures or covariation constraints (Pagel, Meade and Barker, 2004). Marroig and Cheverud (2005) obtained Δ*z* for every branch in their phylogeny as the difference between each species population average and their reconstructed ancestor. As I do not count with covariance matrices for any species in the sample, except *Columba livia*, I decided to take each species as representative of the average phenotypic variation on the species population. Furthermore, Marroig and Cheverud (2005, 2010) transformed their landmark coordinates to linear measurements. However, I decided to base the comparisons entirely in PC scores in order to remain in a geometric morphometric framework comparing landmarks.

For the comparative sample, Δ*z* was obtained by subtracting the vector of PC scores of each descendant from the ancestor's vector of PC scores. For the feral sample, Δ*z* was obtained by subtracting the PC scores vector of each feral pigeon from the ancestor of *C. livia* and *C. rupestris*. Finally, for the domestic fancy sample, Δ*z* was obtained by subtracting each domestic fancy pigeon vector PC scores from the vector of PC scores of the same ancestor of *C. livia* and *C. rupestris*. This ancestor was used because in a molecular phylogeny any domestic fancy pigeon would take the place of *C. livia*. Also, I refrained from simply using the average values of the feral pigeons as the domestic ancestor because this greatly minimized the amount of morphological diversification. I considered $\mathbf{p}_{max}$ as the first principal component (eigenvector) of the phylogenetic PCA (pPCA; Revell, 2009) of the comparative sample. To perform the pPCA I modified the `phyl.pca` function of the

phytools R package (Revell, 2012) and the `plotTangentSpace` function of Geomorph (Adams and Otárola-Castillo, 2013). I obtained the correlation between $\mathbf{p}_{max}$ and each Δz ($LLER_{corr}$) using equation (4.17). The average value of $LLER_{corr}$ for each sample provided a single metric for the overall correlation. I also decided to test the amount of morphological differentiation (m_{amount}; Marroig and Cheverud, 2005) for each of the Δz:

$$m_{amount} = \sum(\Delta z_1^2, \ldots, \Delta z_j^2)$$

(4. 18)

Where j is the number of dimensions in the samples (81). The m_{amount} was tested against $LLER_{corr}$ using the Pearson product moment correlation (Schluter, 1996; Marroig and Cheverud, 2005). If the morphological change is linked to the $\mathbf{p}_{max}$ then a positive Pearson correlation is expected between the LLER*corr* and the m_{amount}. The average Δz and m_{amount} were also recorded for each sample. The m_{amount} is a relatively similar measurement to the "respondability to selection" of Hansen and Houle (2008; Marroig and Cheverud, 2010). Another metric proposed by Marriog and Cheverud (2005) was the pace of morphological differentiation (m_{pace}). However, I decided not to use this metric because it requires branch lengths and this measurement would be strongly influenced by the short (and unknown) branch lengths associated with domestic fancy breeds. I obtained m_{amount}, $LLER_{corr}$ and the Pearson correlation for each of the samples in a phylogenetic context, then the analysis was repeated across 500 phylogenies to take into account the phylogenetic uncertainty of the result (Figure 4.6, Table 4.7). To test for spurious correlations between Δz and $\mathbf{p}_{max}$, in each phylogeny I also compared Δz with a vector obtained using a broken stick method

from a uniform distribution (Table 4.7A, Figure 4.6D; Schluter, 1996; Marroig and Cheverud, 2005, 2010).

Some of the methods implemented in this chapter, such as LLER and random skewers, test the results against random associations between vectors by comparing their results against the correlation obtained using random vectors (Cheverud and Marroig, 2007). In the same way LLER tests against the isometric hypothesis by comparing the obtained results against those obtained by an isometric vector (a vector in which all elements have the same value). To evaluate the validity of these approaches, I simulated 10,000 random vectors and measured their correlation with (1) other random vectors and (2) an isometric vector (Figure S4.3). I found that the average correlation diminishes as the vector length increases, until the correlation stabilized asymptotically (Figure S4.3). The average correlation behaves in the same way for correlations between random or isometric vectors (P= 0.938).

Results

Morphospace

Table 4.2. Variation explained by each PCA. PCA and phylogenetic PCA results

Phylogenetic PCA							
Sample	PC1	PC2	PC3	PC4	PC5	PC6	PC7
Comparative	0.29	0.19	0.12	0.07	0.05	0.04	0.04
Ordinary PCA							
Sample	PC1	PC2	PC3	PC4	PC5	PC6	PC7
All samples	0.46	0.16	0.08	0.07	0.04	0.02	0.02
Feral	0.31	0.19	0.13	0.06	0.06	0.05	0.03
Domestic	0.59	0.15	0.07	0.04	0.02	0.01	0.01

All samples were projected into the phylogenetic principal components analysis of the comparative columbiform sample (PCA: Figure 4.2, Table 4.2). Figure 4.2 shows that the morphospace of the comparative sample of Columbiformes and those of domestic fancy pigeons overlap, nevertheless it also shows that there are distinct regions that have each only been explored by one of these groups. Feral *C. livia* are constrained to a small region of the intersection between domestic fancy pigeons and the comparative sample. For the most part, domestic fancy pigeons and the comparative sample overlap in PC1 morphospace. However, PC1 values higher than 0.8 are only represented by domestic fancy pigeons. *Raphus* is the species from the comparative sample that exhibits the most positive PC1 values. Principal component two shows the overlap of domestic fancy pigeons and the comparative sample in central and negative PC2 morphospace regions, with the domestic sample showing more positive maximum values of PC2. PC2 values higher than 0.7 are only presented by *Treron curvirostra* and *Didunculus*, all comparative sample species with highest PC2 values form part of the frugivorous clusters identified in Chapter Three

(clusters “h” and “g”). When I assess the interplay between PC1 and PC2, it is possible to notice the comparative sample of pigeons mostly occupy the bottom left sector of the morphospace while domestic fancy pigeons occupy the top left and bottom right sectors of the morphospace (Figure 4.2A). The top right sector of the morphospace has not been invaded by either naturally or artificially selected pigeons.

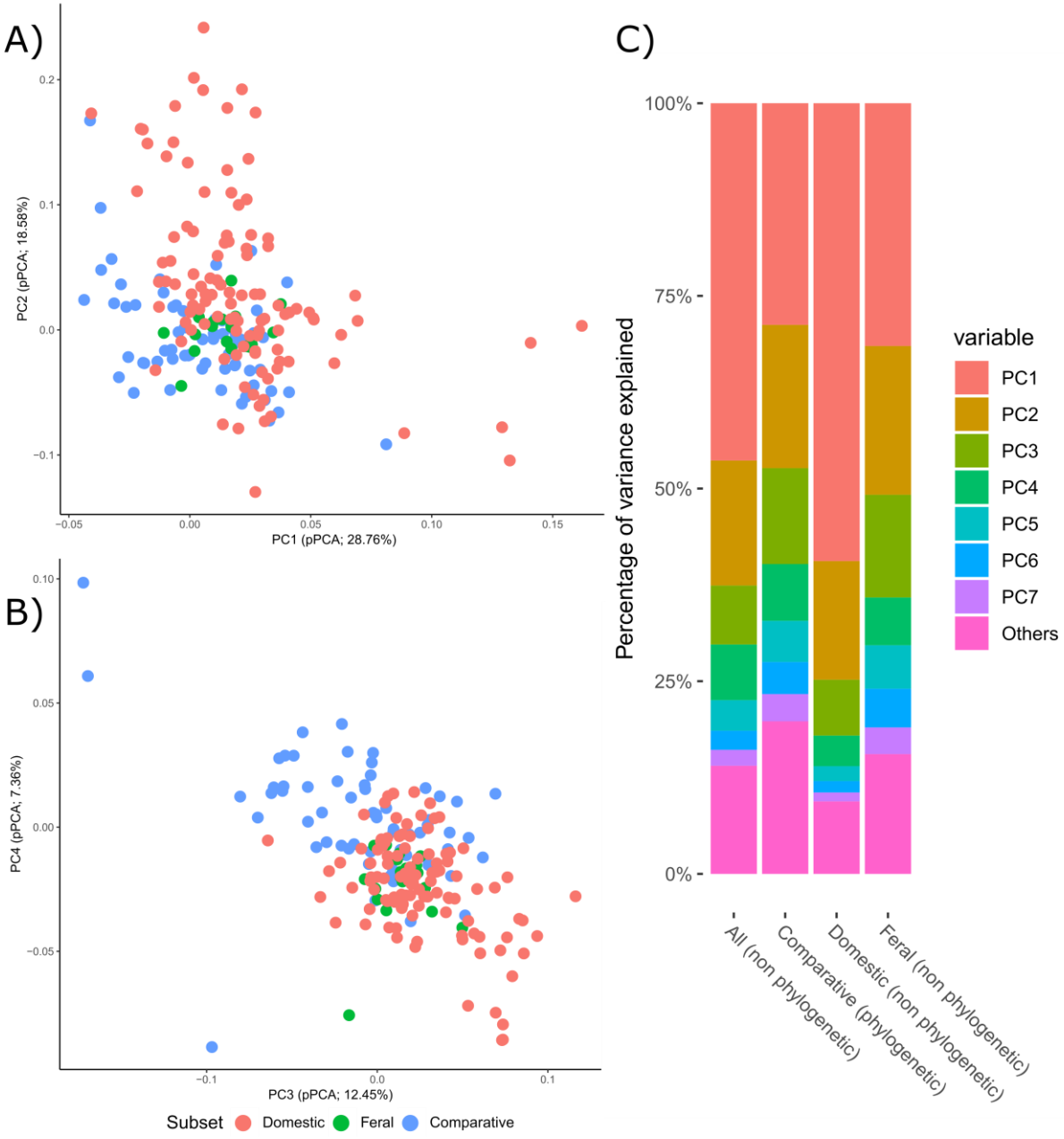


Figure 4.2. Principal component analysis of the complete sample. A) shows the plot of PC1 versus PC2. B) Shows the plot of PC3 versus PC4. C) shows the percentage of variance explained by the first 7 principal component of the complete sample, comparative Columbiformes, feral *C. livia* and domestic fancy pigeons. The PCA of the complete sample, as well as the feral and domestic pigeons samples are ordinary PCA, the comparative sample was examined implementing a phylogenetic PCA (Revell, 2009), and using a randomly selected tree from the tree sample. It is possible to see that the principal components in each subset explain different amounts of variance and explain different aspects of the shape variation (Figure 4.3)

For principal component three (Figure 4.2B), most of the axis is shared between the comparative sample and domestic fancy pigeons. *Raphus*, *Pezophaps*, *Didunculus,* and *Ducula pacifica* show more negative values of PC3 than the domestic fancy pigeons, while PC3 values higher than 0.6 are only shown by the domestic fancy pigeons. For principal component four, the comparative columbiforms, and domestic and feral *C. livia* overlap in central values. PC4 values higher than 0.01 are only exhibited by pigeons from the comparative columbiform sample, while values lower than -0.05 are only shown by the domestic fancy pigeon sample and one feral pigeon (*C. livia*; UMMZ 152906) and one pigeon from the comparative sample (*Didunculus*). When the interplay between PC3 and PC4 is assessed (Figure 4.2B), it is possible to see that only domestic fancy pigeons and some feral *C. livia* occupy the bottom right sector of the morphospace. The comparative columbiform sample occupies the top left quadrant of the morphospace with extreme values shown by *Pezophaps* and *Raphus*. The top right sector of the morphospace is empty while the bottom left sector of the morphospace is populated only by *Didunculus*. Finally, Figure 4.2C shows the comparison between the variance explained by the first principal components of different subsets of the sample. The variance summarized by corresponding principal components is different in all samples. This variation, along with the difference in patterns of morphospace occupation between samples (see below) suggests the possible

change in axes of variation between the comparative Columbiformes and domesticated pigeons.

Identified shape changes

Figures 4.3 and S4.1 show the shape changes summarized by the first four principal components for the two ordinary PCAs (feral and domestic samples) and the phylogenetic PCA (comparative sample). Different shape changes seem to be associated with different samples, with some of the shape changes seemingly corresponding to different PC axes in different samples (*e.g.*, rostrum length reduction along PC1 of the domestic pigeon sample and PC2 of the comparative sample). Low variation was identified in the feral *C. livia* sample, shape changes in PC1 related to the reduction of the frontals in the medio-lateral axis in negative PC values. PC2 shape changes for the feral sample are related to higher of basicranial flexion at negative PC values. In PC3 for the feral sample, negative PC values are related to the increase in size of the orbits, while for PC4 the shape change associated with negative PC values is an increase of ventral beak curvature in the midsagittal plane.

For the comparative sample, positive PC1 values are associated with a higher basicranial flexion and smaller orbit size. Meanwhile, positive PC2 scores are associated with the overall robustness of the skull, including lateral expansion of the braincase and frontals, decrease of rostrum length, and increase in the dorsoventral height at mid-length of the rostrum. Negative values of PC3 for the comparative sample show the dorsoventral compression of the braincase and the lateral expansion of the maxilla-nasal contacts with the jugal (mediolateral expansion of the beak).

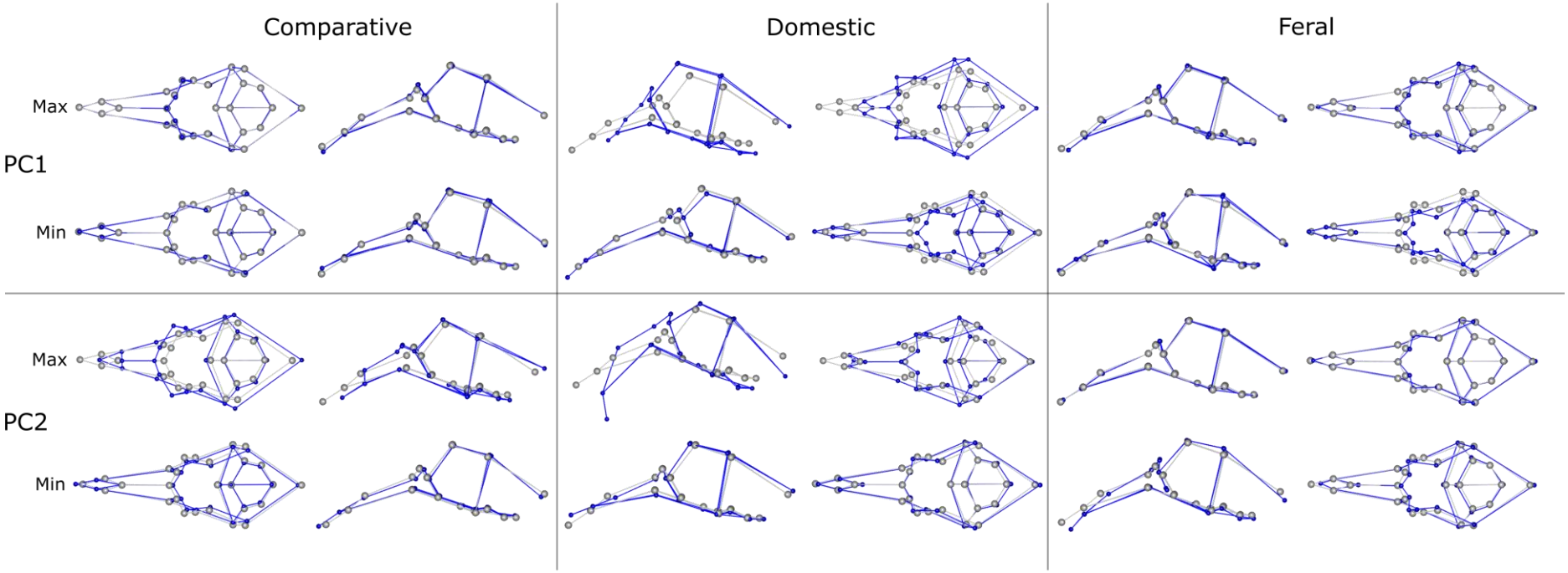


Figure 4.3. Shape changes associated with the first two principal components of the three samples. An ordinary PCA was used to summarize the variation in the domestic fancy pigeons and feral C. livia samples, while a phylogenetic PCA describes the variation in the comparative sample

Finally, negative values of PC4 are associated with the reduction of the frontals in the mediolateral axis; this is a similar shape change to the one identified for PC1 of the feral sample.

The shape changes for the domestic sample were more prominent than in the other samples. Shape changes associated with PC1 range from skulls with elongated beaks and mediolaterally reduced frontals and braincases (negative PC1) to skulls with substantially reduced rostrum length and thick (laterally expanded) rostra and braincases (positive PC1). Along PC2, the shape changes summarize the difference between skulls with thick (high dorsoventral height at mid-length of the rostrum), ventrally curved beaks in the midsagittal plane (positive PC2) and skulls with straight, thin (low dorsoventral height at mid-length of the rostrum) beaks (negative PC2). In PC3 the shape changes summarize the differences between skulls with laterally and anteriorly expanded frontals (negative PC3) versus skulls with frontals reduced in the same planes (positive PC3). Finally, negative PC4 values are associated with laterally expanded lacrimals and frontals.

Overlap of *n*-dimensional hypervolumes

The multidimensional hypervolume overlap was calculated for the three pigeon subsets using the PCA scores of the total samples (Table 4.1) and with the samples projected onto the phylogenetic PCA space. The overlap between the comparative Columbiformes and domestic fancy pigeons hypervolumes is 54% at one standard deviation and 90% at two standard deviations. The overlap was lower when phylogeny was taken into account: 53% at one standard deviation and 79% at two standard deviations. The overlap between the hypervolumes of the comparative columbiform and feral pigeon samples was 79% (one

standard deviation), and 98% (two standard deviations). The overlap between hypervolumes increased at one standard deviation (87%) and decreased at two standard deviations (93%) when phylogeny was taken into account.

Table 4.1. Overlap of variance explained by the multidimensional centroids of different subsets of pigeons.

	Ordinary PCA	
	Overlap (1 sd)	Overlap (2 sd)
Comparative vs Domestic	0.54	0.90
Comparative vs Feral	0.79	0.98
Domestic vs Feral	0.91	0.98
	Phylogenetic PCA	
	Overlap (1 sd)	Overlap (2 sd)
Comparative vs Domestic	0.53	0.79
Comparative vs Feral	0.87	0.93
Domestic vs Feral	0.96	1.00

The overlap between the hypervolumes of the domestic fancy pigeons and feral *C. livia* was 91% at one standard deviation and 98% at two standard deviations. When phylogeny was taken into account, the overlap between hypervolumes increases to 96% at one standard deviation and a total overlap of 100% at two standard deviations. Overall, this metric shows how the hypervolumes of the comparative columbiforms and domestic fancy pigeons overlap but also comprise different areas of phenotypic variation, and might have different axes of variation. The feral pigeons presented the most constrained morphospace (Figure 4.2). The lower variation of the feral *C. livia* is reflected in the almost complete multidimensional hyperspace overlap with the domestic fancy pigeons (100% at two standard deviations). This complete overlap might point to an expected result, the set of overall multivariate features that characterize the skull phenotypic matrices might be more

similar within *Columba livia* (domestic fancy pigeons and feral) than between all Columbiformes.

Geometric angles, scale and difference between vectors

I found high angles between most of the eigenvectors of different samples, with the smallest angles for the first 10 eigenvectors ranging from 48° to 76° in all samples with a mean of around 90° (Table S4.2). The range of minimal angles (62° to 87°) and the average of minimal angles (73°) was higher when comparing the domestic fancy pigeon and feral pigeon samples, while all comparisons with the comparative sample were more similar in both range and average minimum angle (domestic = 62° and feral = 66°). This points to the possibility of domestic fancy pigeons following similar major axes of variation to the naturally selected Columbiformes. However, the similarity of major axes of variation is low because of the high angles observed. The scale between vectors (Table S4.3) points to eigenvectors being mainly independent of a common scale across samples, with a minimum of 68 independent eigenvalues in all pairwise comparisons. These values hint again at the independence of major axes of variation applying to each sample. Finally, the differences between eigenvectors in the first four principal components and their closest eigenvectors (Figure S4.2) showed that there is no clear pattern of differences between all samples. The closest eigenvalues between the three samples seem to summarize different shape components, which change depending on the sample. Nevertheless, some pairwise comparisons showed that the closest eigenvectors summarize similar shape variation in both samples, for example PC1 of domestic fancy pigeons versus PC1 of feral *C. livia*, and PC1 of domestic fancy pigeons versus PC3 of the comparative columbiform sample. These

results might suggest that overall the eigenvectors of different samples are not similar and describe different aspects of shape. However, because each set of PC axes has rotated differentially in each sample, these "naïve" comparison might give spurious results. I further compared PCA results of different samples (see below) in a framework that takes into account the differential rotation of vectors.

Krzanowski principal component comparison (Krzanowski, 1979)

The Krzanowski test asks how similar the subspaces of different groups in their overall features are. To do this, it finds the minimum angle between subspaces and tests it against random association. It found that all the minimum angles were significant for all domestic fancy pigeon comparisons (P=0.001) and for feral-comparative sample comparison (P=0.008; Figure 4.4, Table 4.3). This allowed me to reject the hypothesis that angles generated by random association, and thus the subspaces, are significantly different between samples. The overall similarity (trace of **S**) obtained while comparing the first four principal components via the Krzanowski test were also significant: domestic fancy pigeons versus feral pigeons (P= 0.003); domestic fancy pigeons versus comparative columbiforms (P=0.001) and feral *C. livia* versus comparative columbiforms (P=0.001; Figure 4.4, Table 4.3). This points to the overall similarity of subspaces being largest between domestic fancy pigeons and feral *C. livia* (trace of **S** = 2.22). The second most similar subspace was that shared by the domestic fancy pigeons and the comparative sample (trace of **S** = 1.84). However, this value is close to that obtained from comparison of feral *C. livia* and comparative Columbiformes pigeons (trace of **S** = 1.51).

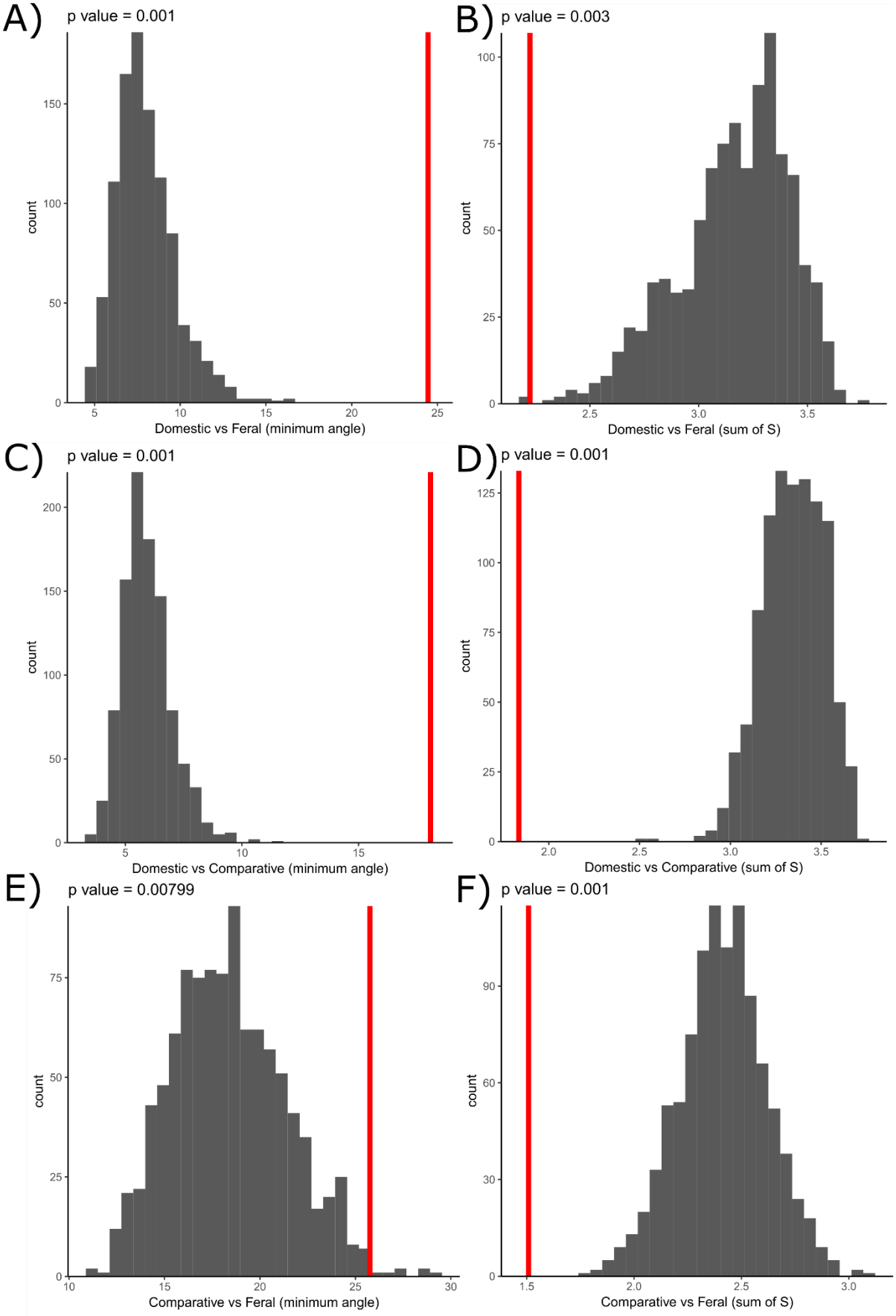

A)
p value = 0.001
count
Domestic vs Feral (minimum angle)
B)
p value = 0.003
count
Domestic vs Feral (sum of S)
C)
p value = 0.001
count
Domestic vs Comparative (minimum angle)
D)
p value = 0.001
count
Domestic vs Comparative (sum of S)
E)
p value = 0.00799
count
Comparative vs Feral (minimum angle)
F)
p value = 0.001
count
Comparative vs Feral (sum of S)

Figure 4.4. Permutation results for the principal component comparison (Krzanowski, 1979). Red lines indicate the value obtained by real data comparison. The minimum angle between principal components (A, C, and E) and the trace of S (B, D, and F) were measured in three different combinations: domestic fancy versus feral C. livia (A and B), domestic fancy pigeons versus comparative columbiform sample (C and D) and comparative columbiform sample versus feral C. livia. All comparisons are significant (P=0.001) and show that the angles observed in the real data are larger than the ones expected by chance while the trace of S shows that the overall similarity of subspaces is smaller in the real data than what is expected by chance.

Table 4.3. Principal component comparison Krzanowski (1979)

Comparison	angle 1	angle 2	angle 3	angle 4	P1	P2	trace of S	P1	P2
Domestic vs Feral	24.5	27.4	41.1	78.6	0.001	0.001	2.22	0.003	0.003
Domestic vs Comparative	18.1	34.8	61.4	80.3	0.001	0.001	1.84	0.001	0.001
Feral vs Comparative	25.8	35.5	81	84	0.008	0.008	1.51	0.001	0.001

Minimum angles between subspaces

The angle results below show that differences between group subspaces can be summarized as follows: (1) the domestic fancy pigeons and the columbiform sample are similar in dimension one; (2) the domestic fancy pigeons and the feral *C. livia* are similar in dimension two; and (3) the feral *C. livia* sample is extremely different to other samples in dimension three. As for detailed angle results, the minimum angles (angles between the closest arbitrary vectors) between these subspaces show that domestic fancy pigeon subspace is more similar in dimension (eigenvalue and eigenvector of **H**) one to the comparative sample (18° dimension one). The subspace of fancy pigeons is more similar to that of feral pigeons in all other dimensions (27° dimension two, 41° dimension three, and 87° dimension four). In all dimensions, the subspace of feral pigeons is more similar to that of domestic fancy pigeons (24° dimension one, 27° dimension two, 41° dimension three, and 79° dimension four), than to the subspace of the comparative columbiform sample.

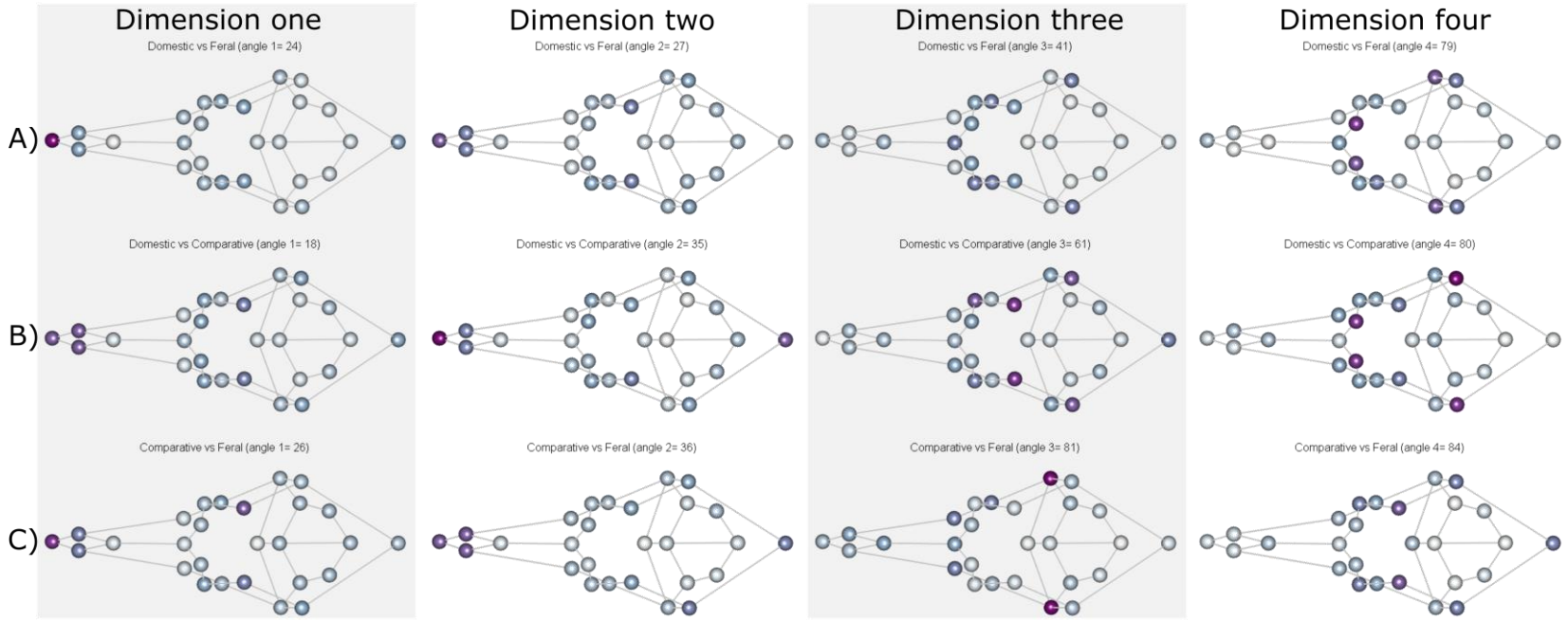


Figure 4.5. Bisector between the first four subspace dimensions. The bisector shows the closest vector to both subspaces in the original variable space. The sum of the absolute loadings for each landmark was calculated. Darker colour represents more similar landmark behaviour between two subspaces. The first two dimensions seem to follow relatively similar eigenvector loadings in the first dimension, however further dimensions are not similar between samples.

However, in dimension one, the angle difference of feral pigeons compared to the other two groups is small (25° with fancy pigeons and 26° with the comparative sample). In dimension three, the largest difference between subspaces is presented by the feral pigeons and the comparative columbiform sample (81° dimension one). The angles in dimension three are notably smaller for other group comparisons: 41° for the fancy pigeon sample versus feral *C. livia* sample, and 61° for the fancy pigeon sample versus the comparative columbiform sample. The columbiform comparative sample is also closer to the domestic fancy pigeon sample in all dimensions (18° dimension one, 34° dimension two, 61° dimension three, and 80° dimension four). Further exploration of the shape significance of these results was obtained by examining the bisector information (Figure 4.5).

Bisector of minimum angles

The bisector information (Figure 4.5) showed the differences in loadings for all four dimensions for the three samples. All samples are relatively close to each other in the first two dimensions (angles 18° to 35°). Dimension one shows that the subspaces are loaded preferentially in the landmarks of the distalmost tip of the premaxilla (all feral comparisons) and in the general tip of the beak area (including nasal contacts for the domestic versus comparative samples). The pattern of dimension two is similar, however differences between samples are more conspicuous. The comparison of domestic fancy pigeons versus the feral pigeons in dimension two shows that the orbital margin was more similar for this pair of sample sets. For the comparison of domestic fancy pigeons versus the comparative columbiforms in dimension two, the tip of the occipital crest has a high loading for both samples. In dimension three, the similarity between subspaces is low for domestic fancy

pigeons and the feral pigeons while the domestic fancy pigeons and comparative sample show a high loading in the orbital region (e.g., orbital margin, posterior orbital rim, and lateral lacrimal-frontal contacts). The similarity in dimension three between the feral and comparative sample is mostly loaded in the lateral points of the jugal bones. Finally, for dimension four the similarities between samples are inconsistent between different comparisons. While the domestic fancy and feral samples are similar mostly in the nasal-frontal contacts and in the lateral-most points of the jugal. The similarities of the domestic fancy and comparative samples are also the nasal-frontal contacts. However, they differ in presenting a high loading in the posterior orbital rim. The similarities in dimension four between the comparative and feral samples is mostly loaded in the orbital margin.

Common subspace between all samples

For the common subspace of all samples (Table 4.4), I found that the first-dimension angle between subspaces was significantly higher than that expected by chance for the three samples (*P*=0.001). The second-dimension angle between the common subspace and the populations behaves differently: the angle between subspaces was significantly higher than random for the domestic fancy pigeons (*P*= 0.009) and comparative columbiform (*P*=0.001) samples but was not significantly higher than random in the feral sample (*P*= 0.176). The third angle was significantly greater than random for the comparative columbiform sample (*P*= 0.001) but was not significantly greater than random (although close to significant) for the feral (*P*=0.059) and domestic fancy pigeons (*P*= 0.418). Finally angle four was significantly greater than random for the comparative sample (*P*= 0.006) but was not significantly different for the feral pigeon (*P*= 0.281) and domestic pigeon (*P*= 0.079) samples.

Table 4.4. Subspace comparison of all samples.

Part 1. Angles between the common subspace and each sample								
	angle 1	*P*	angle 2	*P*	angle 3	*P*	angle 4	*P*
Domestic	13.1	0.001	17.3	0.009	15.5	0.418	34.4	0.079
Feral	17.1	0.001	17.1	0.176	33.6	0.059	48.2	0.281
Comparative	12.5	0.001	22.6	0.001	54.3	0.001	71.6	0.006
Part 2. Eigenvalues of each angle								
	Eigenvalue 1	*P*	Eigenvalue 2	*P*	Eigenvalue 3	*P*	Eigenvalue 4	*P*
Value	2.816	0.001	2.677	0.035	1.963	0.336	1.224	0.543

The first angle with the common subspace is low for all samples (13° to 17°) however it is significantly greater than random, showing the three samples exhibit overall different features (principal components). The second angle between the samples and the common subspace was lower for the domestic fancy pigeons (17°) and comparative samples (23°). The comparative sample exhibited the highest third (54°) and fourth (71°) angles, this point to the Columbiformes presenting a distinctly different subspace to the common subspace of the feral *C. livia* and domestic fancy pigeons.

The eigenvalues of the common subspace (Table 4.4) were significantly lower than would be expected by chance for eigenvalues one (eigenvalue= 2.82; *P*= 0.001) and two (eigenvalue= 2.68; *P*= 0.03). These results show that all sample subspaces are significantly different in these two first dimensions. However, these eigenvalues are relatively high (an eigenvalue= 4 indicates complete alignment) and indicate that some common features (eigenvectors) are similar between all samples. This is reinforced by the low angles obtained, however I recover distinct and definitive subspace traits that would not be expected if all samples presented the same covariation features (eigenvalues).

Test for correlation of matrices (Krzanowski, 1993)

I analysed the correlation matrix of standardized (mean of 0 and variance of 1) Procrustes aligned landmarks (Krzanowski, 1993). When using only four dimensions (Table 4.5A), I found that the overall similarity of the domestic fancy and feral samples is higher (64%, *P*=0.017) than the domestic fancy versus comparative similarity (59%, *P*=0.001) and the comparative versus feral similarity (51%, *P*=0.003). When I assessed the similarity using the maximum 40 dimensions (Table 4.5B) I obtained 58% of similarity for the domestic fancy and feral samples (*P*=0.038), 74% for the domestic fancy and comparative samples (*P*=0.001), and a 57% similarity for the comparative versus feral samples (*P*=0.011). For all comparisons, the similarity values were significantly lower than the similarity of randomly permuted data. The lowest significance was shown by the fancy pigeons and feral *C. livia* comparison when four eigenvectors were analysed (*P*= 0.017) and when 40 dimensions were analysed (*P*= 0,038). This suggests, perhaps unsurprisingly, that Fancy pigeons and feral *C. livia* share more of their correlation matrices.

Table 4.5. Correlation matrices test Krzanowski (1993).

A) Krzanowski (1993) comparison in 4 dimensions

Comparison	trace of **S**	Similarity %	*P*	μ	P_{perm}
Domestic vs Feral	1.905	64	0.017	20.2	0.027
Domestic vs Comparative	1.760	59	0.001	20.2	0.001
Comparative vs Feral	1.518	51	0.003	6.9	0.687

B) Krzanowski (1993) comparison in 40 dimensions

Comparison	trace of **S**	Similarity %	*P*	μ	P_{perm}
Domestic vs Feral	23.159	58	0.038	38.5	0.005
Domestic vs Comparative	29.557	74	0.001	30.2	0.001
Comparative vs Feral	22.878	57	0.011	16.6	0.952

These results suggest that each sample follows the $\mathbf{H}_a$ ($\mathbf{H}_a$: $\boldsymbol{\Upsilon}_i$ arbitrary) of correlation matrices being different in all samples. I decided to measure μ (differences between the eigenvalues) to test the eigenvalues as well, despite the fact that the acceptance of $\mathbf{H}_a$ instantly discards both $\mathbf{H}_0$ ($\boldsymbol{\Upsilon}_i = \boldsymbol{\Gamma} \Delta \boldsymbol{\Gamma}'$; shared eigenvectors and eigenvalues) and $\mathbf{H}_c$ ($\boldsymbol{\Upsilon}_i = \boldsymbol{\Gamma} \Delta_i \boldsymbol{\Gamma}'$; shared eigenvectors). I observed the same pattern in the four- and forty-eigenvector comparison of μ. Relatively high differences of corresponding eigenvalues in all domestic pigeon comparisons were observed. The differences between eigenvalues for domestic pigeons were the same for all comparisons when four eigenvalues were analysed (μ= 20.2). When forty eigenvalues were analysed, μ was higher in the domestic-feral comparison (μ= 38.5) than in the domestic-comparative comparison (μ= 30.2). The differences between eigenvalues were small between the comparative and feral samples when four (μ= 6.9) or 40 eigenvalues (μ= 16.6) were analysed. The value of μ was significantly higher than randomly permuted data in all domestic comparisons ($P_{perm} < 0.03$) and was not significant for the comparative and feral samples when four or forty ($P_{perm} = 0.69$) eigenvalues were analysed ($P_{perm} = 0.95$).

Random skewers

Random skewers revealed a correlation between the response vectors to random selection vectors (Table 4.6). All pairwise comparisons between samples were significant, both against the null hypothesis of correlation against random vectors ($P_{RS} < 0.001$; Table 4.6) and against the hypothesis of samples being drawn from the same population (P_{perm}= 0.001; Table 4.6). The domestic fancy pigeon covariance matrix responds similarly to selection as the comparative sample (RS = 0.568) while the domestic and feral matrices also

present a relatively similar response to selection (RS = 0.507). Finally, there is a less similar response between the comparative and feral samples (RS = 0.437). These results of the random skewers again point to the covariance matrices sharing some structure but not behaving co-linearly or exhibiting the same response to selection. The response to selection is significantly different than the correlation between random vectors. However, the responses to selection pressures are significantly different between the different samples. This gives further evidence for the independent covariance matrices in domestic fancy pigeons, feral pigeons and other Columbiformes.

Table 4.6. Random skewers correlation (Cheverud and Marroig, 2007)

Comparison	correlation	P_{RS}	Correlation (sd)	P_{perm}
RS Domestic vs Feral	0.507	0.000	0.232	0.001
RS Domestic vs Comparative	0.568	0.000	0.253	0.001
RS Comparative vs Feral	0.437	0.000	0.177	0.001

Lines of least evolutionary resistance

$LLER_{corr}$, the average correlation between the maximum line of variation in Columbiformes ($\mathbf{p}_{max}$) with the morphological change vector (Δz) was low in all samples (ranging from 0.109 to 0.124; Table 4.7A), including across phylogenetic PCAs conducted using multiple different phylogenies for the comparative sample (Figure 4.6). Despite all correlation coefficients being low and superficially similar in value, all of them were significantly different to each other (Wilcoxon $P<0.001$; Table 4.7B) with domestic fancy pigeons presenting a higher correlation ($LLER_{corr}= 0.124$) than feral pigeons ($LLER_{corr}= 0.118$) and the comparative columbiform sample ($LLER_{corr}= 0.109$). The mean amount of phenotypic differentiation (m_{amount}) was also significantly different in all samples ($P<0.001$) across all

phylogenies. The m_{amount} was higher in domestic fancy pigeons (m_{amount}= 0.882) than in the feral (m_{amount}= 0.866) and comparative samples (m_{amount}= 0.867). Finally, the Pearson correlation between $\mathbf{p}_{max}$ and m_{amount} was positive in all samples, and was significantly different between samples (P<0.001). Noteworthy, the Pearson correlation was close in the feral (r= 0.39) and comparative samples (r = 0.45), while the Pearson correlation was higher for domestic fancy pigeons (r= 0.74). Figure 4.6D and Table 9A show that the correlation between Δz and $\mathbf{p}_{max}$ obtained for each group was significantly different to the correlation between Δz and random vector (P<0.001). All these results show that the average $LLER_{corr}$ and m_{amount} values were similar between samples, but they were significantly different (Wilcoxon test; P<0.001). The Pearson correlation between $LLER_{corr}$ and m_{amount} showed that the two values were extremely different in domestic fancy pigeons (Figure 4.6C) in comparison to other samples. This suggests that domestication is successfully selecting towards morphologies located across the maximum variation line, obtaining large morphological change in this direction, reflecting possible shared constraints between domestic fancy pigeons and the comparative sample of Columbiformes, imposed by the LLER.

Table 4.7. Lines of least evolutionary resistance (Marroig and Cheverud, 2005)

A) Values and probability versus random					
PC axis	Sample	$LLER_{corr}$	m_{amount}	Pearson	Wilcoxson P
PC1	Domestic	0.124	0.882	0.735	1.3E-60
PC1	Feral	0.118	0.866	0.447	1.1E-59
PC1	Comparative	0.108	0.848	0.024	1.3E-65
PC2	Domestic	0.051		-0.057	4.9E-79
PC2	Feral	0.049		-0.006	6.3E-77
PC2	Comparative	0.050		-0.362	3.3E-79
PC3	Domestic	0.042		0.076	4.6E-81
PC3	Feral	0.040		0.005	1.2E-79
PC3	Comparative	0.048		-0.256	4.6E-80

PC4	Domestic	0.047	0.031	1.2E-80
PC4	Feral	0.046	-0.108	3.7E-79
PC4	Comparative	0.061	-0.204	1.0E-78

B) Comparison between samples (Wilcoxson p)

PC axis	Comparison	$LLER_{corr}$	m_{amount}	Pearson
PC1	Domestic vs Feral	0.000	0.000	0.000
PC1	Domestic vs Comparative	0.000	0.000	0.000
PC1	Comparative vs Feral	0.000	0.000	0.000
PC2	Domestic vs Feral	0.046		0.002
PC2	Domestic vs Comparative	0.369		0.000
PC2	Comparative vs Feral	0.037		0.000
PC3	Domestic vs Feral	0.107		0.010
PC3	Domestic vs Comparative	0.000		0.000
PC3	Comparative vs Feral	0.000		0.000
PC4	Domestic vs Feral	0.638		0.000
PC4	Domestic vs Comparative	0.000		0.000
PC4	Comparative vs Feral	0.000		0.000

The PCA of all samples (Figure 4.2) showed that some domestic fancy pigeons explore regions of morphospace associated with the principal component two that were not explored by other columbiforms. For this reason, I decided to delve into the association patterns of LLER in further principal components. The Pearson correlation between Δz and $\mathbf{p}_{max}$ was different than the correlation of Δz and a random vector for all analyses (all samples and any PC axes; $P<0.001$). When PC2 was taken as $\mathbf{p}_{max}$, the values of the $LLER_{corr}$ were close in all samples: domestic fancy pigeons ($LLER_{corr}$= 0.051), feral *C. livia* ($LLER_{corr}$= 0.049) and the comparative columbiform sample ($LLER_{corr}$= 0.050). These $LLER_{corr}$ values in PC2 for the domestic and comparative samples were not significantly different (P= 0.369). The $LLER_{corr}$ of the domestic and feral samples were not significantly different when PC3 (P= 0.107) or PC4 (P= 0.638) were used as $\mathbf{p}_{max}$. The comparative columbiform sample showed the highest $LLER_{corr}$ in all samples in PC3 ($LLER_{corr}$= 0.048) and PC4 ($LLER_{corr}$= 0.061).

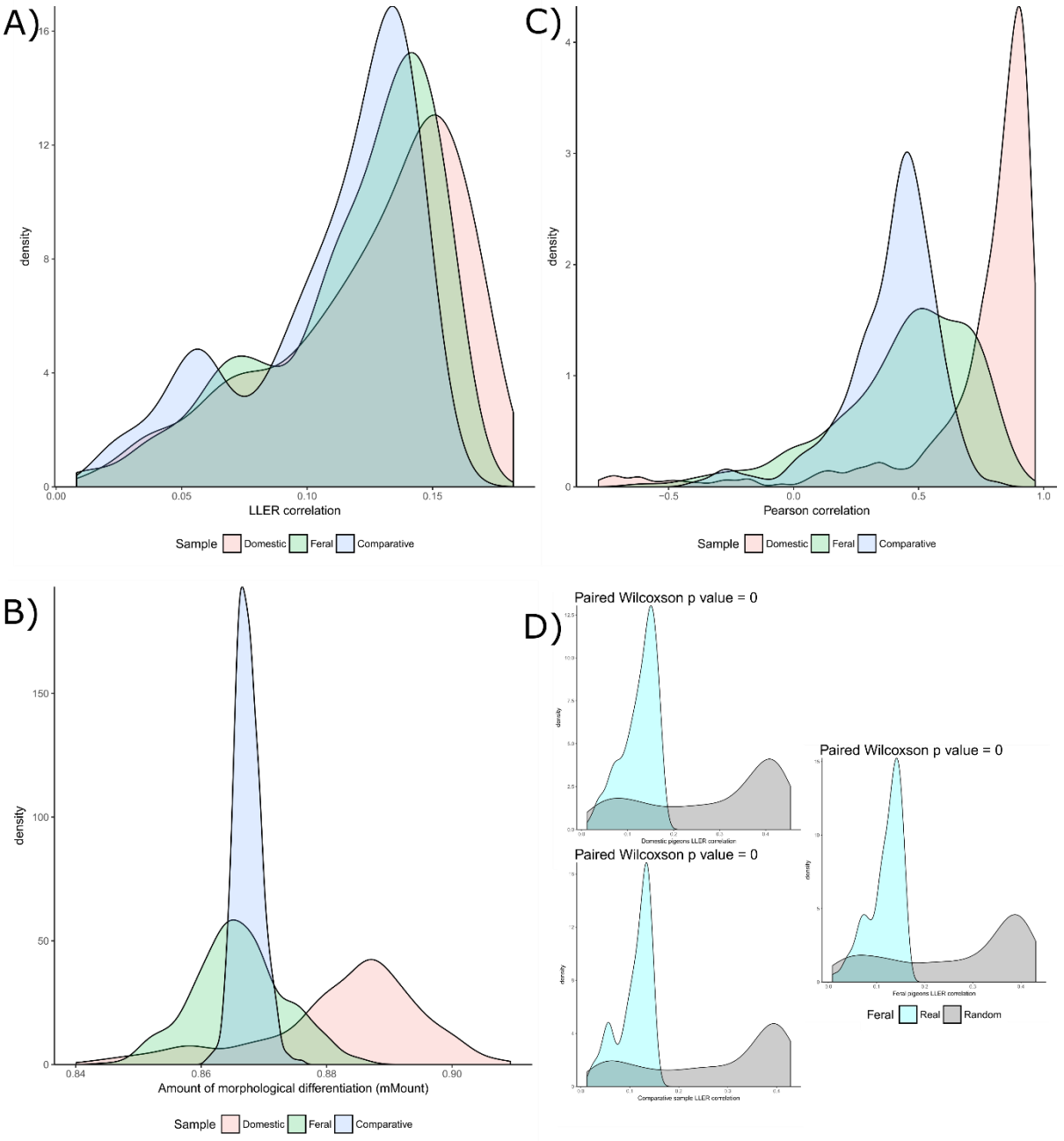


Figure 4.6. Lines of least evolutionary resistance (LLER). A) Mean values of $LLER_{corr}$ in 500 phylogenies, it shows the correlation between the direction of evolution (Δz) and the largest proportion of phenotypic variation ($\mathbf{p}_{max}$). B) Shows the mean values of the amount of morphological variation across 500 phylogenies. C) Pearson correlation of m_{amount} and $LLER_{corr}$ across 500 phylogenies. D) shows the difference in $LLER_{corr}$ for the three samples compared with the $LLER_{corr}$ obtained when comparing Δz and a random vector. A) This shows that the mean correlation between the direction of evolution and the maximum variation is low in all samples (0 to 0.20). However, the correlation is higher in the domestic fancy pigeon sample. $LLER_{corr}$ is also higher in the feral pigeons than the comparative sample although, the distribution is more similar between these two samples. The amount of morphological differentiation is higher in domestic fancy pigeons while feral pigeons seem to be restricted to mean values of m_{amount} of the comparative sample. The Pearson correlation values were similar for the feral and comparative samples.

However, domestic fancy pigeon samples show a more positive correlation, this points to the high correlation of Δz and $\mathbf{p}_{max}$ in domestication. This shows that, in domestication, the phenotypic change is extremely correlated with the $\mathbf{p}_{max}$ direction. D) All comparisons were different to the random $LLER_{corr}$.

As for the Pearson correlation between $LLER_{corr}$ and m_{amount} for further PC axes (Table 4.7, Figure 4.7), the overall results show that in nature (comparative columbiform sample), the morphological variation is highly constrained to follow $\mathbf{p}_{max}$ (PC1). The feral pigeons seem to be less constrained but follow similar patterns, while pigeons under domestication have successfully obtained morphological variation in directions other than $\mathbf{p}_{max}$ (PC1). The Pearson correlation between $LLER_{corr}$ and m_{amount} was significantly different ($P<0.01$) between different samples in all PC axes. When PC2 was used as $\mathbf{p}_{max}$, the Pearson correlation was negative for all the samples; however, it was close to zero for feral *C. livia* (r=-0.006) and smaller for the domestic fancy pigeons (r= -0.057) than for the comparative columbiform sample (r= -0.362). When PC3 was used as $\mathbf{p}_{max}$, the Pearson correlation was negative only for the comparative columbiform sample (r= -0.256), while it was close to zero for the feral *C. livia* sample (r= 0.005) and positive for the domestic fancy pigeon sample (r= 0.076). Finally, when PC4 was used as $\mathbf{p}_{max}$, the Pearson correlation was negative for the feral pigeons (r= -0.108) and the comparative columbiforms (r= -0.204), while it was positive for the domestic pigeon sample (r= 0.031).

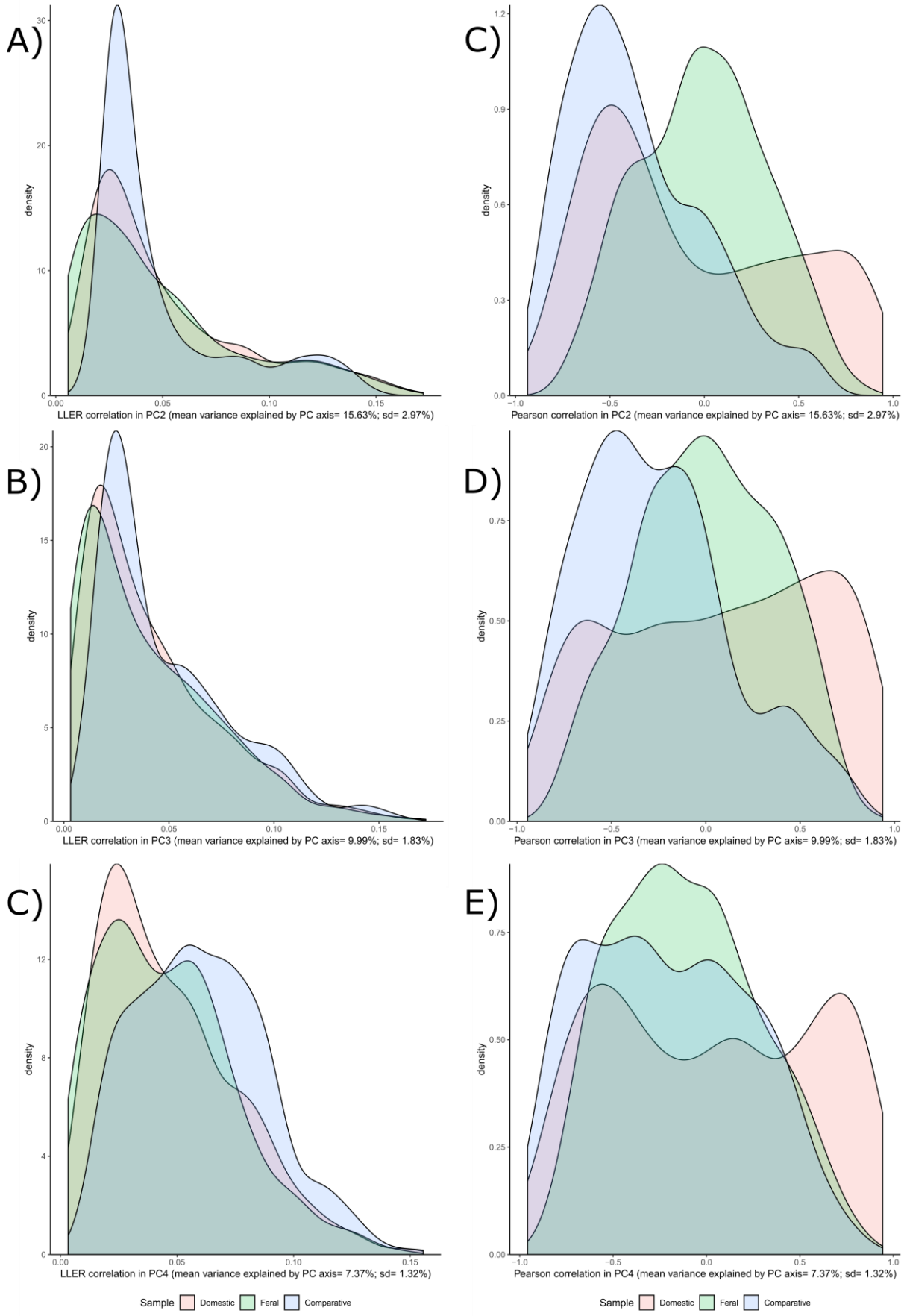

A)
density
LLER correlation in PC2 (mean variance explained by PC axis= 15.63%; sd= 2.97%)
C)
density
Pearson correlation in PC2 (mean variance explained by PC axis= 15.63%; sd= 2.97%)
B)
density
LLER correlation in PC3 (mean variance explained by PC axis= 9.99%; sd= 1.83%)
D)
density
Pearson correlation in PC3 (mean variance explained by PC axis= 9.99%; sd= 1.83%)
C)
density
LLER correlation in PC4 (mean variance explained by PC axis= 7.37%; sd= 1.32%)
E)
density
Pearson correlation in PC4 (mean variance explained by PC axis= 7.37%; sd= 1.32%)
Sample
Domestic
Feral
Comparative

Figure 4.7. Lines of least evolutionary resistance (LLER) using PC axes two, three, and four as $\mathbf{p}_{max}$. A), B) and C) Mean values of $LLER_{corr}$ in 500 phylogenies. D), E) and F) Pearson correlation of m_{amount} and $LLER_{corr}$ across 500 phylogenies. The $LLER_{corr}$ is similar in for the domestic feral pigeons and comparative columbiform sample in PC3 and PC4, in those same axes the Pearson correlation is more variable for the domestic pigeon sample than in the comparative columbiform sample. Finally, the comparative sample is always skewed towards negative Pearson correlations.

Discussion

The overall results show that the covariation and correlation patterns of the domestic, feral and comparative columbiform samples are different. The morphospace occupied by the domestic and comparative samples exhibited remarkable differences (Figure 4.2). While there was overlap between samples, the domestic pigeons colonized morphospace areas beyond those of the comparative sample in PC1 and PC2. Along PC3 and PC4, the morphospace showed overlap between sample occupation: however, specific areas were occupied either only by domestic fancy pigeons or only by the comparative sample of columbiforms (Figure 4.2). The hypervolume overlap (Table 4.1), when phylogeny was taken into account, showed a total overlap between fancy and feral pigeons (100%), and a lower overlap (79%) for domestic and comparative samples. These patterns are somewhat similar to those obtained by Drake and Klingenberg (2010) in which they characterized the morphospace of domestic dog breeds (*Canis familiaris*), wolves (*Canis lupus*) and a comparative sample of Carnivora. The morphospace of dogs also explored a high proportion of the morphospace in which the wolf morphospace was imbedded. When the dogs are compared with Carnivora as a whole, the samples overlap in some regions of morphospace, but dogs explore novel parts of the morphospace beyond anything seen in Carnivora. However, Drake and Klingenberg (2010) suggested that diversity of the dog skull was a product of relaxed constraints (domestication) acting on common patterns of variation (integration and modularity) shared by the wolf and across Carnivora. I demonstrated in Chapter Three that the columbiform skull is a *globally disintegrated* structure (*sensu* Bookstein, 2015), with weak modularity and moderate integration. Considering the weak modularity and moderate integration in Columbiformes, my results

suggest that domestication has produced novel patterns of variation (covariance and correlation) in domestic pigeons. These novel patterns are not shared between domestic Columba livia and the comparative sample of Columbiformes or even among domestic and feral *C. livia*. These results contrasts to those of Young *et al.* (2017) who suggested these patterns were shared across broad ranges of phylogenetic diversity (all birds or even vertebrates).

The comprehensive morphospace reported here was produced by projecting samples into the comparative sample phylogenetic PCA subspace (Figure 4.2). While this is useful in order to visualize morphospace occupation and hypervolume overlap, I found that this naïve approach was less useful for assessing the similarity of axes of variation between samples. This naïve comparison showed that the closest eigenvectors between samples are not a product of a scale difference between samples (Table S4.3) and that the closest eigenvectors do not share a common loading structure between samples (Figure S4.2). The angle comparison indicated that the most similar samples were the domestic and comparative samples albeit large angles were identified (average angle between the closest ten eigenvectors = 62°; Table S4.2).

The naïve comparison of different samples PCAs is challenging, for example in the visual inspection of the shape changes associated to different PC axes in different samples (Figures 4.3 and S4.1). There was no congruence between the shape changes associated with the same PC axis among the different samples. Some of the shape changes seemed to be comparable between samples but these "common" shape changes were associated with different PC axes in different samples. Here I caution against the naïve comparison of

samples when analysing the variance and covariance of different samples. While this comparison is useful for estimating morphospace occupation of each sample, and to measure the hypervolume overlap between samples, this approach is not fit to test for common variation patterns between samples. The misfit comes from each of the samples being imbedded in their own subspace (Krzanowski, 1979, 1993), and therefore my approximation of projecting all samples into the same subspace or the method of analysing all samples in a single PCA (Drake and Klingenberg, 2010) cannot be used to compare the covariance between samples. When all samples are analysed in the same subspace, the information about direction of evolution (Schluter, 1996), modularity and integration (Penna *et al.*, 2017), past selection gradients (Boag, 1983; Lande and Arnold, 1983; Grant and Grant, 1995; but see Marroig, Melo and Garcia, 2012), and constraints and response to selection (Lande, 1979; Cheverud and Marroig, 2007; Klingenberg, 2008) is lost because the covariation and correlation of all samples is calculated from the same matrix. In light of this, I argue in favour of using several statistical analyses when evaluating the variation of different samples.

The statistical comparison of phenotypic matrices showed a much more detailed picture for which the significance could be assessed. Domestic fancy pigeons and feral *C. livia* samples exhibited the highest overall similarity (Krzanowski, 1979; Table 4.3). This similarity between the domestic fancy pigeons and the feral *C. livia* is unsurprising considering that feral pigeons are descendants from escaped domestic pigeons (Johnston, 1992). The minimum angles between subspaces were lower for domestic and comparative samples in dimension one, and for domestic and feral in dimension two. Dimension angle was higher between the feral *C. livia* and comparative columbiform samples than between

other samples. The third angle was higher between the feral *C. livia* and comparative columbiform samples than between any other samples.

The visualization of the bisector (closest vector to both subspaces; Figure 4.4) showed that all samples were highly loaded in the tip of the beak for dimension one, while for dimension two the loading is also higher in the beak tip, but the orbital margin is also similarly loaded in the domestic fancy pigeon and comparative columbiform samples. For dimension two, the occipital crest is similarly loaded in the feral *C. livia* and the comparative columbiform samples. Further dimensions showed no common patterns. The analysis of the common subspace of all samples showed that the first angle is similar but significantly different between all samples (Table 4.4). The second dimension showed the differences between *C. livia* (feral and domestic) and the comparative columbiform sample. Overall, the subspace of the comparative columbiform sample was extremely different from the other samples (Table 4.4). Finally, the relatively high eigenvalues and some low angles showed some shared structure between samples; however, I recover distinct and definitive subspace traits that would not be expected if all samples presented the same covariation features. Further information about the correlation of the phenotypic matrix showed that the highest overall similarity (Krzanowski, 1993; Table 4.5) is shown by the domestic fancy pigeons and feral *C. livia* samples. The random skewers (Cheverud and Marroig, 2007; Table 4.6) showed that some response of variation is shared between samples: however the highest similarity in response to selection was moderate (57%) for the domestic fancy pigeons and comparative columbiform samples.

The series of statistical analysis reported here provide evidence against the generalization of results obtained for one species or clade across a broader taxonomic scale. It has been suggested that common patterns of covariance and correlation might be responsible for all avian cranial variation across taxonomic scales (Young *et al.*, 2017), I find almost no evidence for this for Columbiformes. The only instance where I find shared patterns between samples is in the lines of least evolutionary resistance (LLER; Marroig and Cheverud, 2005, 2010). The LLER approach (Figures 4.6 and 4.7), taking phylogeny and phylogenetic uncertainty into account, showed that the domestic fancy pigeon phenotype has diversified following preferentially the maximum direction of variation of the comparative columbiform covariance matrix. However, the correlation of evolution direction with $\mathbf{p}_{max}$ was low for all samples. The largest amount of morphological variation was identified for the domestic sample. The results from the LLER approach support the hypothesis that fancy pigeons follow the variation found in nature in Columbiformes (Figure 4.6). However, I found clear evidence of artificial selection successfully exploiting different axes of variation than the ones explored by natural selection: when further PC axes of variation were used as $\mathbf{p}_{max}$ (Figure 4.7), the different patterns of variation in the domestic pigeons were confirmed. While the comparative Columbiform sample is constrained to $\mathbf{p}_{max}$ (low Pearson correlation with other PC axes), the domestic pigeons have been able to successfully explore other axes of variation (positive Pearson correlation in PC3 and PC4). These new axes might have originated because accumulation of mutations during the long domestication process of fancy pigeons (Price, 2002).

The LLER approach was useful to describe the sample variation because it allowed me to incorporate the phylogeny and phylogenetic uncertainty into the results. Nevertheless, I

would like to acknowledge and highlight possible problems with the results of the lines of least evolutionary resistance.

First, Mitteroecker *et al.* (2005) showed that it is possible to identify some of the allometric trends like peramorphosis and paedomorphosis in a multivariate framework only if some base precautions are taken. One of these precautions is that principal components analysis should not be used to identify heterochrony (Mitteroecker, Gunza and Bookstein, 2005). This is because other factors besides size can influence PC1 (Mitteroecker, Gunza and Bookstein, 2005). Despite this, PC1 is commonly used as $\mathbf{p}_{max}$ in the LLER approach (Marroig and Cheverud, 2005, 2010; Penna *et al.*, 2017). Furthermore, PC1 can summarize changes in overall size but further principal components can summarize the changes of the size of individual structure (Mitteroecker, Gunza and Bookstein, 2005). Even in a geometric morphometric framework where scale is removed by the Procrustes alignment (Gower, 1975; Rohlf and Slice, 1990), allometric shape changes related to size will influence PC1 (Klingenberg, 2016). While size and allometry have been taken into account in other LLER implementations (Schluter, 1996), here I used the raw Procrustes aligned landmarks to apply the LLER framework as in Marroig and Cheverud (2005, 2010). I acknowledge that the results reported here might be biased because of the controversial use of PC1 as the allometric proxy.

Second, I acknowledge that the covariation between characters was not taken into account for the ancestral character estimation implemented in my LLER analysis. In doing this, the common selective pressures or covariation constraints are ignored (Pagel, Meade and Barker, 2004). Ignoring this covariation might bias the results because it would increase the

uncertainty of estimations (Pagel, Meade and Barker, 2004). However, my LLER implementation only uses the ancestral states inferred for the most recent common ancestors of the species in the sample: these recent nodes are estimated with lower uncertainties than deeper nodes (Pagel, Meade and Barker, 2004).

Third, Lande (1979) formulated the equation of multidimensional evolutionary response to selection in an allometric framework (describing the allometry in brain size during artificial selection). I observed that matrix comparison research (as implimented by Marroig and Cheverud, 2005, 2010; Klingenberg, 2008; Penna *et al.*, 2017) does not take allometry into account. The lack of allometric corrections might be a result of the context in which the equation was formulated (by Lande, 1979). However, Lande (1979) acknowledged that selection could produce interspecific patterns other than allometry and that genetic drift can induce allometry-like patterns because of the pleiotropic effects of correlated genes (Lande, 1979). I suggest therefore, that a future research is needed to further explore the influence of allometry in the LLER framework results.

A cautionary view about the expectations of similarity between patterns of variation in a geometric morphometrics framework.

Here I argue that some of the apparent "common" features between the shape changes across taxonomic levels might reflect the physical constraints of our world, rather than genetic or developmental constraints. To illustrate this, I will use a similar analogy to the classic example of the shape space of triangles (Kendall, 1984; Klingenberg, 2016). In this illustration we can imagine the skull is simplified to a sphere (braincase) and a cone (rostrum), and then we can take a moment to consider what changes could be made to

that structure. These might be of Procrustes nature (size, rotation, and orientation; Gower, 1975) or of topological nature (between the relative position of the elements of the skull): changes of proportional element size, compression or elongation of elements, and changes in alignment between elements. It is possible then to realise that the changes that can modify the structure are limited. These changes are constrained to modify the shape of an existing structure in the three axes (*x*, *y* and *z*) of our 3D world. If a sample of shapes, produced by the discussed shape changes, were analysed in a geometric morphometric framework, the Kendall shape-space (Kendall, 1984) of the sample could be characterized (Adams, Rohlf and Slice, 2013; Klingenberg, 2016).

In this geometric morphometric framework, a series of eigenvectors and eigenvalues could be obtained to summarize the shape variation, and reproduce any change in the shape in the sample (Kendall, 1984; Klingenberg, 1998, 2016). However, certain similarity in the sample could be expected because of the limited number of possible topological changes that produced the sample in the first place.

I argue that the current focus of craniofacial evolution research (Cooney *et al.*, 2017; Young *et al.*, 2017) is misleadingly concentrated on finding similarities between covariation and correlation patterns. As I have illustrated, certain similarity is to be expected because selection can only produce a limited repertoire of shape changes dictated by the geometric and physical laws of an existent structure. Here I argue that the research questions should take this expected similarity into account and focus on the unexpected patterns between samples. I found one of these unexpected patterns in my Columbiform morphospace (Figure 4.2): why has neither natural nor artificial selection selected for pigeon skull shapes

that would occupy the top right sector of the morphospace? I agree with Young *et al.* (2017) who suggested that analysing species with extreme shapes that go beyond characteristic patterns could determine how covariation patterns were generated. On this note, my overall results suggest that restraint should be used when comparing results from one species across ranges of phylogenetic diversity (multiple phylogenetic lineages) because these results might be biased towards spurious similarity of patterns which do not necessarily reflect common molecular signalization but rather common geometrical constraints.

Supplementary material (S4)

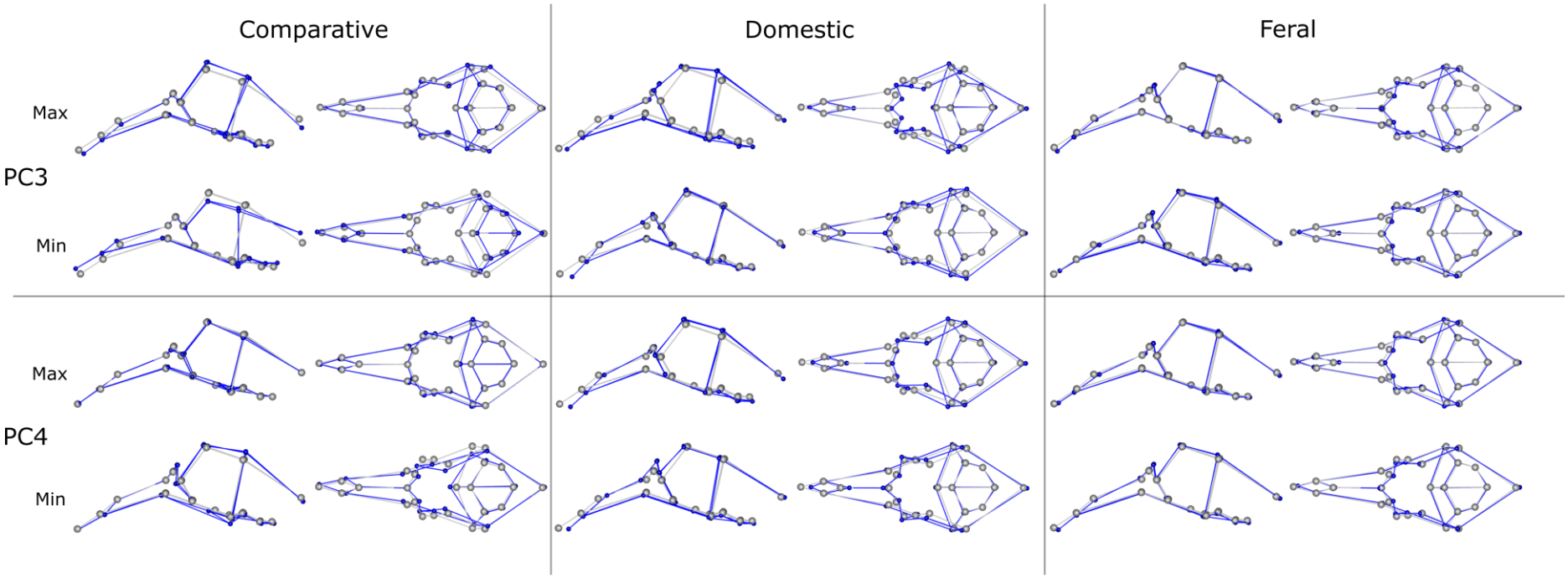


Figure S4.1. Shape changes associated with PC3 and PC4 of the three samples. An ordinary PCA was used to summarize the variation in the domestic fancy pigeons and feral C. livia samples, while a phylogenetic PCA describes the variation in the comparative sample.

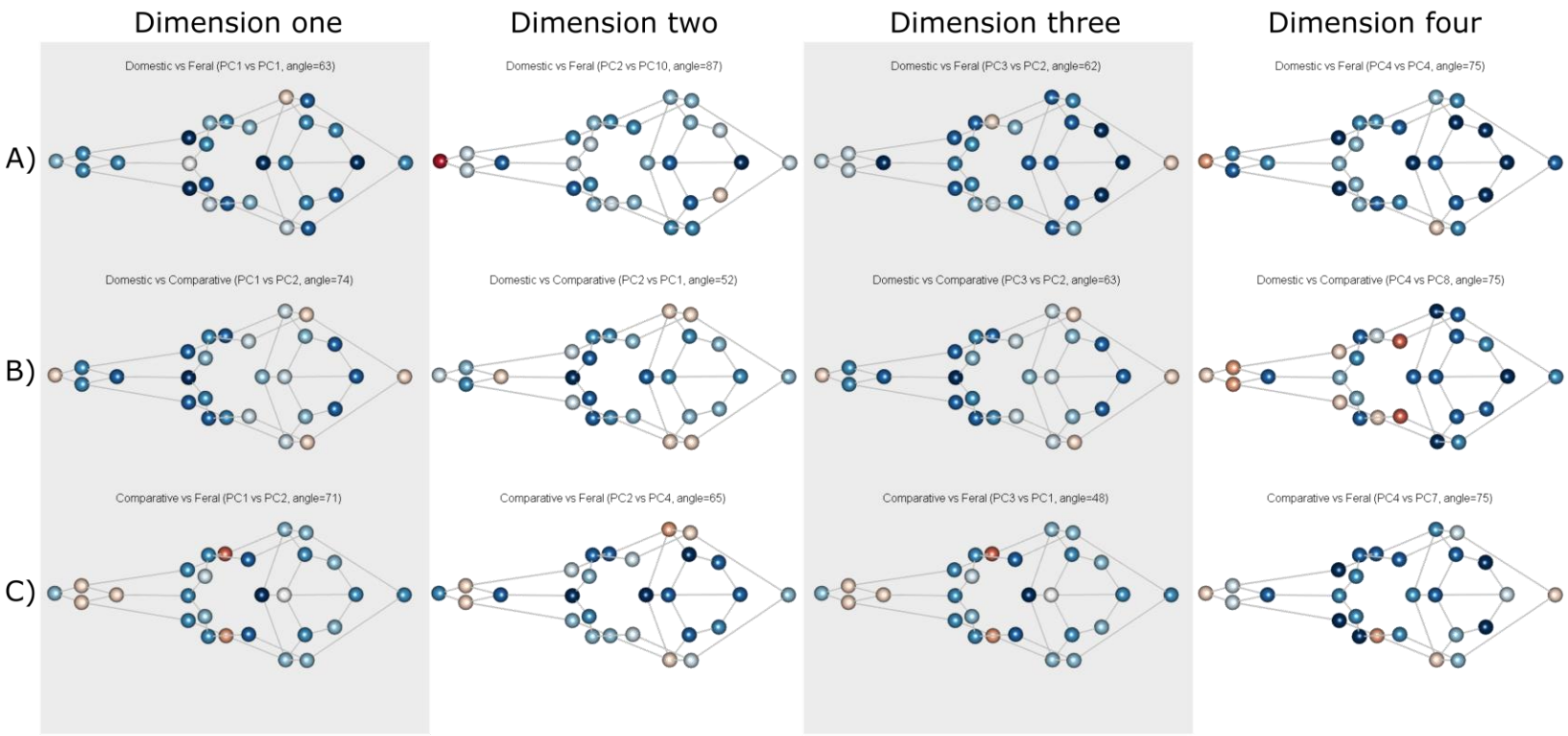


Figure S4.2. Difference between closest vectors.

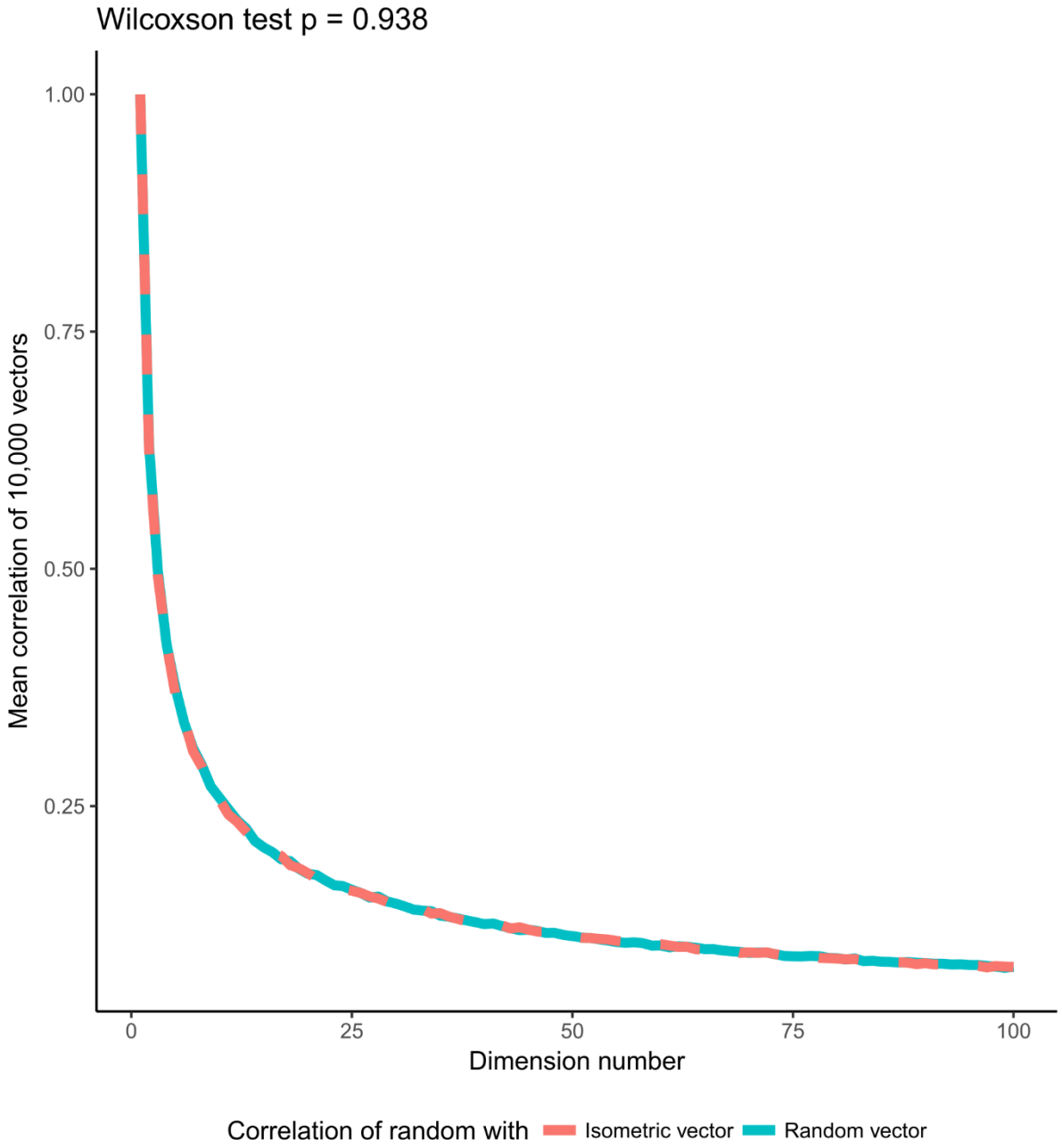

Wilcoxson test p = 0.938
1.00
0.75
0.50
0.25
Mean correlation of 10,000 vectors
0
25
50
75
100
Dimension number
Correlation of random with
Isometric vector
Random vector

Figure S4.3. Correlation between random vectors and random or isometric vectors. The average correlation varies in a predictable way with the dimensionality of the vector. The correlations obtained with random and isometric vectors are not statistically different (P=0.938).

Supplementary tables

Table S4.1. Domestic pigeon specimens and missing landmarks.

Pigeon breed	Collection	Specimen number	N miss.	Which	Why	N miss. Ref.
Fan tail	Darwin	BMNH 1868.2.19.1	0			0
Bassara pigeon	Darwin	BMNH 1868.2.19.2	0			0
Runt	Darwin	BMNH 1868.2.19.3	2	12 and 17	Missing quadrate, difficult to locate symphysis	0
Swallow	Darwin	BMNH 1868.2.19.6	1	18	displaced quadrate	0
Nun	Darwin	BMNH 1868.2.19.7	0			0
Barb	Darwin	BMNH 1868.2.19.10	3	3, 10, and 18	broken zygomatic	1
TurbitXTrumpeteer	Darwin	BMNH 1868.2.19.12	1	18	missing quadrate	0
Carrier Dragon	Darwin	BMNH 1868.2.19.14	0			0
Tumbler	Darwin	BMNH 1868.2.19.16	0			0
Poulter	Darwin	BMNH 1868.2.19.18	0			0
Turbit	Darwin	BMNH 1868.2.19.19	1	5	broken	1
English frill back	Darwin	BMNH 1868.2.19.20	1	7	difficult to locate	0
Jacobin	Darwin	BMNH 1868.2.19.22	0			0
Tumbler roller	Darwin	BMNH 1868.2.19.26	0			0
Bagadotten	Darwin	BMNH 1868.2.19.27	0			0
Scanderoon	Darwin	BMNH 1868.2.19.29	0			0
Trumpeteer	Darwin	BMNH 1868.2.19.30	0			0
Dun dragoon	Darwin	BMNH 1868.2.19.31	0			0

Carrier	Darwin	BMNH 1868.2.19.37	0			0
Archangel	Darwin	BMNH 1868.2.19.38	0			0
Breed reverse feathers	Darwin	BMNH 1868.2.19.39	0			0
Tumbler	Darwin	BMNH 1868.2.19.43	0			0
Laughter	Darwin	BMNH 1868.2.19.48	0			0
Poulter	Darwin	BMNH S/1952.2.387	0			0
Runt Victoria	Darwin	BMNH 1868.2.19.41	0			0
Spot	Darwin	BMNH 1868.2.19.13	1	15	broken	0
Arcangel	Espinoza-Campuzano	CAEC 2015.9.19	0			0
Arcangel	Espinoza-Campuzano	CAEC 2015.9.20	0			0
Brummer	Espinoza-Campuzano	CAEC 2015.9.21	0			0
Brummer	Espinoza-Campuzano	CAEC 2015.9.22	0			0
Buchona	Espinoza-Campuzano	CAEC 2015.9.17	0			0
Buchona	Espinoza-Campuzano	CAEC 2015.9.18	0			0
Carrier	Espinoza-Campuzano	CAEC 2015.9.7	0			0
Carrier	Espinoza-Campuzano	CAEC 2015.9.8	0			0
Colipava India	Espinoza-Campuzano	CAEC 2015.9.1	0			0
Colipava India	Espinoza-Campuzano	CAEC 2015.9.2	0			0
Gigante	Espinoza-Campuzano	CAEC 2015.9.4	0			0
Gigante	Espinoza-Campuzano	CAEC 2015.9.3	0			0
Ladrona	Espinoza-Campuzano	CAEC 2015.9.5	0			0
Ladrona	Espinoza-Campuzano	CAEC 2015.9.6	0			0
Lechuza	Espinoza-Campuzano	CAEC 2015.9.15	1	5	broken	1
Lechuza	Espinoza-Campuzano	CAEC 2015.9.16	0			0
Marchenera	Espinoza-Campuzano	CAEC 2015.9.11	0			0
Marchenera	Espinoza-Campuzano	CAEC 2015.9.12	1	5	difficult to distinguish	1
Maromera	Espinoza-Campuzano	CAEC 2015.9.9	0			0
Maromera	Espinoza-Campuzano	CAEC 2015.9.10	0			0
Mooke	Espinoza-Campuzano	CAEC 2015.9.13	0			0
Mooke	Espinoza-Campuzano	CAEC 2015.9.14	0			0
Trompetera	Espinoza-Campuzano	CAEC 2015.9.23	0			0

Trompetera	Espinoza-Campuzano	CAEC 2015.9.24	0	0
Maltese	Young		0	0
Italian Owl1	Young		0	0
Roller1	Young		0	0
Indian Fantail1	Young		0	0
Hamburg Sticken	Young		0	0
African Owl1	Young		0	0
DSF1	Young		0	0
Archangel1	Young		0	0
Archangel2	Young		0	0
Archangel3	Young		0	0
African Owl2	Young		0	0
African Owl3	Young		0	0
DSF2	Young		0	0
Am Show Racer	Young		0	0
Swallow1	Young		0	0
Swallow2	Young		0	0
Roller2	Young		0	0
Mookie1	Young		0	0
African Owl4	Young		0	0
English Carrier1	Young		0	0
LFCL	Young		0	0
Scandaroon	Young		0	0
English Carrier2	Young		0	0
Indian Fantail2	Young		0	0
Aachen Langer	Young		0	0
GBH1	Young		0	0
African Owl5	Young		0	0
GBH2	Young		0	0
GBH3	Young		0	0
Italian Owl2	Young		0	0

Italian Owl3	Young		0		0
Budapest Shortface1	Young		0		0
Holle Roller	Young		0		0
Indian Fantail	Young		0		0
Magpie1	Young		0		0
Berlin Longface	Young		0		0
Egyptian Bagdad	Young		0		0
American Fantail	Young		0		0
NFlight	Young		0		0
Modena	Young		0		0
Chinese Owl	Young		0		0
Lahore	Young		0		0
Budapest Shortface2	Young		0		0
Dewlap	Young		0		0
VMF	Young		0		0
Helmet	Young		0		0
Bondinette	Young		0		0
Roller3	Young		0		0
Polish Ice Tumbler	Young		0		0
Magpie2	Young		0		0
Archangel	Young		0		0
Polish Srebniack	Young		0		0
Mookie2	Young		0		0
Brunner Pouter	Young		0		0
WoE Tumbler	Young		0		0
Damscene	Young		0		0
Scandaroon1	Young		0		0
Scandaroon2	Young		0		0
		Total	12	Total	4

Table S4.2. Angles and closest eigenvector between the first 10 eigenvectors of each sample.

Domestic vs Feral										
	PC1	PC2	PC3	PC4	PC5	PC6	PC7	PC8	PC9	PC10
PC1	62.76	102.84	135.26	98.96	91.07	85.39	87.08	81.24	88.73	97.74
PC2	69.57	129.22	62.04	98.02	96.49	91.05	90.82	96.09	94.85	90.81
PC3	116.96	105.79	101.09	87.66	83.82	83.15	82.15	105.99	101.43	89.48
PC4	101.87	119.82	93.62	75.32	83.27	75.22	81.26	82.31	80.33	86.98
PC5	86.66	96.76	94.49	103.85	107.83	88.10	84.22	106.12	74.20	84.57
PC6	103.62	94.49	100.28	104.43	112.07	100.01	98.16	99.96	91.70	84.40
PC7	94.57	88.23	88.81	100.01	64.68	68.53	104.37	107.65	96.19	91.93
PC8	106.46	90.48	80.54	111.39	103.76	69.20	107.18	71.99	80.14	94.10
PC9	85.86	92.48	87.84	95.07	81.90	94.41	87.78	82.95	96.20	89.01
PC10	91.00	87.09	89.42	80.72	89.51	79.63	106.13	98.26	67.79	103.41
Closest PC	1	10	2	4	7	7	4	8	10	6
Minimum °	62.76	87.09	62.04	75.32	64.68	68.53	81.26	71.99	67.79	84.40
Average min °	72.59									
Domestic vs Comparative sample										
	PC1	PC2	PC3	PC4	PC5	PC6	PC7	PC8	PC9	PC10
PC1	130.42	51.58	92.32	104.87	91.72	95.92	91.85	79.44	84.75	94.02
PC2	73.97	80.16	63.50	125.55	83.34	100.10	84.95	108.06	86.16	93.62
PC3	82.51	81.51	103.35	77.21	53.77	93.35	77.57	95.51	89.96	100.11
PC4	82.64	70.22	84.48	78.90	92.53	82.81	48.68	89.61	105.85	86.87
PC5	75.91	83.64	87.99	105.67	73.33	102.18	91.78	68.01	94.02	75.87
PC6	106.04	102.84	115.49	100.38	74.01	93.71	79.29	97.00	81.03	92.21

PC7	80.63	75.31	102.73	101.31	97.08	53.22	88.60	106.57	79.19	81.71
PC8	93.91	89.72	68.58	74.72	77.72	89.96	86.82	88.74	59.23	81.10
PC9	82.61	88.44	95.67	101.24	70.13	77.87	105.37	83.74	84.48	97.72
PC10	89.35	94.56	89.74	91.41	79.02	81.17	82.63	75.68	79.96	68.60
Closest PC	2	1	2	8	3	7	4	5	8	10
Minimum °	73.97	51.58	63.50	74.72	53.77	53.22	48.68	68.01	59.23	68.60
Average min °	61.53									

Comparative vs Feral

	PC1	PC2	PC3	PC4	PC5	PC6	PC7	PC8	PC9	PC10
PC1	94.83	95.50	47.89	79.71	83.76	78.36	83.16	110.66	88.73	76.04
PC2	70.78	110.92	106.51	97.10	79.88	69.11	72.40	92.63	86.16	89.71
PC3	84.62	104.52	69.80	98.38	94.29	91.30	90.69	69.16	86.03	93.65
PC4	120.50	64.91	91.97	80.28	88.61	79.07	78.58	79.57	88.69	85.33
PC5	110.52	105.93	97.68	104.52	104.02	89.72	93.74	99.98	87.53	94.64
PC6	107.27	87.62	95.14	97.40	56.44	78.84	100.39	87.17	90.12	93.31
PC7	110.86	125.48	95.74	74.92	92.24	79.42	98.82	93.42	88.02	92.56
PC8	92.82	88.58	104.45	95.11	96.03	100.56	89.84	87.85	75.15	90.47
PC9	94.48	83.18	88.90	103.47	94.52	71.35	107.63	91.87	91.25	89.70
PC10	85.74	78.07	82.29	105.79	88.39	76.12	94.96	94.73	63.20	98.99
Closest PC	2	4	1	7	6	2	2	3	10	1
Minimum °	70.78	64.91	47.89	74.92	56.44	69.11	72.40	69.16	63.20	76.04
Average min °	66.48									

Table S4.3. Scale of vectors

Domestic vs Feral										
	PC1	PC2	PC3	PC4	PC5	PC6	PC7	PC8	PC9	PC10
PC1	74	80	73	75	76	77	74	78	73	75
PC2	73	72	74	79	74	73	69	73	72	69
PC3	77	76	80	78	76	70	73	72	76	78
PC4	80	75	74	76	69	76	76	74	74	73
PC5	77	78	75	78	76	72	77	75	77	78
PC6	75	79	75	77	74	76	75	77	72	78
PC7	73	73	75	76	73	71	76	76	75	75
PC8	73	78	75	76	71	72	75	75	75	75
PC9	78	79	71	75	78	79	79	79	74	77
PC10	77	76	77	75	78	76	74	77	75	76
Min	73	72	71	75	69	70	69	72	72	69
Domestic vs Comparative sample										
	PC1	PC2	PC3	PC4	PC5	PC6	PC7	PC8	PC9	PC10
PC1	72	76	75	76	73	78	72	75	76	75
PC2	76	71	72	73	77	70	72	73	70	74
PC3	75	79	75	79	73	78	76	76	79	79
PC4	79	75	76	68	76	74	76	74	76	78
PC5	77	76	77	79	76	79	76	75	77	78
PC6	75	73	74	80	75	73	77	74	76	77
PC7	71	78	72	78	73	75	75	78	80	73
PC8	74	75	78	80	77	78	74	70	78	74
PC9	77	78	75	79	78	77	77	77	74	80
PC10	76	79	74	79	77	78	76	76	76	77
Min	71	71	72	68	73	70	72	70	70	73
Comparative sample vs Feral										
	PC1	PC2	PC3	PC4	PC5	PC6	PC7	PC8	PC9	PC10
PC1	79	75	70	73	74	69	78	77	72	79
PC2	74	71	74	78	72	70	74	75	74	77
PC3	79	78	75	78	75	74	71	75	78	80
PC4	75	75	75	79	73	76	75	75	75	77
PC5	78	75	69	76	75	76	76	72	72	75
PC6	79	74	77	79	71	78	75	77	73	75
PC7	76	74	70	77	76	76	75	71	76	78
PC8	74	77	74	74	77	75	74	74	72	77
PC9	76	76	70	73	76	75	76	75	74	76
PC10	79	73	75	75	72	74	75	80	75	77
Min	74	71	69	73	71	69	71	71	72	75

Chapter Five. Conclusions

This research contributes to the development versus ecomorphology debate. In doing so, I have subscribed to a pluralistic view of evolution. Throughout this thesis, I have used the skull shape in a geometric morphometric framework to assess the interplay between developmental constraints and ecomorphological factors influencing the evolution of the phenotype.

Allometry and heterochrony in the skull of Columbimorphae

In Chapter Two, I investigated size-related changes (allometry) in the skull shape in Columbimorphae. Columbimorphae is a specious bird clade that contains the Mesitornithiformes (mesites), Pteroclidiformes (sandgrouses) and Columbiformes (pigeons and doves). The extant Columbimorphae range in body mass from 32 grams in the diamond dove (*Geopelia cuneata*) to 2 kg in the Victoria crowned pigeon (*Goura cristata*). Furthermore, the extinct flightless pigeons (Raphini): the dodo (*Raphus cucullatus*) and the Rodrigues solitaire (*Pezophaps solitaria*) could have weighted an order of magnitude more, at 21 and 28 kilograms respectively. Due to this size range, Columbimorphae are a good study system to detect and investigate allometric trends.

In this chapter, I aimed to test allometric trends in skull size and shape in Columbimorphae. I showed that allometry accounts for 11% of the skull shape variation in Columbimorphae, and that negative allometry of head size in comparison to body size is present in the clade,

meaning that many of these species exhibit smaller relative head sizes in comparison to body size as they grow.

I also aimed to explore heterochrony in Columbimorphae. For this, I was able to implement a novel analysis to detect heterochrony in an allometric setting. This test uses shape to predict size. I found that heterochronic patterns can describe the skull shape of Pteroclidiformes (paedomorphosis) and Mesitornithiformes (peramorphosis). My results also showed that allometry and heterochrony can explain a non-negligible proportion of the shape variation in the columbiform skull. Allometry can explain some aspects of the peculiar skull shape of the dodo and the Rodrigues solitaire. However, other aspects of the scull that are not sufficiently explained by allometry or heterochrony are probably related to ecomorphological adaptations (analyses in Chapter Three).

Finally, I found that some species of pigeons (*Didunculus strigirostris* and *Treron curvirostra*) show skull shapes that diverge widely from the overall columbimorph sample and that are impervious to allometric or heterochronic explanations. This suggested that ecomorphological factors might be able to account for the skull shape in these species.

Future work will look in depth into the geometric morphometrics of the skull of Pteroclidiformes and Mesitornithiformes, with a particular emphasis on constructing an ontogenetic sample that might prove the heterochronic relation of these taxa with respect to Columbiformes in a developmental framework.

Ecological factors and their relationship with skull shape in Columbiformes

In Chapter Three, I researched the influence of a series of ecological factors and developmental constraints in columbiform skull shape and biomechanics. One of the objectives of this chapter was to evaluate if these factors could explain the variation left unexplained by allometry and heterochrony (Chapter Two). Particular attention was paid to taxa that were identified as outliers of the purely allometric model of Chapter Two: the dodo, the Rodrigues solitaire, the tooth-billed pigeon (*Didunculus strigirostris*) and the thick-billed green pigeon (*Treron curvirostra*). I found that feeding behaviour factors do explain both skull shape and inferred biomechanical performance. My results suggest that classical Darwinian evolution with selection towards adaptive peaks (frugivory or granivory) has taken place during the evolution of Columbiformes.

I aimed to use dietary and foraging behaviours as ecological factors explaining shape. For this reason, I produced a new characterization of feeding in Columbiformes, which aims to capture the complex interplay between diet and foraging. This new classification, based on a clustering algorithm, divides pigeons into eight different feeding clusters.

I aimed to evaluate the biomechanical landscape of Columbiformes. For this, I designed a model of the pigeon skull which treated the skull as a series of simple machines. This model allowed me to measure the comparative biomechanical performance of several traits in the pigeon skull. I produced a biomechanical "fitness" landscape that allowed me to characterize the differences in performance across the pigeon morphospace. I found clear differences between granivorous and frugivorous pigeon species, frugivorous species showed higher resistance to bending and higher muscle areas, while granivorous species

tend to have straight thin rostra with low bending resistance, small muscle area, and larger eye sizes.

In this chapter, I also aimed to assess developmental constraints (modularity and integration) of the columbiform skull. I found that the columbiform skull is a *globally disintegrated* structure, with weak modularity and moderate integration. These patterns of integration and modularity do not adequately explain the variation found in these skulls. However, I found that different modules are influenced in various degrees by ecological factors, with the rostrum being more affected by ecomorphological variables.

I finally argue for the recognition of an adaptive radiation in Raphinae (a clade within Columbiformes which includes the genera *Didunculus*, *Pezophaps*, *Raphus*, *Caloenas*, *Goura*, *Otidiphaps*, and *Trugon*). This adaptive radiation might be comparable, in terms of morphological disparity, to other remarkable bird adaptive radiations like the Galapagos finches (Geospizinae), Hawaiian honeycreepers (Drepanidinae), and Madagascan vangas (Vangidae) albeit happening on several distant islands. Future directions for this work will be to implement the new pigeon feeding characterization across all columbiform species, taking size into account.

Artificial and natural selection work on different axes of variation

In Chapter four, I investigated the phenotypic matrix of the comparative sample from previous chapters and compared it with a sample of feral *Columba livia* and a sample of domestic fancy *C. livia*. I decided to use a series of multivariate tests to evaluate the

similarity of matrices, response to selection and preferential evolutionary axis (lines of least evolutionary resistance).

I aimed to assess how the axes of variation of one species (*C. livia*) can predict the axes of variation across taxonomic scales. I observed a low similarity of variation patterns between samples and between selection types (artificial versus natural). My results warn against generalizing patterns of variation of one species across broad ranges of phylogenetic diversity (multiple lineages).

I aimed to use the lines of least resistance approach to test which axes of variation have been explored during domestication. I found that novel shapes seen in domesticated pigeons are not only more extreme forms of the natural variation in pigeons but also the exploration of novel axes of variation.

I characterized the morphospace of the comparative sample and projected domestic and feral pigeons into this morphospace. I found that domestic fancy pigeons have occupied a more substantial proportion of the morphospace than the order Columbiformes; however, some specific regions of morphospace have been occupied only by domesticated or only by naturally selected pigeons.

Summary

My overall results highlight the importance of taking a pluralistic view of evolution while assessing the evolutionary history of a group. While developmental factors like allometry were adequate to predict the shape of the Raphini, the Pteroclidiformes and the Mesitornithiformes (Chapter Two), other factors like modularity and integration played a smaller role in pigeon evolution (Chapter Three). I was able to confirm that different

selection regimes (artificial versus natural selection) can modify the phenotypic matrix of species (Chapter Four), and that domestication has used novel axes of variation, possibly derived from mutations occurring and accumulating during the domestication process. My research also suggests that generalizing patterns of one species across taxonomic scales might be incorrect.

Finally, throughout this thesis, I have warned of the dangers of not taking the expected similarity into account while conducting evolutionary research. This is particularly salient when developmental constraints like integration and modularity are being assessed. These approaches might correctly identify a similarity between matrices, but this similarity might be caused by geometric scaling. To this day, the best way to ward against this effect is to take allometry into account. However, more research is needed to estimate the impact of the expected similarity in integration and modularity patterns.

References

Adams, D. C. (2014) 'A method for assessing phylogenetic least squares models for shape and other high-dimensional multivariate data', *Evolution*, 68(9), pp. 2675–2688. doi: 10.1111/evo.12463.

Adams, D. C. (2016) 'Evaluating modularity in morphometric data: Challenges with the RV coefficient and a new test measure', *Methods in Ecology and Evolution*, 7(5), pp. 565–572. doi: 10.1111/2041-210X.12511.

Adams, D. C. and Collyer, M. L. (2016) 'On the comparison of the strength of morphological integration across morphometric datasets', *Evolution*, 70(11), pp. 2623–2631. doi: 10.1111/evo.13045.

Adams, D. C. and Collyer, M. L. (2018) 'Multivariate Phylogenetic Comparative Methods: Evaluations, Comparisons, and Recommendations', *Systematic Biology*, 67(1), pp. 14–31. doi: 10.1093/sysbio/syx055.

Adams, D. C. and Felice, R. N. (2014) 'Assessing trait covariation and morphological integration on phylogenies using evolutionary covariance matrices', *PLoS ONE*, 9(4). doi: 10.1371/journal.pone.0094335.

Adams, D. C. and Otárola-Castillo, E. (2013) 'Geomorph: an R Package for the Collection and Analysis of Geometric Morphometric Shape Data', *Methods in Ecology and Evolution*, 4(4), pp. 393–399. doi: 10.1111/2041-210X.12035.

Adams, D. C., Rohlf, F. J. and Slice, D. E. (2004) 'Geometric morphometrics: Ten years of progress following the "revolution"', *Italian Journal of Zoology*, 71(1), pp. 5–16. doi: 10.1080/11250000409356545.

Adams, D. C., Rohlf, F. J. and Slice, D. E. (2013) 'A field comes of age: Geometric morphometrics in the 21st century', *Hystrix*, 24(1), pp. 7–14. doi: 10.4404/hystrix-24.1-6283.

Aguirre, J. D. *et al.* (2014) 'Comparing G: multivariate analysis of genetic variation in multiple populations', *Heredity*, 112(1), pp. 21–29. doi: 10.1038/hdy.2013.12.

Andersson, K., Norman, D. and Werdelin, L. (2011) 'Sabretoothed carnivores and the killing of large prey', *PLoS ONE*, 6(10), pp. 8–13. doi: 10.1371/journal.pone.0024971.

Angst, D., Buffetaut, E. and Abourachid, A. (2011) 'The end of the fat dodo? A new mass estimate for Raphus cucullatus', *Naturwissenschaften*, 98(3), pp. 233–236. doi: 10.1007/s00114-010-0759-7.

Arnold, S. J. (1983) 'Morphology , Performance and Fitness', *American Zoologist*, 23(2), pp. 347–361. doi: 10.1093/icb/23.2.347.

Arnold, S. J. and Phillips, P. C. (1999) 'Hierarchical Comparison of Genetic Variance-Covariance Matrices. Ii Coastal-Inland Divergence in the Garter Snake, Thamnophis Elegans', *Evolution*, 53(5), pp. 1516–1527. doi: 10.2307/2640897.

Asano, M. *et al.* (2013) 'A model of epigenetic evolution based on theory of open quantum systems', *Systems and Synthetic Biology*, 7(4), pp. 161–173. doi: 10.1007/s11693-013-9109-3.

Ashley, K., Cordell, D. and Mavinic, D. (2011) 'A brief history of phosphorus: From the philosopher's stone to nutrient recovery and reuse', *Chemosphere*. Elsevier Ltd, 84(6), pp. 737–746. doi: 10.1016/j.chemosphere.2011.03.001.

Atwell, D. (1996) 'BIRD IN THE DOVECOTE IS WORTH TWO IN THE BUSH', *The Avicultural Magazine*,

102(4), pp. 169–173.

Auerbach, B. M. and Ruff, C. B. (2004) 'Human body mass estimation: A comparison of "morphometric" and "mechanical" methods', *American Journal of Physical Anthropology*, 125(4), pp. 331–342. doi: 10.1002/ajpa.20032.

Baumel, J. J. (1993) *Handbook of avian anatomy: Nomina anatomica avium*. 2nd edn. Edited by A. Raymond and J. Paymer. Publications of the Nuttal ornithological club.

Bedrick, E. J. and Tsai, C.-L. (1994) 'Model Selection for Multivariate Regression in Small Samples', *Biometrics*, 50(1), p. 226. doi: 10.2307/2533213.

Benson, R. B. J. *et al.* (2017) 'Comparative analysis of vestibular ecomorphology in birds', *Journal of Anatomy*, 231(6), pp. 990–1018. doi: 10.1111/joa.12726.

Benson, R. B. J. and Choiniere, J. N. (2013) 'Rates of dinosaur limb evolution provide evidence for exceptional radiation in Mesozoic birds', *Proceedings of the Royal Society B: Biological Sciences*, 280(1768), pp. 1–7. doi: 10.1098/rspb.2013.1780.

BirdLife International (2018) *IUCN Red List for birds*, *http://www.birdlife.org*.

Blockstein, D. E. and Tordoff, H. B. (1985) 'Gone forever: A contemporary look at the extinction of the passenger pigeon', *American birds*, 39(5), pp. 845–851.

Blonder, B. *et al.* (2014) 'The n-dimensional hypervolume', *Global Ecology and Biogeography*. John Wiley & Sons, Ltd, 23(5), pp. 595–609. doi: 10.1111/geb.12146.

Boag, P. T. (1983) 'The Heritability of External Morphology in Darwin's Ground Finches (Geospiza) on Isla Daphne Major, Galapagos', *Evolution*, 35(5), pp. 877–894. doi: 10.2307/2408404.

Bolnick, D. I. *et al.* (2010) 'Ecological release from interspecific competition leads to decoupled changes in population and individual niche width', *Proceedings of the Royal Society B: Biological Sciences*, 277(1689), pp. 1789–1797. doi: 10.1098/rspb.2010.0018.

Bookstein, F. L. (1991) *Morphometric tools for landmark data: geometry and biology*. Cambridge University Press.

Bookstein, F. L. (1996) 'Shape and the information in medical images: a decade of the morphometric synthesis', *Proceedings of the Workshop on Mathematical Methods in Biomedical Image Analysis*, 66(2), pp. 97–118. doi: 10.1109/MMBIA.1996.534052.

Bookstein, F. L. (1997) 'Landmark methods for forms without lendmarks: morphometrics of group difference in outline shape', *Medical Image Analysis*, 1(3), pp. 225–243. Available at: http://www.ncbi.nlm.nih.gov/pubmed/9873908.

Bookstein, F. L. (2015) 'Integration, Disintegration, and Self-Similarity: Characterizing the Scales of Shape Variation in Landmark Data', *Evolutionary Biology*. Springer US, 42(4), pp. 395–426. doi: 10.1007/s11692-015-9317-8.

Brassey, C. A. *et al.* (2016) 'Convex-hull mass estimates of the dodo (Raphus cucullatus): application of a CT-based mass estimation technique', *PeerJ*, 4:e1432, pp. 1–18. doi: 10.7717/peerj.1432.

Bright, J. A. *et al.* (2016) 'The shapes of bird beaks are highly controlled by nondietary factors', *Proceedings of the National Academy of Sciences*, 113(19), pp. 5352–5357. doi: 10.1073/pnas.1602683113.

Brooke, M. D. L. *et al.* (1999) 'The scaling of eye size with body mass in birds The scaling of eye size with body mass in birds', (October 1998), pp. 405–412. doi: 10.1098/rspb.1999.0652.

Cheverud, J. M. (1988) 'A Comparison of Genetic and Phenotypic Correlations', *Evolution*, 42(5), p. 958. doi: 10.2307/2408911.

Cheverud, J. M. and Marroig, G. (2007) 'Comparing covariance matrices: Random skewers method compared to the common principal components model', *Genetics and Molecular Biology*, 30(2), pp. 461–469. doi: 10.1590/S1415-47572007000300027.

Cignoni, P. *et al.* (2008) 'MeshLab: an Open-Source Mesh Processing Tool', *Sixth Eurographics Italian Chapter Conference*, pp. 129–136. doi: 10.2312/LocalChapterEvents/ItalChap/ItalianChapConf2008/129-136.

Claessens, L. P. A. M., Meijer, H. J. M. and Hume, J. P. (2015) 'The Morphology of the Thirioux dodos', *Journal of Vertebrate Paleontology*, 35(sup1), pp. 29–187. doi: 10.1080/02724634.2015.1121723.

Clarke, K. R., Somerfield, P. J. and Gorley, R. N. (2008) 'Testing of null hypotheses in exploratory community analyses: similarity profiles and biota-environment linkage', *Journal of Experimental Marine Biology and Ecology*, 366(1–2), pp. 56–69. doi: 10.1016/j.jembe.2008.07.009.

Clements, J. F. *et al.* (2017) *The eBird/Clements checklist of birds of the world: v2016*. Available at: http://www.birds.cornell.edu/clementschecklist/download/.

Collyer, M. L., Sekora, D. J. and Adams, D. C. (2015) 'A method for analysis of phenotypic change for phenotypes described by high-dimensional data', *Heredity*. Nature Publishing Group, 115(4), pp. 357–365. doi: 10.1038/hdy.2014.75.

Cooney, C. R. *et al.* (2017) 'Mega-evolutionary dynamics of the adaptive radiation of birds', *Nature*. Nature Publishing Group, 542(7641), pp. 344–347. doi: 10.1038/nature21074.

Cuff, A. R. and Rayfield, E. J. (2013) 'Feeding Mechanics in Spinosaurid Theropods and Extant Crocodilians', *PLoS ONE*, 8(5), pp. 1–11. doi: 10.1371/journal.pone.0065295.

Darwin, C. R. (1859) *On the origin of species by means of natural selection, or the preservation of favoured races in the struggle for life*. London: John Murray.

Darwin, C. R. (1868) *The variation of animals and plants under domestication*. Cambridge University Press. doi: 10.1017/CBO9780511709500.

Davis, B. W. *et al.* (2015) 'Mechanisms underlying mammalian hybrid sterility in two feline interspecies models', *Molecular Biology and Evolution*, 32(10), pp. 2534–2546. doi: 10.1093/molbev/msv124.

Dehling, D. M. *et al.* (2016) 'Morphology predicts species' functional roles and their degree of specialization in plant–Frugivore interactions', *Proceedings of the Royal Society B: Biological Sciences*, 283(1823). doi: 10.1098/rspb.2015.2444.

Demes, B. and Creel, N. (1988) 'Bite force, diet, and cranial morphology of fossil hominids', *Journal of Human Evolution*, 17(7), pp. 657–670. doi: 10.1016/0047-2484(88)90023-1.

Denton, J. S. S. and Adams, D. C. (2015) 'A new phylogenetic test for comparing multiple high-dimensional evolutionary rates suggests interplay of evolutionary rates and modularity in lanternfishes (Myctophiformes; Myctophidae)', *Evolution*, 69(9), pp. 2425–2440. doi: 10.1111/evo.12743.

Diamond, J. M. (1973) 'Distributional Ecology of New Guinea Birds', *Science*, 179(February), pp. 759–770.

Dicker, J. J., Pennock, G. R. and Shigley, J. E. (2003) *Theory of Machines and Mechanisms*. 3rd edn. New York, Oxford: Oxford University Press.

Dobzhansky, T. (1956) 'What is an adaptive trait?', *The American Naturalist*, 90(855), pp. 337–347.

Dollion, A. Y. *et al.* (2017) 'Does diet drive the evolution of head shape and bite force in chameleons of the genus Bradypodion?', *Functional Ecology*, 31(3), pp. 671–684. doi: 10.1111/1365-2435.12750.

Domyan, E. T. and Shapiro, M. D. (2016) 'Pigeonetics takes flight: Evolution, development, and genetics of intraspecific variation', *Developmental Biology*, 427(September 2016), pp. 241–250. doi: 10.1016/j.ydbio.2016.11.008.

Drake, A. G. (2011) 'Dispelling dog dogma: An investigation of heterochrony in dogs using 3D geometric morphometric analysis of skull shape', *Evolution and Development*, 13(2), pp. 204–213. doi: 10.1111/j.1525-142X.2011.00470.x.

Drake, A. G. and Klingenberg, C. P. (2008) 'The pace of morphological change: historical transformation of skull shape in St Bernard dogs', *Proceedings of the Royal Society B: Biological Sciences*, 275(1630), pp. 71–76. doi: 10.1098/rspb.2007.1169.

Drake, A. G. and Klingenberg, C. P. (2010) 'Large-scale diversification of skull shape in domestic dogs: disparity and modularity.', *The American naturalist*, 175(3), pp. 289–301. doi: 10.1086/650372.

Dumont, E. R. *et al.* (2014) 'Selection for mechanical advantage underlies multiple cranial optima in new world leaf-nosed bats', *Evolution*, 68(5), pp. 1436–1449. doi: 10.1111/evo.12358.

Dunning, J. and John, B. (2008) *CRC Handbook of Avian Body Masses*, *CRC handbook of avian body masses. Second edition.* doi: 10.1017/S0963180113000479.

Emerson, S. B. and Radinsky, L. (1980) 'Functional analysis of sabertooth cranial morphology', *Paleobiology*, 6(3), pp. 295–312. doi: 10.1017/S0094837300006813.

Evin, A. *et al.* (2017) 'Data from: A test for paedomorphism in domestic pig cranial morphology. Dryad Digital Repository (doi:10.5061/dryad.c3f25).'

Felice, R. N. and Goswami, A. (2017) 'Developmental origins of mosaic evolution in the avian cranium', *Proceedings of the National Academy of Sciences*, p. 201716437. doi: 10.1073/pnas.1716437115.

Felsenstein, J. (1985) 'Phylogenies and the comparative method', *Am. Nat*, 125(125), pp. 3–147. doi: 10.1086/284325.

Fitch, W. (2000) 'Skull dimensions in relation to body size in nonhuman mammals: The causal bases for acoustic allometry', *Zoology-Analysis of Complex Systems*, pp. 40–58. Available at: http://www.st-andrews.ac.uk/~wtsf/downloads/Fitch2000Zoology.pdf.

Flury, B. (1988) *Common principal components & related multivariate models*. New York, Chichester: Wiley-Blackwell.

Foster, D. J., Podos, J. and Hendry, a. P. (2008) 'A geometric morphometric appraisal of beak shape in Darwin's finches', *Journal of Evolutionary Biology*, 21(1), pp. 263–275. doi: 10.1111/j.1420-9101.2007.01449.x.

Franckowiak, R. P. *et al.* (2017) 'Model selection with multiple regression on distance matrices leads to incorrect inferences', *PLoS ONE*, 12(4), pp. 1–13. doi: 10.1371/journal.pone.0175194.

Futuyma, D. J. and Kirkpatrick, M. (2018) *Evolution*. Massachusetts: Sinauer Associates.

Garamszegi, L. Z. (2014) *Modern phylogenetic comparative methods and their application in evolutionary biology*, *Modern Phylogenetic Comparative Methods and their Application in Evolutionary Biology*. doi: 10.1007/978-3-662-43550-2.

Garamszegi, L. Z., Møller, A. P. and Erritzøe, J. (2002) 'Coevolving avian eye size and brain size in relation to prey capture and nocturnality', *Proceedings of the Royal Society B: Biological Sciences*, 269(1494), pp. 961–967. doi: 10.1098/rspb.2002.1967.

Garland, Jr., T. and Ives, A. R. (2000) 'Using the Past to Predict the Present: Confidence Intervals for Regression Equations in Phylogenetic Comparative Methods', *The American Naturalist*, 155(3), pp. 346–364. doi: 10.1086/303327.

Gibbs, D., Barnes, E. and Cox, J. (2010) *Pigeons and doves: A guide to the pigeons and dove of the world*, *The New Encylopedia of Birds*. doi: 10.1676/0043-5643(2001)113[0257:OL]2.0.CO;2.

Gilbert, M. T. P. and Shapiro, M. D. (2013) 'Pigeons, Domestication of', in Smith, C. (ed.) *Encyclopedia of Global Archaeology*. New York: Springer Science+Business Media, pp. 1–5. doi: 10.1007/978-1-4419-0465-2.

Gill, P. G. *et al.* (2014) 'Dietary specializations and diversity in feeding ecology of the earliest stem mammals', *Nature*. Nature Publishing Group, 512(7514), pp. 303–305. doi: 10.1038/nature13622.

Gillespie, M. J. *et al.* (2012) 'Functional Similarities between Pigeon "Milk" and Mammalian Milk: Induction of Immune Gene Expression and Modification of the Microbiota', *PLoS ONE*, 7(10), pp. 1–10. doi: 10.1371/journal.pone.0048363.

Goodwin, D. (1983) *Pigeons and Doves of the World*. 3rd edn. Ithaca, New York: Cornell University Press.

Gopalakrishnan, S. *et al.* (2018) 'Interspecific Gene Flow Shaped the Evolution of the Genus Canis', *Current Biology*, 28(21), p. 3441–3449.e5. doi: 10.1016/j.cub.2018.08.041.

Goswami, A. and Polly, P. D. (2010) 'Methods for studying morphological integration and modularity', in Alroy, J. and Hunt, G. (eds) *Quantitative methods in paleobiology*. Ithaca (NY): Paleontological Societ, pp. 213–243.

Gould, S. J. (1966) 'Allometry and Size in Ontogeny and Phylogeny', *Biological Reviews*, 41(4), pp. 587–638. doi: 10.1111/j.1469-185X.1966.tb01624.x.

Gould, S. J. (1971) 'Geometric Similarity in Allometric Growth: A Contribution to the Problem of Scaling in the Evolution of Size', *The American Naturalist*, 105(942), pp. 113–136. doi: 10.1086/282710.

Gould, S. J. (1973) 'Positive allometry of antlers in the "Irish elk", Megaloceros giganteus', *Nature*, 244(10), pp. 375–376. doi: 10.1038/227680a0.

Gould, S. J. (1974) 'The origin and function of "bizarre" structures: antler size and skull size in the "Irish elk", Megalocerus giganteus', *Evolution*, 28(June), pp. 191–220. doi: DOI: 10.2307/2407322.

Gould, S. J. (1977) *Ontogeny and phylogeny*. Cambridge: Harvard University Press.

Gould, S. J. and Lewontin, R. C. (1979) 'The Spandrels of San Marco and the Panglossian Paradigm : A Critique of the Adaptationist Programme', *Proceedings of the Royal Society B: Biological Sciences*, 205(1161), pp. 581–598.

Goulet, B. E., Roda, F. and Hopkins, R. (2017) 'Hybridization in Plants: Old Ideas, New Techniques', *Plant Physiology*, 173(1), pp. 65–78. doi: 10.1104/pp.16.01340.

Gower, J. C. (1966) 'Some distance properties of latent root and vector methods used in multivariate analysis', *Biometrika*, 53(3 and 4), pp. 325–338.

Gower, J. C. (1975) 'Generalized procrustes analysis', *Psychometrika*, 40(1), pp. 33–51. doi: 10.1007/BF02291478.

Grafen, A. (1989) 'The phylogenetic regression', *Philosophical Transactions of the Royal Society of London, For 1683-94 (Abridged)*, 326(1233), pp. 119–157.

Grafen, A. and Hails, R. (2002) *Modern Statistics for the Life Sciences*. 1st edn. Oxford University Press, USA.

Grant, P. R. and Grant, B. R. (1995) 'Predicting Microevolutionary Responses to Directional Selection on Heritable Variation', *Evolution*, 49(2), pp. 241–251. doi: DOI: 10.2307/2410334.

Griffin, R. H. (2017) *Missing 3D landmarks in objects with bilateral symmetry: reflecting points across a plane*, *http://rgriff23.github.io/index.html*. Available at: http://rgriff23.github.io/2017/06/09/reflect-3d-points-across-plane.html (Accessed: 14 May 2018).

Gunz, P. *et al.* (2009) 'Principles for the virtual reconstruction of hominin crania', *Journal of Human Evolution*. Elsevier Ltd, 57(1), pp. 48–62. doi: 10.1016/j.jhevol.2009.04.004.

Hackett, S. J. *et al.* (2008) 'A Phylogenomic Study of Birds Reveals Their Evolutionary History', *Science*, 320(5884), pp. 1763–1768. doi: 10.1126/science.1157704.

Hadfield, J. D. (2010) 'MCMC methods for multi-response generalized linear mixed models: the MCMCglmm R package', *Journal of Statistical Software*. doi: 10.1002/ana.22635.

Hailer, F. and Leonard, J. A. (2008) 'Hybridization among three native North American Canis species in a region of natural sympatry', *PLoS ONE*, 3(10). doi: 10.1371/journal.pone.0003333.

Hallgrímsson, B. *et al.* (2009) 'Deciphering the palimpsest: Studying the relationship between morphological integration and phenotypic covariation', *Evolutionary Biology*, 36(4), pp. 355–376. doi: 10.1007/s11692-009-9076-5.

Hansen, T. F. and Houle, D. (2008) 'Measuring and comparing evolvability and constraint in multivariate characters', *Journal of Evolutionary Biology*, 21(5), pp. 1201–1219. doi: 10.1111/j.1420-9101.2008.01573.x.

Hardin, G. (1960) 'The Competitive Exclusion Principle', *Science*, 131(3409), pp. 1292–1297. doi: 10.1126/science.131.3409.1292.

Harmon, L. J. *et al.* (2010) 'Early bursts of body size and shape evolution are rare in comparative data', *Evolution*, 64(8), pp. 2385–2396. doi: 10.1111/j.1558-5646.2010.01025.x.

Helms, J. a. and Brugmann, S. a. (2007) 'The origins of species-specific facial morphology: The proof is in the pigeon', *Integrative and Comparative Biology*, 47(3), pp. 338–342. doi: 10.1093/icb/icm051.

Henderson, D. M. and Snively, E. (2004) 'Tyrannosaurus en pointe: allometry minimized rotational

inertia of large carnivorous dinosaurs', *Proceedings of the Royal Society B: Biological Sciences*, 271(Suppl_3), pp. S57–S60. doi: 10.1098/rsbl.2003.0097.

Herrel, A. *et al.* (2005) 'Evolution of bite force in Darwin's finches: A key role for head width', *Journal of Evolutionary Biology*, 18(3), pp. 669–675. doi: 10.1111/j.1420-9101.2004.00857.x.

Hersh, A. (1934) 'Evolutionary Relative Growth in the Titanotheres', *The American Naturalist*, 68(719), pp. 537–561. Available at: https://www.jstor.org/stable/2456730.

van Heteren, A. H. *et al.* (2017) 'Neither slim nor fat: estimating the mass of the dodo (Raphus cucullatus , Aves, Columbiformes) based on the largest sample of dodo bones to date', *PeerJ*, 5:e4110, pp. 1–19. doi: 10.7717/peerj.4110.

Heupink, T. H., Van Grouw, H. and Lambert, D. M. (2014) 'The mysterious Spotted Green Pigeon and its relation to the Dodo and its kindred', *BMC Evolutionary Biology*, 14(1). doi: 10.1186/1471-2148-14-136.

Hoyo, J. *et al.* (2017) *Handbook of the Birds of the World Alive*, *Lynx Edicions, Barcelona.* Available at: http://www.hbw.com/ (Accessed: 12 February 2017).

Del Hoyo, J. *et al.* (2004) *Handbook of the Birds of the World*, *Lynx Edicions, Barcelona, Spain*.

del Hoyo, J., Elliott, A. and Christie, D. A. (2004) *Handbook of the Birds of the World 1-16*. Barcelona: Lynx Press.

Hubbe, A., Melo, D. and Marroig, G. (2016) 'A case study of extant and extinct Xenarthra cranium covariance structure: Implications and applications to paleontology', *Paleobiology*, 42(3), pp. 465–488. doi: 10.1017/pab.2015.49.

Hume, J. P. (2011) *Systematics, morphology, and ecology of pigeons and doves (Aves: Columbidae) of the Mascarene Islands, with three new species*, *Zootaxa*.

Hume, J. P. (2012) 'The Dodo: From extinction to the fossil record', *Geology Today*, 28(4), pp. 147–151. doi: 10.1111/j.1365-2451.2012.00843.x.

Hung, C.-M. *et al.* (2014) 'Drastic population fluctuations explain the rapid extinction of the passenger pigeon', *Proceedings of the National Academy of Sciences*, 111(29), pp. 10636–10641. doi: 10.1073/pnas.1401526111.

Hutchinson, G. E. (1957) 'Concluding remarks', *Cold Spring Harbor Symposia on Quantitative Biology*, 22, pp. 415–427. doi: http://dx.doi.org/10.1101/SQB.1957.022.01.039.

Ingram, T. and Mahler, D. L. (2013) 'SURFACE: detecting convergent evolution from comparative data by fitting Ornstein-Uhlenbeck models with stepwise Akaike Information Criterion', *Methods in Ecology and Evolution*. Edited by T. Hansen, 4(5), pp. 416–425. doi: 10.1111/2041-210X.12034.

Janoo, A. (2005) 'Discovery of isolated dodo bones [Raphus cucullatus (L.), Aves, Columbiformes] from Mauritius cave shelters highlights human predation, with a comment on the status of the family Raphidae Wetmore, 1930', *Annales de Paleontologie*, 91(2), pp. 167–180. doi: 10.1016/j.annpal.2004.12.002.

Jarvis, E. D. *et al.* (2014) 'Whole-genome analyses resolve early branches in the tree of life of modern birds', *Science*, 346(6215), pp. 1320–1331. doi: 10.1126/science.1253451.

Jetz, W. *et al.* (2012) 'The global diversity of birds in space and time', *Nature*, 491(7424), pp. 444–448. doi: 10.1038/nature11631.

Johnson, K. P. *et al.* (2010) 'The flight of the Passenger Pigeon: Phylogenetics and biogeographic history of an extinct species', *Molecular Phylogenetics and Evolution*. Elsevier Inc., 57(1), pp. 455–458. doi: 10.1016/j.ympev.2010.05.010.

Johnston, R. F. (1990) 'Variation in size and shape in pigeons, Columba livia', *The Wilson Bulletin*, 102(2), pp. 213–225.

Johnston, R. F. (1992) 'Evolution in the Rock Dove - Skeletal Morphology', *Auk*, 109(3), pp. 530–542.

Johnston, R. F. and Janinga, M. (1995) *Feral Pigeons*. Oxford: Oxford University Press.

Jønsson, K. A. *et al.* (2012) 'Ecological and evolutionary determinants for the adaptive radiation of the Madagascan vangas.', *Proceedings of the National Academy of Sciences of the United States of America*, 109(17), pp. 6620–5. doi: 10.1073/pnas.1115835109.

Junker, R. R. *et al.* (2016) 'Dynamic range boxes - a robust nonparametric approach to quantify size and overlap of n -dimensional hypervolumes', *Methods in Ecology and Evolution*. Edited by D. Orme. John Wiley & Sons, Ltd, 7(12), pp. 1503–1513. doi: 10.1111/2041-210X.12611.

Kendall, D. G. (1984) 'Shape manifolds, procrustean metrics, and complex projective spaces', *Bulletin of the London Mathematical Society*, 16(2), pp. 81–121. doi: 10.1112/blms/16.2.81.

Kim, W. and Bush, J. W. M. (2012) 'Natural drinking strategies', *Journal of Fluid Mechanics*, 705, pp. 7–25. doi: 10.1017/jfm.2012.122.

Klingenberg, C. P. (1998) 'Heterochrony and allometry: The analysis of evolutionary change in ontogeny', *Biological Reviews*, 73(1), pp. 79–123. doi: 10.1111/j.1469-185X.1997.tb00026.x.

Klingenberg, C. P. (2008) 'Morphological Integration and Developmental Modularity', *Annual Review of Ecology, Evolution, and Systematics*, 39(1), pp. 115–132. doi: 10.1146/annurev.ecolsys.37.091305.110054.

Klingenberg, C. P. (2009) 'Morphometric integration and modularity in configurations of landmarks: Tools for evaluating a priori hypotheses', *Evolution and Development*, 11(4), pp. 405–421. doi: 10.1111/j.1525-142X.2009.00347.x.

Klingenberg, C. P. (2014) 'Studying morphological integration and modularity at multiple levels: concepts and analysis', *Philosophical Transactions of the Royal Society B: Biological Sciences*, 369(1649), pp. 20130249–20130249. doi: 10.1098/rstb.2013.0249.

Klingenberg, C. P. (2016) 'Size, shape, and form: concepts of allometry in geometric morphometrics', *Development Genes and Evolution*. Development Genes and Evolution, 226(3), pp. 113–137. doi: 10.1007/s00427-016-0539-2.

Klingenberg, C. P. and Marugán-Lobón, J. (2013) 'Evolutionary covariation in geometric morphometric data: Analyzing integration, modularity, and allometry in a phylogenetic context', *Systematic Biology*, 62(4), pp. 591–610. doi: 10.1093/sysbio/syt025.

Kodandaramaiah, U. (2009) 'Use of dispersal-vicariance analysis in biogeography - a critique', *Journal of Biogeography*, 37(1), pp. 3–11. doi: 10.1111/j.1365-2699.2009.02221.x.

Krzanowski, W. J. (1979) 'Between-Groups Comparison of Principal Components', *Journal of the American Statistical Association*, 74(367), pp. 703–707. Available at: https://www.jstor.org/stable/2286995.

Krzanowski, W. J. (1993) 'Permutational tests for correlation matrices', *Statistics and Computing*,

3(1), pp. 37–44. doi: 10.1007/BF00146952.

Krzanowski, W. J. (2000) 'Principles of Multivariate Analysis. A User's Perspective', *Oxford Statistical Science Series No. 23*.

Lande, R. (1979) 'Quantitative Genetic Analysis of Multivariate Evolution , Applied to Brain:Body Size Allometry', *Evolution*, 33(1), pp. 402–416. doi: 10.2307/2407630.

Lande, R. and Arnold, S. (1983) 'The Measurement of Selection on Correlated Characters', *Evolution*, 37(6), pp. 1210–1226. doi: 10.3740/MRSK.2017.27.12.705.

Langerhans, B. and Reznick, D. N. (2010) 'Swimming Performance in Fishes : Predicting Evolution with Biomechanics', in Domenici, P. and Kapoor, B. G. (eds) *Fish locomotion, an eco-etological perspective*. 1st edn. CRC press.

Lapiedra, O. *et al.* (2013) 'Behavioural changes and the adaptive diversification of pigeons and doves', *Proceedings of the Royal Society B: Biological Sciences*, 280(1755). doi: 10.1098/rspb.2012.2893.

Larson, G. and Fuller, D. Q. (2014) 'The Evolution of Animal Domestication', *Annual Review of Ecology, Evolution, and Systematics*, 45(1), pp. 115–136. doi: 10.1146/annurev-ecolsys-110512-135813.

Li, G. *et al.* (2016) 'Phylogenomic evidence for ancient hybridization in the genomes of living cats (Felidae)', *Genome Research*, 26(1), pp. 1–11. doi: 10.1101/gr.186668.114.

Lijtmaer, D. A., Mahler, B. and Tubaro, P. L. (2003) 'Hybridization and postzygotic isolation patterns in pigeons and doves', *Evolution*, 57(6), pp. 1411–1418. doi: 10.1111/j.0014-3820.2003.tb00348.x.

Liu, B., Rooker, S. M. and Helms, J. A. (2010) 'Molecular control of facial morphology', *Seminars in Cell and Developmental Biology*. Elsevier Ltd, 21(3), pp. 309–313. doi: 10.1016/j.semcdb.2009.09.002.

Livezey, B. C. (1993) 'An ecomorphological review of the dodo Raphus cucullatus and solitaire (Pezophaps solitaria), flightless Columbiformes of the Mascarene Islands', *Journal of Zoology*, 230(2), pp. 247–292. doi: 10.1111/j.1469-7998.1993.tb02686.x.

Loog, L. *et al.* (2017) 'Inferring allele frequency trajectories from ancient DNA indicates that selection on a chicken gene coincided with changes in medieval husbandry practices', *Molecular Biology and Evolution*, 34(8), pp. 1981–1990. doi: 10.1093/molbev/msx142.

Louchart, A. and Mourer-Chauviré, C. (2011) 'The dodo was not so slim: Leg dimensions and scaling to body mass', *Naturwissenschaften*, 98(4), pp. 357–358. doi: 10.1007/s00114-011-0771-6.

Luniak, M. (2004) 'Synurbization - adaptation of animal wildlife to urban development', in Shaw, W., Harris, L. K., and Van Druff, L. (eds) *Proceedings of the 4th International Symposium on Urban Wildlife Conservation. Tucson, AZ: University of Arizona*.

MacArthur, R. H. (1958) 'Population Ecology of Some Warblers of Northeastern Coniferous Forests', *Ecology*, 39(4), pp. 599–619.

MacLeod, N. (2006) 'PalaeoMath: Part 7 - Minding your Rs and Qs I', *The Palaeontology Newsletter*, (61), pp. 42–60.

MacLeod, N. (2007) 'PalaeoMath 101 Data Blocks and Partial Least Squares Analysis', *The Palaeontology Newsletter*, (59), pp. 36–48.

MacLeod, N. (2013a) 'PalaeoMath 101 Landmarks and Semilandmarks: Differences without Meaning and Meaning without Difference', *The Palaeontology Newsletter*, 82, pp. 32–43.

MacLeod, N. (2013b) 'Palaeomath101: Semilandmarks and Surfaces', *The Palaeontology Newsletter*, 83, pp. 37–52. doi: 0954-9900.

Mahler, D. L. *et al.* (2010) 'Ecological opportunity and the rate of morphological evolution in the diversification of greater Antillean anoles', *Evolution*, 64(9), pp. 2731–2745. doi: 10.1111/j.1558-5646.2010.01026.x.

Marroig, G. and Cheverud, J. (2010) 'Size as a line of least resistance II: Direct selection on size or correlated response due to constraints', *Evolution*, 64(5), pp. 1470–1488. doi: 10.1111/j.1558-5646.2009.00920.x.

Marroig, G. and Cheverud, J. M. (2005) 'Size as a line of least evolutionary resistance: Diet and adaptive morphological radiation in New World monkeys', *Evolution*, 59(5), pp. 1128–1142. doi: 10.1111/j.0014-3820.2005.tb01049.x.

Marroig, G., Melo, D. A. R. and Garcia, G. (2012) 'Modularity, noise, and natural selection', *Evolution*, 66(5), pp. 1506–1524. doi: 10.1111/j.1558-5646.2011.01555.x.

Marshall, C. R. (2006) 'Explaining the Cambrian "Explosion" of Animals', *Annual Review of Earth and Planetary Sciences*, 34(1), pp. 355–384. doi: 10.1146/annurev.earth.33.031504.103001.

Martínez-Gómez, J. *et al.* (2009) 'Darwin's pigeons and the evolution of the Columbiforms : Recapitulation of ancient genes', *Acta Zoologica Mexicana*, 25(3), pp. 719–741.

Martinez, C. M. *et al.* (2018) 'Feeding ecology underlies the evolution of cichlid jaw mobility', *Evolution*, 72(8), pp. 1645–1655. doi: 10.1111/evo.13518.

Mayr, E. (1983) 'How to Carry Out the Adaptationist Program ?', *The American Naturalist*, 121(3), pp. 324–334.

Mayr, E. (1993) 'What was the evolutionary sythensis?', *Trends in ecology & evolution*, 8(1), pp. 31–34.

McGhee, G. (2012) *The Geometry of Evolution: Adaptive Landscapes and Theoretical Morphospaces*. Cambridge: Cambridge University Press.

McKinney, M. L. and Schoch, R. M. (1985) 'Titanothere allometry, heterochrony, and biomechanics: revisiting an evolutionary classic', *Evolution*, 39(6), pp. 1352–1363. doi: 10.1111/j.1558-5646.1985.tb05700.x.

Melo, D. *et al.* (2016) 'EvolQG - An R package for evolutionary quantitative genetics [version 3; referees: 1 approved, 2 approved with reservations]', *F1000Research 2016*. doi: 10.12688/f1000research.7082.1.

Millien, V. (2006) 'Morphological evolution is accelerated among island mammals', *PLoS Biology*, 4(10), pp. 1863–1868. doi: 10.1371/journal.pbio.0040321.

Mitchell, J. S. (2019) 'Extant-only comparative methods fail to recover the disparity preserved in the bird fossil record'. doi: 10.1111/evo.12738.

Mitteroecker, P. *et al.* (2004) 'Comparison of cranial ontogenetic trajectories among great apes and humans', *Journal of Human Evolution*, 46(6), pp. 679–698. doi: 10.1016/j.jhevol.2004.03.006.

Mitteroecker, P., Gunza, P. and Bookstein, F. L. (2005) 'Heterochrony and geometric morphometrics: a comparison of cranial growth in Pan paniscus versus Pan troglodytes', *Evolution & development*, 7(3), pp. 244–258. doi: EDE05027 [pii]\r10.1111/j.1525-142X.2005.05027.x.

Motani, R. and Schmitz, L. (2011) 'Phylogenetic versus functional signals in the evolution of form-function relationships in terrestrial vision', *Evolution*, 65(8), pp. 2245–2257. doi: 10.1111/j.1558-5646.2011.01271.x.

Motoo Kimura (1968) 'Evolutionary Rate at the Molecular Level', *Nature*, 217, pp. 624–626.

Niklas, K. J. (1994) 'Morphological evolution through complex domains of fitness.', *Proceedings of the National Academy of Sciences*, 91(15), pp. 6772–6779. doi: 10.1073/pnas.91.15.6772.

Niklas, K. J. (1997) 'Adaptive walks through fitness landscapes for early vascular land plants', *American Journal of Botany*, 84(1), pp. 16–25. doi: 10.2307/2445878.

Niklas, K. J. (1999) 'Evolutionary walks through a land plant morphospace', *Journal of Experimental Botany*, 50(330), pp. 39–52. doi: 10.1093/jxb/50.330.39.

Niklas, K. J. (2004) 'Computer Models of Early Land Plant Evolution', *Annual Review of Earth and Planetary Sciences*, 32(1), pp. 47–66. doi: 10.1146/annurev.earth.32.092203.122440.

O'Connor, T. (2013) *Animals as Neighbors: The Past and Present of Commensal Animals*. Michigan State University Press.

Olsen, A. M. and Westneat, M. W. (2015) 'StereoMorph: An R package for the collection of 3D landmarks and curves using a stereo camera set-up', *Methods in Ecology and Evolution*, 6(3), pp. 351–356. doi: 10.1111/2041-210X.12326.

Owen, R. (1866) *Memoir on the Dodo (Didus ineptus, Linn.) with an historical introduction by the late William John Broderip, F.R.S. London (UK)*. Taylor and Francis. Available at: https://www.harvard.edu/.

Pagel, M. (1994) 'Detecting correlated evolution on phylogenies: a general method for the comparative analysis of discrete characters', *Proceedings of the Royal Society B: Biological Sciences*, 255(1342), pp. 37–45. doi: 10.1098/rspb.1994.0006.

Pagel, M. (1999) 'Inferring the historical patterns of biological evolution.', *Nature*, 401(6756), pp. 877–884. doi: 10.1038/44766.

Pagel, M., Meade, A. and Barker, D. (2004) 'Bayesian estimation of ancestral character states on phylogenies.', *Systematic biology*, 53(5), pp. 673–84. doi: 10.1080/10635150490522232.

Paradis, E., Claude, J. and Strimmer, K. (2004) 'APE: Analyses of Phylogenetics and Evolution in R language', *Bioinformatics*, 20(2), pp. 289–290. doi: 10.1093/bioinformatics/btg412.

Parent, C. E. and Crespi, B. J. (2009) 'Ecological Opportunity in Adaptive Radiation of Galápagos Endemic Land Snails', *The American Naturalist*, 174(6), pp. 898–905. doi: 10.1086/646604.

Penna, A. *et al.* (2017) 'The evolution of phenotypic integration: How directional selection reshapes covariation in mice', *Evolution*, 71(10), pp. 2370–2380. doi: 10.1111/evo.13304.

Pereira, S. L. *et al.* (2007) 'Mitochondrial and nuclear DNA sequences support a cretaceous origin of columbiformes and a dispersal-driven radiation in the paleogene', *Systematic Biology*, 56(4), pp. 656–672. doi: 10.1080/10635150701549672.

Petkov, S. (2015) 'The Fitness Landscape Metaphor: Dead but Not Gone', *Philosophia Scientae*, 19(19–1), pp. 159–174. doi: 10.4000/philosophiascientiae.1050.

Phillips, P. C. and Arnold, S. J. (1999) 'Hierarchical Comparison of Genetic Variance-Covariance Matrices. I. Using the Flury Hierarchy', *Evolution*, 53(5), p. 1506. doi: 10.1016/S0925-8388(99)00090-0.

Phipson, B. and Smyth, G. K. (2010) 'Permutation P -values Should Never Be Zero : Calculating Exact P -values When Permutations Are Randomly Drawn', *Statistical Applications in Genetics and Molecular Biology*, 9(1), pp. 1–12. doi: 10.2202/1544-6115.1585.

Pinheiro, J. C. and Bates, D. M. (2010) 'The NLME package', *October*.

Polly, P. D. (2005) 'Development and phenotypic correlations: The evolution of tooth shape in Sorex araneus', *Evolution and Development*, 7(1), pp. 29–41. doi: 10.1111/j.1525-142X.2005.05004.x.

Presgraves, D. C. and Glor, R. E. (2010) 'Evolutionary Biology: Speciation on Islands', *Current Biology*, 20(10), pp. 440–442. doi: 10.1016/j.cub.2010.03.032.

Price, T. D. (2002) 'Domesticated birds as a model for the genetics of speciation by sexual selection', *Genetica*, 116(2–3), pp. 311–327. doi: 10.1023/A:1021248913179.

Prum, R. O. *et al.* (2015) 'A comprehensive phylogeny of birds (Aves) using targeted next-generation DNA sequencing', *Nature*, 526(7574), pp. 569–573. doi: 10.1038/nature15697.

R Core Team (2015) 'R: A language and environment for statistical computing'. Vienna, Austria: R Foundation for Statistical Computing. doi: 3-900051-07-0.

Rauzon, M. J. (2007) 'Island restoration: Exploring the past, anticipating the future', *Marine Ornithology*, 35(2), pp. 97–107.

Rayfield, E. J. (2007) 'Finite Element Analysis and Understanding the Biomechanics and Evolution of Living and Fossil Organisms', *Annual Review of Earth and Planetary Sciences*, 35(1), pp. 541–576. doi: 10.1146/annurev.earth.35.031306.140104.

Revell, L. (2012) 'phytools: An R package for phylogenetic comparative biology', *Methods in Ecology and Evolution*, 3, pp. 217–223.

Revell, L. J. (2009) 'Size-correction and principal components for interspecific comparative studies', *Evolution*, 63(12), pp. 3258–3268. doi: 10.1111/j.1558-5646.2009.00804.x.

Richardson, M. K. *et al.* (2009) 'Heterochrony in limb evolution: Developmental mechanisms and natural selection', *Journal of Experimental Zoology Part B: Molecular and Developmental Evolution*, 312(6), pp. 639–664. doi: 10.1002/jez.b.21250.

Roff, D. A. (1995) 'The estimation of genetic correlations from phenotypic correlations: A test of cheverud's conjecture', *Heredity*, 74(5), pp. 481–490. doi: 10.1038/hdy.1995.68.

Rohlf, F. J., Corti, M. and Olmstead, R. (2000) 'Use of Two-Block Partial Least-Squares to Study Covariation in Shape', *Systematic Biology*, 49(4), pp. 740–753. doi: 10.1080/106351500750049806.

Rohlf, F. J. and Slice, D. (1990) 'Extensions of the Procrustes Method for the Optimal Superimposition of Landmarks', *Systematic Zoology*, 39(1), pp. 40–59. Available at: https://pdfs.semanticscholar.org/12bc/403201e1353303a97bad1c3f2a97ee0f26df.pdf.

Sánchez-Villagra, M. R., Geiger, M. and Schneider, R. A. (2016) 'The taming of the neural crest: A

developmental perspective on the origins of morphological covariation in domesticated mammals', *Royal Society Open Science*, 3(6). doi: 10.1098/rsos.160107.

Sánchez, F., Orero, A. and Soriano, A. (2013) 'ALBIRA : A small animal PET / SPECT / CT imaging system', 40(5), pp. 1–11. doi: https://doi.org/10.1118/1.4800798.

Schluter, D. (1996) 'Adaptive Radiation Along Genetic Lines of Least Resistance', *Evolution*, 50(5), p. 1766. doi: 10.2307/2410734.

Schluter, D. *et al.* (1997) 'Likelihood of Ancestor States in Adaptive Radiation', *Evolution*, 51(6), pp. 1699–1711. doi: 10.2307/2410994?ref=search-gateway:6665e8062931da935aff3ddd9642b536.

Schott, J. R. (1988) 'Common principal component subspaces in two groups', *Biometrika*, 75(2), pp. 229–236. doi: 10.1093/biomet/75.2.229.

Serjeantson, D. (2009) *Birds (Cambridge Manuals in Archaeology)*. Cambridge: Cambridge University Press.

Shapiro, B. *et al.* (2002) 'Flight of the dodo', *Science*, 295(5560), p. 1683. doi: 10.1126/science.295.5560.1683.

Shapiro, M. D. *et al.* (2013) 'Genomic diversity and evolution of the head crest in the rock pigeon', 339(6123), pp. 1063–1067. doi: 10.1126/science.1230422.Genomic.

Sherratt, E. *et al.* (2016) 'Trends in the sand: Directional evolution in the shell shape of recessing scallops (Bivalvia: Pectinidae)', *Evolution; international journal of organic evolution*, 70(9), pp. 2061–2073. doi: 10.1111/evo.12995.

Shifrin, T. (2004) *Multivariable Mathematics: Linear Algebra, Multivariable Calculus, and Manifolds*. 1st edn. Wiley.

Sidlauskas, B. (2008) 'Continuous and arrested morphological diversification in sister clades of characiform fishes: A phylomorphospace approach', *Evolution*, 62(12), pp. 3135–3156. doi: 10.1111/j.1558-5646.2008.00519.x.

Simpson, G. G. (1944) *Tempo and mode in evolution*. Columbia University Press.

Slater, G. J. and Van Valkenburgh, B. (2009) 'Allometry and performance: The evolution of skull form and function in felids', *Journal of Evolutionary Biology*, 22(11), pp. 2278–2287. doi: 10.1111/j.1420-9101.2009.01845.x.

Smith, F. J. *et al.* (2015) 'Divergence of craniofacial developmental trajectories among avian embryos', *Developmental Dynamics*, 244(9), pp. 1158–1167. doi: 10.1002/dvdy.24262.

Soares, A. E. R. *et al.* (2016) 'Complete mitochondrial genomes of living and extinct pigeons revise the timing of the columbiform radiation', *BMC Evolutionary Biology*. BMC Evolutionary Biology, 16(1), pp. 1–9. doi: 10.1186/s12862-016-0800-3.

Sol, D. (2008) 'Artificial selection, naturalization, and fitness: Darwin's pigeons revisited', *Biological Journal of the Linnean Society*, 93(4), pp. 657–665. doi: 10.1111/j.1095-8312.2008.00957.x.

Sol, D., Lapiedra, O. and González-lagos, C. (2013) 'Behavioural adjustments for a life in the city', *Animal Behaviour*. Elsevier Ltd, 85(5), pp. 1101–1112. doi: 10.1016/j.anbehav.2013.01.023.

Spennemann, D. H. and Watson, M. J. (2017) 'Dietary habits of urban pigeons (Columba livia) and implications of excreta pH – a review', *European Journal of Ecology*, 3(1), pp. 27–41. doi:

10.1515/eje-2017-0004.

Stange, M. *et al.* (2018) 'Morphological variation under domestication : how variable are chickens ? Subject Category : Subject Areas : Authors for correspondence ':

Stringham, S. A. *et al.* (2012) 'Divergence, Convergence, and the Ancestry of Feral Populations in the Domestic Rock Pigeon', *Current Biology*, 22(4), pp. 302–308. doi: 10.1016/j.cub.2011.12.045.

Swanson, H. K. *et al.* (2015) 'A new probabilistic method for quantifying n-dimensional ecological niches and niche overlap', *Ecology*. John Wiley & Sons, Ltd, 96(2), pp. 318–324. doi: 10.1890/14-0235.1.

Sykes, N. J. (2007) *The Norman Conquest: A Cooarchaeological Perspective*. Oxford: Archaeopress.

Tanner, J. B. *et al.* (2010) 'Ontogenetic change in skull morphology and mechanical advantage in the spotted hyena (Crocuta crocuta)', *Journal of Morphology*, 271(3), pp. 353–365. doi: 10.1002/jmor.10802.

Taylor, G. and Thomas, A. (2014) *Evolutionary Biomechanics*. 1st edn. Oxford: Oxford University Press.

Therrien, F. and Henderson, D. M. (2007) 'My theropod is bigger than yours … or not: estimating body size from skull length in theropods', *Journal of Vertebrate Paleontology*, 27(1), pp. 108–115. doi: 10.1671/0272-4634(2007)27[108:MTIBTY]2.0.CO;2.

Tokita, M. *et al.* (2016) 'Cranial shape evolution in adaptive radiations of birds: comparative morphometrics of Darwin's finches and Hawaiian honeycreepers', *Philosophical Transactions of the Royal Society B*, 372, pp. 1–17. doi: 10.1098/not.

Trinkaus, E. and Villemeur, I. (1991) 'Mechanical advantages of the Neandertal thumb in flexion: A test of an hypothesis', *American Journal of Physical Anthropology*, 84(3), pp. 249–260. doi: 10.1002/ajpa.1330840303.

Tseng, Z. J. (2013) 'Testing Adaptive Hypotheses of Convergence with Functional Landscapes: A Case Study of Bone-Cracking Hypercarnivores', *PLoS ONE*. Edited by A. A. Farke, 8(5), p. e65305. doi: 10.1371/journal.pone.0065305.

Tseng, Z. J. and Flynn, J. J. (2015) 'Are cranial biomechanical simulation data linked to known diets in extant taxa? A method for applying diet-biomechanics linkage models to infer feeding capability of extinct species', *PLoS ONE*, 10(4), pp. 1–25. doi: 10.1371/journal.pone.0124020.

Van Valen, L. (1965) 'Morphological Variation and Width of Ecological Niche', *The American Naturalist*, 99(908), pp. 377–390. doi: 10.1086/282379.

Van Valen, L. (2009) 'How ubiquitous is adaptation? A critique of the epiphenomenist program', *Biology and Philosophy*, 24(2), pp. 267–280. doi: 10.1007/s10539-008-9142-x.

Vickrey, A. I. *et al.* (2018) 'Introgression of regulatory alleles and a missense coding mutation drive plumage pattern diversity in the rock pigeon', *eLife*, 7, pp. 1–27. doi: 10.7554/elife.34803.

Wheelwright, N. T. (1985) 'Fruit-Size , Gape Width, and the Diets of Fruit-Eating Birds', *Ecology*, 66(3), pp. 808–818. Available at: http://www.jstor.org/stable/1940542.

Whitaker, D. and Christman, M. (2014) 'clustsig: Significant Cluster Analysis'. Available at: https://cran.r-project.org/package=clustsig.

Wilkins, J. F. and Godfrey-Smith, P. (2009) 'Adaptationism and the adaptive landscape', *Biology and Philosophy*, 24(2), pp. 199–214. doi: 10.1007/s10539-008-9147-5.

Worthy, T. H. (2001) 'A giant flightless pigeon gen. et sp. nov. and a new species of Ducula (Aves: Columbidae), from Quaternary deposits in Fiji', *Journal of the Royal Society of New Zealand*, 31(4), pp. 763–794. doi: 10.1080/03014223.2001.9517673.

Young, N. M. *et al.* (2014) 'Embryonic bauplans and the developmental origins of facial diversity and constraint', *Development*, 141(5), pp. 1059–1063. doi: 10.1242/dev.099994.

Young, N. M. *et al.* (2017) 'Craniofacial diversification in the domestic pigeon and the evolution of the avian skull', *Nature Ecology & Evolution*. Macmillan Publishers Limited, part of Springer Nature., 1(March), p. 0095. doi: 10.1038/s41559-017-0095.

Zweers, G. A. (1982) 'Drinking of the Pigeon (Columba livia L.)', *Behaviour*, 80(3/4), pp. 274–317.

Zweers, G. A. (1992) 'Behavioural mechanisms of Avian drinking', *Netherlands Journal of Zoology*, 42(1), pp. 60–84.

Appendix One. Common allometric component and body mass results

Common allometric component results

In Chapter Two, two size proxies were analysed, the skull centroid size and the body mass, however most of the discussion was based on the centroid size results. However, some of the results of body mass were interesting and are briefly reported here. Furthermore the results for the common allometric component of shape are briefly reported here.

To visualize the influence of size on shape (Figure A12) in a phylogenetic framework, the CAC of the D.pgls was plotted against size and residual shape components (RSC) (Mitteroecker *et al.*, 2004). The shape regression scores (Drake and Klingenberg, 2008) were not plotted, but they are mathematically identical to the CAC when only one group is examined (Adams and Otárola-Castillo, 2013; Adams, Rohlf and Slice, 2013), as done here.

Visualisation of the Common Allometric Component (CAC: Figure A1) indicates similar allometric changes to skull shape across Columbiformes. The raphines present CAC similar to other pigeons but have extremely large skull sizes. The other outliers of the CAC are *Didunculus*, Pteroclidiformes and Mesitornithiformes which present sizes similar to Columbiformes but totally different values of CAC.

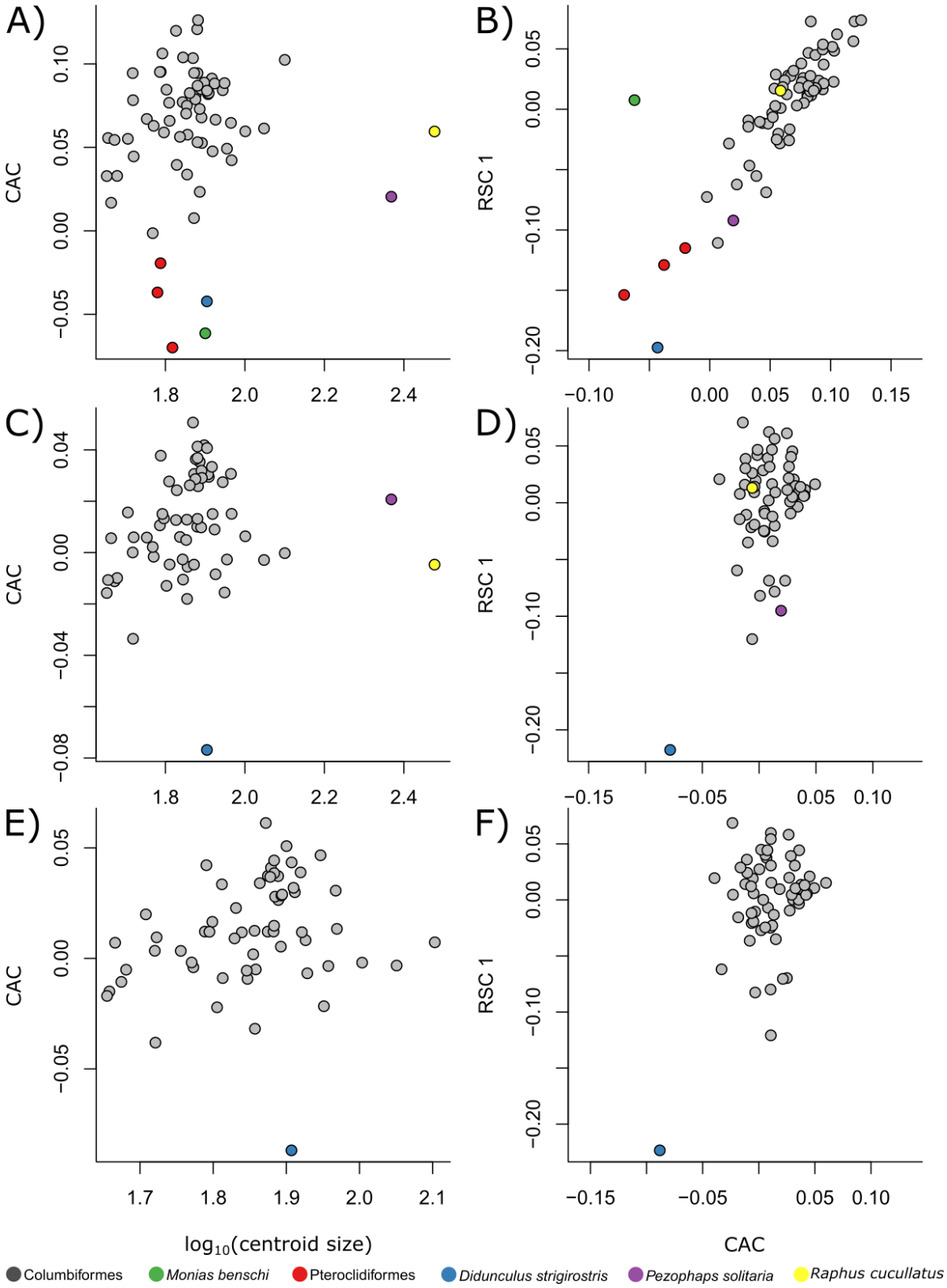


Figure A1.1. Right plots show the comparison between Common Allometric Components (CAC) and the Residual Shape Component (RSC). Left plots show the CRC comparison with the log10 of the centroid size. Columbimorphae (A and B), Columbiformes (C and D), and Columbiformes-nP (excluding Pezophaps and, Raphus) (E and F).

Visualisation of the Common Allometric Component (CAC: Figure A1) indicates similar allometric changes to skull shape across Columbiformes, whether raphines are included or excluded from the sample (Figure 2.1; A, C, E). It is possible to observe that columbiforms form a defined cluster with the exception of *Didunculus strigirostris* and the raphines (Figure A1: C and, E). *D. strigirostris* presents a centroid size similar to other pigeons but a low value of CAC. In contrast, *Pezophaps* and *Raphus* present CAC similar to other pigeons but have extremely large skull sizes. The other outliers of the CAC are the Pteroclidiformes and Mesitornithiformes which present sizes similar to Columbiformes but totally different values of CAC.

When the Residual Shape Components (RSC) is compared with CAC (Figure A1: D and F), the raphines show similar RSC values other Columbiformes while it is possible to observe that *D. strigirostris* shows different values of both CAC and RSC. Finally, Figure A1B shows Pteroclidiformes fall at the lower end of the distribution of columbiform residual shapes and present low CAC. *Monias* is another outlier presenting a low value of CAC and similar values of RSC to Columbiformes, showing that this group presents a morphology that seems to be located in a different part of the shape-size space than the one of the other two clades.

The common allometric component (CAC) of the shape calculated for centroid size (Figure A1) showed similar patterns across samples. Pteroclidiformes, *Monias*, Raphinae and, *Didunculus strigirostris* are outliers. When comparing CAC against centroid size (Figure A1A) the Pteroclidiformes, Mesitornithiformes and *D. strigirostris* present low values of the common allometric components but regular centroid sizes while Raphinae presents the inverse relationship. Figure A1B shows that only D. *strigirostris* and *M. benschi* are outliers

of the linear relationship of Columbimorphae. Pteroclidiformes seem to follow a similar allometric path to Columbiformes. However, *Monias* presents a skull shape morphology that is extremely different to the one of the other two clades. It is impossible to assess if the allometric trends in *Monias* is parallel to the one of Columbiformes, this would require a higher sample. The skull morphology of *Monias* can be contemplated as apomorphic from the group and might point to the evolutionary change either of morphology but also in allometry of the group.

The skull shapes cluster around a central value of CAC. This points at the low explanatory power of CAC while the spread of points in the RSC axis is larger (Figure A1D), accounting for most of the shape variation. Further analysis of this heterochronic hypothesis in a CAC framework would need the inclusion of a larger sample of Pteroclidiformes. Pteroclidiformes showed a large residual shape component (Figure A1) that fell in ranges similar to other columbiformes, with a low common allometric component. The CAC and RSC (Figure A1) show that shape-wise the Raphinae group along other Columbiforms. *Treron curvirostra* was identified as an outlier using the SSR but did not show extreme values of CAC or RSC.

Detailed mass results

I acknowledge that results produced using the mean species body mass instead of the specimen body mass should be viewed with caution. The skull shapes of all three Pteroclidiformes, plus *Didunculus* and *Pezophaps*, predict body masses lower than their species body size mean that fall outside the 95% confidence intervals of the ols models (Figure 2.7). The skull shape of *Monias* predicts a higher body mass than it's recorded

species mean body mass (10244g vs 138g), and *Raphus* presents a higher predicted mass than the literature estimate (30kg vs 9.6kg; Livezey (1993): Table S2.1). However, one pteroclidiform (*Pterocles quadricinctus*) and *Raphus* fell within the 95% confidence interval of the model.

The predicted body masses for Pteroclidiformes, based on their skull shapes, were lower than their real sizes: *Syrrhaptes paradoxus* differed from 257g to 28g and 62mm to 44mm. *Pterocles senegallus* differed from 264g to 111g and from 67mm to 65mm. *Pterocles quadricinctus* differed from 180g to 52g and from 61.mm to 52mm. Only the centroid size prediction for *Pterocles senegallus* was similar to the real centroid size (61 vs 51.8g). For *Monias* the size estimations based on skull shape were larger than its actual size: the body mass differed from 138g to 10244g and the centroid size from 81mm to 168mm. For the Raphinae clade the size estimation was lower than the real data except in the body mass prediction of *Raphus*: the size differed from 9.6kg to 30kg (the upper limit of evaluated sizes) and the centroid size from 30cm to 23cm while *Pezophaps* body mass differed from 11.3 kg to 3.5kg and its centroid size from 24 cm to 17 cm. Other columbiforms like *Didunculus strigirostris* predicted size was lower that the real size: from 400g to 238g and the centroid size from 81mm to 74mm. *Treron curvirostra* body mass differed from 134.5g to 277g and from a centroid size of 75mm to 86mm while *Chalcophaps indica* predicted body mass differed from 136g to 429g and the centroid size differed from 64mm to 82mm.

The improvement in shape prediction when the heterochronic size (predicted) was used was not uniform across the outlier species: *Syrrhaptes paradoxus* improved 22% (body mass) and of 12% (centroid size). *Pterocles senegallus* improved in 1.18% (body mass) but

presented no improvement in shape prediction when evaluating the heterochronic centroid size. *Pterocles quadricinctus* improved in 7.34% (body mass) and 2.56% (centroid size). *Monias* improved in 23% (body mass) and 13.93% (centroid size). *Raphus* improved in 3.05% for body mass but the shape prediction was -5.15% more inaccurate for the best centroid size, while *Pezophaps* presented basically no improvement in shape prediction (1.63%, body mass; 2.3%, centroid size). *Didunculus strigirostris* improved in 0.45% (body mass) and 0.17% (centroid size). *Treron curvirostra* improved in 2.98% (body mass) and in 0.71% (centroid size). *Chalcophaps indica* improved in 5.18% (body mass) and 1.94% (centroid size).

Detailed discussion: shape-based mass prediction and its significance for the "fat" dodo hypothesis

The mass of *Raphus* has been a point of heated discussion for some time. This debate probably originated because the exaggerated accounts of sailors ("fifty pound" about 22kg; Angst, Buffetaut and Abourachid, 2011), however modern mass estimations ordinarily recover a much lighter bird (9.5 to 15.4 kg). Only the mass estimation of Livezey (1993) was much larger for males (21.2 kg) when the basal estimation was increased twofold to account for flightlessness and "fat" condition. I estimated the mass of the dodo in my analysis and it seems fit to discuss these results (in light of the body mass results) because of the importance of this species. The body mass of the dodo might have been larger than the 9.6 kilos (Livezey, 1993) used in this chapter as suggested by these results: (1) the predicted body mass was higher than the expectation in an ordinary least squares model of predicted versus empirical body masses. (2) Heterochrony of body mass explained

19.56% of the variance that was not explained by allometry. (3) the predicted body mass was 30kg (the upper bound in the analysed hypothetical body mass sequence). This 30kg estimate for the body mass of *Raphus* could be interpreted as evidence supporting “fat” dodo of historical accounts. However, I demonstrated that skull shape in Raphini can be partly explained by allometry and heterochrony did not improve the shape prediction for this species. Thus, my evidence is insufficient to argue in favour of the “fat” dodo theory. Instead I highlight the importance of taking into account the heterochrony and its explanatory power when predicting body mass.

Appendix Two: New classification and evolution of feeding behaviour in Columbiformes

In Chapter Three, I used a clustering algorithm and a principal coordinates analysis to summarize the feeding behaviour (diet and foraging) of columbiforms. As a by-product of this I propose a new classification of feeding behaviour of pigeons and used this new classification to explore the evolution of this behaviour in all columbiforms. In this appendix, I explore in detail this new classification and discuss the evolutionary history of feeding in pigeons.

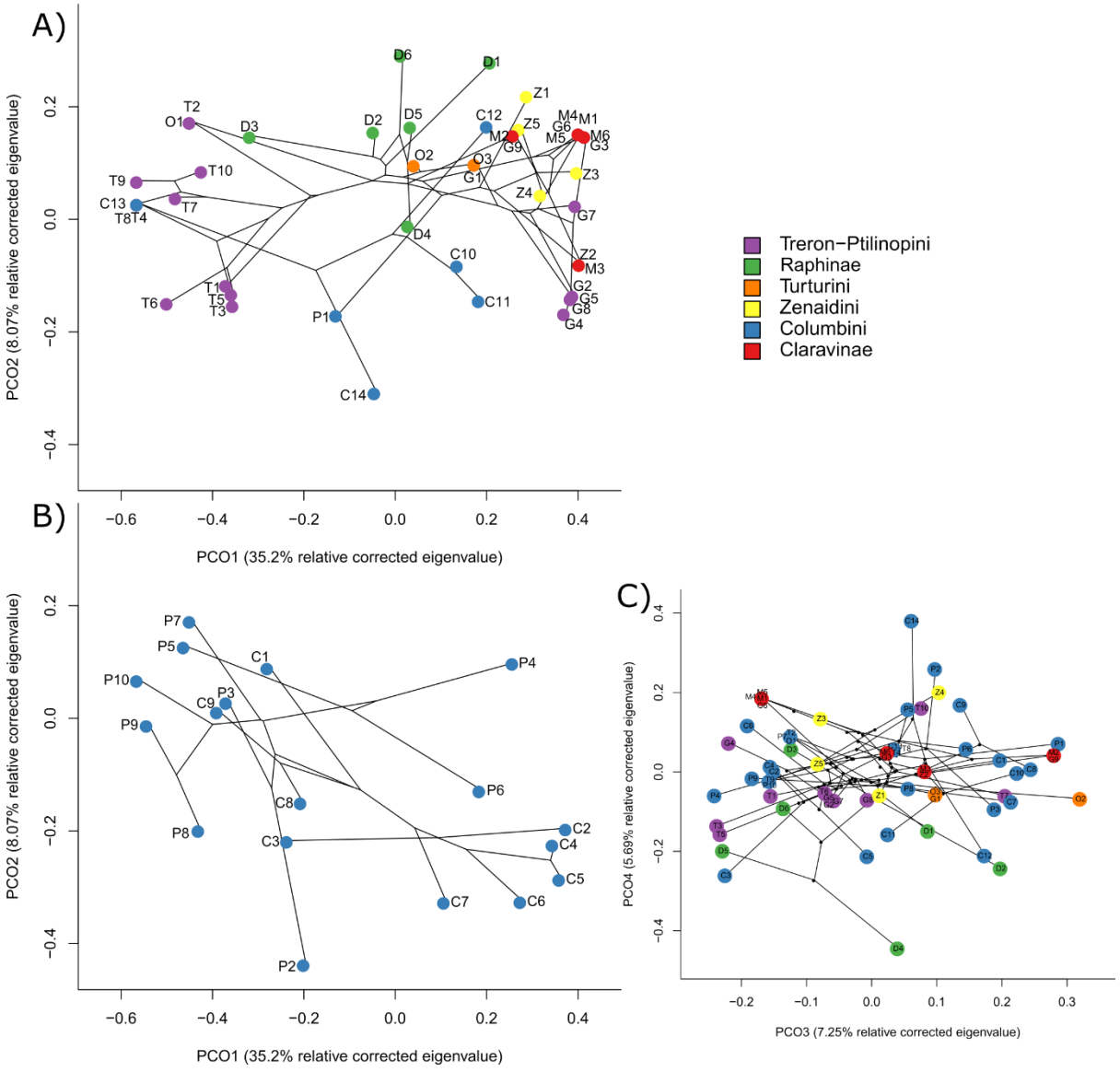


Figure A2.1. Phylogenetic feeding space (phylofeedingspace). This figure shows the feeding space of the first four principal coordinates axis of the diet (binary dissimilarity matrix). The pigeon phylogeny is plotted in this feeding space in a similar way to a phylomorphospace (Sidlauskas, 2008); A) shows the Columbiform feeding space in PCO1 and PCO2 excluding the genera Columba and Patagioenas; B) shows the feeding space in PCO1 and PCO2 of the genera Columba and Patagioenas; C) shows the feeding space in PCO3 and PCO4 for the complete columbiform sample. This figure shows: A) most clades inside Columbiformes occupy restricted areas of the feeding space; B) how Columba and Patagioenas have occupied disparate areas of the feeding space; C) that feeding strategies are less restricted in PCO3 and PCO4.Legend: *Leucosarcia melanoleuca* (G1), *Ocyphaps lophotes* (G2), *Phaps elegans* (G3), *Phaps histrionica* (G4), *Phaps chalcoptera* (G5), *Petrophassa albipennis* (G6), *Geopelia cuneata* (G7), *Geophaps plumifera* (G8), *Gallicolumba luzonica* (G9), *Phapitreron leucotis* (O1), *Treron curvirostra* (T1), *Treron formosae* (T2), *Hemiphaga novaeseelandiae* (T3*), Lopholaimus antarcticus* (T4), *Ducula pacifica* (T5), *Ducula goliath* (T6), *Ptilinopus dupetithouarsii* (T7), *Drepanoptila holosericea* (T8), *Alectroenas madagascariensis* (T9), *Alectroenas pulcherrimus* (T10), *Caloenas nicobarica* (D6), *Pezophaps* (D5), *Raphus* (D4), *Didunculus* (D3), *Goura cristata* (D2), *Otidiphaps nobilis* (D1), *Turtur tympanistria* (O2), *Chalcophaps indica* (O3), *Geotrygon versicolor* (Z5), *Starnoenas cyanocephala* (Z4), *Geotrygon mystacea* (Z3), *Zenaida macroura* (Z2), *Leptotila rufaxilla* (Z1), *Patagioenas speciosa* (P10), *P. leucocephala* (P9), *P. squamosa* (P8), *P. plumbea* (P7), *P. picazuro* (P6), *P. cayennensis* (P5), *P. maculosa* (P4), *P. nigrirostris* (P3), *P. fasciata* (P2), *Ectopistes migratorius* (P1), *Columba arquatrix* (C1), *C. guinea* (C2), *C. trocaz* (C3), *C. rupestris* (C4), *C. livia* (C5), *C. oenas* (C6), *C. palumbus* (C7), *C. vitiensis* (C8), *C. pulchricollis* (C9), *Streptopelia turtur* (C10), *Streptopelia decaocto* (C11), *Aplopelia larvata* (C12), *Turacoena manadensis* (C13), *Macropygia unchall* (C14), *Columbina cruziana* (M1), *Columbina passerina* (M2), *Columbina talpacoti* (M3), *Metriopelia melanoptera* (M4), *Metriopelia ceciliae* (M5), and *Claravis pretiosa* (M6).

Results for the phylogeny and feeding behaviour ("phylofeedingspace")

When the phylogeny is plotted against PCO1 and PCO2 (Figure A2.1B) it was possible to observe that the genera *Columba* and *Patagioenas* (Columbini) occupy large parts of the feeding space. Indeed, members of this group exhibit feeding behaviours as disparate as a mostly frugivorous diet and a mostly granivorous diet. Neither *Patagioenas* nor Columba have invaded the obligate terrestrial feeding of cluster "A" (central PCO1 values and highly positive PCO2 values). No species of *Columba* in the sample has occupied the mostly arboreal/mostly frugivorous portion of the feeding space (highly negative PC01 values and highly positive PCO2 values). However, *P. plumbea, P. speciosa, and P. cayennensis* have occupied the mostly arboreal foraging and mostly frugivorous part of the feeding space. It is also possible to see

in Figure A2.1A that most of the other clades show more restricted feeding behaviours and occupy discrete parts of the feeding space. Species of the *Treron* clade present low values of PCO1 and medium to low values of PCO2. This clade includes genera like *Treron*, *Hemiphaga*, *Lopholaimus*, *Ducula*, *Ptilinopus*, *Drepanoptila* and *Alectroenas* which are included in the complete linkage clusters "f", "g", and "h", which characterize for mostly arboreal foraging and diets that range from generalist to specialist frugivory (main cluster "M1"). The sister group to this clade includes the genera *Leucosarcia*, *Ocyphaps*, *Phaps*, *Petrophassa*, *Geopelia*, *Geophaps*, and *Gallicolumba*. These species are contained in the significant clusters "D" and "E" from the clustering analyses, which represent mostly terrestrial foragers with specialist granivorous diets or mostly granivorous diets that can incorporate some fruit. The Raphinae presents medium values of PC1 but medium to high values of PC2. This clade includes the dodo-related species and are contained in complete linkage clusters: "A", "g", and "d", and represent mostly frugivorous species with mostly arboreal feeding or the specialist terrestrial foraging frugivorous species. The genera *Turtur* and *Chalcophaps* occupy medium/positive values of PCO1 and PCO2, that represent mostly terrestrial foragers that include fruit in their mostly granivorous diets. Zenaidini includes pigeons like *Geotrygon*, *Starnoenas*, *Zenaida* and *Leptotila* which present high values of both PCO1 and PCO2. These pigeons are contained in the significant cluster "E", which represent mostly terrestrial foragers with mostly granivorous diets. Claravinae includes the genera *Columbina Metriopelia* and *Claravis* which are contained in the significant clusters "D" and "E". This clade presents high positive values of PCO1 and medium to highly positive values of PCO2, which represent mostly terrestrial granivorous species.

When the phylofeedingspace constructed with PCO3 and PCO4 is constructed (Figure A2.1) the Columbini also occupied the largest part of the feeding space. The other clades do not present such a discrete distribution in the feeding space as in PCO1 and PCO2. Most clades occupy large parts of PCO3 while PCO4 shows a better clade separation. Rhapinae present the most negative values of PCO4 while Claravinae tends to present mostly positive PCO3 values. Zenaidini (*Geotrygon*, *Starnoenas*, *Zenaida* and *Leptotila*) presents medium values of PCO3 and 4 while *Turtur* presents a high positive value of PCO3.

Discussion of diet classification and feeding evolution in Columbiforms

Diet classification of Pigeons

I propose a new classification of pigeon feeding behaviour based on diet and foraging. This new classification defined between seven and eight pigeon clusters (Table 3.1). Pigeon classification has previously been defined in two different axes: diet (frugivorous, granivorous or both) and foraging (terrestrial, arboreal or both). However, these axes do not take into account the interplay between both these aspects of feeding behaviour. Different species of pigeons have been noted to inhabit the same geographic areas and forage on similar resources (Diamond, 1973), these species, and other bird species might avoid competition because of differences on sizes and foraging strategies (MacArthur, 1958; Diamond, 1973).

I acknowledge that the proposed new classification of pigeon foraging is imperfect because it does not take the food item size and body size into account (Diamond, 1973; Emerson and Radinsky, 1980; Wheelwright, 1985). However, this classification (Figure S3.1) corrects some of the problems derived from the inflexibility of previous classifications. For example, the

Raphini have been described as particular cases of the standard pigeon classifications: "*R. cucullatus* and *P. solitaria* are considered most simply to be 'obligate,' perhaps specialized, members of the terrestrial group." (Livezey, 1993). The Raphini were included in this new classification by scoring original accounts and early descriptions (fruit; Owen, 1866; Livezey, 1993) and some proposed feeding strategies (snails and insects) for their diet (Livezey, 1993) and foraging characters were deduced from the fact they were massive flightless birds (= exclusive terrestrial foraging; Livezey, 1993). The new classification recovers the Raphini, along with *Caloenas nicobarica*, as members of a distinctive terrestrial frugivorous clade (cluster "A"). This classification also allows identification of specialist or obligate species like cluster "E", which are an extreme example of terrestrial pigeons that only forage on the ground. Cluster "E" includes the genera *Phaps*, *Geopelia*, *Columbina*, *Zenaida*, *Starnoenas*, *Geotrygon*, *Ocyphaps*, *Metriopelia*, *Petrophassa*, *Leptotila*, and *Claravis* and species of the ubiquitous Columbini (*C. rupestris*, *C livia*, and *C. guinea*) and *Patagioenas maculosa*. Feeding cluster "E" is the exact opposite of feeding cluster "g" which is almost entirely composed of arboreal frugivore species like the genera *Didunculus*, *Turacoena*, *Drepanoptila*, *Lopholaimus*, *Alectroenas*, Phapitreron and species like *Treron formosae*, *P. cayennensis, P. speciosa*, and *P. plumbea.* I also note that some combinations of feeding and foraging that are not present in known Columbiformes: granivorous specialists with entirely arboreal foraging.

Future directions: The proposed classification could be improved by incorporating size into the database. A future area of research would be the classification of diet in all Columbiform species, taking size into account. This database could be characterised as a distance matrix using the Gower dissimilarity index (Gower, 1966; MacLeod, 2006) to obtain a classification

that takes into account how size can interact with the competitive exclusion principle (Hardin, 1960).

Feeding evolution (phylofeedingspace)

The matter of the evolution of feeding behaviour in Columbiformes has not been considered with enough detail in the literature (Goodwin, 1983; Janoo, 2005; Gibbs, Barnes and Cox, 2010). One noticeably exception is Lapiedra *et al.* (2013) which found terrestrial foraging to be the ancestral foraging strategy in Columbiformes, increased rates of evolution in arboreal foraging pigeons and a constrains to subsequent reversals to terrestrial foraging. However, little attention has been paid towards possible ancestral states and the putative feeding behaviour (foraging and diet) convergence of some distantly related pigeon groups (Figure A2.1A): (1) granivory of some *Columba* and *Patagioenas*, and Claravinae, Zenaidini or Turturini, or (2) the frugivory of some *Columba* and *Patagioenas*, and species of the, hereby called, “fruit pigeons” (*Alectroenas*, *Drepanoptila*, *Ptilinopus*, *Ducula*, *Lopholaimus*, *Hemiphaga*, and *Treron*).

The phylomorphospace is a standard visualization of the evolution of morphology (Sidlauskas, 2008; *e.g.*, Benson and Choiniere, 2013; Bright *et al.*, 2016; Sherratt *et al.*, 2016), and it has previously done using the results of a morphological principal coordinates analysis (PCO). However, to my knowledge, it has not been used on the results of a feeding PCO to visualise the evolution and occupation of the feeding space "phylofeedingspace" (Figure A2.1). This visualisation helped me to shed some light on the evolutionary history and disparity of feeding ecology among pigeon clades, and to compare how variable is within-clade feeding behaviour. I found that *Columba* and *Patagioenas* occupy a more substantial proportion of the feeding

space than other groups of Columbiformes (Figure A2.1A). A possible explanation for this is that some *Columba* and *Patagioenas* species are medium-sized generalists. Generalist lineages could have invaded new unoccupied geographical locations or become specialist in already occupied locations to avoid competition from other species, contributing towards the high feeding diversity of this clade. One example of this is the successful invasion of urban environments by the common pigeon (*C. livia*), which has a generalist diet that variates along their geographical range. *C. livia* shows an opportunistic feeding in cities but presents a mostly granivorous diet in natural or rural environments (Sol, Lapiedra and González-lagos, 2013; Spennemann and Watson, 2017). Similar characteristics are shared by wood pigeons (*Columba palumbus*), which have also invaded urban environments (Luniak, 2004).

In the phylogeny of Columbiformes (Jetz *et al.*, 2012), the first clade to diverge is a clade comprised by *Metriopelia*, *Claravis* and *Columbina* (M in Figure A2.2; Claravinae in Figure A2.1). This clade occupied regions of the feeding space that are related with a mostly granivorous diet of the cluster "E". After this clade, the second clade to diverge is divided into two large clades: (1) Zanaidini (clade “Z” Figure A2.1 and A2.2) containing *Leptotila*, *Zenaida*, *Geotrygon* and *Starnoenas*. Columbini (clade "C" of Figure A2.1; clades “C” and “P” of Figure A2.2) is a clade containing *Macropygia*, *Turacoena*, *Aplopelia*, *Streptopelia*, *Ectopistes*, *Patagioenas* and *Columba*. Zenaidini also occupies a feeding space of the seed-eating terrestrial foraging cluster "E" (Figure A2.1). For Columbini, some genus like *Aplopelia* and *Streptopelia* show a granivorous-generalist diet that includes fruit and tree foraging (cluster "D"). Conversely, the other genera in Columbini occupy large areas of the feeding space; *Columba* and *Patagioenas* present extreme radiation of feeding behaviour (Figure A2.1 and A2.2) that is accompanied by a high species diversity in both genera (35 and 17 spp.

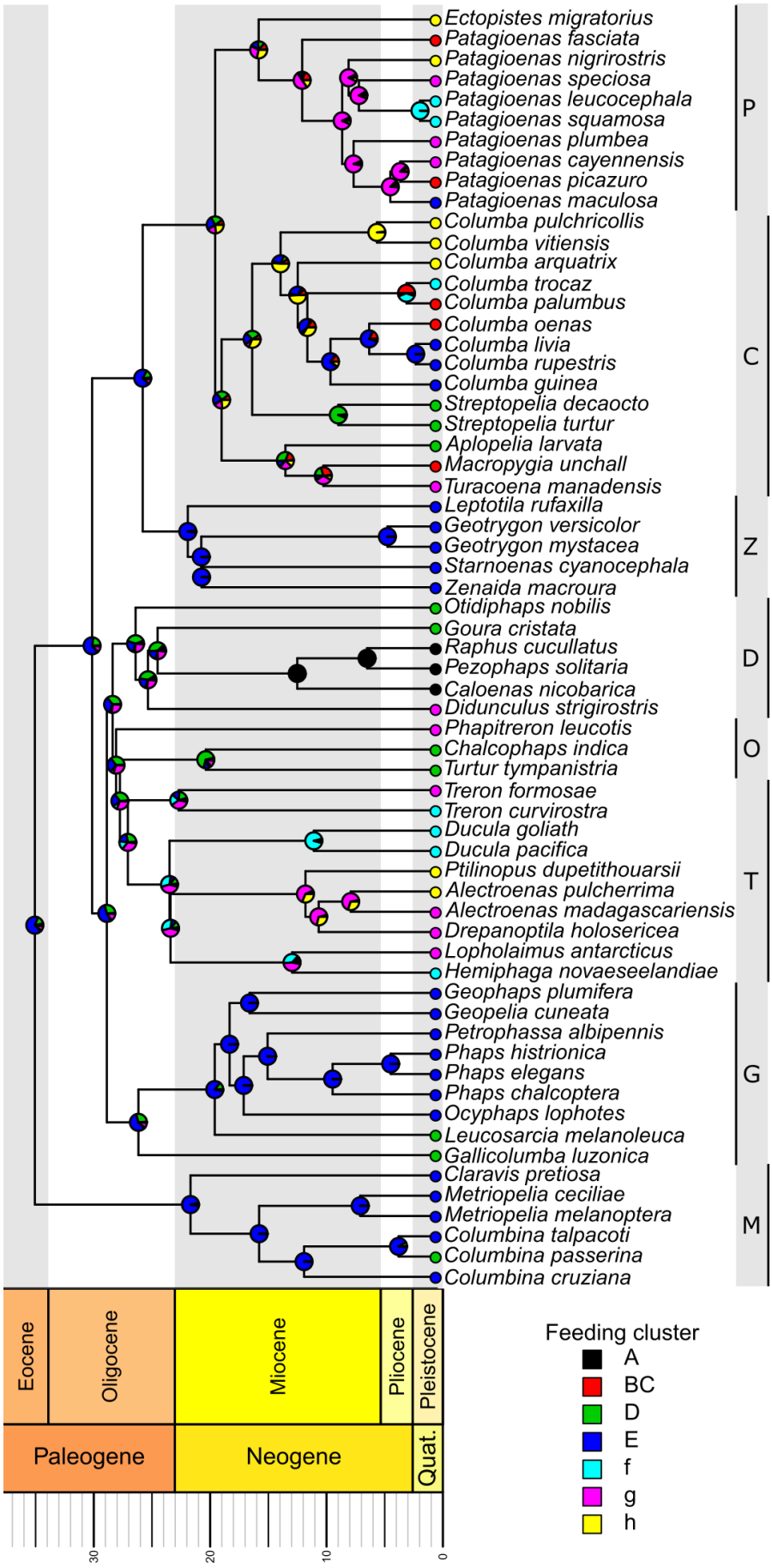

Ectopistes migratorius
Patagioenas fasciata
Patagioenas nigrirostris
Patagioenas speciosa
Patagioenas leucocephala
Patagioenas squamosa
Patagioenas plumbea
Patagioenas cayennensis
Patagioenas picazuro
Patagioenas maculosa
Columba pulchricollis
Columba vitiensis
Columba arquatrix
Columba trocaz
Columba palumbus
Columba oenas
Columba livia
Columba rupestris
Columba guinea
Streptopelia decaocto
Streptopelia turtur
Aplopelia larvata
Macropygia unchall
Turacoena manadensis
Leptotila rufaxilla
Geotrygon versicolor
Geotrygon mystacea
Starnoenas cyanocephala
Zenaida macroura
Otidiphaps nobilis
Goura cristata
Raphus cucullatus
Pezophaps solitaria
Caloenas nicobarica
Didunculus strigirostris
Phapitreron leucotis
Chalcophaps indica
Turtur tympanistria
Treron formosae
Treron curvirostra
Ducula goliath
Ducula pacifica
Ptilinopus dupetithouarsii
Alectroenas pulcherrima
Alectroenas madagascariensis
Drepanoptila holosericea
Lopholaimus antarcticus
Hemiphaga novaeseelandiae
Geophaps plumifera
Geopelia cuneata
Petrophassa albipennis
Phaps histrionica
Phaps elegans
Phaps chalcoptera
Ocyphaps lophotes
Leucosarcia melanoleuca
Gallicolumba luzonica
Claravis pretiosa
Metriopelia ceciliae
Metriopelia melanoptera
Columbina talpacoti
Columbina passerina
Columbina cruziana
P
C
Z
D
O
T
G
M
Eocene
Oligocene
Miocene
Pliocene
Pleistocene
Paleogene
Neogene
Quat.
30
20
10
0
Feeding cluster
A
BC
D
E
f
g
h

Figure A2.2. Phylogeny of Columbiformes with the feeding clusters mapped. Ancestral characters were estimates using an equal rates model. The significant clusters of the complete linkage algorithm were used as tip states to be reconstructed along the phylogeny. The ancestral feeding strategy for Columbiformes is the cluster “E”, which is a cluster of mainly terrestrial foragers with granivorous diets. Columbiformes have occupied different parts of the feeding space (or acquired novel feeding) in several occasions: (1) by clade “T” (“fruit pigeons” *sensu lato*); (2) by Raphinae (clade “D”); (3) by members of clades “P” and “C”. albeit (1) and (2) could form part of an older feeding diversification (clades “D”, ”O”, and ”T”).

respectively; Clements *et al.*, 2017). These genera, however, show a similar skull morphology that is close to the average columbiform shape. When the phylofeedingspace of *Columba* and *Patagioenas* is analysed (Figure A2.1B), there is an apparent division of the feeding space with *Patagioenas* being more frugivorous and *Columba* being more granivorous/generalists. However, species of the two genera are distributed widely across the feeding space, which suggests that species with generalist diets might have more labile skull shapes. These generalist species might preferentially follow the lines of least evolutionary resistance (Schluter, 1996; Marroig and Cheverud, 2005) in their speciation process. These species might also change their body size/shape relation using heterochrony along these lines of least evolutionary resistance.

Chalcophaps, *Turtur* and Raphinae (except *Didunculus*) share a different region of the feeding-space marked by positive PCO2 values and central PCO1 values (Figure A2.1). This region of the feeding space relates to various feeding behaviours of clusters "D" (terrestrial foragers with diets that include fruit) and "A" (specialist terrestrial frugivorous species). I note that the specialist cluster “A” is only exhibited by a clade of closely related species (*Raphus*, *Pezophaps* and *Caloenas*; Figure A2.2). The obligate terrestrial frugivory of this clade possibly evolved

from a frugivorous, mainly terrestrial foraging ancestor. However, the ancestors of Raphus and Pezophaps should have remained flighted at least until the emergence of the Rodrigues 1.5 million years ago (mya) and Mauritius islands 6.8 to 7.8 mya (Shapiro *et al.*, 2002).

The clade *Treron-Ptilinopus* (Figure A2.1; “T” in Figure A2.2) includes the "fruit pigeons” occupy negative values of PCO1 and represent feeding clusters "h", "g", "f" (mainly arboreal forager with diets that range from mainly fruit to specialist frugivory) from the mostly arboreal and frugivorous "M1" main cluster. *Phapitreron* (“O1” of Figure A2.1; “O” in Figure A2.2) and Didunculus (“D3” of Figure A2.1; “D clade” in Figure A2.2) are also in this region of the feeding space and is included in the frugivorous arboreal cluster "g". Finally, the Geopelia-Gallicolumba clade (“G” in Figures A2.1 and A2.2) which includes *Gallicolumba*, *Geophaps*, *Geopelia*, *Petrophassa*, *Phaps*, *Ocyphaps* and *Leucosarcia* occupy an area close to the feeding space of the basal columbiforms: terrestrial mainly granivorous clusters "D" and "E" (Figure S3.1 and A2.1).

The evolutionary history in the feeding space shows that the granivorous, terrestrial foraging behaviour is the likely ancestral condition in Columbiformes (Figure A2.1). This ancestral condition was confirmed by the ancestral character reconstruction of feeding clusters (Figure A2.2). My findings support the ancestral foraging strategy of columbiforms reported by from Lapiedra *et al.* (2013) and shed light into the evolution of diet along foraging in this clade. The phylofeedingspace and the ancestral character reconstruction show that Columbiformes have occupied other regions (besides the ancestral terrestrial granivory) of the feeding space at least three times (Figure A2.2): (1) by *Columba* and *Patagioenas* around 29 to 25 million years ago (mya) (Late Rupelian to Early Aquitanian; Oligocene to Early Miocene), (2) by Raphinae

around 34 mya (Middle Rupelian; Oligocene) and (3) by "fruit pigeons" around 30 mya (Rupelian; Oligocene). The ancestral feeding behaviour hypothesis is further supported by the feeding behaviour of the sister clade to Columbiformes. This clade includes the Pteroclidiformes and the Mesitornithiformes. Both clades are terrestrial foragers and Pteroclidiformes species are granivorous. However, the diet of the Mesitornithiformes is mostly based on invertebrates (Hoyo *et al.*, 2017).

Our findings contrast with previous research which found a mean of 20 transitions in columbiform evolution: five times from terrestrial to arboreal foragers and six times from generalist to arboreal foragers (Lapiedra *et al.*, 2013). A lower number of transitions were expected because the sample analysed in this chapter is smaller compared to the one analysed by Lapiedra *et al*. (2016, 65 versus 156 spp.). However, my findings might indicate that when complex feeding behaviour (foraging and diet) is used in an ancestral character reconstruction, it might reduce the number of identifiable significant transitions along the phylogenetic tree.

Future directions: to analyse the feeding evolution of the Columbiformes was not the primary objective of this research. Nevertheless, the obtained results shed light into the ancestral states and the evolution of this behaviour. The proposed evolutionary hypotheses of feeding behaviour need to be further analysed in a phylogenetic framework in which a larger sample is analysed. This sample should summarize all the dietary, foraging and size information available for Columbiformes, Mesitornithiformes, and Pteroclidiformes. Furthermore, the feeding characterization (foraging and diet) should be used to reassess the rates of evolution and evolutionary constraints analyses of foraging published by Lapiedra *et al.* (2013).

Appendix Three. Biomechanical landscape and its relationship with diet of Columbiformes and Raphini (dodo and Rodrigues Solitaire)

Detailed biomechanical landscape results

The principal component analysis of all 29 Procrustes aligned landmarks of the sample showed that the first six principal components summarize 80% of the shape variation in the sample (32,4%, 23.1%, 9.2%, 6%, 5.2%, and 4.3% respectively; Figures A3.1 to A3.4). The analysis of patterns in the biomechanical landscape pointed out for PC1 and PC2 are the biomechanical dimensions that seem to be more closely related to the feeding behaviour clusters: when the performance of different biomechanical characters is plotted against the first two principal components of shape (56% of the sample variation), it is possible to observe the non-linear patterns of performance across morphospace. Principal components three and four (Figures A3.3 and A3.4) summarize 15.2% of the sample variation (9.2 and 6% respectively). When I visually examine Figures A3.3 and A3.4, it was difficult to identify a clear correlation between the biomechanical performance and the significant feeding clusters.

In subsequent paragraphs, I will report the results of the biomechanical performance landscape. It is pertinent to remind the reader about some aspects of this morphospace that otherwise might seem incongruous. (1) All hypothetical shapes across the performance landscape were calculated from the PCA of Procrustes aligned coordinates. The Procrustes alignment removes size (geometric but not allometric) which makes it possible to compare different skulls based only on shape differences. For a hypothetical

example, the identified eye size could be larger in a tiny pigeon (Columbina) than in a giant pigeon (Raphus), albeit this would not be true empirically. The performance landscape is thus visualizing the comparative performance between shapes in the selected PC axes. (2) In this context, the reported performance for a particular species is not an empirical measurement but the performance measured for an idealized skull shape, with the same PC scores as the ones of that species in the selected PC axes. While this might appear to be counterintuitive, it allows one to dissect the components of shape and performance. The inclusion of the species ordination in the performance landscape allows to visually assess if different performance corresponds to different feeding clusters or phylogenetic clades. (3) Because of limitations of data visualization, I compare first the PC1 against PC2 (55% of the sample variation) and then the PC3 against PC4 (15.2% of the sample variation), and the performance is measured in the shapes representing combinations of values across those axes. This approach might produce results in which one taxon has the comparatively highest performance one plot (PC1 versus PC2) and low performance in another plot (PC3 versus PC4). These differences reflect different contributions of shape components to the overall the performance. However, as each subsequent component in the PCA analysis captures less variance, it can be expected that the contribution of subsequent PC axes to the biomechanical performance will diminish as well.

Input force (muscle centroid size)

The input force (muscle centroid size) increases with lower values of PC1 and PC2 (Figure A3.1E). A similar pattern was obtained when the muscle area (Fi) was used as an approximation of input force (not shown). For PC1 versus PC2, *Raphus*, *Pezophaps* and

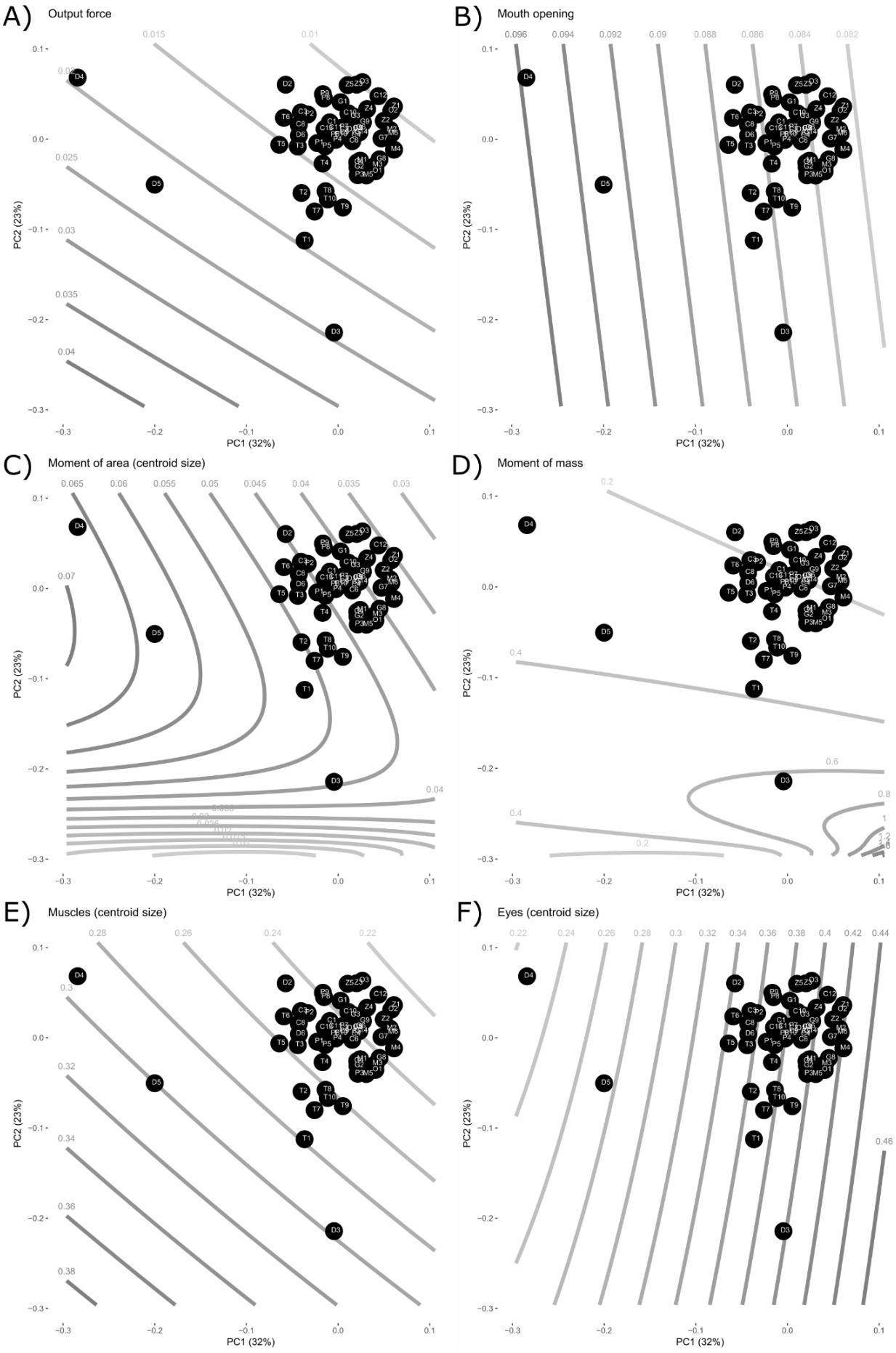

A)
Output force
B)
Mouth opening
C)
Moment of area (centroid size)
D)
Moment of mass
E)
Muscles (centroid size)
F)
Eyes (centroid size)
PC1 (32%)
PC2 (23%)

Figure A3.1. Biomechanical landscape in PC1 and PC2. A) Output force; B) mouth opening; C) moment of area; D) moment of mass; E) muscle size; F) eye size. Shapes were simulated for values across the PC2 and PC2, and the comparative biomechanical performance was measured for these shapes. Biomechanical performance is displayed as contour lines across the morphospace. Species in the sample are plotted in the biomechanical landscape according to their shape (PC scores). Legend: *Leucosarcia melanoleuca* (G1), *Ocyphaps lophotes* (G2), *Phaps elegans* (G3), *Phaps histrionica* (G4), *Phaps chalcoptera* (G5), *Petrophassa albipennis* (G6), *Geopelia cuneata* (G7), *Geophaps plumifera* (G8), *Gallicolumba luzonica* (G9), *Phapitreron leucotis* (O1), *Treron curvirostra* (T1), *Treron formosae* (T2), *Hemiphaga novaeseelandiae* (T3*), Lopholaimus antarcticus* (T4), *Ducula pacifica* (T5), *Ducula goliath* (T6), *Ptilinopus dupetithouarsii* (T7), *Drepanoptila holosericea* (T8), *Alectroenas madagascariensis* (T9), *Alectroenas pulcherrimus* (T10), *Caloenas nicobarica* (D6), *Pezophaps* (D5), *Raphus* (D4), *Didunculus* (D3), *Goura cristata* (D2), *Otidiphaps nobilis* (D1), *Turtur tympanistria* (O2), *Chalcophaps indica* (O3), *Geotrygon versicolor* (Z5), *Starnoenas cyanocephala* (Z4), *Geotrygon mystacea* (Z3), *Zenaida macroura* (Z2), *Leptotila rufaxilla* (Z1), *Patagioenas speciosa* (P10), *P. leucocephala* (P9), *P. squamosa* (P8), *P. plumbea* (P7), *P. picazuro* (P6), *P. cayennensis* (P5), *P. maculosa* (P4), *P. nigrirostris* (P3), *P. fasciata* (P2), *Ectopistes migratorius* (P1), *Columba arquatrix* (C1), *C. guinea* (C2), *C. trocaz* (C3), *C. rupestris* (C4), *C. livia* (C5), *C. oenas* (C6), *C. palumbus* (C7), *C. vitiensis* (C8), *C. pulchricollis* (C9), *Streptopelia turtur* (C10), *Streptopelia decaocto* (C11), *Aplopelia larvata* (C12), *Turacoena manadensis* (C13), *Macropygia unchall* (C14), *Columbina cruziana* (M1), *Columbina passerina* (M2), *Columbina talpacoti* (M3), *Metriopelia melanoptera* (M4), *Metriopelia ceciliae* (M5), and *Claravis pretiosa* (M6).

Didunculus seem to be the taxa with skull shapes that present larger muscle areas (these taxa were assigned to clusters “A” and “g”). *Treron*, *Ducula pacifica*, *Ptilinopus*, and *Alectroenas* present the second highest muscle size (from clusters “f”, “g”, and “h”). Most other columbiform species present lower values of input force. The lowest muscle areas were obtained for *Chalcophaps Geotrygon*, *Aplopelia*, *Leptotila* and *Turtur* (clusters “E” and “D”).

For PC3 versus PC4, taxa like *Metriopelia*, *Ocyphaps*, *Geophaps*, and *Pezophaps* present low input force (clusters “E” and “A”), while taxa like *Geotrygon versicolor*, *Lopholaimus antarcticus*, and *Didunculus* present high input forces (clusters “E” and ”g”). The input force pattern was non-linear, incrementing towards positive values of PC4 and in extreme values of PC3. In these axes the centroid size of the muscle is more linear (Figure A3.3E),

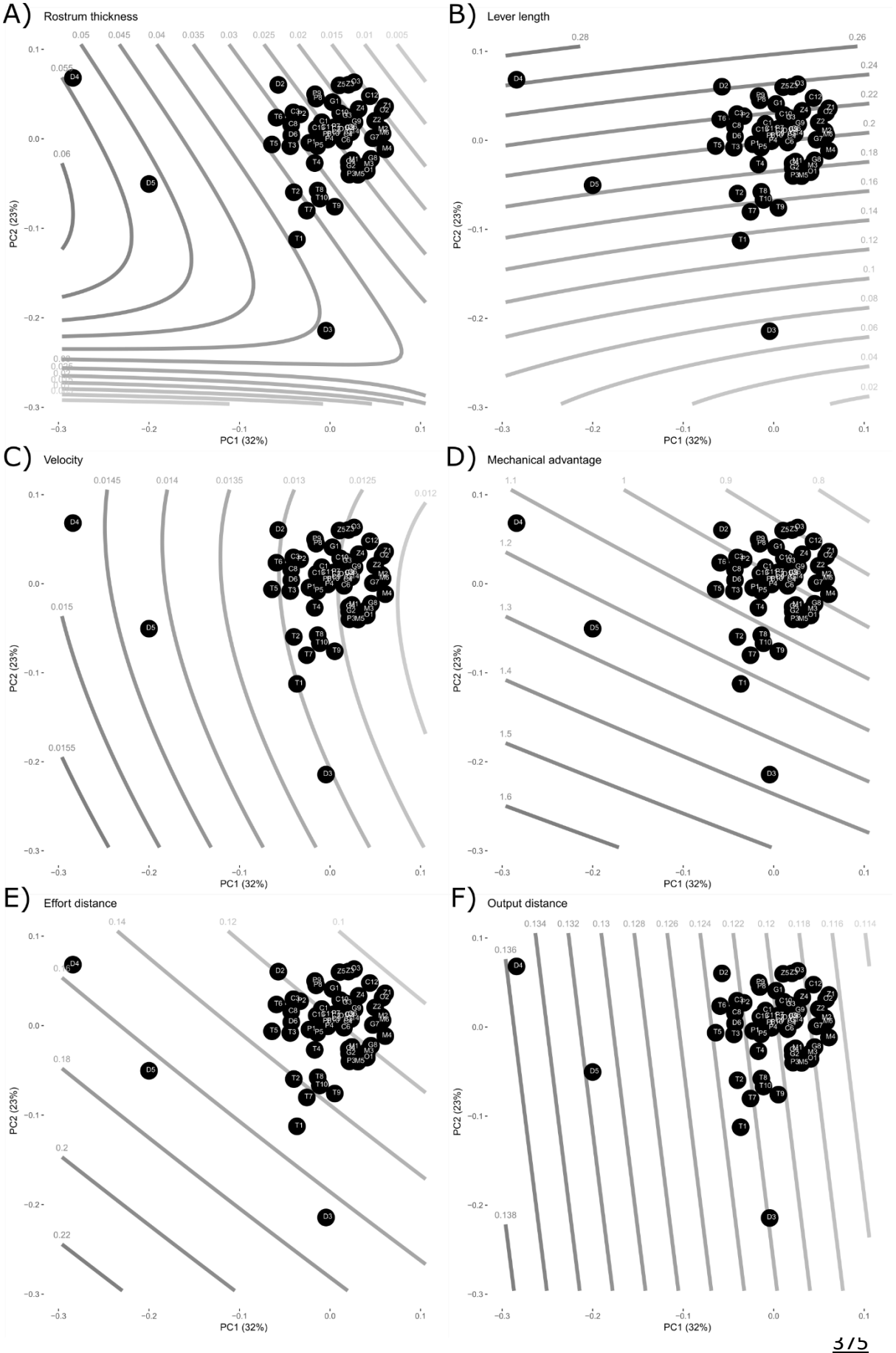

A) Rostrum thickness
B) Lever length
C) Velocity
D) Mechanical advantage
E) Effort distance
F) Output distance
PC1 (32%)
PC2 (23%)

Figure A3.2. Biomechanical landscape in PC1 and PC2 (continued). A) Rostrum dorsoventral thickness; B) anteroposterior lever length; C) velocity of bite; D) mechanical advantage; E) effort distance; F) output distance. Shapes were simulated for values across the PC2 and PC2, and the comparative biomechanical performance was measured for these shapes. Biomechanical performance is displayed as contour lines across the morphospace. Species in the sample are plotted in the biomechanical landscape according to their shape (PC scores). Legend for code names as in Figure A3.1.

incrementing towards negative values of PC3 and positive values of PC4, however the trends identified are similar when muscle area is used as a proxy for input force.

Mechanical advantage

For PC1 versus PC2, The taxon with higher mechanical advantage is *Didunculus* while *Treron curvirostra* and *Pezophaps* present the second highest mechanical advantage values (clusters “g”, “A”, and ”f”). *Raphus* shares the third highest mechanical advantage values with *Treron formosae*, Drepanoptila, Alectroenas and Ptilinopus (clusters “A”, “g”, and ”h”). The mechanical advantage (MA) showed a pattern which increments toward negative values of PC1 and PC2 (Figure A3.2D).

For PC3 versus PC4, the taxa with low mechanical advantages are *Metriopelia*, *Geophaps*, and *Pezophaps* (clusters “E” and “A”). While the taxa with high mechanical advantages are *Didunculus*, *Lopholaimus*, *Drepanoptila*, *Ducula goliath*, *Caloenas*, and *Otidiphaps* (clusters “g”, “f”, “A”, and “D”). The mechanical advantage closely follows the PC3 values (Figure A3.4D), it increments towards negative values and is slightly skewed towards positive values of PC4.

Effort distance and output force

For PC1 versus PC2, the effort distance (Figure A3.2E) and output force (Figure A3.1A) follow a similar pattern than the mechanical advantage. For PC3 versus PC4, the effort distance (Figure A3.4E) and output force show similar distributions (Figure A3.3A), with taxa like *Metriopelia*, *Geophaps*, *Pezophaps*, and *Ocyphaps* (clusters "E" and "A") showing low values of effort distance and output force. High values for these two biomechanical traits are shown by taxa like *Didunculus*, *Lopholaimus*, *Geotrygon*, *Alectroenas pulcherrimus*, *Geotrygon*, *Drepanoptila*, *Ducula*, *Caloenas*, *Otidiphaps*, *Goura*, *Chalcophaps*, *Hemiphaga*, and *Patagioenas* (clusters "g", "E", "h", "f", "A", and "D").

Output distance and mouth opening

For PC1 versus PC2, taxa with higher values of output distance (Do) and mouth (Mo) opening are *Raphus*, followed by *Pezophaps* and *Treron*, *Ptilinopus*, *Ducula*, *Hemiphaga*, *Goura*, *Caloenas*, *Columba vitiensis*, and *Columba trocaz* (clusters "A", "f", "g", "h", and "D"). The output distance is highly correlated with PC2 (Figure A3.2F), it increments towards negative values of PC2 although the increment of the output distance is slightly skewed towards negative values of PC1. Mouth opening (Figure A3.1B) follows a similar pattern to the output distance but the increment in mouth opening is more skewed towards negative values of PC1 than the output distance.

For PC3 versus PC4, taxa with low output distances are *Drepanoptila*, *Ducula*, and *Caloenas* ("g", "f", and "A") while other taxa with large output distances are *Columba guinea*, *Raphus*, *Metriopelia*, and *Pezophaps* ("E" and "A"). The output distance (Figure A3.4F) increments

towards positive values of PC3 and PC4. Mouth opening follows a similar pattern to output distance when PC3 is compared with PC4 (Figure A3.3B).

Velocity of bite

For PC1 versus PC2, *Raphus* shows the highest bite velocity, followed by *Pezophaps* and a group composed by *Didunculus*, *Treron*, *Ducula* and *Goura* (clusters "A", "g", "f", and "D"). The velocity of bite (Figure A3.2C) show a less linear relationship than other biomechanical variables. Broadly, it increments towards negative values of PC1 while it increments toward medium values of PC2. For PC3 versus PC4, velocity of bite (Figure A3.4C) is more linear than in previous principal components. This pattern closely resembles the mouth opening and output force.

Eye size

For PC1 versus PC2, the Raphini present the smallest eye sizes, while pigeons like *Metriopelia*, *Columbina passerina*, *Claravis*, *Turtur*, and *Leptotila rufaxilla* are characterized by large eye sizes (clusters "E" and "D"). Eye size increments with positive values of PC1 and is slightly skewed towards negative values of PC2 (Figure A3.1F).

For PC3 versus PC4, small eye sizes are presented by *Drepanoptila*, *Ducula*, *Caloenas*, *Otidiphaps*, *Goura*, *Chalcophaps*, *Hemiphaga*, *Patagioenas fasciata*, *Patagioenas plumbea*, *Leucosarcia*, *Didunculus*, *Patagioenas speciosa*, *Lopholaimus*, and *Geotrygon* mystacea (clusters "g", "f", "A", "D", "BC", and "E") and large eye sizes are present in *Metriopelia*, *Pezophaps*, and *Geophaps plumifera* followed by *Columba guinea*, *Raphus*, *Columba oenas*, *Columba rupestris*, and *Ocyphaps* (clusters "E", "A", and "BC"). The eye size increments in

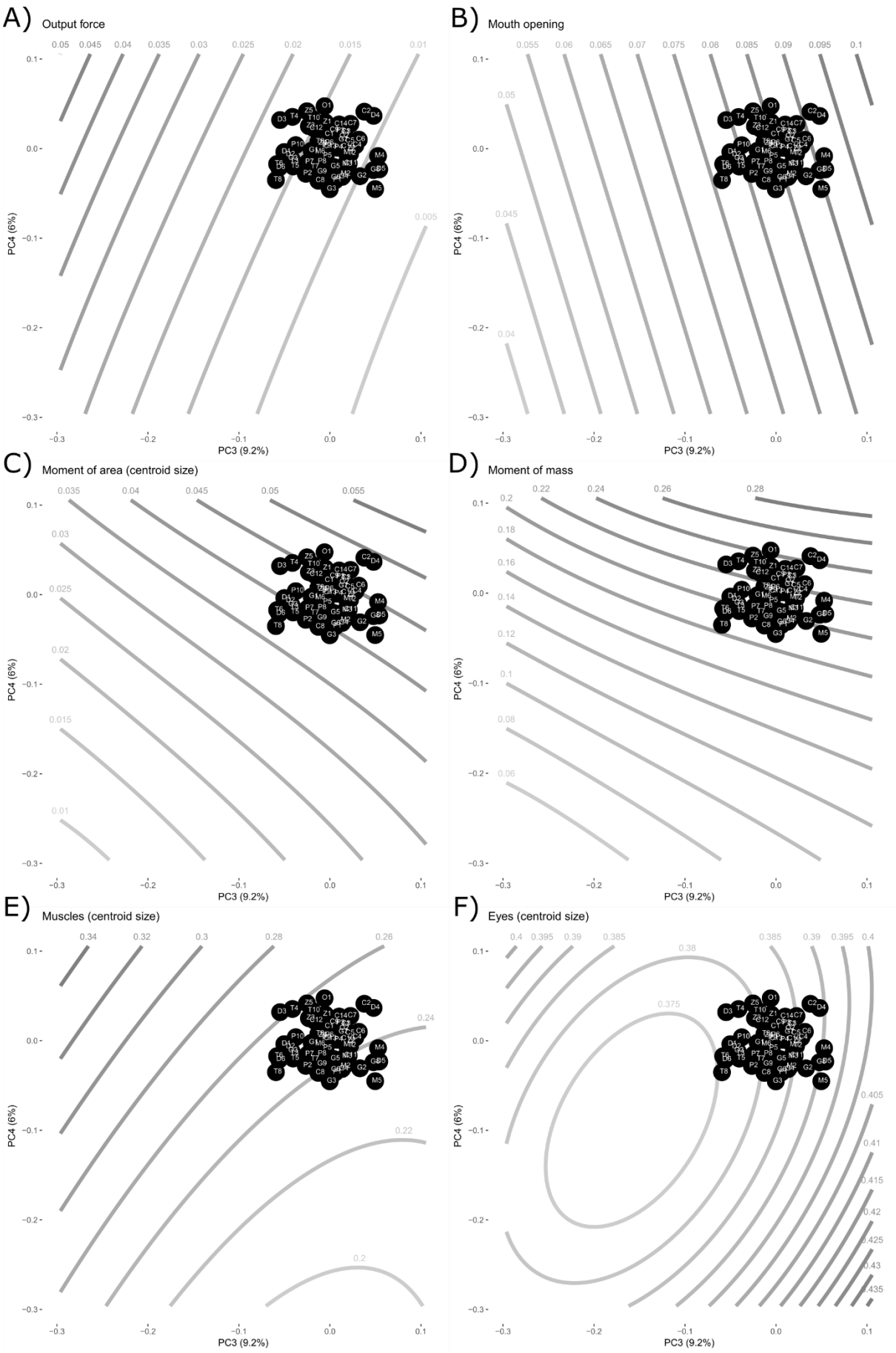

A)
Output force
B)
Mouth opening
C)
Moment of area (centroid size)
D)
Moment of mass
E)
Muscles (centroid size)
F)
Eyes (centroid size)
PC3 (9.2%)
PC4 (6%)

Figure A3.3. Biomechanical landscape in PC3 and PC4. A) Output force; B) mouth opening; C) moment of area; D) moment of mass; E) muscle size; F) eye size. Principal components 3 and 4 were used to simulate and evaluate the biomechanical function of the columbiform morphospace. Legend for code names as in Figure A3.1.

a concentric manner (Figure A3.3F). With the smallest eye sizes located at -0.1 in PC4 and at -0.2 in PC3.

Dorsoventral height (thickness) at mid length of the rostra

For PC1 versus PC2, the pigeons with thickest rostra are the Raphini, followed by *Didunculus*, *Treron* and *Ptilinopus* (clusters "A", "g", "f", and "h"). The rostrum thickness increments non-linearly following the negative values of PC1 and central values of PC2 (Figure A3.2A).

For PC3 versus PC4, pigeons with large dorsoventral height at mid-length of the rostrum are *Columba guinea*, *Raphus*, *Phapitreron, Columba palumbus*, and *Geotrygon* (clusters "E", "A", "g", and "BC") while taxa with low dorsoventral rostral height are *Drepanoptila*, *Caloenas*, *Ducula*, *Phaps*, *Columba vitiensis*, *Patagioenas fasciata*, and *Ducula* (clusters "g", "A", "f", "E", "h", and "BC"). The dorsoventral height at mid length of the rostrum (Figure A3.4A) increments towards the positive values of PC3 and PC4.

Moment of area

For PC1 versus PC2, the proxy for the moment of area (Figure A3.1C) follows a similar pattern to rostrum thickness, in which highest moment of area is shown by the Raphini, followed by *Treron* and then for a large cluster of pigeons including *Didunculus*. For PC3 versus PC4, pigeons with low moment of area are *Drepanoptila*, *Ducula*, *Caloenas*, *Patagioenas fasciata*, *Columba vitiensis*, *Metriopelia melanoptera* (clusters "g", "f", "A",

"BC", "h", and "E") and the taxa with high moment of area are *Columba guinea*, *Raphus*, *Phapitreron*, and *Columba palumbus* (clusters "E", "A", "g", and "BC"). The proxy for

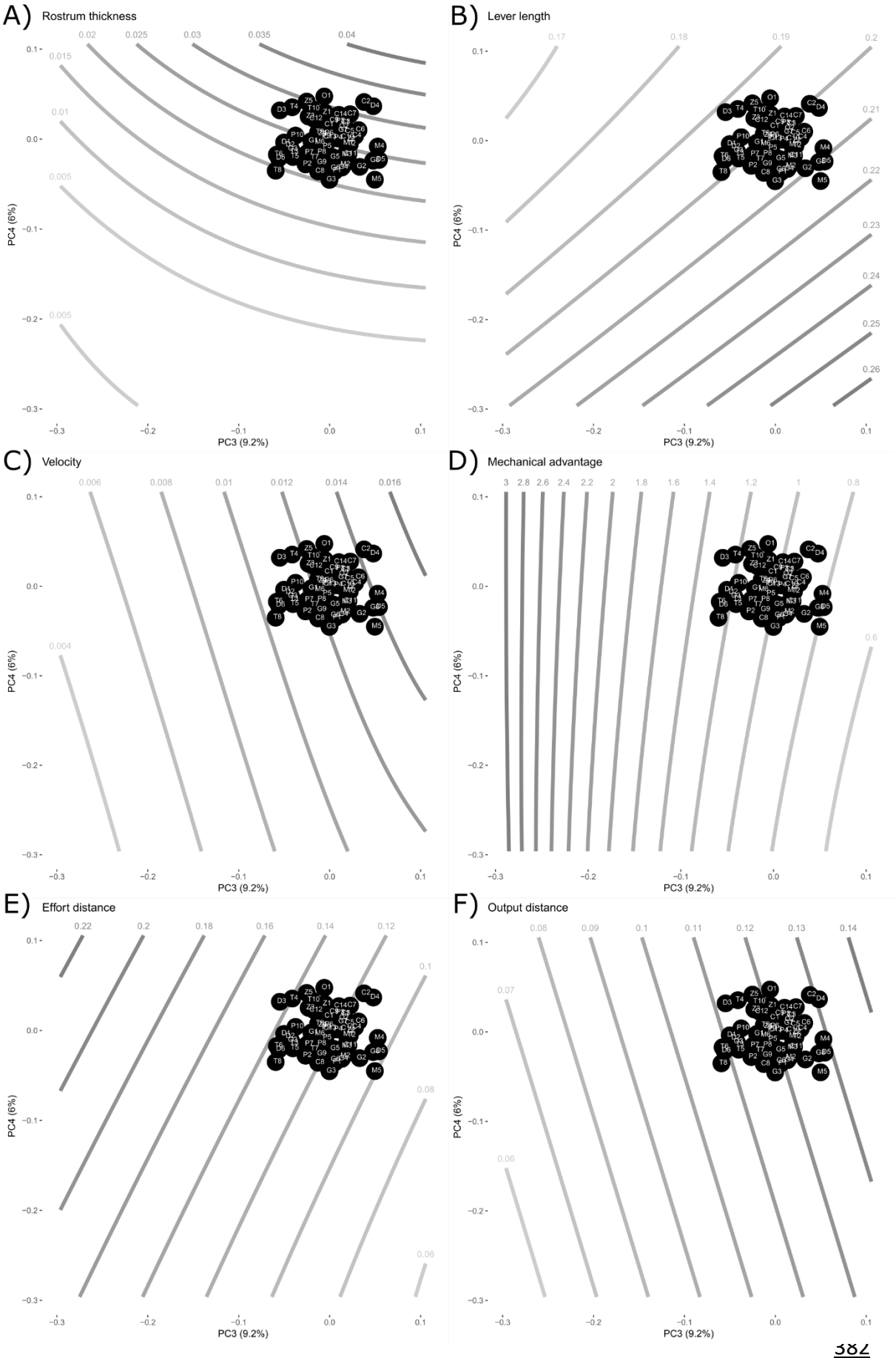

A) Rostrum thickness
B) Lever length
C) Velocity
D) Mechanical advantage
E) Effort distance
F) Output distance
PC3 (9.2%)
PC4 (6%)

Figure A3.4. Biomechanical landscape in PC3 and PC4 (continued). A) Rostrum dorsoventral thickness; B) anteroposterior lever length; C) velocity of bite; D) mechanical advantage; E) effort distance; F) output distance. Principal components 3 and 4 were used to simulate and evaluate the biomechanical function of the columbiform morphospace. Legend for code names as in Figure A3.1.

moment of area (Figure A3.3C) follows a similar pattern to the output distance (Figure A3.4F) with the moment of area incrementing towards positive values of PC3 and PC4.

The lever length (Dlever)

For PC1 versus PC2, the pigeons with larger lever length (Dlever) with respect to other (Procrustes aligned) pigeons in the morphospace, are *Raphus* and *Goura* while the shorter lever is presented by *Didunculus*, followed by *Treron*. The lever length is closely related to higher values of PC2 (Figure A3.2B).

For PC3 versus PC4, taxa with large lever length are *Ocyphaps*, *Geophaps plumifera*, *Pezophaps*, and *Metriopelia* (clusters "E" and "A") and short lever length taxa are *Didunculus*, *Lopholaimus*, *Geotrygon*, *Phapitreron* and *Alectroenas pulcherrimus* (clusters "g", "E", and "h"). Lever length (Figure A3.4B) increments towards negative values of PC4 and positive values of PC3.

Moment of mass

For PC1 versus PC2, the moment of mass (moment of area accounting for structure length) presents extremely different patterns than those of the moment of area (Figure A3.1D), *Didunculus* is the pigeon with highest moment of mass while the Raphini present similar resistance to bending than other pigeons. For PC3 versus PC4, the increment of the moment of mass (Figure A3.3D) closely follows PC4. Taxa with large moment of mass are *Phapitreron*, *Columba guinea*, and *Raphus* ("A", "g", and "E"). While taxa with low resistance to bending are *Drepanoptila*, *Ducula*, *Caloenas*, *Patagioenas fasciata*, *Columba*

vitiensis, *Metriopelia*, *Petrophassa*, *Ectopistes*, *Gallicolumba*, and *Phaps* ("g", "f", "A", "BC", "h", "E", and "D").

Detailed discussion of columbiform biomechanical landscape

The biomechanical landscape approach allowed me to assess the species distribution in the performance space. From which the first two principal components of shape (55% of the sample variation) are related to the feeding behaviour classification proposed here. The use of the biomechanical landscape allowed not only to spot the species with extremely different morphology/performance but to assess the differences in performance among these species based on shape alone.

The species with distinct biomechanical performance are, not surprisingly, the pigeons with distinctive morphology. These pigeon species are *Pezophaps*, *Raphus*, *Didunculus*, and *Treron curvirostra*. However, even in the pigeons with a conservative shape (closer to the mean shape of the sample), I noted that frugivorous species (Cluster M1; "fruit pigeons", frugivorous *Columba* and *Patagioenas*, and Raphinae) show higher biomechanical performance than granivorous species. This high performance corresponded to large muscle area and high mechanical advantage. These frugivorous species skull shapes also showed high resistance to bending (high rostrum thickness and moments of area and mass).

Pigeon species with a granivorous diet were distributed in a contiguous area of the morphospace to frugivorous pigeons. The granivorous species show slender rostra, large eye sizes, and small mouth openings that close at high velocity. The granivorous species also show low mechanical advantages and low output forces with small muscle areas and low bending resistance (moments of area and mass). Some biomechanical characters like

large lever length were not correlated with any specific feeding categories. For PC3 and 4 (15.2% of sample variation), only muscle area and lever length seem to be related with any feeding strategies (ancestral granivorous diet).

The assessment of the biomechanical performance was useful to understand how the species with peculiar skull shapes differ in performance. While *Raphus* and *Pezophaps* presented high rostrum thickness, this was not related to bending resistance when the structure length was taken into account (moment of mass). The Raphini presented the highest velocity of bite, largest mouth opening, and smallest eye sizes. *Didunculus* is the pigeon with a skull shape that presents a higher bending resistance and output force, this species also presents relatively large eye sizes, unlike the Raphini.

The skull shape of the Raphini, especially the dodo, has been hypothesized to be related to the inclusion of animals in the diet (Owen, 1866; Livezey, 1993). However, animals would be included in the diet of Raphini sporadically and as supplement of their diets of fallen fruit and seeds, with bulbs also hypothesized to be used as a food resources by these obligate ground dwelling birds (Owen, 1866; Goodwin, 1983; Livezey, 1993; Angst, Buffetaut and Abourachid, 2011). The biomechanical performance of the skull shape in Raphini, compared to that of other pigeons, seems to contradict some of the feeding behaviour hypotheses. While the high bite velocity could suggest the inclusion of animal matter in the diet, other biomechanical traits suggest otherwise. First, the eye size of Raphini is the smallest in the sample, which might imply a lower visual acuity unsuited for the targeting of small or fast prey. However, the calculated eye size should be carefully considered because it was measured in the Procrustes aligned skulls and does not take in

account the real large size of the Raphini skulls. Second, the eye position in both *Raphus* and *Pezophaps* seems to support a preferentially peripherical rather than binocular vision. However, the field of vision overlap was not measured or simulated. Third, the moment of area could support the hypothesis of the inclusion of animals on the diet because high performance would allow the Raphini to capture and retain struggling prey without suffering structural damage. However, the moment of mass (taking lever length into account) showed that comparatively, the bending resistance of the Raphini is similar to the one of *Treron curvirostra* or other "fruit pigeons". Overall these results support the classical view of the Raphini feeding behaviour (Owen, 1866; Livezey, 1993). The Raphini probably feed on fallen fruit on the forest ground, while the inclusion of fast or small live prey or heavily armoured prey with armour like crustaceans and molluscs (Hachisuka, 1953 in Livezey, 1993) seems unlikely.

Appendix Four. Scripts

A) Script used in Chapter Two

```
################################################
#This script was used to predict size based on  #
#  skull as part of the Heterochronic test      #
################################################
library(ape)
library(geiger)
library(nlme)
library(phytools)
library(geomorph)
library(ggplot2)
load("CoordinatesMassCs.rda")


GetCoefficients<-function(x){
Coeff<-x$coefficients
return(Coeff)
}
###For body mass
###similar to a pigmy parrot
MinCsise<-min(Compare$Csize)*.5
#From maximum estimation by Livezey min
MaxCsize<-max(Compare$Csize)*1.5
MassSeq<-log10(seq(1,30000))
#MassSeq<-log10(seq(1,30000,by=50))
Intercept<-rep(1,length(MassSeq))
Coefficients<-lapply(DpglsMultiColumbiformesnpMass,GetCoefficients)
MeanCoefficients<-Reduce("+", Coefficients) / length(Coefficients)

#########predict shapes for Size ranges and for acual sizes
NewX<-as.matrix(data.frame(Intercept=Intercept,LogMass=MassSeq))
Predicted<-NewX %*% MeanCoefficients
PredictedOnlyAllom<-
as.matrix(data.frame(Intercept=rep(1,length(Compare$Mass)),LogMass=log10(
Compare$Mass)))%*% MeanCoefficients

#########
Coefficients<-lapply(DpglsMultiColumbiformesnpCsize,GetCoefficients)
MeanCoefficients<-Reduce("+", Coefficients) / length(Coefficients)

CsizeSeqNormal<-
seq(MinCsise*1.5,MaxCsize*.5,length.out=length(Intercept))
CsizeSeq<-log10(CsizeSeqNormal)
NewXCsize<-as.matrix(data.frame(Intercept=Intercept,LogMass=CsizeSeq))
PredictedCsize<-NewXCsize %*% MeanCoefficients
PredictedCsizeOnlyAllom<-
as.matrix(data.frame(Intercept=rep(1,length(Compare$Csize)),LogMass=log10
(Compare$Csize)))%*% MeanCoefficients

###Predict the best size for the shape
GetDiff<-function(x){
DataTemp<-data.frame(x,y)
abs(DataTemp$x-DataTemp$y)
}
```

```
Results<-NULL
SppNumber<-seq(1,dim(ProWild)[1])
for (i in SppNumber){
y=ProWild[i,]
Test<-apply(Predicted,1,GetDiff)
Test2<-colSums(Test)
PBodyMass<-which(Test2==min(colSums(Test)))
Results<-c(Results,PBodyMass)
}

ResultsCS<-NULL
ResultsCSNum<-NULL
for (i in SppNumber){
y=ProWild[i,]
Test<-apply(PredictedCsize,1,GetDiff)
Test2<-colSums(Test)
PCsizeNUM<-which(Test2==min(colSums(Test)))
ResultsCSNum<-c(ResultsCSNum,PCsizeNUM)
PCsize<-CsizeSeqNormal[PCsizeNUM]
ResultsCS<-c(ResultsCS,PCsize)
}


ResutlsTable<-
data.frame(Names=rownames(ProWild),Mass=Compare$Mass,Predicted_mass=Resul
ts,Csize=Compare$Csize,Predicted_Csize=ResultsCS)
write.csv(ResutlsTable,file="ResultsMassPrediction2.csv")
#################Get percentage of shape explained
AllNames<-rownames(Compare)
AllBestMass<-Predicted[Results,]
rownames(AllBestMass)<-rownames(PredictedOnlyAllom)<-AllNames
AllReal<-arrayspecs(ProWild,27,3)
AllBestMass<-arrayspecs(AllBestMass,27,3)
PredictedOnlyAllom<-arrayspecs(PredictedOnlyAllom,27,3)
#
AllBestCsize<-PredictedCsize[ResultsCSNum,]
rownames(AllBestCsize)<-rownames(PredictedCsizeOnlyAllom)<-AllNames
AllBestCsize<-arrayspecs(AllBestCsize,27,3)
PredictedCsizeOnlyAllom<-arrayspecs(PredictedCsizeOnlyAllom,27,3)

GetRealCentroids<-function(x){
Centroids<-NULL
Test2<-colMeans(x)
Centroids<-rbind(Centroids,Test2)
return(Centroids)
}

RealCentroids<-t(apply(AllReal,3,GetRealCentroids))

GetDistances<-function(x,y){
Distances<-NULL
GeomDist<-NULL
for (i in seq(1,length(x[,1]))){
Test2<-x[i,]-y[i]
Distances<-rbind(Distances,Test2)
GeomDist2<-sqrt(sum(Distances^2))
GeomDist<-c(GeomDist,GeomDist2)
#AbsDist<-sum(abs(Distances))
```

```
}

return(GeomDist)

}
DistReal<-apply(AllReal,3,GetDistances,y=RealCentroids)
DistBestMass<-apply(AllBestMass,3,GetDistances,y=RealCentroids)
DistAllomModel<-apply(PredictedOnlyAllom,3,GetDistances,y=RealCentroids)
DistBestCsize<-apply(AllBestCsize,3,GetDistances,y=RealCentroids)
DistAllomModelCsize<-
apply(PredictedCsizeOnlyAllom,3,GetDistances,y=RealCentroids)

ColsumsReal<-colSums(DistReal)
PercentageBestMass<-100-colSums(abs(DistReal-
DistBestMass))/ColsumsReal*100
PercentageAllometry<-100-colSums(abs(DistReal-
DistAllomModel))/ColsumsReal*100
PercentageBestCsize<-100-colSums(abs(DistReal-
DistBestCsize))/ColsumsReal*100
PercentageAllometryCsize<-100-colSums(abs(DistReal-
DistAllomModelCsize))/ColsumsReal*100

ResultsPercentage<-
data.frame(PercentageBestMass,PercentageAllometry,PercentageBestCsize,Per
centageAllometryCsize)
write.csv(ResultsPercentage,file="ResultsMassPredictionPercent.csv")
```

B) Script used in Chapter Three

```
#########################################################################
#This script calculates the biomechanical performance across the
morphospace#
#########################################################################

library(geomorph)
library("scatterplot3d")
library(ggplot2)
library(reshape2)
library(RColorBrewer)
library(plyr)
library(NISTunits)
setwd("C:/Users/penta/Desktop/Analysis/Pigeons Columbiformes
environment/Function")
load("EcologyData.rda")

Distance3D<-function(x,y){
sqrt(sum((x-y)^2))
}
#Areas calculated using Heron's formula
Heron<-function(x,y,z){
A<-Distance3D(x,y)
B<-Distance3D(x,z)
C<-Distance3D(z,y)
S<-(A+B+C)/2
A<-sqrt(S*(S-A)*(S-B)*(S-C))
return(A)
}
####Proyection od point C to a AB line
GetCoordToLine<-function(A,B,C){ #A B line, C point projected
Dir<-(B-A)/Distance3D(B,A)
VectorLinetoUpper<-C-B
DistToProyection<-crossprod(VectorLinetoUpper,Dir)
Proyected27<-B+crossprod(DistToProyection,Dir)
return(Proyected27)
}
#GetCSize<-function(x){sqrt(sum((x-mean(x))^2))}
###Fix Fitness
FixFitness<-function(i){
RealFitness2 <-
data.frame(Fe=numeric(0),De=numeric(0),Do=numeric(0),Mo=numeric(0),MA=num
eric(0),Vel=numeric(0),Fo=numeric(0))
for (j in i){
RealFitness2<-rbind(RealFitness2,j)
}
rownames(RealFitness2)<-(rownames(ProColumbiformes))
return(RealFitness2)
}
FixFitness2<-function(i){
RealFitness2 <-
data.frame(Fe=numeric(0),De=numeric(0),Do=numeric(0),Mo=numeric(0),MA=num
eric(0),Vel=numeric(0),Fo=numeric(0))
for (j in i){
RealFitness2<-rbind(RealFitness2,j)
}
#rownames(RealFitness2)<-(rownames(ProColumbiformes))
```

```
return(RealFitness2)
}
####FitnessCentroidSize
CentroidSizes<-function(x){
NewCooordinates<-arrayspecs(t(x),4,3)
Icentroid<-gpagen(NewCooordinates[2:4,,])$Csize
MuscleI<-gpagen(procrustesCoord[c(6,16,18),,])$Csize
MuscleR<-gpagen(procrustesCoord[c(6,15,17),,])$Csize
MuscleT<-MuscleI+MuscleR
EyeI<-gpagen(procrustesCoord[c(14,25,20,29),,])$Csize
EyeR<-gpagen(procrustesCoord[c(13,26,19,28),,])$Csize
EyeT<-EyeI+EyeR
data.frame(Icentroid,MuscleI,MuscleR,MuscleT,EyeI,EyeR,EyeT)
}
#x=Fitness coordinates, y= original coordinates
CentroidSizes2<-function(x,y){
NewCooordinates<-arrayspecs(t(x),4,3)
Icentroid<-gpagen(NewCooordinates[2:4,,])$Csize
MuscleI<-gpagen(y[c(6,16,18),,])$Csize
MuscleR<-gpagen(y[c(6,15,17),,])$Csize
MuscleT<-MuscleI+MuscleR
EyeI<-gpagen(y[c(14,25,20,29),,])$Csize
EyeR<-gpagen(y[c(13,26,19,28),,])$Csize
EyeT<-EyeI+EyeR
data.frame(Icentroid,MuscleI,MuscleR,MuscleT,EyeI,EyeR,EyeT)
}
###Get Fitness
Fitness<-function(i,j){
Fulcrum<-(i[18,]+i[17,])/2
MidDe<-(i[15,]+i[16,])/2
De<-Distance3D(Fulcrum,MidDe)
Do<-Distance3D(Fulcrum,i[18,])
#Areas calculated using Heron's formula
Mai<-Heron(i[6,],i[16,],i[18,])
Mar<-Heron(i[6,],i[15,],i[17,])
#force of effot
Fe<-Mai+Mar
###Fitness
#Mouth opening at 45 degrees
Mo=Do*sin(NISTdegTOradian(45))
#Mechanical advantage
MA<-De/Do
#force/ Velocity
Vel<-(Fe*Do)/De
#Bite force
Fo<-Fe*MA
################New####################
####Second moment of inertia
RostrumProx<-(i[9,]+i[10,])/2
RostrumDist<-(i[7,]+i[8,])/2
Proy27<-GetCoordToLine(RostrumProx,RostrumDist,i[27,])
Thickness<-Distance3D(i[27,],Proy27)
Dlever<-Distance3D(RostrumProx,RostrumDist)
ProyR<-GetCoordToLine(i[7,],i[9,],Proy27)
ProyL<-GetCoordToLine(i[8,],i[10,],Proy27)

#######################################
```

```
Fitness<-
data.frame(Fe=Fe,De=De,Do=Do,Mo=Mo,MA=MA,Vel=Vel,Fo=Fo,Thick=Thickness,Dl
ever=Dlever)
#Fitness<-data.frame("Effort force"=Fe,"Effort distance"=De,"Output
distance"=Do,"Mouth opening"=Mo,
#"Mechanical advantage"=MA,"Velocity"=Vel,"Output force"=Fo,"Rostrum
thickness"=Thickness,
#"Lever length"=Dlever)

Coordinates<-cbind(as.vector(Proy27),ProyR,ProyL,i[27,])
#Results<-list("Fitness"=Fitness,"Coords"=Coordinates)
ifelse(j=="Coordinates",return(Coordinates),ifelse(j=="Fitness",return(Fi
tness),return("Error")))
#return(Results)
#return(Coordinates)
}

#################################################################
#                   Calculate Real Fitness                      #
#################################################################
RealFitness<-apply(procrustesCoord,c(3),Fitness,j="Fitness")
RealNewCooordinates<-apply(procrustesCoord,c(3),Fitness,j="Coordinates")
RealFitness<-FixFitness(RealFitness)
RealFitnessCsizes<-CentroidSizes(RealNewCooordinates)

RealFitnessCsizes$Icentroid/RealFitness$Dlever
FinFitnessReal<-
data.frame(RealFitness,RealFitnessCsizes,Bending=RealFitnessCsizes$Icentr
oid/RealFitness$Dlever)
#save(FinFitnessReal,file="ResultsRealFitness.rda")

#################################################################
#                       Get rasters                             #
#################################################################

#Get Procrustes
PCA<-plotTangentSpace(procrustesCoord,labels=TRUE)
#min(PCA$pc.scores[,"PC2"])
#max(PCA$pc.scores[,"PC2"])
Min<-min(apply(PCA$pc.scores,2,min))*1.05
Max<-max(apply(PCA$pc.scores,2,max))*1.05
#Min<-.30*-1
#Max<-.11

SimulList<-
expand.grid(seq(Min,Max,length.out=100),seq(Min,Max,length.out=100))
x <- two.d.array(procrustesCoord)
    ref <- mshape(procrustesCoord)
    retx <- TRUE
    scale.<-FALSE
    center<-TRUE
    d <- prcomp(x)$sdev^2
    cd <- cumsum(d)/sum(d)
    cd <- length(which(cd < 1))
    tol <- max(c(d[cd]/d[1], 0.005))
    k <- dim(procrustesCoord)[2]
    p <- dim(procrustesCoord)[1]
    n <- dim(procrustesCoord)[3]
pc.res <- prcomp(x, center = center, scale. = scale., retx = retx,
```

```
    tol = tol)
shapes <- shape.names <- NULL

############list of  combinations, y and z are the desired PC
Working<-function(i,y,z){
pc.yz <- rep(0, dim(pc.res$x)[2])
pcaxis.y<-i[[1]]
pcaxis.z<-i[[2]]
pc.yz[[y]] <- pcaxis.y
pc.yz[[z]] <- pcaxis.z
pc.yz <- as.matrix(pc.yz %*% (t(pc.res$rotation))) +
    as.vector(t(ref))
shapes2 <- arrayspecs(pc.yz, p, k)
shapes2 <- lapply(seq(dim(shapes2)[3]), function(x) shapes2[,
        , x])
}
Maybe<-apply(SimulList, 1, Working ,y=1,z=2)
```

C) Script used in Chapter Four

```
#########################################################################
# This Script Performs analyses of the Chapter 4 (Domestication) #
#########################################################################

library(ggplot2)
library(geomorph)
library(RColorBrewer)
library(MCMCglmm)
library(statmod)
library(evolqg)
library(phytools)
library(geiger)
library(reshape2)
library(scales)

rad2deg <- function(rad) {(rad * 180) / (pi)}
deg2rad <- function(deg) {(deg * pi) / (180)}
setwd("C:/Users/penta/Desktop/Analysis/Pigeons        Domestication/Clean
Script")
load("DomesticationData.rda")
wires<-read.csv("WiresFinal.csv",header=FALSE)
wires<-data.matrix(wires)

#########################################################################
#                          Centroids                                    #
#########################################################################
colSd   <-   function   (x,   na.rm=FALSE)   apply(X=x,   MARGIN=2,   FUN=sd,
na.rm=na.rm)

CentroidWild<-colMeans(subset(DataPCA[,1:74], Subset=="Wild"))
CentroidWildsd<-colSd(subset(DataPCA[,1:74], Subset=="Wild"))
CentroidDomestic<-colMeans(subset(DataPCA[,1:74], Subset=="Domestic"))
CentroidDomesticsd<-colSd(subset(DataPCA[,1:74], Subset=="Domestic"))
CentroidFeral<-colMeans(subset(DataPCA[,1:74], Subset=="Feral"))
CentroidFeralsd<-colSd(subset(DataPCA[,1:74], Subset=="Feral"))

#one sd
SpanWild<-t(rbind(CentroidWild-
(1*CentroidWildsd),CentroidWild+(1*CentroidWildsd)))
SpanDomestic<-t(rbind(CentroidDomestic-
(1*CentroidDomesticsd),CentroidDomestic+(1*CentroidDomesticsd)))
SpanFeral<-t(rbind(CentroidFeral-
(1*CentroidFeralsd),CentroidFeral+(1*CentroidFeralsd)))

GetOverlap<-function(x){
A<-x[1:2]
B<-x[3:4]
AB<-c(A,B)
#Smaller<-
ifelse(which(AB==min(AB))==3,Smaller<-
B,ifelse(which(AB==min(AB))==1,Smaller<-A,"error"))

#Larger<-
ifelse(Smaller==A,Larger<-B,ifelse(Smaller==B,Larger<-A,"error"))

Overlap<-ifelse(
```

```
#if minLarger is larger than maxSmaller then overlap is zero
Smaller[2]<Larger[1],0,ifelse(
#if maxSmaller is larger than maxLarger then overlap is 1
Smaller[2]>Larger[2],1,
#Percentage of overlap from minSmaller to maxLarger
(Smaller[2]-Larger[1])/(Larger[2]-Smaller[1])
))
return(Overlap)
}

Overlap1sd<-
c(sum(apply(cbind(SpanWild,SpanDomestic),1,GetOverlap)*Importance.All[1:7
4]),
sum(apply(cbind(SpanWild,SpanFeral),1,GetOverlap)*Importance.All[1:74]),
sum(apply(cbind(SpanDomestic,SpanFeral),1,GetOverlap)*Importance.All[1:74
]))

#2 sd
SpanWild<-t(rbind(CentroidWild-
(2*CentroidWildsd),CentroidWild+(2*CentroidWildsd)))
SpanDomestic<-t(rbind(CentroidDomestic-
(2*CentroidDomesticsd),CentroidDomestic+(2*CentroidDomesticsd)))
SpanFeral<-t(rbind(CentroidFeral-
(2*CentroidFeralsd),CentroidFeral+(2*CentroidFeralsd)))

Overlap2sd<-
c(sum(apply(cbind(SpanWild,SpanDomestic),1,GetOverlap)*Importance.All[1:7
4]),
sum(apply(cbind(SpanWild,SpanFeral),1,GetOverlap)*Importance.All[1:74]),
sum(apply(cbind(SpanDomestic,SpanFeral),1,GetOverlap)*Importance.All[1:74
]))

TableOverlap<-rbind(Overlap1sd,Overlap2sd)
colnames(TableOverlap)<-c("Wild vs Domestic","Wild vs Feral","Domestic vs
Feral")
write.csv(file="TableOverlap.csv",t(TableOverlap))

##########Function unit vectors#################
 scalar1 <- function(x) {x / sqrt(sum(x^2))}

##########Function to get the norma##############
 Norma <- function(x) sqrt(sum(x^2))

######Get Angles (to determine better comparissons)
###we Could use also Raphines
Weirdos<-c("Raphus_cucullatus", "Pezophaps_solitaria")
Normies<-setdiff(rownames(ProWild),Weirdos)
#Withour Raphines
A.WildNR<-plotTangentSpace(arrayspecs(ProWild[Normies,],27,3))

GetAngle<-function(x,y){
Angle<-acos(sum(x*y)/(Norma(x)*Norma(y)))
return(Angle)
}

AnglesDomesticWild<-matrix(,nrow=0,ncol=10)
for(i in seq(1,10)){
TempAngle<-
apply(A.WildNR$rotation[,1:10],2,GetAngle,A.Domestic$rotation[,i])
```

```
AnglesDomesticWild<-rbind(AnglesDomesticWild,TempAngle)
}
AnglesDomesticWild<-
rbind(rad2deg(AnglesDomesticWild),closest=apply(AnglesDomesticWild,2,whic
h.min))

AnglesDomesticFeral<-matrix(,nrow=0,ncol=10)
for(i in seq(1,10)){
TempAngle<-
apply(A.Feral$rotation[,1:10],2,GetAngle,A.Domestic$rotation[,i])
AnglesDomesticFeral<-rbind(AnglesDomesticFeral,TempAngle)
}
AnglesDomesticFeral<-
rbind(rad2deg(AnglesDomesticFeral),closest=apply(AnglesDomesticFeral,2,wh
ich.min))

AnglesWildFeral<-matrix(,nrow=0,ncol=10)
for(i in seq(1,10)){
TempAngle<-
apply(A.Feral$rotation[,1:10],2,GetAngle,A.WildNR$rotation[,i])
AnglesWildFeral<-rbind(AnglesWildFeral,TempAngle)
}
AnglesWildFeral<-
rbind(rad2deg(AnglesWildFeral),closest=apply(AnglesWildFeral,2,which.min)
)

write.csv(file="AnglesDomesticWild.csv",AnglesDomesticWild)
write.csv(file="AnglesDomesticFeral.csv",AnglesDomesticFeral)
write.csv(file="AnglesWildFeral.csv",AnglesWildFeral)
#########################################################################
##
#                  Compare distance of closest vectors                  #
#########################################################################
##
CompDW<-rbind(seq(1,10),AnglesDomesticWild["closest",])
CompDF<-rbind(seq(1,10),AnglesDomesticFeral["closest",])
CompWF<-rbind(seq(1,10),AnglesWildFeral["closest",])

# No signs
GetDiff<-function(x,y,z){#x=groupA,y=groupB,z=Equivalence
CompResult<-matrix(,nrow=81,ncol=0)

for (i in seq(1,10)){
#TempCorresp<-z[,i][2]
TempName<-paste0("comp",i,z[,i][2])
TempDiff<-abs(x[,1])-abs(y[,z[,i][2]])
assign(TempName,TempDiff)
CompResult<-cbind(CompResult,get(TempName))
}
return(CompResult)}

#Diff in 81 dimensions
DiffDW<-GetDiff(A.Domestic$rotation,A.WildNR$rotation,CompDW)
DiffDF<-GetDiff(A.Domestic$rotation,A.Feral$rotation,CompDF)
DiffWF<-GetDiff(A.WildNR$rotation,A.Feral$rotation,CompDW)
#Dif per landmark
DiffLandDW<-apply(abs(arrayspecs(t(DiffDW),27,3)),3,rowSums)
DiffLandDF<-apply(abs(arrayspecs(t(DiffDF),27,3)),3,rowSums)
DiffLandWF<-apply(abs(arrayspecs(t(DiffWF),27,3)),3,rowSums)
```

```
##############################Define heat3Dplot
#Plots distance with each axis as the color scale
PlotDistance2<-function(x,links,y){#x     any     coords     for     mean
shape,links,y=axis
ColTest<-as.numeric(cut2(y, g=10))
cols<-rev(brewer.pal(10, "RdBu"))
ColTest<-cols[ColTest]
plot3d(mshape(arrayspecs(x,27,3)), type = "s", col = ColTest, main =
paste("Eigenvector effect difference"), size = 2, aspect = FALSE,
                  xlab = "", ylab = "", zlab = "", box = FALSE,
                  axes = FALSE)
M1<-mshape(arrayspecs(x,27,3))
gP <- gridPar()
                linkcol <- rep(gP$link.col, nrow(links))[1:nrow(links)]
                linklwd <- rep(gP$link.lwd, nrow(links))[1:nrow(links)]
                linklty <- rep(gP$link.lty, nrow(links))[1:nrow(links)]
                tarlinkcol            <-            rep(gP$tar.link.col,
nrow(links))[1:nrow(links)]
                tarlinklwd            <-            rep(gP$tar.link.lwd,
nrow(links))[1:nrow(links)]
                tarlinklty            <-            rep(gP$tar.link.lty,
nrow(links))[1:nrow(links)]
                for (i in 1:nrow(links)) {
                  segments3d(rbind(M1[links[i, 1], ], M1[links[i,
                    2], ]), col = linkcol[i], lty = linklty[i],
                    lwd = linklwd[i])
                    }
}


#####################################################################
#                       Check for similar but diff scALE            #
#####################################################################
GetScales<-function(x,y){#x and y are matrices to be compared
Scales<-matrix(,ncol=10)
for (i in seq(1,10)){
ScaleTemp<-apply(round(x$rotation[,i]/y$rotation[,1:10],2),2,function(x)
length(unique(x)))
Scales<-rbind(Scales,ScaleTemp)
}
Scales<-Scales[-1,]
Min<-apply(Scales,2,min)
Scales<-rbind(Scales,Min)
return(Scales)}
ScaleDW<-GetScales(A.Domestic,A.WildNR)
ScaleDF<-GetScales(A.Domestic,A.Feral)
ScaleWF<-GetScales(A.WildNR,A.Feral)
write.csv(ScaleDW,file="ScaleDW.csv")
write.csv(ScaleDF,file="ScaleDF.csv")
write.csv(ScaleWF,file="ScaleWF.csv")


#####################################################################
#                  Krzanowski     1972                              #
#####################################################################

#####Cumulative variance
GetNImportances<-function(x){
```

```
rbind(Dometic=A.Domestic$pc.summary$importance[3,x],
WildNR=A.WildNR$pc.summary$importance[3,x],
Feral=A.Feral$pc.summary$importance[3,x])
}
GetNImportances(4)
#####Getmatrices for comparison
KrazaDomestic<-A.Domestic$rotation[,1:4]
KrazaWildNR<-A.WildNR$rotation[,1:4]
KrazaFeral<-A.Feral$rotation[,1:4]

#Original function seemed to be wrong in vecs, it used vectors without any
reason
krzanowski.test2<-function (CA, CB, vecsA, vecsB,corr = FALSE,...){#  ...)
    if (length(vecsA) != length(vecsB)) {
        stop("vecsA amd vecsB must be same length")
    }
    if (length(vecsA) > c(dim(CA)[1]/2)) {
        warning("component spaces must be ", floor(c(dim(CA)[1]/2)),
            " dimension", "s"[floor(c(dim(CA)[1]/2)) > 1], " or less")
    }
    if (corr) {
        CA <- cov2cor(CA)
        CB <- cov2cor(CB)
    }
    #CA <- as.matrix(eigen(CA)$vectors[, vecsA])
    #CB <- as.matrix(eigen(CB)$vectors[, vecsB])
    N <- t(CA) %*% CB %*% t(CB) %*% CA
    eigval <- eigen(N)$values
    eigvec <- as.matrix(eigen(N)$vectors)
    bisector <- matrix(NA, dim(CA)[1], vecsA)
    I <- diag(dim(CA)[1])
    for (i in 1:vecsA) {
        bisector[, i] <- sqrt(2 * (1 + sqrt(eigval[i]))) * ((I +
            (1/sqrt(eigval[i])) * CB %*% t(CB)) %*% CA %*% eigvec[,
            i])
        bisector[, i] <- bisector[, i]/sqrt(sum(bisector[, i]^2))
    }
    angles <- acos(eigval^0.5)/(pi/180)
    sumofS <- sum(eigval)
    list(sumofS = sumofS, angles = angles, bisector = bisector,N=N)
}
I <- diag(dim(KrazaDomestic)[1])
RealDF<-krzanowski.test2(KrazaDomestic,KrazaFeral,4,4)
RealDW<-krzanowski.test2(KrazaDomestic,KrazaWildNR,4,4)
RealWF<-krzanowski.test2(KrazaWildNR,KrazaFeral,4,4)

#####################Permutation
GetResampleKraza<-function(x,y,z,w){#two matrices to compare, z number of
PC, what to get(string):sumofS or angles
Lx<-nrow(x)
Ly<-nrow(y)
All<-rbind(x,y)
La<-nrow(All)
#New Permutation without replacement
SampleAll<-sample(La)
x2<-All[SampleAll[seq(1,Lx)],]
y2<-All[SampleAll[seq(Lx+1,La)],]

Kraza.x2<-plotTangentSpace(arrayspecs(x2,27,3))$rotation[,1:z]
```

```
Kraza.y2<-plotTangentSpace(arrayspecs(y2,27,3))$rotation[,1:z]
rgl.close()
rgl.close()
dev.off()

ResT<-krzanowski.test2(Kraza.x2,Kraza.y2,z,z)
ifelse(w=="angles",return(ResT$angles[1]),ifelse(w=="sumofS",return(ResT$
sumofS),return("error")))
}



############################ Nice plots

PlotHisto<-function(x,y,z,w){#x permu, y real, z name sting,w angle or
sumofS
Bper<-
ifelse(w=="angle",length(which(x>=y)),ifelse(w=="sumofS",length(which(x<=
y)),"error"))
Mper<-length(x)
pPerm<-round((Bper+1)/(Mper+1),5)
qplot(x,geom="histogram")+
geom_vline(aes(xintercept=y),colour="red",size=2)+
theme_bw() + theme(panel.border = element_blank(), panel.grid.major =
element_blank(),
panel.grid.minor = element_blank(), axis.line = element_line(colour =
"black"))+
scale_y_continuous(expand = c(0, 0))+labs(x=z,title=paste0("p value =
",pPerm))
}

##############################TableKraza#################################
####

#################################################################
#             bisector plots                                    #
#################################################################

PlotDistanceBis<-function(x,links,y,z,w){#x any coords for mean
shape,links,y=axis,z=Matrix dataset,Title
#This function takes in account maximum and minimum number to scale each
axis from bisector
#Max<-max(abs(range(z)))
ColTest<-as.numeric(cut(z[,y],breaks=seq(0,max(z),length.out=9)))
#good#ColTest<-
as.numeric(cut(z[,y],breaks=seq(min(z),max(z),length.out=11)))
cols<-(brewer.pal(9, "BuPu"))
ColTest<-cols[ColTest]
plot3d(mshape(arrayspecs(x,27,3)), type = "s", col = ColTest, main = w,
size = 2, aspect = FALSE,
                  xlab = "", ylab = "", zlab = "", box = FALSE,
                  axes = FALSE)
M1<-mshape(arrayspecs(x,27,3))
gP <- gridPar()
                linkcol <- rep(gP$link.col, nrow(links))[1:nrow(links)]
                linklwd <- rep(gP$link.lwd, nrow(links))[1:nrow(links)]
                linklty <- rep(gP$link.lty, nrow(links))[1:nrow(links)]
                tarlinkcol            <-            rep(gP$tar.link.col,
nrow(links))[1:nrow(links)]
```

```
                tarlinklwd            <-            rep(gP$tar.link.lwd,
nrow(links))[1:nrow(links)]
                tarlinklty            <-            rep(gP$tar.link.lty,
nrow(links))[1:nrow(links)]
                for (i in 1:nrow(links)) {
                  segments3d(rbind(M1[links[i, 1], ], M1[links[i,
                    2], ]), col = linkcol[i], lty = linklty[i],
                    lwd = linklwd[i])
                    }
}

#####Transform 81 to 27 dimensions
BisectorLandDW<-apply(abs(arrayspecs(t(RealDW$bisector),27,3)),3,rowSums)
BisectorLandDF<-apply(abs(arrayspecs(t(RealDF$bisector),27,3)),3,rowSums)
BisectorLandWF<-apply(abs(arrayspecs(t(RealWF$bisector),27,3)),3,rowSums)
#####
PlotBisector<-function(x,name,angles){
#dim(DiffLandDF)[1]
for(h in seq(1,dim(x)[2])){
  for(j in views){
Title<-paste0(name," (angle ",h,"= ",round(angles[h]),")")
open3d(FOV=0,     userMatrix=as.name(paste("usrMat",     j,     sep=".")),
windowRect=windowRect)
PlotDistanceBis(ProFeral,links=wires,y=h,z=x,w=Title)
filename <- paste("Bisector/",name," Bisector. ",h,"_",j,".png", sep="")
    rgl.snapshot(filename, fmt="png", top=TRUE)
    rgl.close()
  }}}
  #Create Bisector folder beforehand
  #red is the most likely
PlotBisector(BisectorLandDF,name="Domestic                                    vs
Feral",angles=RealDF$angles)
PlotBisector(BisectorLandDW,name="Domestic                                    vs
Comparative",angles=RealDW$angles)
PlotBisector(BisectorLandWF,name="Comparative                                 vs
Feral",angles=RealWF$angles)

#########################################################################
#
#                        Three Groups                                   #
#########################################################################
#
GetResampleKraza2<-function(x,y,m,z,w){#two matrices to compare, z number
of PC, what to get(string):sumofS or angles
Lx<-nrow(x)
Ly<-nrow(y)
Lm<-nrow(m)

All<-rbind(x,y,m)
La<-nrow(All)

SampleAll<-sample(La)
x2<-All[SampleAll[seq(1,Lx)],]
y2<-All[SampleAll[seq(Lx+1,Lx+Ly)],]
m2<-All[SampleAll[seq(Lx+Ly+1,La)],]

CovX<-cov(x2)
CovY<-cov(y2)
CovZ<-cov(m2)
```

```
MList<-list(CovX,CovY,CovZ)


ResT<-KrzSubspace(MList,z)
ifelse(w=="angles",return(ResT$k_angles),ifelse(w=="eVals",return(ResT$k_
eVals_H),return("error")))
}

##########################################################################
#              Krzanowski 1993                                           #
##########################################################################
Krazanowsky.test.1993<-function (CA, CB, vecsA, vecsB, corr = FALSE, ...)
{
    if (length(vecsA) != length(vecsB)) {
        stop("vecsA amd vecsB must be same length")
    }
    if (length(vecsA) > c(dim(CA)[1]/2)) {
        warning("component spaces must be ", floor(c(dim(CA)[1]/2)),
            " dimension", "s"[floor(c(dim(CA)[1]/2)) > 1], " or less")
    }
    if (corr) {
        CA <- cov2cor(CA)
        CB <- cov2cor(CB)
    }
    #Mu
    EA <- eigen(CA)$values[seq(1,length(vecsA))]
    EB <- eigen(CB)$values[seq(1,length(vecsB))]
    Mu<-sum(abs(EA-EB))
    CA <- as.matrix(eigen(CA)$vectors[, vecsA])
    CB <- as.matrix(eigen(CB)$vectors[, vecsB])
    N <- t(CA) %*% CB %*% t(CB) %*% CA
    eigval <- eigen(N)$values
    eigvec <- as.matrix(eigen(N)$vectors)
    bisector <- matrix(NA, dim(CA)[1], length(vecsA))
    I <- diag(dim(CA)[1])
    for (i in 1:length(vecsA)) {
        bisector[, i] <- sqrt(2 * (1 + sqrt(eigval[i]))) * ((I +
            (1/sqrt(eigval[i])) * CB %*% t(CB)) %*% CA %*% eigvec[,
            i])
        bisector[, i] <- bisector[, i]/sqrt(sum(bisector[, i]^2))
    }
    angles <- acos(eigval^0.5)/(pi/180)
    sumofS <- sum(eigval)

    list(sumofS = sumofS, eigval = eigval,Mu=Mu)
}

#Y standardized matrices
YW<-(scale(ProWild[Normies,],center=TRUE,scale=TRUE))
YD<-(scale(ProDomestic,center=TRUE,scale=TRUE))
YF<-(scale(ProFeral,center=TRUE,scale=TRUE))
#REAL
YCovW<-cov(YW)
YCovD<-cov(YD)
YCovF<-cov(YF)
#corr=TRUE to work with correlation matrices
Kraza1993DF<-
Krazanowsky.test.1993(YCovD,YCovF,seq(1,4),seq(1,4),corr=TRUE)
```

```
Kraza1993DW<-
Krazanowsky.test.1993(YCovD,YCovW,seq(1,4),seq(1,4),corr=TRUE)
Kraza1993WF<-
Krazanowsky.test.1993(YCovW,YCovF,seq(1,4),seq(1,4),corr=TRUE)

#PERM
GetResampleKraza1993<-function(x,y,z,w){#two matrices to compare, z number
of PC, what to get(string):sumofS or angles
Lx<-nrow(x)
Ly<-nrow(y)

All<-rbind(x,y)
La<-nrow(All)

SampleAll<-sample(La)
x2<-All[SampleAll[seq(1,Lx)],]
y2<-All[SampleAll[seq(Lx+1,La)],]

xCov<-cov(x2)
yCov<-cov(y2)

ResT<-Krazanowsky.test.1993(xCov,yCov,seq(1,z),seq(1,z),corr=TRUE)
Mu<-ResT
ifelse(w=="Mu",return(ResT$Mu),ifelse(w=="sumofS",return(ResT$sumofS),ret
urn("error")))
}

K1993MuDF<-replicate(1000,{GetResampleKraza1993(YD,YF,4,"Mu")})

#########################################################################
#
#                                Random Skewers                         #
#########################################################################
#
#RandomSkewers(m.list,num.vectors=10000)
RS.RealDF<-RandomSkewers(CovD,CovF,num.vectors=10000)
RS.RealDW<-RandomSkewers(CovD,CovW,num.vectors=10000)
RS.RealWF<-RandomSkewers(CovW,CovF,num.vectors=10000)

#################Resample
GetResampleRS<-function(x,y,z){#m,z,w){#two matrices to compare, z number
of PC, what to get(string):sumofS or angles
Lx<-nrow(x)
Ly<-nrow(y)
#Lm<-nrow(m)

All<-rbind(x,y)
La<-nrow(All)

SampleAll<-sample(La)
x2<-All[SampleAll[seq(1,Lx)],]
y2<-All[SampleAll[seq(Lx+1,La)],]
#m2<-All[SampleAll[seq(Lx+Ly+1,La)],]

CovX<-cov(x2)
CovY<-cov(y2)

ResT<-RandomSkewers(CovX,CovY,num.vectors=z)
return(ResT)
```

```
}

#####################################Lines least evol resistance to
Penna and all evolvability
#Phylogenetic PCA
load(file="FunctionPlotTangentSpacePhyl.Rdata")
#Get Phylogenies
load(file="5000TreesDodoMoniasJetz.rda")
Sample500Trees<-sample(MultiTreeEctoPezoDodo,size=500)
Sample500TreesColumbiformesNR<-
lapply(Sample500Trees,drop.tip,tip=c("Monias_benschi","Pterocles_senegall
us","Pterocles_quadricinctus","Syrrhaptes_paradoxus",
"Raphus_cucullatus","Pezophaps_solitaria"))
Sample500TreesColumbiformes<-
lapply(Sample500Trees,drop.tip,tip=c("Monias_benschi","Pterocles_senegall
us","Pterocles_quadricinctus","Syrrhaptes_paradoxus"))

#Ancestor
ANCESTRAl<-NULL
for (i in seq(1,ncol(ProWild[Normies,]))){
Temp<-as.vector(fastAnc(Consensus,ProWild[Normies,i]))
ANCESTRAl<-cbind(ANCESTRAl,Temp)
}
rownames(ANCESTRAl)<-names(fastAnc(Consensus,ProWild[Normies,i]))

AncestorF<-
findMRCA(Consensus,tips=c("Columba_livia","Columba_rupestris"))-61
AncestorF<-ANCESTRAl[AncestorF,]
AncestorD<-colMeans(PredictFeral)
######For some reason not 61 PC in projected
pMax<-PpcaWild$rotation[1:60,"PC1"]

#Zd mean feral to each domestic
Zd<-NULL
for (i in seq(1,dim(PredictDomestic)[1])){
Temp<-AncestorD-PredictDomestic[i,]
Zd<-rbind(Zd,Temp)
}
#Zf ancestor livia rupestriis to every feral
Zf<-NULL
for (i in seq(1,dim(PredictFeral)[1])){
Temp<-AncestorF[1:60]-PredictFeral[i,]
Zf<-rbind(Zf,Temp)
}
#Zw ancestors to each decendant
Zw<-NULL
for (i in seq(1,dim(PpcaWild$pc.scores)[1])){
Des<-which(Consensus$edge[,2]==i)
Anc<-Consensus$edge[Des,1]-61
Temp<-ANCESTRAl[Anc,1:60]-PpcaWild$pc.scores[i,]
Zw<-rbind(Zw,Temp)
}
##########LLERcorr
GetCorr<-function(x,y){
Corr<-cos(crossprod(x,y)/(Norma(x)*Norma(y)))
return(Corr)
}

LLERcorrD<-apply(Zd,1,GetCorr, y=pMax)
```

```
LLERcorrF<-apply(Zf,1,GetCorr, y=pMax)
LLERcorrW<-apply(Zw,1,GetCorr, y=pMax)

##########mMount
mMountD<-apply(Zd,1,function(x) sum(x^2))
mMountF<-apply(Zf,1,function(x) sum(x^2))
mMountW<-apply(Zw,1,function(x) sum(x^2))
##########Pearson
#plot(LLERcorrD,mMountD)
PearsonD<-cor.test(LLERcorrD,mMountD,method="pearson")$estimate
#plot(LLERcorrF,mMountF)
PearsonF<-cor.test(LLERcorrF,mMountF,method="pearson")$estimate
#plot(LLERcorrW,mMountW)
PearsonW<-cor.test(LLERcorrW,mMountW,method="pearson")$estimate


#####################################################################
#                                MultyPCA                           #
#####################################################################
#Phylogenetic PCA
Raphini<-setdiff(rownames(ProWild),Normies)


GetCorr<-function(x,y){
Corr<-sum(x*y)/(Norma(x)*Norma(y))
return(abs(Corr))
}

broken.stick <- function(p){
Stick<-1
Result<-NULL
for (i in seq(1,p-1)){
Piece<-runif(1,min=0,max=Stick)
Result<-c(Result,Piece)
Stick<-Stick-Piece
}
Result<-c(Result,1-sum(Result))
return(Result)
}

#Takes between 25 and 33 mins for 500 phylogenies

for (i in seq(1,500)){
Consensus<-Sample500TreesColumbiformesNR[[i]]
PpcaWild<-
PlotTangentSpacePhyl(arrayspecs(ProWild[Normies,],27,3),Sample500TreesCol
umbiformesNR[[i]])
rgl.close()
dev.off()
#predictions of species in PhyPCA space
class(PpcaWild)<-c("prcomp")
PredictDomestic<-predict(PpcaWild,ProDomestic)
PredictFeral<-predict(PpcaWild,ProFeral)
PredictRaphini<-predict(PpcaWild,ProWild[Raphini,])
#Ancestor
ANCESTRAl<-NULL
for (j in seq(1,ncol(ProWild[Normies,]))){
Temp<-
as.vector(fastAnc(Sample500TreesColumbiformesNR[[i]],ProWild[Normies,j]))
```

```
ANCESTRAl<-cbind(ANCESTRAl,Temp)
}
#changed this a lot
rownames(ANCESTRAl)<-
names(fastAnc(Sample500TreesColumbiformesNR[[i]],ProWild[Normies,1]))

AncestorF<-
findMRCA(Sample500TreesColumbiformesNR[[i]],tips=c("Columba_livia","Colum
ba_rupestris"))-61
AncestorF<-ANCESTRAl[AncestorF,]
#################This gave a constant 0.0132759
AncestorD<-AncestorF[1:60]


######For not 61 PC in projected
pMax<-PpcaWild$rotation[1:60,"PC1"]
pMax2<-PpcaWild$rotation[1:60,"PC2"]
pMax3<-PpcaWild$rotation[1:60,"PC3"]
pMax4<-PpcaWild$rotation[1:60,"PC4"]

pRand<-broken.stick(81)[1:60]

#Zd mean feral to each domestic
Zd<-NULL
for (j in seq(1,dim(PredictDomestic)[1])){
Temp<-AncestorD-PredictDomestic[j,]
Zd<-rbind(Zd,Temp)
}
#Zf ancestor livia rupestriis to every feral
Zf<-NULL
for (j in seq(1,dim(PredictFeral)[1])){
Temp<-AncestorF[1:60]-PredictFeral[j,]
Zf<-rbind(Zf,Temp)
}
#Zw ancestors to each decendant
Zw<-NULL
for (j in seq(1,dim(PpcaWild$pc.scores)[1])){
Des<-which(Consensus$edge[,2]==j)
Anc<-Consensus$edge[Des,1]-61
Temp<-ANCESTRAl[Anc,1:60]-PpcaWild$pc.scores[j,]
Zw<-rbind(Zw,Temp)
}
TempRaphiP<-PpcaWild$pc.scores["Caloenas_nicobarica",]-
PredictRaphini["Pezophaps_solitaria",]
TempRaphiR<-PpcaWild$pc.scores["Caloenas_nicobarica",]-
PredictRaphini["Raphus_cucullatus",]
Zw<-rbind(Zw,TempRaphiP,TempRaphiR)
##########LLERcorr
T.LLERcorrD<-apply(Zd,1,GetCorr, y=pMax)
T.LLERcorrF<-apply(Zf,1,GetCorr, y=pMax)
T.LLERcorrW<-apply(Zw,1,GetCorr, y=pMax)
M.LLERcorrD<-c(M.LLERcorrD,T.LLERcorrD)
M.LLERcorrF<-c(M.LLERcorrF,T.LLERcorrF)
M.LLERcorrW<-c(M.LLERcorrW,T.LLERcorrW)
Mean.LLERcorrD<-c(Mean.LLERcorrD,mean(T.LLERcorrD))
Mean.LLERcorrF<-c(Mean.LLERcorrF,mean(T.LLERcorrF))
Mean.LLERcorrW<-c(Mean.LLERcorrW,mean(T.LLERcorrW))

##########mMount
```

```
T.mMountD<-apply(Zd,1,function(x) sqrt(sum(x^2)))
T.mMountF<-apply(Zf,1,function(x) sqrt(sum(x^2)))
T.mMountW<-apply(Zw,1,function(x) sqrt(sum(x^2)))
M.mMountD<-c(M.mMountD,T.mMountD)
M.mMountF<-c(M.mMountF,T.mMountF)
M.mMountW<-c(M.mMountW,T.mMountW)
Mean.mMountD<-c(Mean.mMountD,mean(T.mMountD))
Mean.mMountF<-c(Mean.mMountF,mean(T.mMountF))
Mean.mMountW<-c(Mean.mMountW,mean(T.mMountW))

##########Pearson
T.PearsonD<-cor.test(T.LLERcorrD,T.mMountD,method="pearson")$estimate
T.PearsonF<-cor.test(T.LLERcorrF,T.mMountF,method="pearson")$estimate
T.PearsonW<-cor.test(T.LLERcorrW,T.mMountW,method="pearson")$estimate
M.PearsonD<-c(M.PearsonD,T.PearsonD)
M.PearsonF<-c(M.PearsonF,T.PearsonF)
M.PearsonW<-c(M.PearsonW,T.PearsonW)
#####################################################################
#PC2
T.LLERcorrD2<-apply(Zd,1,GetCorr, y=pMax2)
T.LLERcorrF2<-apply(Zf,1,GetCorr, y=pMax2)
T.LLERcorrW2<-apply(Zw,1,GetCorr, y=pMax2)
M.LLERcorrD2<-c(M.LLERcorrD2,T.LLERcorrD2)
M.LLERcorrF2<-c(M.LLERcorrF2,T.LLERcorrF2)
M.LLERcorrW2<-c(M.LLERcorrW2,T.LLERcorrW2)
Mean.LLERcorrD2<-c(Mean.LLERcorrD2,mean(T.LLERcorrD2))
Mean.LLERcorrF2<-c(Mean.LLERcorrF2,mean(T.LLERcorrF2))
Mean.LLERcorrW2<-c(Mean.LLERcorrW2,mean(T.LLERcorrW2))
T.PearsonD2<-cor.test(T.LLERcorrD2,T.mMountD,method="pearson")$estimate
T.PearsonF2<-cor.test(T.LLERcorrF2,T.mMountF,method="pearson")$estimate
T.PearsonW2<-cor.test(T.LLERcorrW2,T.mMountW,method="pearson")$estimate
M.PearsonD2<-c(M.PearsonD2,T.PearsonD2)
M.PearsonF2<-c(M.PearsonF2,T.PearsonF2)
M.PearsonW2<-c(M.PearsonW2,T.PearsonW2)
#PC3
T.LLERcorrD3<-apply(Zd,1,GetCorr, y=pMax3)
T.LLERcorrF3<-apply(Zf,1,GetCorr, y=pMax3)
T.LLERcorrW3<-apply(Zw,1,GetCorr, y=pMax3)
M.LLERcorrD3<-c(M.LLERcorrD3,T.LLERcorrD3)
M.LLERcorrF3<-c(M.LLERcorrF3,T.LLERcorrF3)
M.LLERcorrW3<-c(M.LLERcorrW3,T.LLERcorrW3)
Mean.LLERcorrD3<-c(Mean.LLERcorrD3,mean(T.LLERcorrD3))
Mean.LLERcorrF3<-c(Mean.LLERcorrF3,mean(T.LLERcorrF3))
Mean.LLERcorrW3<-c(Mean.LLERcorrW3,mean(T.LLERcorrW3))
T.PearsonD3<-cor.test(T.LLERcorrD3,T.mMountD,method="pearson")$estimate
T.PearsonF3<-cor.test(T.LLERcorrF3,T.mMountF,method="pearson")$estimate
T.PearsonW3<-cor.test(T.LLERcorrW3,T.mMountW,method="pearson")$estimate
M.PearsonD3<-c(M.PearsonD3,T.PearsonD3)
M.PearsonF3<-c(M.PearsonF3,T.PearsonF3)
M.PearsonW3<-c(M.PearsonW3,T.PearsonW3)
#PC4
T.LLERcorrD4<-apply(Zd,1,GetCorr, y=pMax4)
T.LLERcorrF4<-apply(Zf,1,GetCorr, y=pMax4)
T.LLERcorrW4<-apply(Zw,1,GetCorr, y=pMax4)
M.LLERcorrD4<-c(M.LLERcorrD4,T.LLERcorrD4)
M.LLERcorrF4<-c(M.LLERcorrF4,T.LLERcorrF4)
M.LLERcorrW4<-c(M.LLERcorrW4,T.LLERcorrW4)
Mean.LLERcorrD4<-c(Mean.LLERcorrD4,mean(T.LLERcorrD4))
Mean.LLERcorrF4<-c(Mean.LLERcorrF4,mean(T.LLERcorrF4))
```

```
Mean.LLERcorrW4<-c(Mean.LLERcorrW4,mean(T.LLERcorrW4))
T.PearsonD4<-cor.test(T.LLERcorrD4,T.mMountD,method="pearson")$estimate
T.PearsonF4<-cor.test(T.LLERcorrF4,T.mMountF,method="pearson")$estimate
T.PearsonW4<-cor.test(T.LLERcorrW4,T.mMountW,method="pearson")$estimate
M.PearsonD4<-c(M.PearsonD4,T.PearsonD4)
M.PearsonF4<-c(M.PearsonF4,T.PearsonF4)
M.PearsonW4<-c(M.PearsonW4,T.PearsonW4)

############################Random###################################
T.LLERcorrD<-apply(Zd,1,GetCorr, y=pRand)
T.LLERcorrF<-apply(Zf,1,GetCorr, y=pRand)
T.LLERcorrW<-apply(Zw,1,GetCorr, y=pRand)
Mean.LLERcorrD.R<-c(Mean.LLERcorrD.R,mean(T.LLERcorrD))
Mean.LLERcorrF.R<-c(Mean.LLERcorrF.R,mean(T.LLERcorrF))
Mean.LLERcorrW.R<-c(Mean.LLERcorrW.R,mean(T.LLERcorrW))

###########Pearson
T.PearsonD<-cor.test(T.LLERcorrD,T.mMountD,method="pearson")$estimate
T.PearsonF<-cor.test(T.LLERcorrF,T.mMountF,method="pearson")$estimate
T.PearsonW<-cor.test(T.LLERcorrW,T.mMountW,method="pearson")$estimate
M.PearsonD.R<-c(M.PearsonD.R,T.PearsonD)
M.PearsonF.R<-c(M.PearsonF.R,T.PearsonF)
M.PearsonW.R<-c(M.PearsonW.R,T.PearsonW)
}


########################################random    association    between
vectors a) random b) isometric
#https://stackoverflow.com/questions/1897704/angle-between-two-vectors-
in-r

######Expected values for random
RandomCorr<-replicate(500,{
Rand60A<-runif(60,-1,1)
Rand60B<-runif(60,-1,1)
RandIso<-rep(1,60)
Res<-c(Rand=GetCorr(Rand60A,Rand60B),Iso=c(GetCorr(Rand60A,RandIso)))
})
```